A proteomic study of an in-vitro model of TGF-1-induced fibrosis and mechanisms of herbal antifibrotics

Zhou, Shujun

Awarding institution:
King's College London

A Proteomic Study of an *In-Vitro* Model of TGF-β1-induced Fibrosis and Mechanisms of Herbal Antifibrotics

A thesis submitted for the degree of Doctor of Philosophy
By Shujun Zhou

King's College London

September 2019

Abstract

Fibrosis is scarring of tissues characterised by excessive accumulation of collagen proteins, in which transforming growth factor (TGF)-β1 plays a central role. Fibrosis affects virtually all organs and is a common pathology behind chronic organ failure and mortality. Few anti-fibrotic drugs are available to prevent or reverse fibrosis, thus, it represents a significant unmet medical need to better understand fibrosis and to develop novel antifibrotics.

Botanicals could be both cause and cure of fibrosis. Aconiti Radix (AR) and Aconiti Lateralis Radix (ALR) were suggested pro-fibrotic and potentially nephrotoxic, while Scutellariae Radix (SR) and SR flavonoids were reportedly anti-fibrotic. I hypothesised that AR/ALR and SR might affect fibrogenesis as a function of AR/ALR alkaloids and SR flavonoids, respectively. This project aimed to (i) further scrutinise effects of AR, ALR, AR/ALR alkaloids, SR and SR flavonoids in a TGF-β1-induced *in-vitro* model of fibrosis; and (ii) develop a proteomic view of the *in-vitro* model of fibrosis and the differential mechanisms of action of selected antifibrotics.

In NRK-49F renal fibroblasts with and without treatment by TGF-β1 and antifibrotics, fibrogenesis was quantified by total collagen assays and examination of fibrogenic molecular markers. Cell lysates and conditioned media were harvested for proteomic analysis. Proteins of interest were validated by enzyme-linked immunosorbent assay (ELISA).

Results showed that aqueous and ethanolic extracts of unprocessed and processed AR did not affect fibrogenesis. Seven of nine AR alkaloids showed anti-fibrotic effects. These disapproved my hypothesis on AR/ALR and their alkaloids. Supporting SR flavonoids as the main anti-fibrotic compounds in SR, however, methanolic extract of SR (SRM), which contained 8-fold higher flavonoids than SR aqueous (SRA) extract, is more potently anti-fibrotic than SRA. Five tested SR flavonoids were more or less anti-fibrotic, with baicalein being the most anti-fibrotic and least toxic. Hence, in further proteomic studies, I focused on mechanisms of TGF-β1-induced *in-vitro* model of fibrosis and the anti-fibrotic mechanisms of SRM and baicalein, in comparison with IN1130, an inhibitor of TGF-β type I receptor. In cell lysates of TGF-β1-stimulated NRK-49F cells, there was an apparent mismatch between increased ribosomal proteins and reduced proteins involved in multiple metabolism pathways, in between which there was increased Impdh2, a druggable target. Secretomic analysis indicated that TGF-β1-induced fibrosis was mediated by dysregulation of key regulators of matrix degradation (PAI-1and Mmp3), signalling mediators (Ccn1, Ccn2, Ccn3 and Tsku) and a collagen crosslinker (Plod2), and was coupled with increased chemokines Ccl2 and Ccl7. SRM, baicalein and IN1130 all significantly regulated the ribosome pathway; SRM and baicalein, but not IN1130, regulated the lysosome pathway, while they

differentially regulated metabolism pathways. They all reversed TGF-β1-induced PAI-1, Plod2, Ccn2, Ccl2 and Ccl7. Baicalein and IN1130, but not SRM, reversed TGF-β1-induced Ccn1 and Tsku. Only baicalein reversed TGF-β1 repression of Mmp3. Only IN1130 reversed TGF-β1 induction of Impdh2 and repression of Aldh3a1 and Ccn3. Among all proteins in cell lysates, Enpp1 was most dramatically induced by TGF-β1 and it was also among the most dramatically repressed by SRM, baicalein and IN1130.

In conclusion, TGF-β1-induced fibrogenesis in renal fibroblasts involves dysregulation of multiple secreted proteins involved in regulation of collagen synthesis, crosslinking and degradation, and is characterised by dysregulation of intracellular metabolism. It is inherently coupled with increased secretion of chemokines, suggestive of a pro-inflammatory role for TGF-β1 and myofibroblasts. Comparative proteomic analysis has uncovered overlapping mechanisms of the three antifibrotics. Besides known anti-fibrotic targets e.g. PAI-1 and Ccn2, it deserves further investigation to determine whether ribosome, lysosome, metabolism pathways and individual proteins e.g. Aldh3a1, Ccn1, Ccn3, Enpp1, Impdh2, Mmp3, Plod2 and Tsku are novel targets for developing antifibrotics.

Acknowledegement

Firstly, I would like to thank my supervisors, Dr Qihe Xu and Professor Peter Hylands for offering me the opportunity to embark on this PhD project and for their continuous support, help, and advice throughout my PhD training. Their generosity of time and spirit has been very much appreciated.

Secondly, I would like to thank PuraPharm and Sino-British Fellowship Trust for their generosity in supporting me with this PhD project. Their finical support is truly appreciated.

I would also like to thank Prof. Zhongzhen Zhao, Dr Zhitao Liang and Miss Jun Yuan in Hong Kong Baptist University for performing the herbal extraction and processing; Dr Yunxia Li in Chengdu University of Traditional Chinese Medicine for providing flavonoids and alkaloids compounds; Prof. Yung-Chi Cheng in Yale University for supplying 30 chemically modified baicalein derivatives; Prof. Lin Ge in Chinese University of Hong Kong for her professional advice; Prof. Manuel Mayr and Dr. Xiaoke Yin in King's college London for providing technical support of proteomics study.

Last but not least, I would like to express my gratitude to all members of renal laboratory. I still want to thank my parents and the whole family for their warm support and encouragement.

Contents

Abstract 2

Acknowledegement 4

Contents 5

List of figures 9

List of tables 12

Abbreviations 14

Chapter 1 Introduction 17

1.1. Chronic kidney disease (CKD) 17

1.2. TIF 20

1.3. Anti-fibrotic and pro-fibrotic activities of botanicals 23

1.4. *Aconitum carmichaeli* Debx. and its alkaloid compounds 24

1.5. *Scutellaria baicalensis* Georgi and its flavonoid compounds 28

1.6. Hypothesis and aims 33

Chapter 2 Materials and Methods 34

2.1. Herbs and herbal compounds 34

2.2. Reagents, buffers and solutions 34

2.2.1. *In-vitro* model of fibrosis 35

2.2.2. Immunocytochemistry 37

2.2.3. Protein preparation 38

2.2.4. Enzyme-linked immunosorbent assay (ELISA) 38

2.3. Preparation of herbal extracts 39

2.3.1. Processing and extraction of AR and ALR 39

2.3.2. Extraction of SR 40

2.4. Authentication of herbal compounds 42

2.5. Cell culture and quality control 42

2.5.1. Cell species identification 44
2.5.2. Cellular morphology and immunocytochemical characterisation 48
2.5.3. Mycoplasma contamination detection 50
2.6. *In-vitro* model of fibrosis 52
2.7. Lactate dehydrogenase (LDH) release assays 53
2.8. Immunocytofluorescence assay 54
2.9. Protein extraction 54
2.10. QuickZyme total collagen assay 55
2.11. Sicrol soluble collagen assay 56
2.12. Proteomic analysis 56
2.12.1. Sample preparation 56
2.12.2. HPLC-MS/MS analysis 58
2.13. Bioinformatics 59
2.14. ELISA validation 59
Chapter 3 Effects of AR and aconite alkaloids on fibrogenesis 60
3.1. Quality control of AR/ALR extracts 60
3.2. Effects of unprocessed and processed AR extracts on fibrogenesis 65
3.3. Effects of aconite alkaloids on fibrogenesis 65
3.4. Discussion and Conclusions 71
Chapter 4 *In-vitro* anti-fibrotic activities of SR and SR flavonoids 74
4.1. Quality control of SR extracts 74
4.2. Anti-fibrotic activities of SR extracts in an *in-vitro* model of fibrosis 78
4.3. Anti-fibrotic activities of SR flavonoids in an *in-vitro* model of fibrosis 82
4.4. Discussions and Conclusions 86
Chapter 5 Proteomics of TGF-β1-induced *in-vitro* model of fibrosis 88
5.1. TGF-β1-induced *in-vitro* model of fibrosis 88
5.2. Proteomic profiling analysis of cell lysates 88
5.3. ELISA validation of selected cell-lysate proteins 106

5.4. Effect of Sappanone A, an Impdh2 inhibitor, on TGF-β1-induced fibrogenesis 107
5.5. Proteomic profiling analysis of conditioned media 109
5.6. ELISA validation of selected proteins in conditioned media 121
5.7. Discussions 123
5.7.1. Comparison with a proteomic study of TGF-β1-induced fibrogenesis in NRK-49F cells in the literature 123
5.7.2. TGF-β1-induced fibrogenesis may be an intracellular metabolic disorder 125
5.7.3. TGF-β1 most significantly induced Enpp1 and repressed Aldh3a1 and Cat 126
5.7.4. TGF-β1 triggered pro-fibrotic and anti-fibrotic signals 127
5.7.5. TGF-β1 induced chemokines Ccl2 and Ccl7 129
5.8. Conclusions 130
Chapter 6: Comparative proteomic analysis of the fibrotic effects of SRM, baicalein and IN1130 131
6.1. Experimental design and workflow 131
6.2. Results on cell lysates 133
6.2.1. Proteomic analysis and data interpretation 133
6.2.2. ELISA validation 140
6.3. Results on conditioned media 142
6.3.1. Proteomic analysis and data interpretation 142
6.3.2. ELISA validation 150
6.4. Discussions 152
6.4.1. Discussion on cell-lysate results 152
6.4.2. Discussion on condition-media results 154
6.4.3. Discussion on integrated analysis of findings on cell-lysate and condition-media proteins 156
6.5. Conclusions 160
Chapter 7. General discussion and future work 161
7.1. General discussion 161
7.1.1. Quality control of materials and methods 161

7.1.2. Choice of cellular model and *in-vitro* model of fibrosis 162
7.1.3. Toxicity of SR and SR flavonoids 163
7.1.4. Proteomic approach to guide mechanistic studies 164
7.2. Future work 166
7.2.1. Confirmation of the effects of AR/ALR on fibrogenesis 166
7.2.2. Anti-fibrotic activities of synthetic baicalein derivatives 167
7.2.3. Further validation 168
7.2.4. Integrating proteomics and metabolomics 168
Chapter 8 Bibliography 169
Chapter 9 Appendix 189
Supplementary Fig. 1. Authentication of AR. 189
Supplementary Fig. 2. Authentication of ALR. 192
Supplementary Fig. 3. Authentication of SR. 195
Supplementary Table. 1. Cell-lysate proteins significantly regulated by TGF-β1. (listed in the order of fold change (TGF-β1/control). 198
Supplementary Table. 2. SRM, baicalein and IN1130 all significantly regulated proteins involved in the focal adhesion pathway. 214
Supplementary Table. 3. SRM and IN1130 significantly regulated proteins involved in the amoebiasis pathway pathway. 215
Supplementary Table. 4. Baicalein and IN1130 significantly regulated proteins involved 13 KEGG pathways. 216
Supplementary Table. 5. SRM significantly regulated proteins involved 5 KEGG pathways. 223
Supplementary Table. 6. Baicalein significantly regulated proteins involved 18 KEGG pathways. 224
Supplementary Table. 7. IN1130 significantly regulated proteins involved 9 KEGG pathways. 228
Supplementary Table. 8. Validation of the molecular weights of synthetic baicalein derivatives by HRMS. 229

List of figures

Fig. 1.1. Origin of matrix-producing myofibroblasts that directly mediate TIF 22
Fig. 1.2. Photographs of *Aconitum carmchaeli* Debx. and its derived herbal drugs. 25
Fig. 1.3. Schematic representation of two step hydrolysis of alkaloids. 26
Fig. 1.4. The form of traditional processing of AR/ALR in the Chinese Pharmacopoeia. 27
Fig. 1.5. Photographs of *Scutellaria baicalensis* Georgi and its derived herbal drug. 29
Fig. 1.6. Structures of five SR flavonoids. 29
Fig. 2.1. The procedure flow of AR and ALR extraction and downstream assays. 39
Fig. 2.2. The procedure of SR extraction and downstream analysis. 41
Fig. 2.3. PCR amplification with species-specific human, mouse and rat primer pairs. 47
Fig. 2.4. PCR amplification with human and mouse primer pairs. 48
Fig. 2.5. NRK-49F cells in culture. 48
Fig. 2.6. Characterisation of NRK-49F cells by immunocytofluoresence assays. 49
Fig. 2.7. PCR amplification for mycoplasma detection. 51
Fig. 2.8. Protein sample preparation for proteomic analysis. 57
Fig. 3.1. BPCs of unprocessed and processed AR. 62
Fig. 3.2. BPCs of unprocessed and processed ALR. 63
Fig. 3.3. EICs of nine alkaloids in unprocessed and processed AR and ALR. 64
Fig. 3.4. Unprocessed AR aqueous (AR-A) and ethanolic (AR-E) extracts did not affect fibrogenesis. 66
Fig. 3.5. Processed AR aqueous (AR-A) and ethanolic (AR-E) extracts did not affect fibrogenesis. 67
Fig. 3.6a. Alkaloids A1 and A2, but not A3, showed dose-dependent anti-fibrotic activities. 68
Fig. 3.6b. A5 and A6, but not A4, showed dose-dependent anti-fibrotic activities. 69
Fig. 3.6c. Alkaloids A7, A8 and A9 showed dose-dependent anti-fibrotic activities. 70
Fig. 4.1. BPCs of SRA and SRM. 75
Fig. 4.2. EICs of F5 in SRA and SRM. 76
Fig. 4.3. BPCs of the “F5 fraction” (SRA-F5) and “F5-depleted fraction” (SRA-F5D) of SRA. 77
Fig. 4.4. BPCs of the “F5 fraction” (SRM-F5) and the “F5-depleted fraction” (SRM-F5D) of SRM. 78
Fig. 4.5. SRA and SRM extracts inhibited fibrogenesis in an in-vitro model of fibrosis induced by TGF-β1. 80
Fig. 4.6. At 80 μg/mL, SRM, but not SRA, significantly inhibited TGF-β1-induced total collagen accumulation in NRK-49F cells. 81

Fig. 4.7. 80 μg/mL SRM, but not SRA, significantly down-regulated TGF-β1-induced collagen type I, collagen type III, α-SMA and fibronectin in NRK-49F cells. 81
Fig. 4.8. Among F5, baicalin and baicalein were the most potent in inhibiting fibrogenesis in the presence of TGF-β1. 83
Fig. 4.9. Among 60 μM F5, baicalein showed the best anti-fibrotic activity and little cytotoxicity. 84
Fig. 4.10. 60 μM F5 down-regulated TGF-β1-induced collagen type I, collagen type III, α-SMA and fibronectin in NRK-49F cells. 85
Fig. 5.1. TGF-β1 induced accumulation of total collagen in cell lysates and soluble collagen in conditioned media. 89
Fig. 5.2. GO cellular component enrichment analysis of the proteins significantly regulated by TGF-β1 in cell lysates. 91
Fig. 5.3. GO biological process enrichment analysis of the proteins significantly regulated by TGF-β1 in cell lysates. 92
Fig. 5.4. GO molecular function enrichment analysis of the proteins significantly regulated by TGF-β1 in cell lysates. 93
Fig. 5.5. KEGG pathway and STRING network analyses of 628 proteins in cell lysates significantly regulated by TGF-β1. 96
Fig. 5.6. KEGG pathway analysis of 127 proteins in cell lysates significantly regulated by TGF-β1 with fold-change >1.5 or < 0.67 101
Fig. 5.7. TGF-β1 significantly regulated multiple metabolic pathways and the ribosome pathway, with Impdh2 sitting in between as a possible “middleman” 102
Fig. 5.8. Volcano plot displaying the proteins differentially regulated by TGF-β1 105
Fig. 5.9. ELISA validation of selected cell-lysate proteins. 107
Fig. 5.10. Sappanone A, an Impdh2 inhibitor, did not affect TGF-β1-induced fibrogenesis. 108
Fig. 5.11. GO cellular component enrichment analysis of the proteins in conditioned media significantly regulated by TGF-β1. 112
Fig. 5.12. GO biological processe enrichment analysis of the proteins in conditioned media significantly regulated by TGF-β1. 115
Fig. 5.13. GO molecular function enrichment analysis of the proteins in conditioned media significantly regulated by TGF-β1. 118
Fig. 5.14. STRING analysis illustrates predicted direct (physical) and indirect (functional) associations among proteins in conditioned media significantly regulated by TGF-β1. 120
Fig. 5.15. KEGG pathways of proteins in conditioned media regulated by TGF-β1 120
Fig. 5.16. Volcano plot shows the proteins in conditioned media regulated by TGF-β1. ... 121
Fig. 5.17. Validation of selected proteins in conditioned media by ELISA. 122

Fig. 5.18. Venn diagram showing similarities and differences between the proteins significantly changed by TGF-β1 in reference data (141) and the proteins detected in present study. 124
Fig. 5.19. Possible mechanisms and potential therapeutic targets of TGF-β1-induced fibrosis in NRK-49F cells 130
Fig. 6.1. Experimental design, workflow and establishment of TGF-β1-induced *in-vitro* model of fibrogenesis in NRK-49F cells and effects of anti-fibrotic drugs. 132
Fig. 6.2. Venn diagram analysis of cell-lysate proteins regulated by SRM, baicalein and IN1130 in TGF-β1-induced *in-vitro* model of fibrosis. 133
Fig. 6.3. KEGG pathway analysis of cell-lysate proteomics significantly regulated by SRM, baicalein and IN1130. 135
Fig. 6.4. Venn diagram analysis of ribosomal proteins regulated by SRM, baicalein and IN1130 136
Fig. 6.5. Volcano plots of cell-lysate proteins regulated by SRM, baicalien and IN1130 in TGF-β1-induced *in-vitro* model of fibrosis. 139
Fig. 6.6. Comparison of proteomoic analysis and ELISA validation of selected cell-lysate proteins regulated by SRM, baicalein and/or IN1130. 141
Fig. 6.7. Venn diagram analysis of secreted proteins significantly regulated by SRM, baicalein and IN1130. 142
Fig. 6.8. KEGG pathway analysis of proteins in conditioned media significantly regulated by SRM and baicalein in TGF-β1-induced *in-vitro* model of fibrosis. 143
Fig. 6.9. Venn diagram analysis of secreted proteins involved in the ribosome pathway, which were regulated by SRM and/or baicalein. 143
Fig. 6.10. Volcano-plot analysis of SRM, baicalien and IN1130 effects on proteomics of conditioned media in TGF-β1-induced *in-vitro* model of fibrosis. 148
Fig. 6.11. Comparison of proteomic analysis and ELISA validation of selected proteins in conditioned media regulated by SRM, baicalein and IN1130. 150
Fig. 6.12. Effect of SRM, baicalein and IN1130 on proteins of interest in cell lysates of TGF-β1-induced fibrosis. 152
Fig. 6.13. Effects of TGF-β1, SRM, baicalein and IN1130 on proteins in conditioned media and their possible roles in fibrosis and inflammation. 154
Fig. 7.1. Structures of synthetic baicalein derivatives 167

List of tables

Table 1.1 Anti-fibrotic drugs tested in clinical trials. 18
Table 1.2. SR and its flavonoids showed anti-fibrotic activities in fibrotic disease models.. 31
Table 2.1. List of herbal materials..... 35
Table 2.2. Herbal extracts and compounds prepared as stocks for biology studies. 36
Table 2.3. List of antibodies..... 37
Table 2.4. List of ELISA kits. 38
Table 2.5. Validation of molecular weights of AR/ALR alkaloids by HRMS. 43
Table 2.6. Validation of molecular weights of SR flavonoids by HRMS..... 43
Table 2.7. List of cell lines and primary cell cultures. 45
Table 2.8. Species-specific primers..... 46
Table 2.9. The reaction composition for species-specific amplification..... 46
Table 2.10. Cycling protocol for species-specific amplification. 46
Table 2.12. Cycling protocol for mycoplasma amplification..... 51
Table 3.1. Percent contents of nine alkaloids in unprocessed and processed AR and ALR.. 61
Table 4.1. Percent contents of F5 in SRA and SRM..... 74
Table 5.1. Cell-lysate proteins significantly regulated by TGF-β1 are involved in 42 KEGG pathways..... 97
Table 5.2 Proteins in clusters a and b (Fig. 5.7a) listed in order of fold-change..... 103
Table 5.3 KEGG pathways and the involved proteins significantly regulated by TGF-β1 in clusters a and b. 104
Table 5.4 Cell-lysate proteins most significantly up-regulated by TGF-β1 with fold change>2. 106
Table 5.5. Cell-lysate proteins most significantly down-regulated by TGF-β1 with fold change <0.5. 106
Table 5.6. Proteins significantly up-regulated by TGF-β1 in conditioned media..... 109
Table 5.7. Proteins significantly down-regulated by TGF-β1 in conditioned media..... 110
Table 5.8. GO cellular component analysis of proteins in conditioned media significantly regulated by TGF-β1. 113
Table 5.9. GO biological process analysis of proteins in conditioned media significantly regulated by TGF-β1. 116
Table 5.10. GO molecular function analysis of proteins in conditioned media significantly regulated by TGF-β1 118
Table 5.11. Comparison of proteomic studies of TGF-β1-induced fibrogenesis in NRK-49F cells..... 123

Table 5.12. The overlapping proteins significantly changed by TGF-β1 in reference data and the present study 124
Table 6.1. SRM, baicalein and IN1130 all significantly regulated the proteomic profiling of the ribosome pathway. 136
Table 6.2. SRM and baicalein, but not IN1130, significantly regulated proteins involved in the lysosome pathway. 138
Table 6.3. Both concentrations of SRM and 80 μM baicalein regulated proteins in conditioned media enriched in the ribosome pathway. 144
Table 6.4. Baicalein significantly regulated proteins in conditioned media enriched in 10 KEGG pathways. 145

Abbreviations

AKI	Acute kidney injury
Aldh3a1	Aldehyde dehydrogenase, dimeric NADP-preferring
ALR	Aconiti Lateralis Radix
AR	Aconiti Radix
BCA	Bicinchoninic acid
BDL	Bile duct ligation and scission
BPCs	Base peak chromatograms
BSA	Bovine serum albumin
Cat	Catalase
Ccdc80	Coiled-coil domain-containing protein 80
Ccl2	C-C motif chemokine 2
CCl4	Carbon tetrachloride
Ccl7	C-C motif chemokine 7
Ccn3	Protein Nov
CCR2/5	Chemokine receptor 2/5
CKD	Chronic kidney disease
Cox I	Cytochrome oxidase subunit
Ctgf	Connective tissue growth factor
Cyr61	Cysteine Rich Angiogenic Inducer 61
DAVID	Database for Annotation, Visualization and Integrated Discovery
DDAs	Diester-diterpenoid alkaloids
DMEM	Dulbecco's Modified Eagle Medium
DMN	Dimethylnitrosamine
DMSO	Dimethyl sulfoxide
DN	Diabetic nephropathy
DTT	Dithiothreitol
EDTA	Ethylenediaminetetraacetic acid
EICs	Extracted ion chromatograms
ELISA	Enzyme-linked immunosorbent assay
EMT	Epithelial-to-mesenchymal transition
EndoMT	Endothelial-to-mesenchymal transition
Enpp1	Ectonucleotide pyrophosphatase/phosphodiesterase family member 1
ESI	Electrospray ionization
ET-1	Endothelin-1
FCS	Fetal calf serum
FDR	False discovery rate
GAP	Good Agricultural Practices
GFR	Glomerular filtration rate
GO	Gene Ontology

GPx	Glutathione peroxidase
HCl	Hydrochloric acid
HPLC	High-performance liquid chromatography
HRMS	High-resolution mass spectrometry
HSC	Hepatic stellate cell
HSP	Heishunpian
Impdh2	Inosine-5'-monophosphate dehydrogenase 2
ITS	Insulin-transferrin-sodium selenite
JAK	Janus kinase
LD_{50}	Lethal dose 50%
LDH	Lactate dehydrogenase
MCP-1	Monocyte chemotactic protein-1
MDA	Malondialdehyde
MDAs	Monoester-diterpenoid alkaloids
MMP	Matrix metalloproteinase
Mmp3	Matrix Metalloproteinase 3
mTOR	Mechanistic Target of Rapamycin
NaOH	Sodium hydroxide
NFκB	Nuclear factor-kappaB
PAI-1	Plasminogen activator inhibitor 1
PBS	Phosphate buffered saline
PCR	Polymerase chain reaction
Plod2	Procollagen Lysine-2-Oxoglutarate-5-Dioxygenase 2
PPAR	Peroxisome proliferator-activated receptors
PSR	Picro-Sirius red
PTM	Post-translational modification
RAAS	Renin-angiotensin-aldosterone system
RFU	Relative fluorescence unit
ROS	Reactive oxygen species
SOD	Superoxide dismutase
Sqstm1	Sequestosome-1
SR	Scutellariae Radix
SRM	Methanolic extract of SR
STAT	Signal transducer and activator of transcription
TCA	Citrate
TCM	Traditional Chinese medicine
TEAB	Triethylammonium bicarbonate
TFA	Trifluoroacetic acid
Tfrc	Transferrin receptor
TGF	Transforming growth factor
TIF	Renal tubulointerstitial fibrosis

TMT	Tandem mass tags
TNBS	2,4,5-trinitrobenzene sulphonic acid
Tsku	Tsukushin
UDAs	Unesterified-diterpene alkaloids
UPLC/Q-TOF-MS	Ultra-high-performance liquid chromatography-quadrupole time-of-flight mass spectrometry
UUO	Unilateral ureteral obstruction
ZFZ	Zhengfuzi
α-SMA	alpha smooth muscle actin

Chapter 1 Introduction

1.1. Chronic kidney disease (CKD)

The definition and classification of CKD have evolved over time, but current international guidelines define this condition as decreased kidney function shown by glomerular filtration rate (GFR) of less than 60 mL/min per 1.73 m^2, or markers of kidney damage, or both, of at least 3 months duration, regardless of the underlying cause (1). The most common causes of CKD are hypertension and diabetes, both aggravated by aging. Other diseases and conditions that may also induce CKD, such as glomerulonephritis (i.e. the inflammation of the glomeruli), polycystic kidney disease (i.e. gradual growth of masses of cysts in both kidneys), interstitial nephritis (i.e. the inflammation of the kidney's tubules and surrounding structures), pyelonephritis (i.e. recurrent kidney infections), failure of normal kidney development during pregnancy and the long-term consumption of some medicaments (e.g. non-steroidal anti-inflammatory drugs like aspirin and ibuprofen)(2, 3).

CKD affects around 10% of the worldwide population with high mortality, partly due to limited available and affordable treatment (4, 5). There is no direct cure for CKD actually and treatment usually depends on the stages of CKD. In the early stages (1-3), the treatment mainly consists in having a healthy and balanced diet, moderating the alcohol consumption, stopping smoking, getting regular physical exercise, losing weight in case of overweight/obesity and taking medication to control the blood pressure and lower the blood cholesterol levels. On the advanced stages (4-5), additional medications can be prescribed to control or prevent the symptoms of CKD. Finally, in case of end-stage kidney disease, it is fatal without renal-replacement therapy like dialysis or kidney transplantation (6, 7).

Currently new strategies for the treatment of CKD include more comprehensive blockade of the renin-angiotensin-aldosterone system (RAAS) with direct renin inhibitors (4, 8), endothelin receptor antagonists (9), drugs that target TGF-β system (10) and connective tissue growth factor (Ctgf) inhibitors, etc (11). Many clinical trials have been undertaken aiming at blocking and/or reversing CKD progression (**Table 1.1)**, with some of the trials directly or indirectly targeting renal fibrosis, including glomerulosclerosis (i.e. scarring of glomeruli) and tubulointerstitial fibrosis (TIF, i.e. scarring of the tubulointerstitial compartment). Despite the primary aetiology of CKD, tubulointerstitial injury and TIF appear to be the common pathway to end-stage kidney disease (https://www.ncbi.nlm.nih.gov/pubmed/14964574). Thus, the following discussions will focus on TIF, including its mechanisms, prevention and treatment.

Table 1.1. Some recent clinical trials on treatments of CKD.

Group	Drug	Target	Kidney disease (Stage)	Outcome	Reference
TGF-β blockers	LY2382770	TGF-β	DN (Phase 2)	Terminated prematurely due to a lack of efficacy	(12), NCT01113801
	Pirfenidone	TGF-β	DN ((Phase 1)	Slowed the rate of eGFR decline	(13)
	Pirfenidone	TGF-β	CKD (Phase 2)	Ongoing	NCT02408744
	Pirfenidone	TGF-β	DN (Phase 3)		NCT02689778
Ctgf blockers	FG-3019	Ctgf	DN (Phase 1)	Reduced microalbuminuria	(14)
	FG-3019	Ctgf	DN (Phase 2)	Prematurely stopped for suboptimal study design	NCT00913393
Endothelin receptor antagonists	Atrasentan	ET-1	DN (Phase 3)	Terminated (strategic considerations)	NCT01858532
	Avosentan	ET-1	DN (Phase 1)	Stopped because of fluid retention	(15)
	Atrasentan	ET-1	DN (Phase 2)	Reduced albuminuria	(16, 17)
	Atrasentan	ET-1	CKD (Phase 2)	Ongoing	NCT01424319
	Avosentan	ET-1	DN (Phase 1)	Reduced urinary albumin	(18)
	TAK-044	ET-1	CKD (Phase 1)	No significant effects on GFR decline	(19)
Chemokine antagonists	MLN1202	CCR2	DN (Phase 2)	Prematurely stopped for unknown reasons	NCT02410499
	BMS-813160	CCR2/5	DN (Phase 2)	Discontinuation of clinical development of the drug	NCT01752985
	PF-04634817	CCR2/5	DN (Phase 2)	Reduced urinary albumin	NCT01712061
	NOX-E36	CCR2	DN (Phase 2)	Reduced albuminuria	(20)
	CCX140-B	CCR2	DN (Phase 2)	Reduced albuminuria	(21), NCT01447147
PPAR antagonists	Fenofibrate	PPAR-α	DN (Phase 1)	Reduced albuminuria, slowed the rate of GFR decrease	(22)
	Elafibranor	PPAR-α & -δ	type 2 diabetes mellitus	Ongoing	NCT01261494

Group	Drug	Target	Kidney disease (Stage)	Outcome	Reference
			(Phase 2)		
	Rosiglitazone	PPAR-γ	type 2 diabetes mellitus (Phase 3)	Reduced albuminuria and proteinuria	(23, 24) NCT00279045
BMP-7 agonists	THR-184	BMP	CKD (Phase 2)	No effects on GFR decline, reduced incidence of AKI	NCT01830920
Nrf2 activator	Bardoxolone	Nrf2	CKD (Phase 1)	Slowed the rate of GFR decrease, increased albuminuria	(25, 26)
	Bardoxolone	Nrf2	DN, CKD (Phase 2)	Ongoing	NCT02316821
	Bardoxolone	Nrf2	DN, CKD (Phase 3)	Terminated (safety concerns)	(27), NCT01351675
NFκB blockers	ACTH	MCP-1	DN (Phase 4)	Slowed the rate of GFR decrease, reduced proteinuria	(28), NCT01028287
	Bindarit	MCP-1	DN (Phase 2)	Reduced albuminuria	NCT01109212
JAK-STAT inhibitors	Baricitinib	JAK	DN (Phase 2)	Reduced albuminuria, no changes in kidney function	(29), NCT01683409
Galectin-3 antagonists	GCS-100	galectin-3	DN (Phase 2)	Discontinuation of clinical development of the drug because the Company was required to conduct additional chemical characterization	(30), Poster
	GCS-100	galectin-3	CKD (Phase 2)	Slowed the rate of GFR decrease	NCT01843790
GPR40&GPR84 antagonists	PBI-4050	GPR40&GPR84	type 2 diabetes mellitus (Phase 2)	Terminated (Failure to meet recruitment target during the recruitment period)	NCT03081598
Thromboxane receptor antagonists and thromboxane synthase inhibitors	SER150	thromboxane A2	DN (Phase 2)	Decreased in albuminuria, no safety or tolerability concern Ongoing	http://www.serodus.com/Pipeline/SER150DN

Note: AKI, acute kidney injury; ACTH, adrenocorticotropic hormone; CKD, chronic kidney disease; CTGF, connective tissue growth factor; CCR2/5, chemokine receptor 2/5; DN, diabetic nephropathy; ET-1, endothelin-1; GFR, glomerular filtration rate; JAK, Janus kinase; MCP-1, monocyte chemotactic protein-1; NFκB, nuclear factor-kappaB; PPAR, peroxisome proliferator-activated receptors; STAT, signal transducer and activator of transcription.

1.2. TIF

TIF is characterised by excessive extracellular matrix (ECM) accumulation in the tubulointerstitial compartment and is considered as a common final feature of almost all progressive CKD (31, 32). The tubulointerstitium consists of multiple cell components including tubular epithelial, endothelial, mesenchymal (fibroblasts and pericytes) and inflammatory cells, all of which involve and participate in some way in the pathogenesis of TIF, illustrating the immense complexity of this process.

Tubular epithelia are targeted by acute and chronic injuries. The injured epithelia differentiate and proliferate resulting in repair after acute kidney injury (33). When epithelial injury occurs repetitively or persists over time, tubular apoptosis may occur and lead to progressive TIF (34). These dying epithelial cells may produce growth factors and cytokines such as TGF-β and PDGF. These growth factors may initially promote regeneration of the injured epithelia but, in persistent injury, may have some effects on surrounding cells such as fibroblasts causing them to transform into myofibroblasts. It was also known that the injured epithelia undergo epithelial to mesenchymal transition (EMT) and contribute to ECM production and ultimately fibrosis. Similarly, myofibroblasts might derive from capillary endothelium by endothelial-mesenchymal transition (EndoMT). EndoMT is considered to be a unique form of EMT, as endothelial cells are a specialized type of epithelia (35). Although epithelial cells can clearly respond to fibrotic stimuli resulting in loss of epithelial features and acquisition of mesenchymal markers, its role as a potential source of myofibroblasts in TIF has been questioned (36, 37). Nonetheless, emerging evidence supports a role for epithelial cells as efficient producers of stable extracellular matrix and thus contributing to renal tubule thickening and TIF (36, 37).

Fibroblasts are quiescent cells found within the interstitial space, important for maintaining the structural integrity of kidneys by producing basal level of extracellular matrix. During the normal tissue repair process after damage, these cells can be activated by cytokines including TGF-β (38) and tumour necrosis factor alpha (TNFα) (39) as well as stress stimuli including hypoxia (40) to proliferate and produce collagens to make new connective tissue. Activated fibroblasts have increased stress fibres, proliferate, and produce ECM components like collagens leading to progressive TIF. It is commonly regarded that fibroblast activation and the expression of α smooth muscle actin (α-SMA) is indicative of its transformation into myofibroblasts, which are the main contributors to TIF (41). However, the expression of α-SMA is not exclusive to myofibroblasts, being also expressed on vascular smooth cells. In addition, vimentin and CD73 expressed by fibroblasts and myofibroblasts are also expressed

by immune cells (42). Thus, it is difficult to conclude on what exact percentage of myofibroblasts are derived from fibroblasts, due to the lack of specific cellular markers for both fibroblasts and myofibroblasts.

Fibrocytes are circulating bone marrow-derived cells that are positive for the leukocyte marker CD45 and are capable of producing type I collagen (43). Fibrocytes also express certain chemokine receptors, such as CCR7. The differentiation of fibrocytes is critically dependent on other inflammatory cells, such as CD4(+) T cells, through secreted cytokines (44). The relative importance of fibrocytes in renal fibrosis is unclear, at least in part because of the lacking of specific markers for these cells, making it a great challenge to clearly differentiate fibrocytes from monocytes, macrophages, fibroblasts and myofibroblasts.

Inflammatory cells, specifically macrophages and dendritic cells (DC), are also important modulators of CKD. Macrophages/DCs populate the uninjured renal interstitium and act as antigen-presenting cells and macrophages also have an important phagocytic function (45). After renal injury, these inflammatory cells expand both through local proliferation and infiltration of circulating monocytes and subsequent differentiation. The classic view on the connection between inflammation and fibrosis is that they are mediated in a paracrine manner, whereby inflammatory cells secrete profibrotic cytokines that act on resident fibroblasts and tubular cells to promote fibrogenesis (46).

In the pathogenesis of TIF, infiltrated inflammatory cells become activated after a sustained kidney injury, which sets up the fibrogenic stage and triggers the activation and expansion of ECM-producing cells from multiple sources through various mechanisms, mainly including activation of interstitial fibroblasts and pericytes, phenotypic conversion of tubular epithelial and endothelial cells and recruitment of circulating fibrocytes. These ECM-producing cells integrate input from various fibrogenic signals to drive the production of matrix components and their extracellular assembly (42). Myofibroblasts are the principal ECM-producing cells and have been identified as key cellular mediators of TIF, thus to understand the cellular and molecular mechanisms responsible for the creation of myofibroblasts and their activities is central to the development of therapies.

Myofibroblasts are characterised by expression of the intermediate filaments desmin, vimentin and the contractile protein α-SMA (47). Myofibroblasts can be derived from several sources, as shown in **Fig. 1.1**, including proliferation and activation of quiescent tissue-resident fibroblasts into a myofibroblastic phenotype, recruitment and activation of fibrocytes from bone marrow, and trans-differentiation of epithelial or endothelial into a

mesenchymal phenotype (31, 32, 48). In view that resident fibroblasts are believed to be the most important sources of myofibroblasts (47), this project will mainly use renal fibroblasts for *in-vitro* modelling of fibrosis and for testing antifibrotic activities.

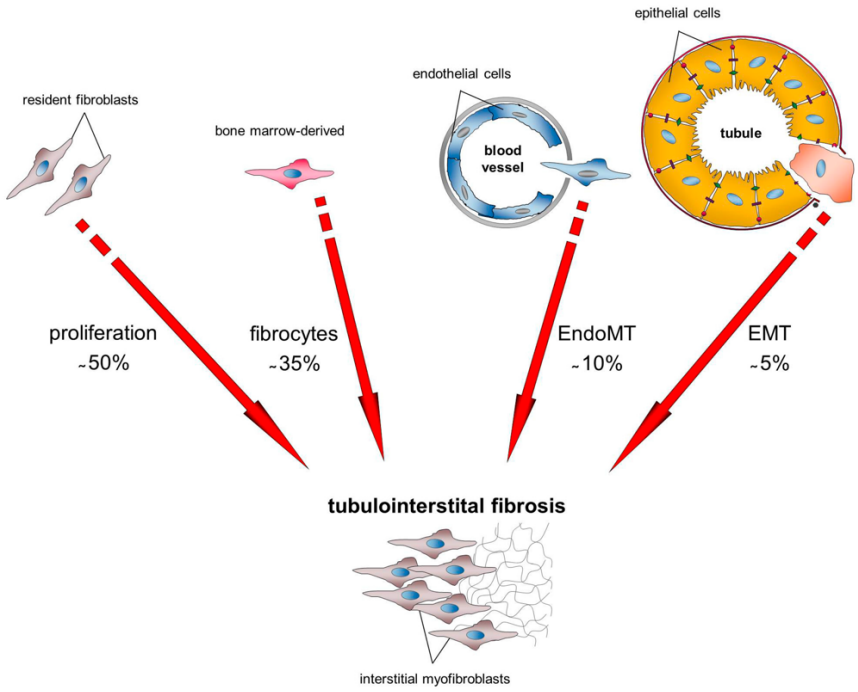

Fig. 1.1. Origin of matrix-producing myofibroblasts that directly mediate TIF (48). Schematic illustration shows the possible mechanisms via myofibroblasts can originate during kidney fibrosis with their proposed proportions on the total number of interstitial myofibroblasts. Recent studies estimate that approximately 35% of fibroblasts arise from bone marrow, 10% and 5% via local EndoMT or EMT, respectively, and 50% of myofibroblasts result from proliferation and activation of resident fibroblasts.

TGF-β is considered one of the strongest pro-fibrotic growth factors due to its ability to activate fibroblasts into myofibroblasts and stimulate matrix production. TGF-β belongs to the TGF-β superfamily of cytokines, playing important roles in embryogenesis and adult tissue homeostasis by regulating cell proliferation, differentiation and migration. TGF-β is made up of three isoforms, TGF-β 1, 2 and 3 (49). TGF-β1 is the most broadly studied of the TGF-β isoforms and it promotes progressive renal fibrosis by stimulating ECM synthesis, preventing its degradation, activating fibroblasts and mediating EMT or EndoMT (48, 50). In addition, TGF-β1 induces the expression of a variety of ECM molecules including collagens type I, III and IV, fibronectin and plasminogen activator inhibitor (PAI)-1, all of which are increased in TIF (49).

Active TGF-β1 is released via proteolytic cleavage and binds to the TGF-β type II receptor and initiates Smad-dependent and -independent signalling pathways. In the canonical TGF-β1/Smad pathway, phosphorylated Smad2/3 complexes together with Smad4 translocate into the nucleus to modulate transcription of a number of target genes. Increasing evidence has demonstrated that TGF-β-induced activation of downstream Smad signalling is a major driver for renal fibrosis (51). The expression of TGF-β and its receptor is increased in human and experimental models of CKD (52), overexpression of active TGF-β in mice promotes the development of glomerulosclerosis and TIF (53) and inhibition of TGF-β activity attenuates renal disease in experimental models of renal fibrosis (54). In addition, TGF-β released from injured tubular cells or inflammatory cells promotes TIF by increasing ECM gene transcription, tubular cell apoptosis, myofibroblast differentiation and EMT depending on the cellular context of TGF-β action (55). In addition to the Smad pathway, multiple Smad-independent signalling pathways are also involved in renal fibrosis (51), such as Wnt/β-catenin (56), JNK/STAT3 (57), and MAPKs (56, 57).

Despite the aforementioned mechanisms, our knowledge on the exact intracellular and extracellular mechanisms in myofibroblasts remains very limited. Further understanding such intracellular and extracellular mechanisms promises to discover novel therapeutic targets and to guide developing effective strategies to prevent or even reverse TIF and CKD.

1.3. Anti-fibrotic and pro-fibrotic activities of botanicals

Despite the commonly accepted role for TIF in CKD progression, there are currently few approved treatments in conventional medicine that directly target the mechanisms of fibrosis [33-36]. A range of biological activities offered by natural products and herbal medicines have aroused increasing interests thanks to their potentials for treating fibrotic diseases (58-62). For example, GQ5, a small molecular phenolic compound isolated from the dried resin of *Toxicodendron vernicifluum*, hindered renal fibrosis in obstructive nephropathy by selectively inhibiting TGF-β1-induced Smad3 phosphorylation (63). On the other hand, some botanicals also cause fibrosis. For example, aristolochic acid, a natural compound present in plants of the *Aristolochia*, *Bragantia* and *Asarum* genera, has been known to induce a fibrotic nephropathy, designated aristolochic acid nephropathy, as well as urothelial cancer (64).

To discover and compare inflammation-independent anti-fibrotic and pro-fibrotic activities, a high-throughput cellular model of fibrosis was established in my supervisor's laboratory, based on TGF-β1 induced total collagen accumulation, a gold standard for clinical diagnosis of fibrosis (65, 66). On this *in-vitro* platform, five herbal compounds, eleven individual herbal extracts and sixteen herbal formulae showed anti-fibrotic activities and three ethanolic

extract had potent *in-vitro* pro-fibrotic activities (66, 67). For instance, anti-fibrotic activities are identified in Scutellariae Radix and two flavonoids derived from this herb; unprocessed Aconiti Radix (AR), which have alkaloids-mediated acute poisonous effects, showed potent *in-vitro* pro-fibrotic activities. Nevertheless, the anti-fibrotic and pro-fibrotic chemical principles in SR and AR and exact mechanisms remain poorly understood. Therefore, the present study set out to study the chemical principles and molecular mechanisms of SR and AR, with particular focuses on SR flavonoids and AR alkaloids, in TGF-β1-induced *in-vitro* models of fibrosis.

1.4. *Aconitum carmichaeli* Debx. and its alkaloid compounds

The *Aconitum* genus are widely used in traditional Chinese medicine (TCM) and have been used in TCM clinics for 2000 years. *Aconitum carmchaeli* Debx. is one of the almost 80 aconite species used for medical purposes (68). Two herbal drugs recorded in the 2015 edition of the Chinese Pharmacopoeia are mainly derived from this species - Aconiti Radix (AR), the main roots, and Aconiti Lateralis Radix (ALR), the lateral roots (**Fig. 1.2**).

AR and ALR are mostly producted in Sichuan Province, the south-western of China. Local people normally use it as a vegetable to make soup, by cutting the roots into slices and boiling with different vegetables and meat. Since the local climate in these areas is very humid and according to TCM theory, pungent and bitter tasting herbs can counteract the influence of a damp environment on the human body. Therefore, *Aconitum* is believed to help to treat cold-damp type of illness. However, the improper use of *Aconitum* in China and other Asian countries still poses a high risk of poisoning as it can cause severe cardiotoxicity and neurotoxicity. The typical symptoms of poisoning include palpitation, vomiting, nausea, arrhythmia, shock, dizziness, hypotension, coma, even lead to death if the rescue is not timely (68).

Both AR and ALR are known to be highly poisonous because they contain abundant toxic components-aconite alkaloids. Currently, chemical studies have shown that three major groups of aconite alkaloids have been extensively studied: (i) diester-diterpenoid alkaloids (DDAs), mainly comprise aconitine, mesaconitine and hypaconitine; (ii) monoester-diterpenoid alkaloids (MDAs), such as benzoylaconine, benzoylmesaconine and benzoylhypaconine; and (iii) unesterified-diterpene alkaloids (UDAs), mainly containing aconine, mesaconine and hypaconine. In particular, the DDAs have the highest toxicity to the cardiovascular and nervous system. DDAs are not stable, which are easily hydrolysed into MDAs in the presence of water and/or heat. As shown in **Fig. 1.3**, MDAs can be further

converted into UDAs through a second hydrolysis (68, 69). Hydrolysis of the DDAsmarkedly decreases their toxicities by over 100-fold (70). The three lethal dose 50% (LD_{50}) values of the rat oral administration were 1.0-1.8 mg/kg, 1.9 mg/kg, and 5.8 mg/kg respectively (68). Therefore, aconitum toxicity can be reduced by adding water and heat processing, this is mainly due to the promotion of hydrolysis of DDAs into the low toxicity MDAs and UDAs.

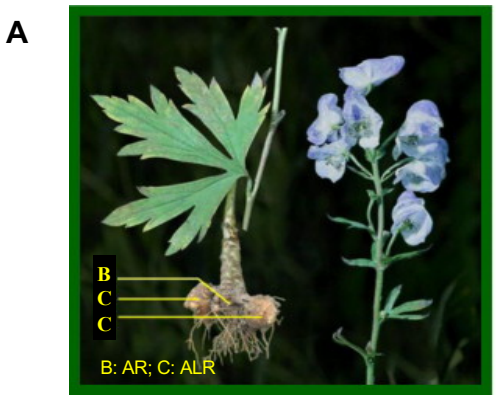

Aconitum carmchaeli Debx.

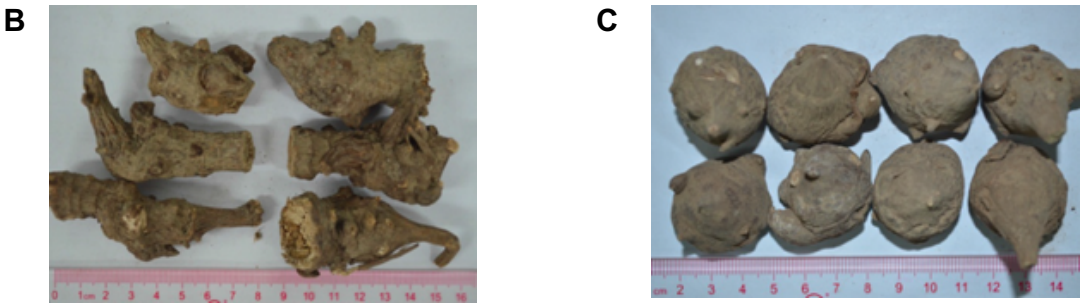

Aconiti Radix (AR)

Aconiti Lateralis Radix (ALR)

Fig. 1.2. Photographs of *Aconitum carmchaeli* Debx. and its derived herbal drugs. (A) The morphology of *Aconitum carmchaeli* Debx. (69); (B) AR, the principal root: Irregularly conical, slightly curved. Externally brown or greyish-brown, shrunken, with tuberculate rootlets and scars of daughter roots. Texture compact, fracture whitish or greyish-yellow, cambium ring polygonal. Odour, slight; taste, pungent and numb. (C) ALR, the lateral root: Irregularly spherical, matte. Texture compact. Externally slate grey or greyish-brow, fracture oyster whitish. Odour, slight fishy; taste, pungent and numb.

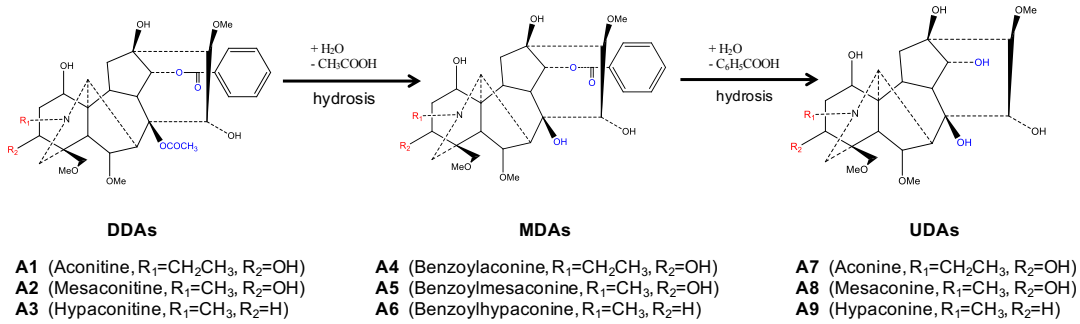

Fig. 1.3. Schematic representation of two step hydrolysis of alkaloids.

This detoxicating procedure, known as Paozhi in TCM, is the traditional processing method of TCM, playing an important role in detoxifying toxic herbs. *Aconitum* processing methods can be broadly divided into three categories: water processing (soaking, moistening or rinsing in water, wine, vinegar or other liquid adjuvants, etc.), fire processing (baking, roasting, stir-frying, etc.) and fire and water processing (steaming, decocting with or without adjuvants) (71). Only processed AR and ALR are allowed to be clinically used in TCM practice (72). In the 2015 edition of the Chinese Pharmacopoeia, five decoction pieces of AR and ALR were recorded, as shown in **Fig. 1.4**: Zhichuanwu, Heishunpian, Baifupian, Danfupian, and Paofupian. In addition, the clinical dosage and decoction time of AR and ALR decoction pieces are exactly described: AR, 1.5-3 g and ALR, 3-15 g, a day. It should be decocted first and for a long period of time. Moreover, doctors should remind users to pay attention to the occurrence of adverse reactions, to avoid serious consequences due to the treatment.

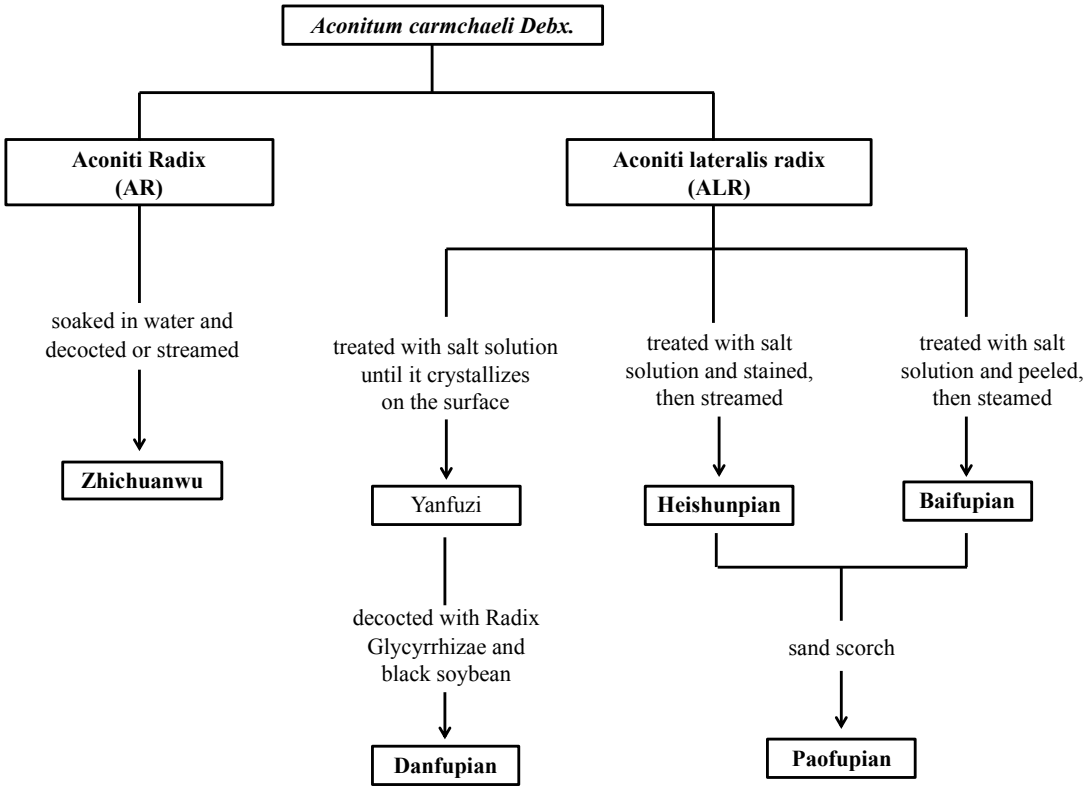

Fig. 1.4. The form of traditional processing of AR/ALR in the Chinese Pharmacopoeia.

Aconite alkaloids also served as quality markers for the chemical evaluation of AR and ALR. Due to the high toxicity of AR/ALR and the DDAs, accurate qualitative and quantitative determination of DDAs is of great importance. Intoxications could probably be prevented if a standardized method for quality control could be established. Some publications show that high-performance liquid chromatography (HPLC) is an appropriate method of quality control for aconite preparations (73). According to the Chinese Pharmacopeia 2015, HPLC method is accepted for the quantitative analysis of alkaloids in AR and ALR. The legal ranges of DDAs in AR and ALR, calculated taking aconitine, mesaconitine and hypaconitine into consideration, are 0.050%−0.17% and < 0.20%, respectively.

The processed AR and ALR are known to have important pharmaceutical properties, e.g. the effects on the cardiovascular system, oedema, abdominal colic and irregular menstruation, antinociceptive, analgesic and anti-epileptic activities, and around 600 formulae containing processed AR and ALR are on the Chinese market alone (68, 69, 74). Despite the well-established acute toxicities of the genus *Aconitum*, the chronic adverse effects of AR, ALR and other products containing *Aconitum* species are largely unknown. In an ealier screening expriemnt, my supervisor's laboratory found that the ethanolic extracts of unprocessed AR had potent *in-vitro* pro-fibrotic activities at concentrations as low as 20 μg/mL (75), which is

the first report linking AR to potent pro-fibrotic activities as far as we know. This *in-vitro* finding also has important clinical implications as consumption of an ethanolic extract of *Aconitum* species is known to cause acute kidney injury (76) and consumption of an ALR-containing product was recently linked to end-stage renal failure (77). Thus, it is important to determine the reliability of the screeing findings by repeating experiments and to establish if the potent pro-fibrotic effect of this toxic herb could be reduced or even eliminated through traditional "Paozhi" and if this newly identified adverse effect is attributable to any aconite alkaloids.

1.5. *Scutellaria baicalensis* Georgi and its flavonoid compounds

Scutellaria baicalensis Georgi is one of the most commonly used medical plant in China, Korean, Japan, Mongolia and Russian Federation (**Fig. 1.5**). Scutellariae Radix, the dry roots of the plants, is officially recorded in the Chinese (78), European (79), and American Herbal Pharmacopoeias (80). SR is used as a local medicine to clear away the "heat-evil" and expel "superficial evils", eliminate stasis and activate blood circulation, induce diuresis and reduce edema. In TCM clinics, extracts of SR are widely applied to treat pneumonia, hypertension, jaundice, dysentery and intestinal catarrh, pyogenic infection, etc (81). Apart from the above properties, SR alone, or used as a key ingredient in combination with other herbs, has been shown to have wide therapeutic effects on cancer (82, 83), liver disease (84, 85) and kidney diseases (86, 87).

SR is especially rich in flavonoids (88). Flavonoids, from the Latin word *flavus* meaning yellow, their color in nature, are a class of plant secondary metabolites. Epidemiological studies have shown that dietary intake of flavonoids is significantly associated with a reduced risk of cancer, inflammation and heart disease (89, 90). Indeed, the flavonoids isolated from SR have been shown to exert antioxidant (91), anti-viral (92), anti-inflammatory (93, 94) and cardiovascular protective effects (95).

A

Scutellaria baicalensis Georgi

B

Scutellariae Radix (SR)

Fig. 1.5. Photographs of *Scutellaria baicalensis* Georgi and its derived herbal drug. (A) The morphology of *Scutellaria baicalensis* Georgi (96). (B) SR: Irregularly cylindrical. Externally medium brown beige. Texture hard and fragile. Odour, woody and beany; taste, strong bitter.

SR contains five major flavonoid compounds which have similar structures (**Fig. 1.6**): baicalin (7-glucuronic acid, 5, 6-dihydroxy-flavone), baicalein (5, 6, 7-trihydroxyfavone), wogonin (5, 7-dihydroxy-8-methoxyflavone), wogonoside (wogonin-7-glucuronic acid) and oroxylin-A (Oroxylin A 7-O-beta-D-glucuronide). One or more flavonoids are usually adopted for qualitative and quantitative analysis of SR. For example, baicalin, the main flavonoid with the highest content, is employed to control the quality of SR-containing medicinal materials and related products. In Chinese Pharmacopeia 2015, the content of baicalin should be at least 9% in dried SR (78).

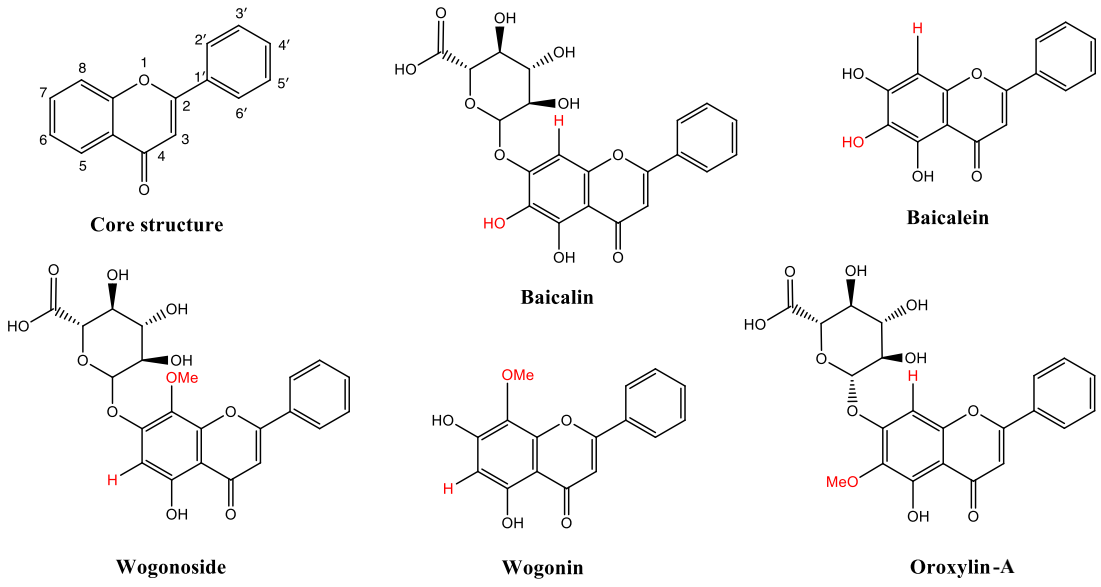

Fig. 1.6. Structures of five SR flavonoids.

SR and its flavonoids, have been reported as potential anti-fibrotic agents (97-100). **Table 2** summarises the effects and mechanisms of SR extracts and five aforementioned flavonoids on fibrosis in various experimental fibrotic disease models. SR ethanolic extracts attenuated liver fibrosis in rat models induced by dimethylnitrosamine (101) and lipopolysaccharide (84). SR methanol extract is effective in preventing liver (102) and colonic fibrosis (103). Baicalin can inhibit hepatic stellate cells activation (104) and progression of liver fibrosis in carbon tetrachloride-induced rat model (105, 106). In addition, baicalin attenuated the accumulation of inflammatory cells and fibrotic changes in lung tissues (107) and also alleviated renal interstitial fibrosis *in vivo* (108). Baicalein was used as a potential antioxidant against hepatic (109, 110), pulmonary fibrosis (111) and protective potential for myocardial fibrosis (112-115). Baicalein treatment can inhibit stellate cell activation and proliferation (116, 117) and attenuate tubulointerstitial fibrosis by inducing myofibroblast apoptosis (118) and inhibiting inflammation (98). Wogonoside was reported to prevent liver fibrosis (119) and wogonin can suppressed collagen deposition in cardiac fibroblasts (115) and mitigated cardiac fibrosis through inhibiting inflammation and oxidative stress (120). In addation, my supervisor's laboratory has reported that methanolic extract of the SR has potent *in-vitro* anti-fibrotic activities, and so do baicalin and baicalein (65, 66).

Table 1.2. SR and its flavonoids showed anti-fibrotic activities in fibrotic disease models.

Herbal agents	Type	*In-vivo*	*In-vitro*	Signalling	Reference
SR aqueous extracts	N/A	N/A	N/A	N/A	N/A
SR ethanol extracts	Liver	DMN-induced rat model	HSC-T6	ERK-p53-p21 ERK-p53-bax-caspase-3/9	(121)
		LPS- induced rat model	primary rat liver endothelial cells and HSCs	attenuates LPS-induced liver endothelial cell activation and inhibits HSC migration (MCP-1/Ccl2 ↓)	(84)
		DMN-induced rat model	N/A	attenuate oxidative stress (SOD↑ GPx ↑Catalase↑)	(101)
SR methanol extracts	Liver	BDL- and CCl4-induced rat models	N/A	reduced levels of connective tissue (α-SMA, hydroxyproline) and lipid peroxidation MDA	(102)
	Colon	TNBS-induced rat model	N/A	TGF-β1/smad3 pathway	(103)
	Kidney	N/A	NRK-49F	Total collagen (PSR staining) ↓; α-SMA↓ ; Collagen I ↓	(66)
Baicalin	Liver	N/A	primary HSCs	interaction between PPARγ (↑) and Wnt pathway (↓)	(104)
		CCl4-induced rat model	N/A	interaction between PPARγ (↑) and TGF-β1 pathway (↓)	(105)
		Colchicine-induced rat model	HSCs	inhibit proliferation and promote apoptosis; MDA ↓; SOD↑ reduce ECM (TIMP-1/MMP-1↓); Collagen I&III ↓; TGF-β1 ↓	(122)
		CCl4-induced rat model	N/A	TGF-β1↓; TNF-α ↓; IL-6 ↓; IL-10 ↑	(106)
	Lung	silica-induced mice model	N/A	inhibit Th17 cells differentiation; inhibit inflammatory (IL-6 ↓; IL23 ↓)	(107)
	Kidney	UUO rat model	N/A	Notch1pathway; TGF-β1↓	(108)
Baicalein	Liver	CCl4-induced rat model	N/A	inhibits the activation and proliferation of HSCs (PDGF-β receptor ↓)	(116)
		N/A	primary HSCs	inhibit proliferation	(117)

Baicalein	Lung	bleomycin-induced rat model	N/A	improve antioxidant activity; attenuate inflammation; repress miR-21 inhibit TGF-β1/smad3	(111)
	Heart	abdominal aorta constriction rat model	H9c2	prevent apoptosis; reduce ECM (Mmp2↓; Mmp9 ↓)	(112)
		Aortic banding mice model	H9c2	MEK-ERK1/2 pathway	(113)
		spontaneously hypertensive rat model	N/A	pro-collagen I & III↓; 12-lipoxygenase ↓ p-ERK/PEK ↓; MMP-9 ↓	(114)
		N/A	primary cardiac fibroblasts from neonatal normotensive and hypertensive rats	12-lipoxygenase ↓ p-ERK/PEK ↓; MMP-9 ↓	(115)
	Kidney	UUO mice model	NRK-49F	PI3k/Akt pathway; induce myofibroblast apoptosis	(118)
		UUO mice model	N/A	NF-κB ↓; MAPK signal pathway	(98)
Wogonoside	Liver	CCl4-induced rat model	HSCs	PI3K/Akt/mTOR pathway	(119)
Wogonin	Heart	N/A	primary cardiac fibroblasts from neonatal normotensive and hypertensive rats	12-lipoxygenase ↓ p-ERK/PEK ↓; MMP-9 ↓	(115)
		Streptozotocin-induced diabetic mice model	N/A	anti-inflammatory (IL-1β ↓; IL-6 ↓; TNF-α↓; PAI-1↓; NF-κB ↓) anti-oxidative (SOD1/2 ↑; Catalase ↑)	(120)
Oroxylin-A	N/A	N/A	N/A	N/A	N/A

Note: DMN: dimethylnitrosamine; GPx: glutathione peroxidase; SOD: superoxide dismutase; BDL: bile duct ligation and scission; CCl4: carbon tetrachloride; MDA: malondialdehyde; TNBS: 2,4,5-trinitrobenzene sulphonic acid; PSR: Picro-Sirius red; HSC: Hepatic stellate cell; UUO: unilateral ureteral obstruction; NRK: normal rat kidney fibroblasts; H9c2: rat heart myoblast.

1.6. Hypothesis and aims

My hypothesis is that the pro-fibrotic effect of AR and anti-fibrotic activity of SR can be attributed to AR alkaloids and SR flavonoids, respectively. This project is designed to test the above hypothesis and to explore underlying molecular mechanisms by a proteomic approach.

Specifically, the objectives of this project are:

- To examine effects of unprocessed and processed AR/ALR extracts in a TGF-β1-induced *in-vitro* model of fibrosis;
- To examine whether the pro-fibrotic activities of unprocessed and processed AR are attributable to alkaloids or non-alkaloids in the herb;
- To compare the SR methanolic and aqueous extracts in a TGF-β1-induced *in-vitro* model of fibrosis;
- To compare the anti-fibrotic activities of five SR flavonoids;
- To establish a proteomic view of an *in-vitro* model of TGF-β1-induced fibrogenesis;
- To explore mechanisms underlying the anti-fibrotic activities of the most promising SR extract and flavonoid through a proteomic approach.

Chapter 2 Materials and Methods

This chapter describes the materials and methods used for all laboratory work, including procurement and quality control of herbal materials, processing, extraction and chemical profiling of herbs, authentication and quality control of cell lines, establishing *in-vitro* models of fibrosis, testing anti- and pro-fibrotic activities of the herbal materials, mechanistic investigations by proteomic approach and further validation.

2.1. Herbs and herbal compounds

Aconiti Radix (AR), Aconiti Lateralis Radix (ALR) and Scutellariae Radix (SR), as shown in **Fig. 1.2** and **Fig. 1.5,** were supplied and authenticated through stringent quality control by PuraPharm International Ltd. (Hong Kong) as detailed in **Supplementary Fig. 1-3**. The voucher samples have been deposited at Royal Botanic Gardens Kew, UK (Economic Botany Collection number: 84041, 84042, 84040 for AR, ALR and SR, respectively). **Fig. 1.3 and 1.6** illustrate the structure of herbal compounds, which were supplied as HPLC-grade compounds of >98% purity and their molecular weights have been confirmed at King's by high-resolution mass spectrometry (HRMS), as to be shown in **2.4. Authentication of herbal compounds**. All herbs and herbal compounds used in this project are listed in **Table 2.1**.

2.2. Reagents, buffers and solutions

All buffers, solutions and reagents were prepared following the recipes and protocols demonstrated below. Ultrapure water dispensed from a Maxima USF Alsa machine was used for dilution and dissolution of reagents. A Metler teledo AB204-S weighting balance was used for weighting chemical reagents; a Stutart CB161 magenetic stirrer (with Fisher Brand magnetic stir bar) and a Grant Bio PV-1vortex mixer were used for mixing purpose; and a Metler Toledo 340 pH meter was used for pH measurement.

Table 2.1. List of herbal materials.

Herbs and herbal compounds	Manufacturers
Aconiti Radix (AR)	PuraPharm International Ltd., Hong Kong, China.
Aconiti Lateralis Radix (ALR)	
Scutellariae Radix (SR)	
Aconitine (CAS: 302-27-2, $C_{34}H_{47}NO_{11}$)	Santa Cruz Biotechnology, Inc., Heidelberg, Germany.
Mesaconitine (CAS: 2752-64-9, $C_{33}H_{45}NO_{11}$)	Chengdu Must Bio-Technology Co. Ltd., Chengdu, China.
Hypaconitine (CAS: 6900-87-4, $C_{33}H_{45}NO_{10}$)	
Benzoylaconine (CAS: 466-24-0, $C_{32}H_{45}NO_{10}$)	
Benzoylmesaconine (CAS: 63238-67-5, $C_{31}H_{43}NO_{10}$)	
Benzoylhypaconine (CAS: 63238-66-4, $C_{31}H_{43}NO_9$)	
Aconine (CAS: 509-20-6, $C_{25}H_{41}NO_9$)	
Mesaconine (CAS: 6792-09-2, $C_{24}H_{39}NO_9$)	Chengdu Chroma-Biotechnology Co. Ltd., Chengdu, China.
Hypaconine (CAS: 63238-68-6, $C_{24}H_{39}NO_8$)	
Baicalin (CAS: 21967-41-9, $C_{21}H_{18}O_{11}$)	Chengdu Must Bio-Technology Co. Ltd. (Chengdu, China)
Baicalein (CAS: 491-67-8, $C_{15}H_{10}O_5$)	
Wogonin (CAS: 632-85-9, $C_{16}H_{12}O_5$)	
Wogonoside (CAS: 51059-44-0, $C_{22}H_{20}O_{11}$)	
Oroxylin A 7-O-beta-D-glucuronide (Oroxylin-A; CAS: 36948-76-2, $C_{22}H_{20}O_{11}$)	

2.2.1. *In-vitro* model of fibrosis

TGF-β1: Human platelet TGF-β1 (R&D Systems, Abingdon, UK) was reconstituted in sterile 4 mM hydrochloric acid (HCl; VWR International Ltd, Lutterworth, UK) and 0.1% bovine serum albumin (BSA; PAA Laboratories GmbH) that had been filter-sterilised through polyethersulfone membrane with 0.2 μm pore size. A stock solution of 10 ng/μL TGF-β1 was stored at -80 °C until use.

IN1130: A selective inhibitor of TGF-β type I receptor (Alk5), is a kind gift from Dr. Dae-Kee Kim (Ewha Woman's University, Korea). A stock of 2 mM IN1130 in normal saline was stored at -80 °C until use.

Herbal stock solutions: Stock solutions of herbal extracts and compounds were prepared by dissolving the lyophilized powder in dimethyl sulfoxide (DMSO) as described in **Table 2.2**.

Table 2.2. Herbal extracts and compounds prepared as stocks for biology studies.

Herbal agents	Molecular weight (g/mol)	Weight (mg)	DMSO (µL)	Stock solution
Herbal extracts	-	16	1000.0	16 mg/mL
Aconitine	645.74	10	774.3	20 mM
Mesaconitine	631.71	10	791.5	20 mM
Hypaconitine	615.71	10	812.1	20 mM
Benzoylaconine	603.7	10	828.2	20 mM
Benzoylmesaconine	589.67	10	847.9	20 mM
Benzoylhypaconine	573.67	10	871.6	20 mM
Aconine	499.59	10	1000.8	20 mM
Mesaconine	485.57	10	1029.7	20 mM
Hypaconine	469.57	10	1064.8	20 mM
Baicalin	446.36	10	1120.2	20 mM
Wogonoside	460.39	10	1086.0	20 mM
Baicalein	270.24	10	925.1	40 mM
Wogonin	284.26	10	879.5	40 mM
Oxylin-A	460.39	10	1086.0	20 mM

All stock solutions were stored at -80 °C until use. The protocols and procedures of herbal extraction are described in **2.3 Preparation of herbal extracts** section.

Picro-Sirius red (PSR) stain (0.1%): 1.5 g of picric acid (Sigma-Aldrich, UK) was added to 100 mL H_2O to make saturated picric acid. Then add 0.1 g of Sirius Red 80 (Sigma-Aldrich, UK) to make 0.1% PSR.

Acetic acid solution (0.1%): 5 mL of acetic acid (VWR International Ltd) was added to 500 mL of H_2O to make 1% stock solution. Stock solution was further diluted 10× to make 0.1% acetic acid solution.

Sodium hydroxide (NaOH) solution (0.1M): 20 g of NaOH (Sigma-Aldrich, UK) was added to 500 mL H_2O to make 1 M stock solution. Stock solution was then diluted 10× to make 0.1 M NaOH.

Phosphate buffered saline (PBS): To make 1 L of 10× PBS, 80 g NaCl (Sigma-Aldrich, UK), 2 g KCl (Sigma-Aldrich, UK), 14.4 g Na_2PO_4 (Sigma-Aldrich, UK) and 2.4 g KH_2PO_4 (Sigma-Aldrich, UK) were dissolved in H_2O to a volume of 1 L and adjusted to pH 7.4 using 1 M NaOH (Sigma-Aldrich, UK). For use in experiments 1× PBS was made by adding 100 mL 10× PBS to 900 mL H_2O.

2.2.2. Immunocytochemistry

Antibodies: Antibodies used in this project and their sources are listed in **Table 2.3**. All antibodies were stored according to recommendations form the suppliers.

Paraformaldehyde solution (3.7%): 2 mL of 37% formaldehyde solution (Sigma-Aldrich) was added to 18 mL PBS.

Triton X solution (0.1%): 10 µL Triton X-100 (Sigma-Aldrich) was added to 10 mL PBS.

BSA blocking reagent (1%): 0.1 g BSA was added to 10 mL PBS.

Table 2.3. List of antibodies.

Antibodies	Suppliers
Non-immune mouse IgG (sc-2025)	Santa Cruz Biotechnology, Inc. (Heidelberg, Germany)
Non-immune goat IgG (sc-2028)	
Anti-factor VIII goat polyclonal IgG (E-16, sc-27649)	
Anti-fibronectin rabbit polyclonal IgG (H-300, sc-9068)	
Anti-vimentin mouse monoclonal IgG1 (V6389)	Sigma-Aldrich (Gillingham, UK)
Anti-cytokeratin mouse monoclonal IgG1 (ab49779)	Abcam (Cambridge, UK)
Anti-collagen I rabbit polyclonal IgG (ab292)	
Anti-collagen III rabbit polyclonal IgG (ab778)	
Alexa Fluor 488 goat anti-mouse IgG (H&L) (ab150113)	
Alexa Fluor 555 donkey anti-goat IgG (H&L) (A21432)	Invitrogen (Paisley, UK)
Anti-α-smooth muscle actin (α-SMA) mouse monoclonal IgG (A2547)	Sigma-Aldrich (Gillingham, UK)

2.2.3. Protein preparation

RIPA lysis and extraction buffers: To make 10× stock solution of RIPA lysis and extraction buffer, add a vial of protease and phosphatase inhibitors (MS-SAFE, Sigma-Aldrich) into 2 mL of RIPA lysis and extraction buffer (R0278, Sigma-Aldrich) and stored at -20 °C. Stock solution was then diluted 10× into 1× RIPA lysis and extraction buffer working solution.

2.2.4. Enzyme-linked immunosorbent assay (ELISA)

The ELISA kits used in this study and their sources are listed in **Table 2.4** and stored according to recommendations from the suppliers.

Table 2.4. List of ELISA kits.

ELISA kits	**Suppliers**
Protein Nov (Ccn3), ab205570	Abcam (Cambridge, UK)
Plasminogen activator inhibitor 1 (PAI-1/Serpine1), ab201283	
Connective Tissue Growth Factor (Ctgf), MBS261004	MyBiosource (San Diego, USA)
Matrix Metalloproteinase 3 (Mmp3), MBS762109	
Procollagen Lysine-2-Oxoglutarate-5-Dioxygenase 2 (Plod2), MBS9391878	
C-C motif chemokine 2 (Ccl2), MBS824584	
C-C motif chemokine 7 (Ccl7), MBS8244676	
Protein Cyr61, MBS9425693	
Inosine-5'-monophosphate dehydrogenase 2 (Impdh2), XPER1807	Express biotech International (Frederick, USA)
Ectonucleotide pyrophosphatase/phosphodiesterase family member 1 (Enpp1), ER0419	Fine Biotech (Wuhan, China)
Transferrin receptor (Tfrc), ER1375	
Aldehyde dehydrogenase, dimeric NADP-preferring (Aldh3a1), E02A1034	BlueGene Biotech (Shanghai, China)
Coiled-coil domain-containing protein 80 (Ccdc80), E02C1111	
Tsukushin (Tsku), E02T0739	
Sequestosome-1 (Sqstm1), E12411744	Sincere Biotech (Beijing, China)

2.3. Preparation of herbal extracts

Herbal extracts were produced and analysed by Ms. Jun Yuan and Zhitao Liang in Professor Zhongzhen Zhao's Laboratory (Hong Kong Baptist University, Hong Kong) and the specific protocols and procedures for each herb were described below.

2.3.1. Processing and extraction of AR and ALR

Fig.2.1 illustrates the workflow of processing and extraction of AR and ALR. To make processed AR, AR was graded according to size and macerated in Milli-Q water until there was no dry core. Taken out and boiled in water until there was no white core. AR was then cut into slices and dried at 50 °C for 24 h.

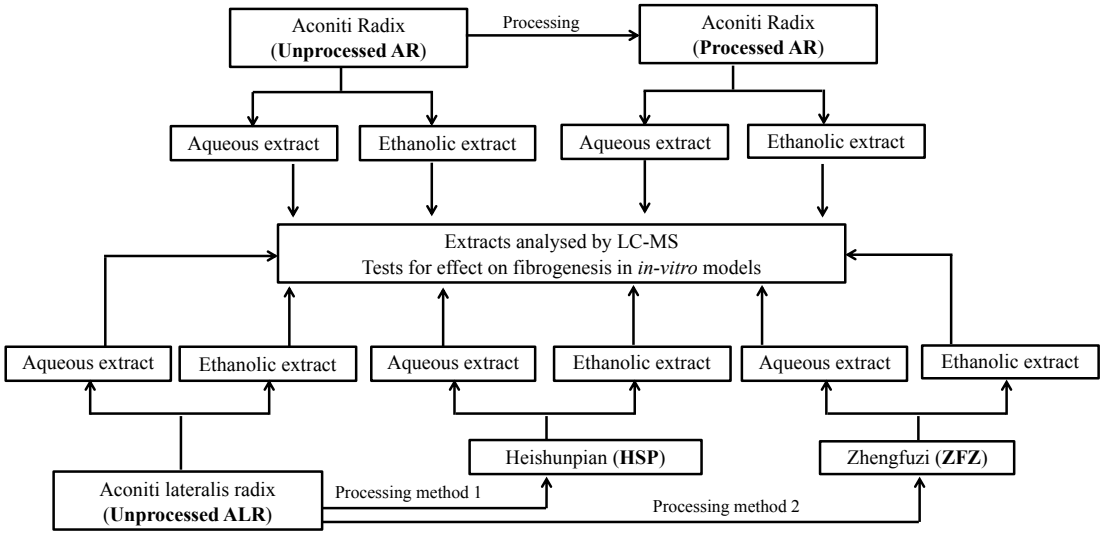

Fig. 2.1. The procedure flow of AR and ALR extraction and downstream assays.

Three types of processed ALR are recorded in the Chinese pharmacopoeia 2015 edition. The most commonly used, known as Heishunpian (HSP), was chosen for this study. Besides, another type of processed ALR, known as Zhengfuzi (ZFZ), which is recommended by the Japanese Pharmacopoeia 17th edition was also chosen for study.

To make HSP, ALR was graded according to size and macerated in saturated Danba solution (86.42 % $CaCl_2$, Penglai Salt Chemical Co. Ltd., Chengdu, China) until there was no dry core. After washing with distilled water, slices were cut and autoclaved at 121 °C (0.1 Mpa) for 2 h. The slices were then dried at 50 °C for 24 h.

To make ZFZ, ALR was graded and macerated in Milli-Q water for 2 days, cut halfway, and then macerated in Milli-Q water until there was no dry core. Autoclaved at 121 °C (0.1 Mpa) for 2 h, followed by moisture overnight, the herb was autoclaved for another 2 h at 121 °C (0.1 Mpa) and then dried at 50 °C for 24 h.

For ultra-high-performance liquid chromatography-quadrupole time-of-flight mass spectrometry (UPLC/Q-TOF-MS)-based chemical analysis and quality control, 0.5 g fine powders were dissolved in 5 mL 50% methanol and then diluted 4 times by 50% methanol.

For testing activities of unprocessed and processed AR and ALR in *in-vitro* models of fibrosis, 85 g fine powders were mixed in 600 mL Milli-Q water or 80% ethanol, simmered for 2 h under reflux on electric heating-jacket, cooled, filtered, dried under vacuum freeze and the extracts were stored at -20 °C until use.

2.3.2. Extraction of SR

The procedure flow of SR extraction is illustrated in **Fig.2.2**.

SR aqueous and methanolic (SRA and SRM) extracts: 85 g SR powder (through 40 meshes) was simmered in 600 mL Milli-Q water or 70% methanol for 2 h under reflux on electric heating-jacket, cool and filter. Extracts were dried under vacuum freeze and stored at -20 °C until use.

Sample preparation for MS analysis: Lyophilised powder of aqueous/methanolic extracts were accurately weighed and dissolved in 100% methanol to obtain 1 mg/mL solutions prior to UPLC/Q-TOF-MS analysis.

Mass spectrometry: UPLC was carried out using an Agilent 6540 accurate-mass Q-TOF LC/MS (Agilent Technologies, U.S.A.). Liquid chromatographic separation was performed at room temperature of 20 °C, using a UPLC C18 analytical column (dimensions: 2.1 mm ×

100 mm I.D., 1.7 μm, ACQUITY UPLC®BEH, Waters, U.S.A.), attached with a C18 pre-column (2.1 mm × 5 mm I.D., 1.7 μm, VanGuardTM BEH, Waters, U.S.A.). MS analyses were performed under the following operation parameters: dry gas temperature 300 °C, dry gas (N_2) flow rate 8 L/min, nebulizer pressure 45 psi, Vcap 4500 V, nozzle voltage 500 V and fragment voltage 150 V. Mass spectra were acquired in the positive ion mode by scanning from 50 to 1700 in the mass-to- charge ratio (m/z). The mobile phase composition used for UHPLC-QTOF MS comprised of a mixture of H_2O (A) and CH_3CN (B), both containing 0.1% HCOOH, with an optimized linear gradient elution as follows: 0-10 min, 5-25% B; 10-25 min, 25-75% B; 25-28 min, 75-100% B; 28-31 min, 100-100% B; 31-31.1 min, 100-5% B with 3.9 min of equilibrium time. The injection volume was 2 μL. The flow rate was set at 0.4 mL/min.

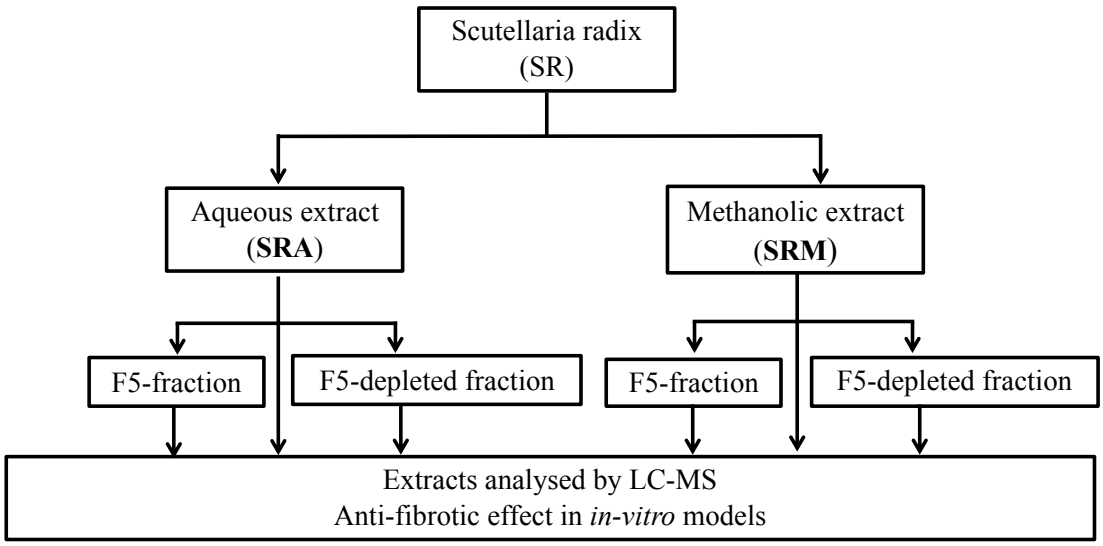

Fig. 2.2. The procedure of SR extraction and downstream analysis.

Note: F5: five SR flavonoids, including baicalin, baicalein, wogonoside, wogonin, oroxylin-A.

F5 depletion: To address whether major SR flavonoids (F5: baicalin, baicalein, wogonoside, wogonin and oroxylin-A) are the main contributors to the anti-fibrotic activities in NRK-49 cells, F5 compounds were isolated from SRA and SRM extracts and pooled as the F5 fractions and the rest as F5-depleted fractions. Freeze-dried powder of SRA (110.6 mg) and SRM (142.4 mg) were added 5 mL methanol respectively, mixed well and filter through a

0.22 μm membrane. Preparative liquid chromatography was carried out using Waters 2489 UV/visible detector, Waters 2545 binary gradient module, an Empower workstation (Waters, USA) and a reversed phase C18 column (40×300 mm, 12 μm, Symmetry Prep TM). The mobile phase composition used for depletion comprising of a mixture of H_2O (A) and methanol (B), with an optimised linear gradient elution as follows: 0-60 min, 35% B; 60-70 min, 35-100% B; 70-90 min, 100% B; 90-100 min, 35% B; 100-110 min, 35% B. The flow rate was set at 10 mL/min.

2.4. Authentication of herbal compounds

To examine if aconite alkaloids have pro-fibrotic effects *in vitro* and could account for the reported pro-fibrotic effect of AR, nine aconite alkaloids were procured and their molecular weights were validated, with the mass errors lower than 2.5961 ppm (**Table 2.5**).

To examine if SR flavonoids have anti-fibrotic effects and could account for the previously reported anti-fibrotic activities of the herb, five SR flavonoids (baicalin, wogonoside, baicalein, wogonin, oroxylin-A) were purchased and examined to validate their molecular weights, as listed in **Table 2.6**. The five flavonoids were found to have the expected molecular weights with the mass errors lower than 3.3823 ppm.

2.5. Cell culture and quality control

Normal rat kidney fibroblasts (NRK-49F; LGC Standards, Teddington, UK) were an established cell line derived from an adult non-inbred Osborne-Mendel rat kidney and developed as a fibroblastic clone. This cell type has been widely used in TGF-β1-induced fibrogenesis studies and the culture conditions to maximise the fibrogenesis and minimise proliferation in response to TGF-β1 have already been developed. Likewise, in our previous research, a TGF-β1-induced *in-vitro* model of fibrosis has been established in NRK-49F cells for screening the anti-fibrotic activities of herbs and herbal compounds. Therefore, NRK-49F cell line was chosen as a cellular model in this project.

Table 2.5. Validation of molecular weights of AR/ALR alkaloids by HRMS.

Compound	Molecular formula	Measured mass (m/z)	Theoretical exact mass (m/z)	Error (ppm)	Mode
A1	$C_{34}H_{47}NO_{11}$	646.3219 $[M+H]^+$	646.3227 $[M+H]^+$	-1.2378	ESI+
A2	$C_{33}H_{45}NO_{11}$	632.3061 $[M+H]^+$	632.3071 $[M+H]^+$	-1.5815	ESI+
A3	$C_{33}H_{45}NO_{10}$	616.3106 $[M+H]^+$	616.3122 $[M+H]^+$	-2.5961	ESI+
A4	$C_{32}H_{45}NO_{10}$	604.3107 $[M+H]^+$	604.3122 $[M+H]^+$	-2.4822	ESI+
A5	$C_{31}H_{43}NO_{10}$	590.2953 $[M+H]^+$	590.2965 $[M+H]^+$	-2.0329	ESI+
A6	$C_{31}H_{43}NO_9$	574.3004 $[M+H]^+$	574.3016 $[M+H]^+$	-2.0895	ESI+
A7	$C_{25}H_{41}NO_9$	500.2852 $[M+H]^+$	500.2860 $[M+H]^+$	-1.5991	ESI+
A8	$C_{24}H_{39}NO_9$	486.2963 $[M+H]^+$	486.2703$[M+H]^+$	-2.0565	ESI+
A9	$C_{24}H_{39}NO_8$	470.2743 $[M+H]^+$	470.2754 $[M+H]^+$	-2.3391	ESI+

Note: ESI: Electrospray ionization.

Table 2.6. Validation of molecular weights of SR flavonoids by HRMS.

Compound	Molecular formula	Measured mass (m/z)	Theoretical exact mass (m/z)	Error (ppm)	Mode
Baicalin	$C_{21}H_{18}O_{11}$	445.0782 $[M-H]^-$	445.0771 $[M-H]^-$	2.5164	ESI-
Wogonoside	$C_{22}H_{20}O_{11}$	459.0937 $[M-H]^-$	459.0927 $[M-H]^-$	2.1129	ESI-
Baicalein	$C_{15}H_{10}O_5$	269.0459 $[M-H]^-$	269.0449 $[M-H]^-$	3.3823	ESI-
Wogonin	$C_{16}H_{12}O_5$	283.0612 $[M-H]^-$	283.0606 $[M-H]^-$	1.9784	ESI-
Oroxylin-A	$C_{22}H_{20}O_{11}$	459.0939 $[M-H]^-$	459.0927 $[M-H]^-$	2.6106	ESI-

NRK-49F cells were maintained in Dulbecco's Modified Eagle Medium (DMEM, Thermo Fisher Scientific Inc.) supplemented with 5% fetal calf serum (FCS, Sigma-Aldrich, UK), penicillin 100 IU/mL, streptomycin 100 µg/mL (PAA Laboratories, GmbH) and amphotericin B 2.5 µg/mL (Invitrogen, Paisley, UK) at 37 °C and 5% CO_2. For passaging or use in experiments, adherent cells were first washed with sterile PBS (PAA Laboratories GmbH) then incubated in 1 mL trypsin (0.5 mg/mL)-ethylenediaminetetraacetic acid (EDTA, 0.22mg/mL) (PAA, GE Healthcare LTD) for 3 min. Complete trypsinisation was confirmed

by examining the cells under microscope. Fresh culture medium was added, then aspirated and dispensed into new culture flasks. A sub-cultivation ratio of 1:3 to 1:4 was used as recommended by supplier.

2.5.1. Cell species identification

Misidentification and cross-contamination of cell lines are common problems of cell cultures that can make scientific results and their reproducibility unreliable. Simple and quick polymerase chain reaction (PCR)-based method was used to identify the species of cultured cells and to detect inter-species cross contamination. DNA was extracted from the tested cells and PCR was conducted by using oligonucleotide primer pairs for cytochrome oxidase subunit (*Cox I*) sequences for *Homo sapiens, Rattus norvegicus* and *Mus musculus*. The cell lines and primary cell cultures used for species identification was listed in **Table 2.7**.

DNA extraction: Total DNA was extracted using PureLink Genomic DNA Mini Kit (K1820, Life technologies) according to the manufacturer's guidelines. Briefly, cell culture medium was removed and cells were harvested by trypsinisation, then the cells were resuspended in 200 µL PBS. 20 µL Proteinase K, 20 µL RNase and 200 µL Lysis/Binding Buffer were added and mixed well to obtain a homogenous solution. After incubation at 55 °C for 10 min, 200 µL 100% ethanol was added to the lysates and samples were transferred to a Spin Column, centrifuged at 10,000 × *g* for 1 min, washed once with 500 µL Wash Buffer 1 then centrifuged at 10,000 × *g* for 1 min. Further washing was performed using 500 µL Wash Buffer 2 then centrifuged at maximum speed. Finally, DNA was eluted into 1.5 collection tubes by adding 100 µL Elution Buffer directly to the spin column followed by centrifugation for 1 min at full speed. The purity of the eluted total DNA was confirmed using a NanoDrop 8000 Spectrophotometer (Thermo Fisher Scientific) and stored at -20 °C until use.

Table 2.7. List of cell lines and primary cell cultures.

Name	Expected species	Expected cell type	Supplier
HUVEC	Human	Endothelial	Dr. Lingfang Zeng, King's College London, London, UK
HEK	Human	Embryonic	LGC Standards, Teddington, UK
HKC-8	Human	Epithelial	Dr. Lorraine Racusen, Johns Hopkins University, Baltimore, USA
"TK173"	Human	Fibroblastic	Prof. Gerhard Müller, University of Göttingen, Goettingen, Germany
"TK188"	Human	Fibroblastic	Prof. Gerhard Müller, University of Göttingen, Goettingen, Germany
NRK-49F	Rat	Fibroblastic	LGC Standards, Teddington, UK
SM43	Rat	Mesangial	Dr. Masanori Kitamura, UCL, London, UK
mPTECs	Mouse	Epithelial	Dr. Mark Dockrell, South West Thames Institute for Renal Research, London, UK
mIMCD-3	Mouse	Epithelial	LGC Standards, Teddington, UK

Primers: Oligonucleotide primer pairs, GenBank information and amplification product sizes were listed in **Table 2.8**. Oligonucleotides were supplied by Sigma-Aldrich and *Cox I* sequences for *Homo sapiens, Rattus norvegicus, Mus musculus* were employed to select highly specific application primers (123).

PCR amplification: Amplification was carried out in a Thermal Cycler (Applied Biosystems). Genomic DNA from each cell line was used as the template and amplified by PCR using DreamTaq PCR Master Mix (K1071, Life technologies). Gradient PCR was performed to determine the optimal annealing temperature for each pair of primers. The reaction composition and cycling protocol that were used for amplification are shown in **Table 2.9** and **Table 2.10**. The amplification product (10 μL) was run on 2% agarose gel Sigma-Aldrich (Gillingham, UK), stained with ethidium bromide (Invitrogen), visualised under UV light, and photographed.

Table 2.8. Species-specific primers.

Species	Gene/GenBank Accession No.	Position	Direction	Sequence	Size (bp)
Human	cox I/J01415	5967-5988 6173-6194	for: 5' rev: 5'	TTCGGCGCATGAGCT GGAGTCC TATGCGGGGAAACGC CATATCG	228
Mouse	cox I/J01420	9570-9589 10055-10074	for: 5' rev: 5'	TGCGGATTCGACCCT ACAAG GGCTGCGAAAACTAA GGTGA	505
Rat	cox I/NC001665	6022-6043 6196-6217	for: 5' rev: 5'	CGGCCACCCAGAAGT GTACATC GGCTCGGGTGTCTAC ATCTAGG	196

Table 2.9. The reaction composition for species-specific amplification.

Reagent	Concentration	Volume
Dream Taq PCR Master Mix	2×	10.0 µL
Forward primer	100 µM	0.2 µL
Reverse primer	100 µM	0.2 µL
Template DNA	100 ng/µL	5.0 µL
Water (nuclease-free)	-	4.6 µL
Total	-	20.0 µL

Table 2.10. Cycling protocol for species-specific amplification.

Stage	Temperature (°C)	Time	Number of Cycles
Initial denaturation	95	3 min	1
Denaturation	95	30 sec	35
Annealing	52 (mouse) 62 (Human) 67 (rat)	30 sec	
Extension	72	1 min	
Final Extension	72	5 min	1
Incubation	4	Infinity	1

NRK-49F cells were set for authentication in present study, alongside with “TK173” and “TK188”, which were expected to be human kidney fibroblast cell lines originated from healthy and fibrotic kidneys, respectively, in comparison with a range of other cells as species and phenotype controls. “TK173” and “TK188”, if authenticated as human kidney fibroblasts, were candidate cells for developing human cell-based *in-vitro* models for validating the human relevance of findings from NRK-49F cells.

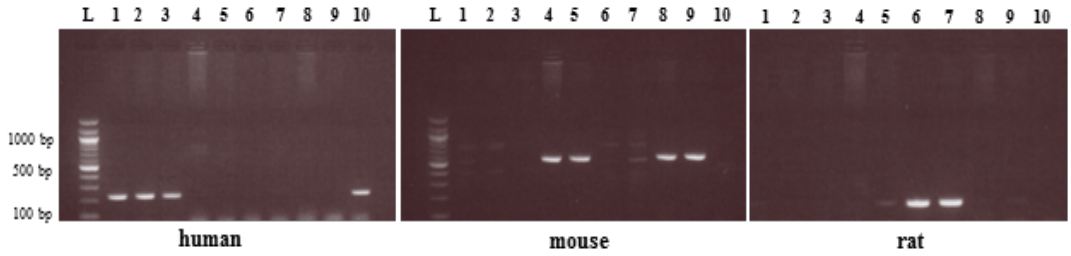

Fig. 2.3. PCR amplification with species-specific human, mouse and rat primer pairs. Amplified fragments were detected by ethidium bromide staining after 2% agarose gel electrophoresis. On each gel, the amplified products were loaded in the same order. L: DNA ladder (100 bp, New England Biolabs); lane 1: HUVEC (human); lane 2: HEK (human); lane 3: HKC-8 (human); lane 4: “TK173” (expected to be human); lane 5: “TK188” (expected to be human); lane 6: NRK-49F (rat); lane 7: SM43 (rat); lane 8: mPTECs (mouse); lane 9: mIMCD-3 (mouse) and lane 10: Human control DNA (Qiagen).

As shown in **Fig. 2.3**, most cells were confirmed of their expected species, with the exception of “TK173” and “TK188” cells, which were expected as human cells. However, DNAs extracted from these cells were unexpectedly amplified by mouse specific primers, but not human. To further confirm the species of “TK173” and “TK188” cells, fresh DNAs of each cell line were extracted and subjected to PCR amplification using human and mouse specific primers. As illustrated in **Fig. 2.4**, “TK173” and “TK188”, once again were characterised as of murine origin rather than human.

In conclusion, the above studies confirmed that NRK-49F cells were of rat origin as expected, however, “TK173” and “TK188” were not human renal fibroblasts and were of mouse origin instead.

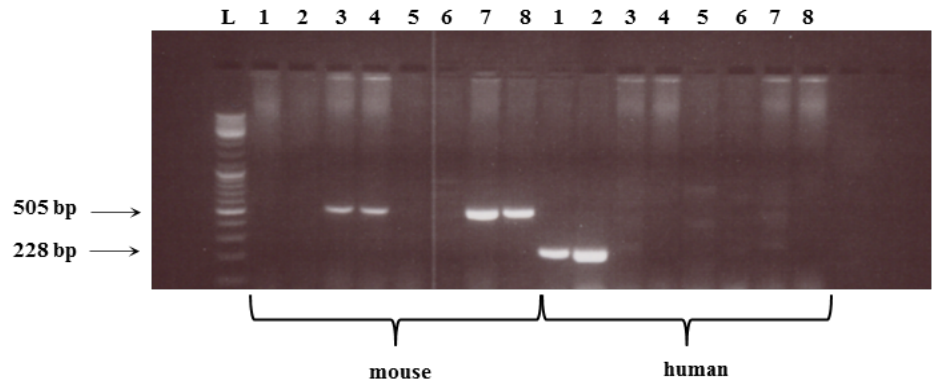

Fig. 2.4. PCR amplification with human and mouse primer pairs. Amplified fragments were detected by ethidium bromide staining after 2% agarose gel electrophoresis. L: 100 bp DNA ladder; lane 1: HUVEC (human); lane 2: HKC-8 (human); lane 3: "TK173"; lane 4: "TK188"; lane 5: NRK-49F (rat); lane 6: SM43 (rat); lane 7: mPTECs (mouse); lane 8: mIMCD-3 (mouse).

2.5.2. Cellular morphology and immunocytochemical characterisation

Cell morphology was observed under Nikon Eclipse TE2000-S microscope (Nikon Instruments Europe BV, Amstelveen, the Netherlands) regularly to confirm the healthy status of the cells. The phase contrast images (**Fig. 2.5**) show the morphology of healthy NRK-49F cells in adherent at 60% confluence. The cells were always passaged before they reach confluence to avoid transformation.

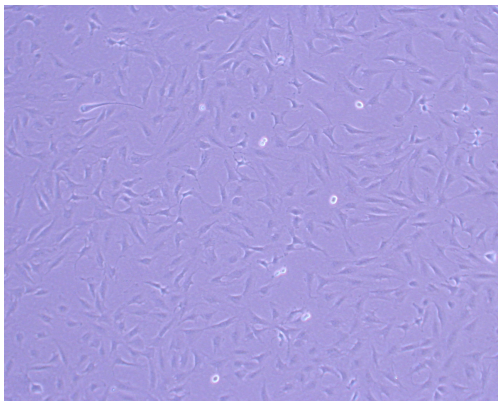

Fig. 2.5. NRK-49F cells in culture. The figure shows NRK-49F cells cultured for 48 h with sub-cultivation ratio of 1:4.

A basic cell characterisation was performed to confirm identify of NRK-49F cells. Expression of vimentin, cytokeratin and factor viii, the markers of fibroblasts, epithelial cells and endothelial cells, respectively, were examined by indirect immunocytofluorescence. Cells were seeded at 5×10^3 cells/well into 96 well plates in DMEM with 10% FCS (NRK-49F, "TK177", "TK188"); DMEM/F12 (1:1) with 5% FCS (HKC-8); Medium199 with 10% FCS (HUVEC). After an overnight incubation, cells were fixed with ice-cold 100% methanol at -20 °C for 10 min, followed by washing with three changes of PBS, 5 min each. Cells were then permeabilised with 0.1% Triton X-100 for 5 min, washed with PBS three times and blocked with 1% BSA for 1 h at room temperature. Cells were then stained for 1 h at room temperature with anti-vimentin mouse monoclonal IgG1, anti-cytokeratin mouse monoclonal IgG1 and anti-factor VIII goat polyclonal IgG, as well as negative control non-immune mouse IgG and goat IgG, respectively. **Table 2.3** lists the antibodies used in experiments and their sources. After three PBS washing, cells were incubated for 1 h with Alexa Fluor 488 goat anti-mouse IgG and Alexa Fluor 555 donkey anti-goat IgG, respectively, followed by washing, counterstain with 4'6-diamidino-2-phenylindole (DAPI) and visualisation under a Nikon Eclipse TE2000-S fluorescence microscope.

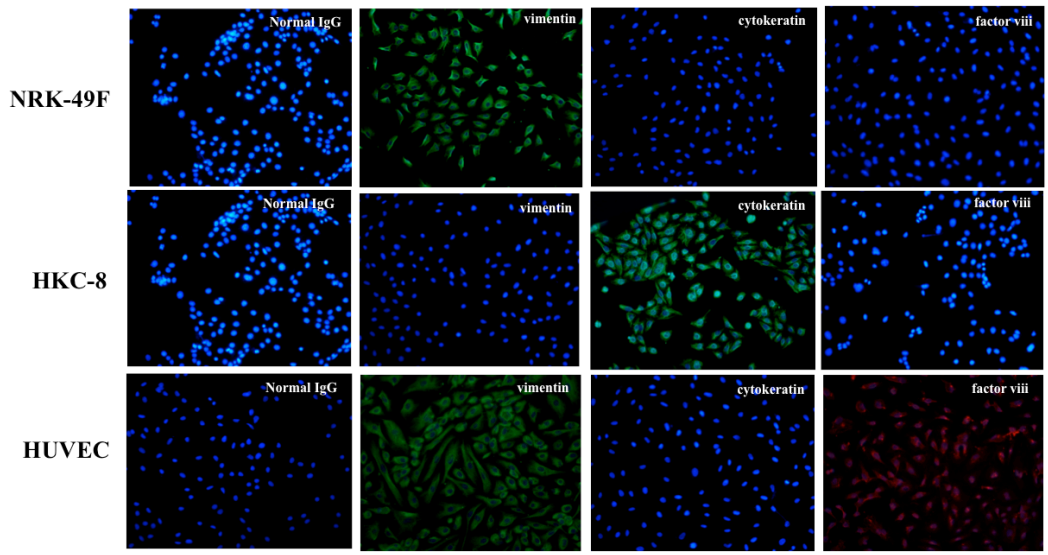

Fig. 2.6. Characterisation of NRK-49F cells by immunocytofluoresence assays.

As shown in **Fig. 2.6**, NRK-49F stained positive for the fibroblast maker vimentin and negative for the epithelial maker cytokeratin and the endothelial maker factor viii as expected. HKC-8 cells stained positive for cytokeratin and negative for vimentin and factor viii; and HUVEC stained positive not only for factor viii but also vimentin, and negative for cytokeratin.

2.5.3. Mycoplasma contamination detection

Conditioned media were harvested for PCR with a LookOut Mycoplasma PCR Detection Kit (MP 0035, Sigma-Aldrich). The reaction composition and cycling protocol that were used for amplification are shown in **Table 2.11** and **Table 2.12**. 20 µL amplification product was run on 1.2% agarose gel with ethidium bromide and photographed under UV light.

NRK-49F and mIMCD-3 cells were examined for mycoplasma detection. As shown in **Fig. 2.7**, the negative control and positive control samples showed distinct a 481 bp band and a 260 bp band, respectively. Both NRK-49F cells and mIMCD-3 cells were confirmed free of mycoplasma contamination.

Table 2.11. The reaction composition for mycoplasma amplification.

Reagent	**Sample**	**Positive**	**Negative**
Rehydration buffer/DNA Polymerase*	23 µL	25 µL	23 µL
Sample volume	2 µL	-	-
DNA-free water	-	-	2 µL
Total	25 µL	25 µL	25 µL

Note: one unit of DNA Polymerase is required per reaction.*

Table 2.12. Cycling protocol for mycoplasma amplification.

Stage	Temperature (°C)	Time	Number of Cycles
Initial denaturation	94	2 min	1
Denaturation	94	30 sec	40
Annealing	55	30 sec	
Extension	72	40 sec	
Incubation	4	Infinity	1

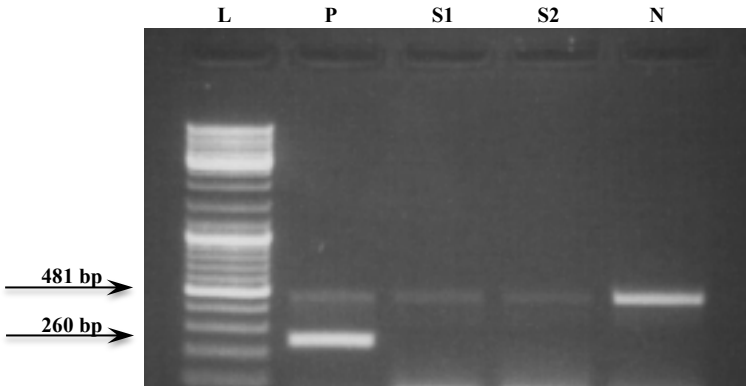

Fig. 2.7. PCR amplification for mycoplasma detection. Amplified fragments were detected by ethidium bromide staining after 1.2% agarose gel electrophoresis. L: 100 bp DNA ladder; P: Positive control; S1: NRK-49F cells; S2: mIMCD-3 cells; N: Negative control.

In summary, NRK-49F cells were confirmed as rat cells that showed typical morphology of fibroblasts, positive for mesenchymal cell marker and negative for epithelial and endothelial markers, and the cells were free of mycoplasma contamination.

The initial plan was to use “TK173” and “TK188” cells to validate findings in NRK-49F cells to establish human relevance of findings. Unexpectedly, these cells were proven to be of mouse origin. In interest of time, I decided to stick to NRK-49F cells for further studies.

2.6. *In-vitro* model of fibrosis

The *in-vitro* model of TGF-β1-induced fibrosis was used to determine the effect of herbal extracts and compounds on fibrogenesis in NRK-49F cells. This model is qualitatively stained by strong anionic dye PSR for the total collagen and quantified by spectrophometric analysis of the eluted stain. PSR contains the small anionic picric acid and the large hydrophobic Sirius Red, which can bind to collagens via the interaction of its acid sulfonic groups with the basic groups of collagen molecules. Since collagens are abundant in basic amino acids, PSR can strongly react with these collagens.

NRK-49F cells were seeded at a density of 1×10^4 cells/well in 96-well collagen type I-coated tissue culture plates in DMEM supplemented with 2.5% FCS and 2.5% Nu-Serum (Collaborative Biomedical, Bedford, MA, USA) for 3 days then change to DMEM supplemented with 1× insulin-transferrin-sodium selenite Liquid Media Supplement (ITS; Sigma) for 4 days. Cells were treated with herbal compounds and/or TGF-β1 in 1% ITS DMEM for further 48 h. Control groups were treated by equivalent concentrations of vehicles only. Changes in cell morphology were observed and captured by photomicroscopy using a Nikon Eclipse TE2000-S epifluorescence microscope (Nikon Instruments Europe BV, Amstelveen, the Netherlands) and a DXM 1200F Nikon digital camera (Nikon UK Limited, Kingston upon Thames, UK).

Cell detachment index in each well was recorded under microscope and categorised using the following scoring criteria: a score of 0 represents no cell detachment and 4 represents a complete disruption of the cell monolayer. Scores 0.5, 1, 1.5, 2, 2.5, 3, 3.5 stand for detachment of 5%, 10%, 20%, 30%, 40%, 60, and 80% cells, respectively. The cells were then fixed with 100% ice-cold methanol overnight at -20 °C, rinsed twice for 5 min with PBS before staining with 200 µL 0.1% PSR for 6 h on a rocking platform at room temperature. PSR solution was removed and washed twice with 0.1% acetic acid. The plate air-dried overnight at room temperature and cell staining for PSR was observed and captured

by photomicroscopy. The PSR eluted with 200 µL 0.1 M NaOH for 1 h on a rocking platform at room temperature. Following elution, PSR staining was quantified by spectrophotometric analysis at 540 nm using a spectrophotometer (Dynex Technologies, Worthing, UK). Experiments were repeated independently at least three times.

2.7. Lactate dehydrogenase (LDH) release assays

LDH assay was used to assess *in-vitro* cytotoxic effects, using Promega's CytoTox 96® Non-Radioactive Cytotoxicity Assay kits (Promega, Southampton, UK). LDH is a cytosolic enzyme that can release into cell culture media when cells are damaged. The amount of LDH in the media can be measured by a coupled enzymatic reaction in which LDH catalyses the conversion of lactate to pyruvate via NAD^+ reduction to NADH. Diaphorase then uses NADH to reduce a tetrazolium salt to a red formazan product that can be measured by spectrophotometry. The level of formazan formation is directly proportional to the amount of LDH released into the medium, which is indicative of cytotoxicity.

NRK-49F cells were seeded in quadruplicate into 96 well collagen type I-coated plates and treated as per protocol for the *in-vitro* model. A medium control without cells, a cell spontaneous LDH release control and a control to determine maximum LDH release from cells were included in the plates. To measure the maximum LDH release from cells, 20 µL lysis solution was added to the medium control and cell control for complete lysis and the plates were incubated at 37 °C and 5% CO_2 for 45 min. 50 µL conditioned media from control and experimental wells were transferred to 96 well flat bottom enzymatic assay plates (Nunc, Roskilde, Denmark) and an equal volume of substrate mix was added. Plates were incubated at room temperature for 30 min protected from light then 50 µL of stop solution was added to stop the reaction and the absorbance recorded at 490 nm using a spectrophotometer.

Percentage cytotoxicity for the test conditions was calculated as follows:

Maximum LDH release= (cells + lysis solution) - (medium + lysis solution)

Baseline LDH release= (cells alone) - (medium alone)

Test LDH release= (cells in test conditions) - (medium alone)

$$\% \text{ cytotoxicity} = \frac{(\text{test LDH release}) - (\text{baseline LDH release})}{\text{Maximum LDH release}} \times 100$$

% cytotoxicity was presented as an average of quadruplicates.

2.8. Immunocytofluorescence assay

1×10^4 cells/well NRK-49F cells were seeded in quadruplicate into 96 well collagen type I-coated plates and treated as per protocol for the *in-vitro* model. Cells were fixed with 3.7% paraformaldehyde on ice for 10 min, followed by washing with three times of PBS. Cells were then permeabilized with 0.1% Triton X-100 for 5 min, washed with PBS three times and blocked with 1% BSA for 1 h at room temperature, then incubated with anti-collagen I, anti-collagen III, anti-α-SMA and anti-fibronectin primary antibodies, as well as negative control non-immune IgG overnight at -4°C, respectively. After three times PBS washing, cells were incubated for 1 h with Alexa Fluor 488 or 555 conjugated secondary antibodies respectively, followed by washing with PBS and counterstaining with DAPI. Fluorescence intensity was then measured using a Cytation 5 Multi-Mode reader (Bio Tek) and expressed in a relative fluorescence unit (RFU)/well.

2.9. Protein extraction

2.0×10^6 NRK-49F cells were grown in 75 mm^2 flask in DMEM with 2.5% FCS and 2.5% Nu-serum replacement for 3 days, then changed the medium to 15 mL 1% ITS-DMEM for another 4 days. Cells were washed with serum free, phenol red-free DMEM (Thermo Fisher Scientific, 31053028) and added fresh one then incubated at 37 °C for 30 min. Repeat this step once. The medium was removed and the cells were treated with 40, 80 μg/mL SRM, 40 μM, 80 μM baicalein and 1 μM IN1130 with 5 ng/mL TGF-β1 in serum-free, phenol red-free DMEM for 2 days.

The conditioned media were collected and added protease and phosphatase inhibitors (MS-SAFE, Sigma), then centrifuged at 500 *g* for 5 min at 4 °C to pellet detached cells and large debris. The supernatant was collected and then centrifuged at 2,500 *g* for 5 min at 4 °C to pellet smaller debris. The final supernatant was saved and kept at -80 °C until use.

For extraction of total cell lysates, cell culture flasks were placed on ice and washed thrice with cold PBS. 1.0 mL/flask RIPA buffer (R0278, Sigma) with protease and phosphatase inhibitors were added to cover cell monolayer. Cell lysates were harvested by scraper and centrifuged at a full speed for 10 min to pellet debris. The bicinchoninic acid (BCA) protein assay (Pierce Protein Research products, Thermo Scientific, Rockford, USA) was used to measure the protein concentration of the samples. The BCA protein assay combines the reduction of $Cu2^{+}$ to $Cu1^{+}$ by protein in an alkaline medium with the highly sensitive and selective colorimetric detection of the cuprous cation ($Cu1^{+}$) by BCA. The resulting intense purple-coloured product can be measured by spectrophotometric analysis at 540 nm. Total cell lysate was stored at -80°C until use.

2.10. QuickZyme total collagen assay

The total collagen content was measured indirectly through measurement of hydroxyproline using the QuickZyme total Collagen Assay (QZBtotcol, QuickZyme, Leiden, Netherlands). Hydroxyproline is a non-proteinogenic amino acid, which in mammals occurs in elastin and collagen. It is formed post-translationally form specific proline residues by action of the enzyme prolyhydroxylase. This assay measures the total amount of hydroxyproline present in the sample, which represents all the types of collagens including pro-collagen, mature collagen and collagen degradation products. The measurement of collagen is started by complete hydrolysis of the sample in 6 M HCl at 95 °C. The hydrolysate hydroxyproline residues are quantified using a modification of the method described by Prockop and Udenfriend (124). Cell lysate and standards were mixed with 12 mol/L HCl and hydrolysis was performed for 20 h at 95 °C, following assay as described by the manufacturer. After the

hydrolysis procedure, the tubes were cooled to room temperature and then centrifuged for 10 min at 13,000 *g*. The supernatants were collected and diluted the samples with demi H_2O (200 µL hydrolysate + 100 µL H_2O). The samples are now in 4 M HCl. 35 µL diluted hydrolyzed samples and prepared collagen standards were added into 96-well plates, 75 µL assay buffer was added to each well. The plate was covered with an enclosed adhesive plate seal and incubated 20 min at room temperature, while shaking the plate. 75 µL mixed detection reagents A and B (2:3) were added into each well and incubated for 60 min at 60 °C. The absorbance was recorded at 540 nm.

2.11. Sicrol soluble collagen assay

The Sircol assay is a dye-binding method designed for the analysis of acid and pepsin-soluble collagens. The amount of soluble collagen in conditioned media was colorimetrically detected by the Sicrol soluble collagen assay (Biocolor Ltd., Northern Ireland, UK) according to the manufacturer's protocol. In brief, 1.0 mL culture supernatant was harvested and concentrated by 200 µL collagen isolation and concentration reagent overnight at 4 °C. The supernatant was gently removed followed by centrifugation at 13,000 *g* for 10 min (The pellet of hydrated transparent collagen is invisible). 1.0 mL of the dye (Sirius-Red) in picric acid was added and shaked for 30 min, the pellet was carefully collected and washed with 750 µL washing solution. The pellet bound dye was dissolved in 250 µL alkaline solution, and measured the absorbance of the pellet solution at 540 nm.

2.12. Proteomic analysis

2.12.1. Sample preparation

Sample preparation is a critical step in proteomics workflow, because the quality and reproducibility of sample extraction and preparation could significantly affect the results from MS systems.

The protein preparation procedure is illustrated in **Fig. 2.8**. Medium samples were first concentrated by Amicon Ultra-0.5® 3kD centrifugal filtration device (Millipore, Billerica, MA). Then cell lysate and medium samples were denatured by adding 6 M urea/2 M thiourea and reduced with 10 mM dithiothreitol (DTT) for 1 h at 37 °C in the dark. 50 mM iodoacetamide were added for alkylation and the samples were briefly spinned down and incubated for 1 hour at room temperature in the dark.

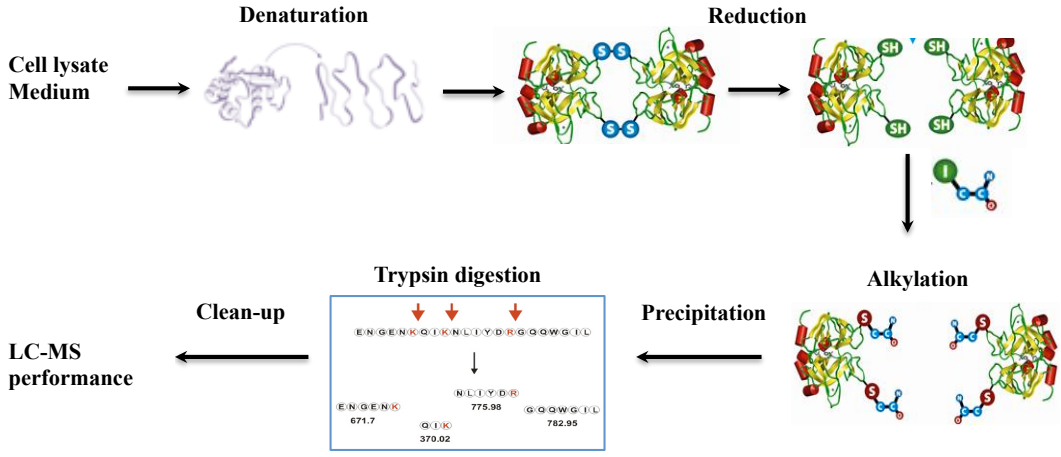

Fig. 2.8. Protein sample preparation for proteomic analysis. Sample preparation procedure mainly includes denaturation, reduction, alkylation, precipitation, digestion and clean-up steps.

Protein content was extracted by pre-chilled (-20 °C) acetone precipitation (8× volume) overnight at -20 °C. Samples were centrifuged at 14,000 *g* for 25 min at 4 °C and the supernatant subsequently discarded. The residue was dried in a Speed Vac vacuum centrifuge and re-suspended in 0.1 M triethylammonium bicarbonate (TEAB, pH=8.2) and followed by digestion with trypsin (1:50, enzyme: substrate) overnight at 37 °C. The digestion was stopped by acidification of samples with 1% trifluoroacetic acid (TFA) then the samples were loaded onto 96-well MACROSpin C18 plates (Harvard Apparatus) for clean-up and peptide concentrations were measured according to manufacturer's instructions. The plate was firstly activated using 200 µL methanol and centrifuged at 1,000 *g* for 1 minute, followed by washing steps with 200 µL of 80% acetonitrile, 0.1% TFA in H_2O, and

three equilibration steps using 200 µL of 1% acetonitrile, 0.1% TFA in H_2O with centrifugation (1,000 *g* for 1 min) after each step. Samples were loaded into the plate and centrifuged at 1,500 *g* for 1 min; the flow through was reloaded onto the plate a second time and centrifugation repeated. The plate was then washed three times with 200 µL 1% acetonitrile, 0.1% TFA in H_2O, then centrifuged at 1,500 *g* for 1 min. Finally, the samples were eluted with 170 µL of 50% acetonitrile, 0.1% TFA in H_2O and centrifuged at 1,500 *g* for 1 min; this step was repeated and the eluates were combined. The eluted peptides were dried in a Speed Vac vacuum centrifuge and re-suspended in 2% acetonitrile containing 0.05% TFA. Isobaric labelling of the digested peptides was performed using 10-plex Tandem mass tags (TMT) reagents (Thermo Fisher, Loughborough, Leics., UK).

2.12.2. HPLC-MS/MS analysis

Samples were injected onto a nano-trap column (Acclaim® PepMap100 C18 Trap, 5 mm × 300 µm, 5 µm, 100 Å), at a flow rate of 25 µL/min for 3 min, using mobile phase (A) 0.1% formic acid in H_2O and (B) 2% ACN. The following nano-LC gradient was then used to separate the peptides at 0.3 µL/min: 0-10 min, 2-10% B; 10-200 min, 10-30% B; 200-210 min, 30-40% B; 210-220 min, 99% B; 220-250 min, 2% B. The nano column (Acclaim® PepMap100 C18, 50 cm × 75 µm, 3 µm, 100 Å) was set at 40 °C and coupled to a nano spray source (Picoview, New Objective, US). The MS spectra are collected from Orbitrap mass analyzer (LTQ-Orbitrap XL, Thermo Fisher Scientific) with full ion scan mode over the mass-to-change (*m/z*) range 350-1550 *m/z*. MS/MS were performed on the Top Speed method to fit as many MS^2 scan in 3 sec cycle time, and use SPS-MS^3 method to acquire the TMT reporter ion signal. Raw files were analyzed using Proteome Discoverer 2.1 and Mascot 2.3.01 (Matrix science). The mass tolerance was set at 10 ppm for precursor ions. Proteins with at least two independent peptides were used for quantification.

2.13. Bioinformatics

Volcano plot (GraphPad Prism software 6.0) was used to illustrate the distribution of quantified proteins according to *p*-value and fold change. DAVID (Database for Annotation, Visualisation, and Integrate Discovery, https://david.ncifcrf.gov/) was used to investigate the biological pathways in which the differentially expressed proteins may participate. The STRING database (https://string-db.org) was then used to build protein-protein interaction networks to further explore their functions.

2.14. ELISA validation

Based on the TMT-labelling MS-based proteomic findings, the proteins most robustly changed or particularly relevant to fibrosis were chosen for further validation by ELISA. Nine proteins in conditioned media (PAI-1, Ctgf, Plod2, Ccl2, Ccl7, Cyr61, Tsku, Nov and Mmp3) and six in cell lysates (Enpp1, Aldh3a1, Tfrc, Ccdc80, Sqstm1 and Impdh2) were selected and subjected to ELISA according to the manufactures' instructions (**Table 2.4**). Absorbance was determined using micro-plate reader. Experiments were in triplicates.

Chapter 3 Effects of AR and aconite alkaloids on fibrogenesis

3.1. Quality control of AR/ALR extracts

Nine alkaloids in raw AR and ALR, as well as processed AR and ALRs (HSP and ZFZ) were analysed. Percent contents of alkaloids in raw and processed ARs and ALRs are presented in **Table 3.1** and their base peak chromatograms (BPCs) and extracted ion chromatograms (EICs) are shown in **Fig. 3.1-3.3,** respectively.

In the BPCs (**Fig. 3.1 A**), most of the tested standards achieved the baseline separation, except A1 and A3, peaks of which were partially overlapping. The overlapping of A1 and A3 was also observed in the sample analysis of raw AR and ALR (**Fig. 3.1B and Fig. 3.2A**), as well as processed AR (**Fig. 3.1C)** and ALRs (HSP and ZFZ, **Fig. 3.2B&C**), which seemed difficult to quantify. Luckily, by using the Q/TOF-MS detector, specific target analyte with unique accurate molecular weight can be extracted as peaks without other interference for quantitative analysis (**Fig. 3.3**).

As shown in **Table 3.1**, the total content (0.070%) of A4, A5 and A6 in processed AR met the legal range required by the Chinese pharmacopoeia (0.070%-0.150%). The content of A5 was 0.041%, meeting the Hong Kong Chinese Materia Medica Standards, i.e. >0.035%. The total content of A1, A2 and A3 in processed AR was 0.0040%, which was in line with the requirements of the Chinese pharmacopoeia (≤ 0.040%) and Hong Kong Chinese Materia Medica Standards (≤0.022%).

Table 3.1. Percent contents of nine alkaloids in unprocessed and processed AR and ALR.

Alkaloids	Unprocessed AR	Processed AR	Unprocessed ALR	Processed ALR type A (HSP)	Processed ALR type B (ZFZ)
A1	0.012249	0.000132	0.015511	0.000044	0.000037
A2	0.044884	0.000430	0.040740	0.000066	0.000042
A3	0.038604	0.003462	0.056877	0.000367	0.000049
A4	0.012043	0.012014	0.021293	0.023439	0.019488
A5	0.050283	0.041275	0.054304	0.040225	0.038998
A6	0.010309	0.013210	0.014327	0.027763	0.026331
A7	0.005383	0.002255	0.002577	0.003831	0.008461
A8	0.038566	0.020804	0.017257	0.018136	0.041255
A9	0.011134	0.004883	0.002207	0.004469	0.009835

Note: (A1) aconitine, (A2) mesaconitine, (A3) hypaconitine, (A4) benzoylaconine, (A5) benzoylmesaconine, (A6) benzoylhypaconine, (A7) aconine, (A8) mesaconine and (A9) hypaconine.

Two types of processed ALRs, HSP and ZFZ were produced. In HSP, the total content of A4, A5 and A6 was 0.091% and that of A1, A2 and A3 was 0.0038%, both meeting the standards of the Chinese pharmacopoeia (≥0.010% and ≤0.020%, respectively). In ZFZ, the contents of A1, A2 and A3 were 0.000037%, 0.000042% and 0.000049%, fulfilling the requirements of Japanese pharmacopoeia (≤ 0.006%, 0.014% and 0.028%, respectively).

A4, A5, and A6 were the most abundant among the nine tested alkaloids, both in HSP and ZFZ. The content of A1, A2 and A3 in ZFZ (0.000128%) was 3 times lower than in HSP (0.000450%). The total content of A7, A8 and A9 in HSP (0.029670%) was >2-fold lower than in ZFZ (0.062246%).

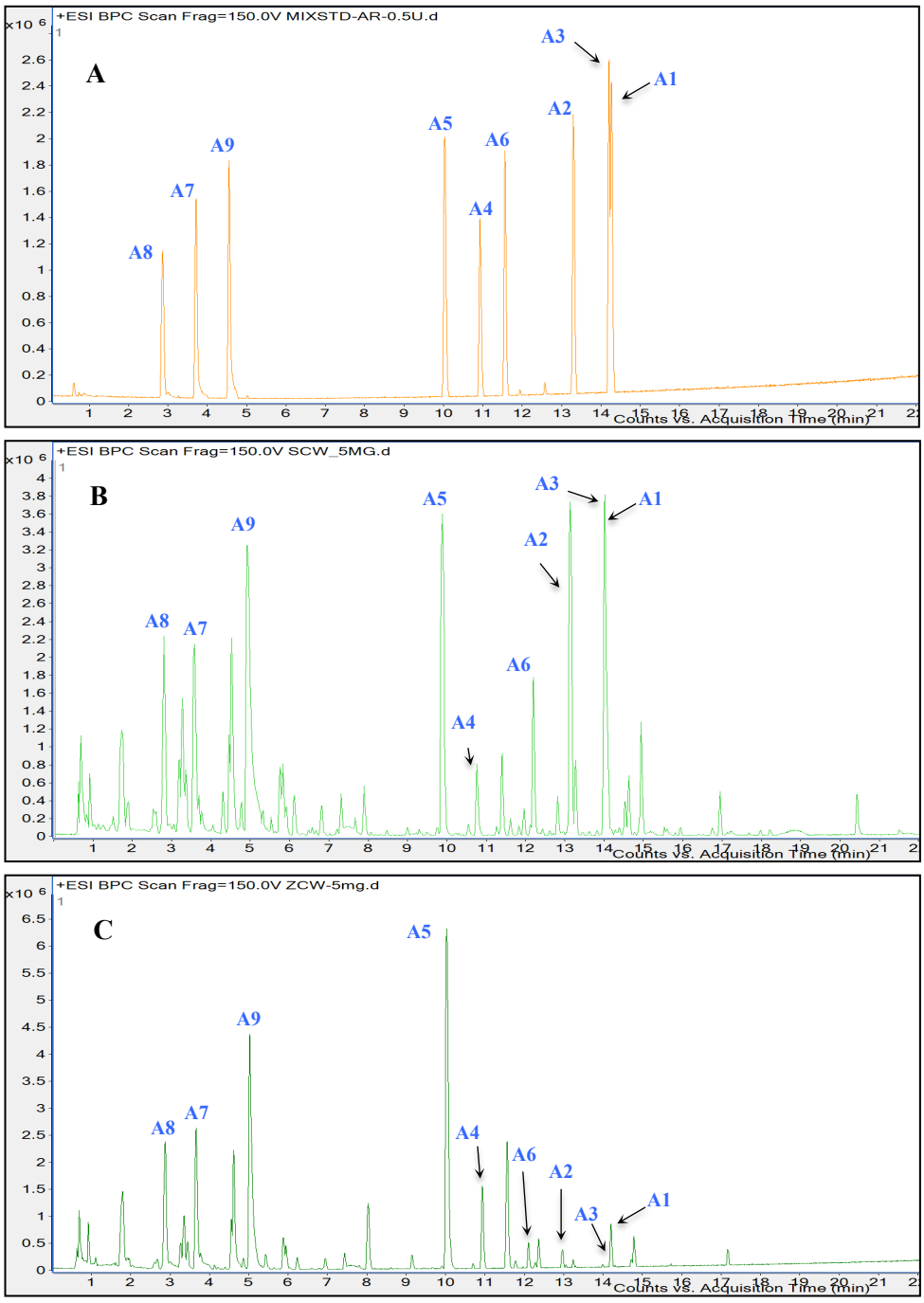

Fig. 3.1. BPCs of unprocessed and processed AR. (A) mix standards, (B) unprocessed AR and (C) processed AR. Alkaloid peaks: (A1) aconitine, (A2) mesaconitine, (A3) hypaconitine, (A4) benzoylaconine, (A5) benzoylmesaconine, (A6) benzoylhypaconine, (A7) aconine, (A8) mesaconine and (A9) hypaconine.

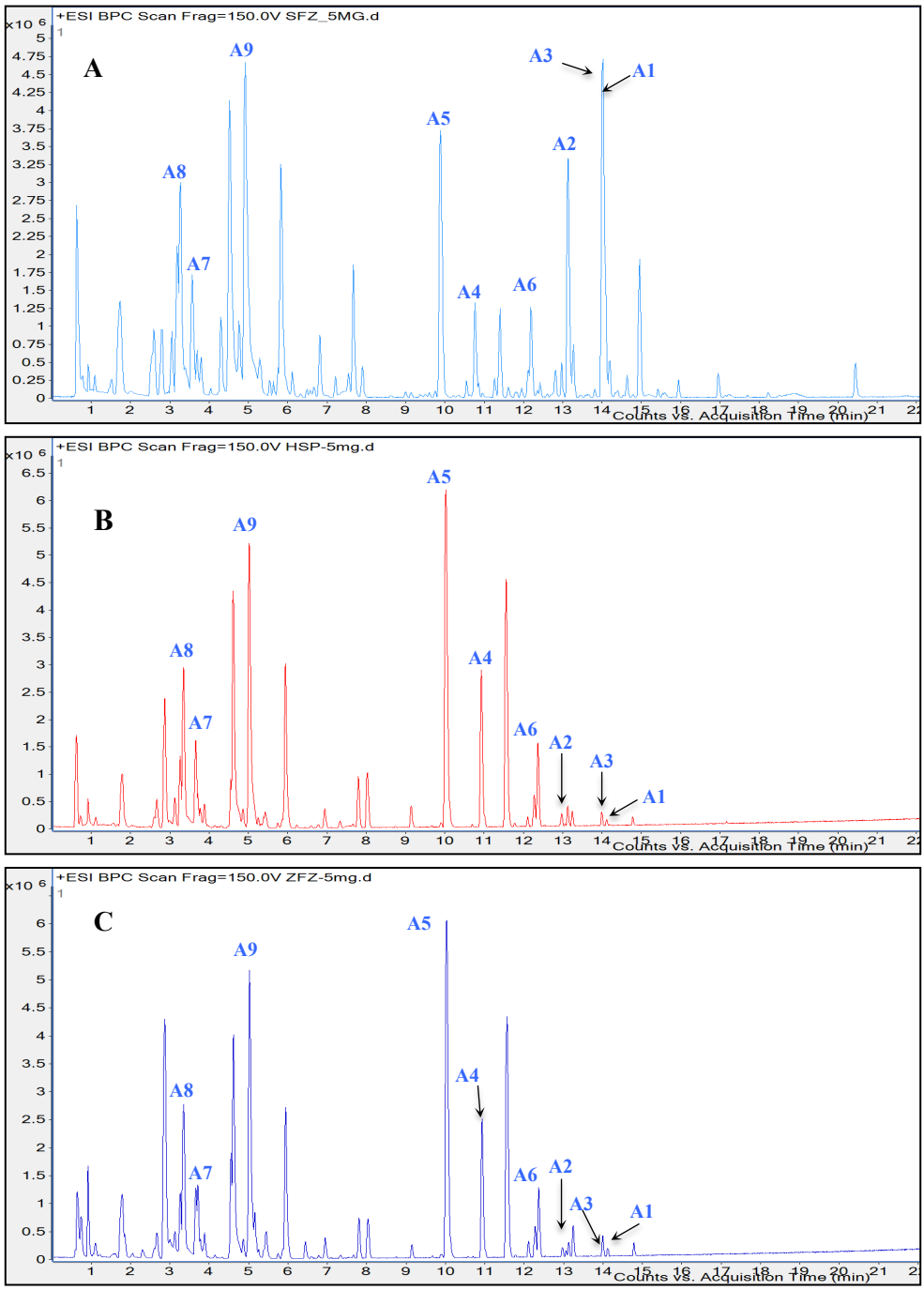

Fig. 3.2. BPCs of unprocessed and processed ALR. (A) Unprocessed ALR and two types of processed ALR: (B) HSP and (C) ZFZ. Alkaloid peaks: (A1) aconitine, (A2) mesaconitine, (A3) hypaconitine, (A4) benzoylaconine, (A5) benzoylmesaconine, (A6) benzoylhypaconine, (A7) aconine, (A8) mesaconine and (A9) hypaconine.

Fig. 3.3. EICs of nine alkaloids in unprocessed and processed AR and ALR. EICs were generated using exact masse of targeted compounds from positive mode of LC-MS for the quantitation of nine alkaloids (A1-A9) in unprocessed and processed AR and ALR, togarther with the retention time (RT), peak height and area, concentration of each alkaloid.

3.2. Effects of unprocessed and processed AR extracts on fibrogenesis

An ethanolic extract of unprocessed AR was previously suggested to have *in-vitro* pro-fibrotic activities at the concentrations of 20-80 μg/mL in the presence of TGF-β1 (66, 67). This *in-vitro* finding had important clinical implications as consumption of an ethanolic extract of *Aconitum* species has been reported to cause acute kidney injury (76). In addition, three cases of severe side effects of *Aconitum*-containing products has been reported, two cases suffered from acute poisonous effects and the third case developed chronic kidney failure and required dialysis (77). Before solid conclusions can be drawn, the potential pro-fibrotic effect of unprocessed AR must be reproducible in new batches of quality-assured herbal extracts. Furthermore, effect of unprocessed AR in the absence of TGF-β1 remains unknown. To answer these questions, aqueous and ethanolic extracts of unprocessed AR were examined in NRK-49F cells in the absence and presence of TGF-β1. As shown in **Fig. 3.4,** the aqueous and ethanolic extracts of unprocessed AR, with or without TGF-β1, did not affect fibrogenesis at the concentrations of 10-80 μg/mL, without inducing significant cell detachment.

Since AR has well known toxic effects, such as cardiotoxicity and neurotoxicity (125-127), unprocessed AR is never used as a medicinal material. According to the Chinese Pharmacopeia, only processed AR is allowed to be use legally, with great caution, as decoction pieces. It is important to examine whether detoxicating process procedure, known as Paozhi (68), could change its effects in *in-vitro* models of fibrosis. As shown in **Fig. 3.5** the aqueous and ethanolic extracts of processed AR did not affect fibrogenesis in the range of 10-80 μg/mL, with little cytotoxicity.

3.3. Effects of aconite alkaloids on fibrogenesis

To test the hypotheses that the previously reported potential pro-fibrotic activity of AR may be attributed to aconite alkaloids. Nine aconite alkaloids, i.e. (A1) aconitine, (A2) mesaconitine, (A3) hypaconitine, (A4) benzoylaconine, (A5) benzoylmesaconine, (A6) benzoylhypaconine, (A7) aconine, (A8) mesaconine, (A9) hypaconine, were tested in an *in-vitro* model of fibrosis. As shown in **Fig. 3.6**, all the nine alkaloids did not show any pro-fibrotic activities. On the contrary, seven of them, i.e. A1, A2, A5 A6, A7, A8 and A9, suppressed TGF-β1 induced fibrogenesis, without inducing significant cell detachment.

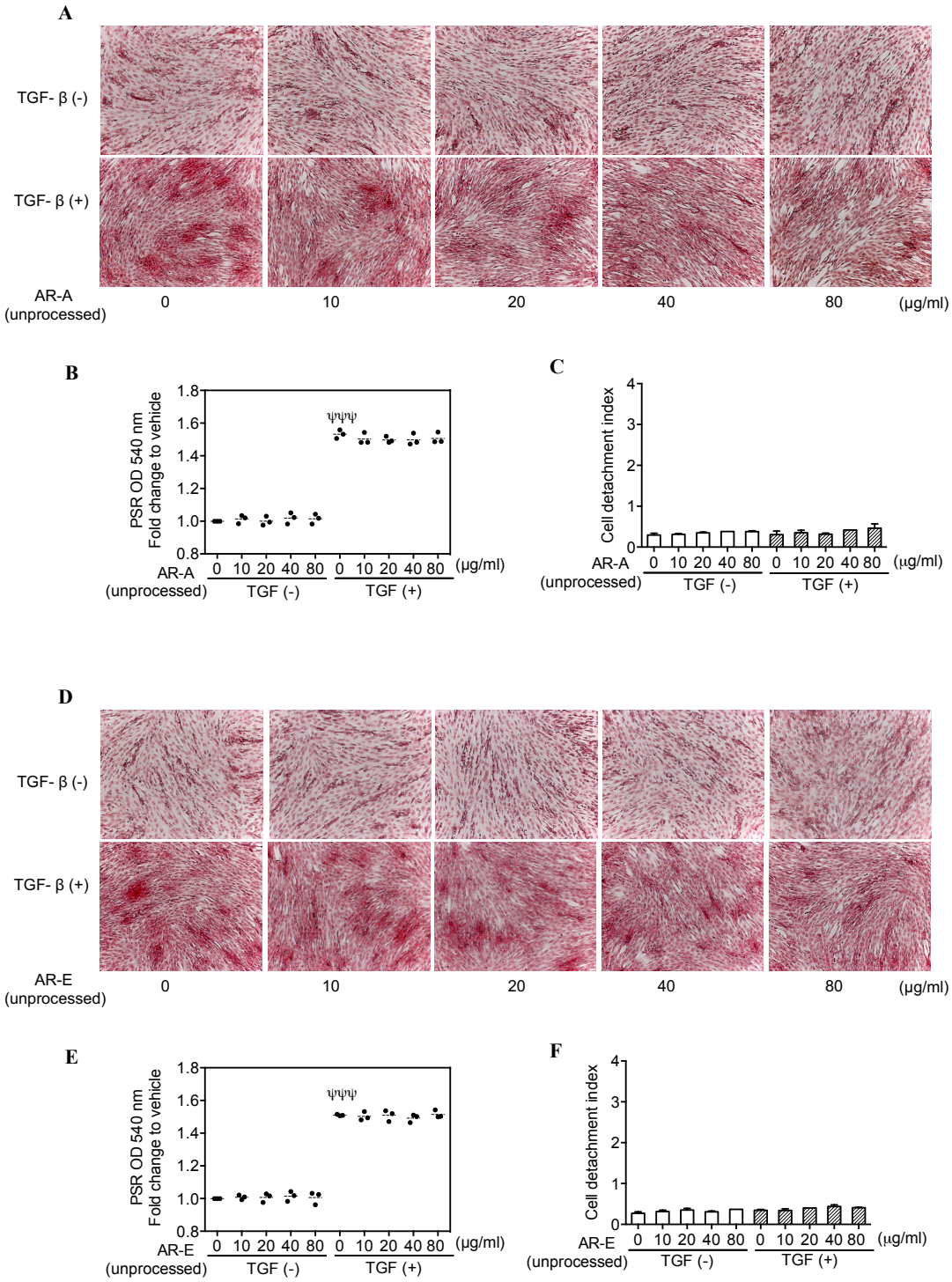

Fig. 3.4. Unprocessed AR aqueous (AR-A) and ethanolic (AR-E) extracts did not affect fibrogenesis. NRK-49F cells were treated with 10-80 μg/mL extracts of unprocessed AR with or without 5 ng/ml TGF-β1 for 48 h. Effects on fibrogenesis were illustrated by representative PSR staining images (A, D), which visualised total collagen deposition in red colour; eluted PSR was quantified by spectrophotometric analysis (B, E) and cytotoxicity was approximated by recording a mean cell detachment index (C, F). Experiments were performed in quadruplicate and repeated three times independently. ψψψ $p < 0.001$ *vs* control group.

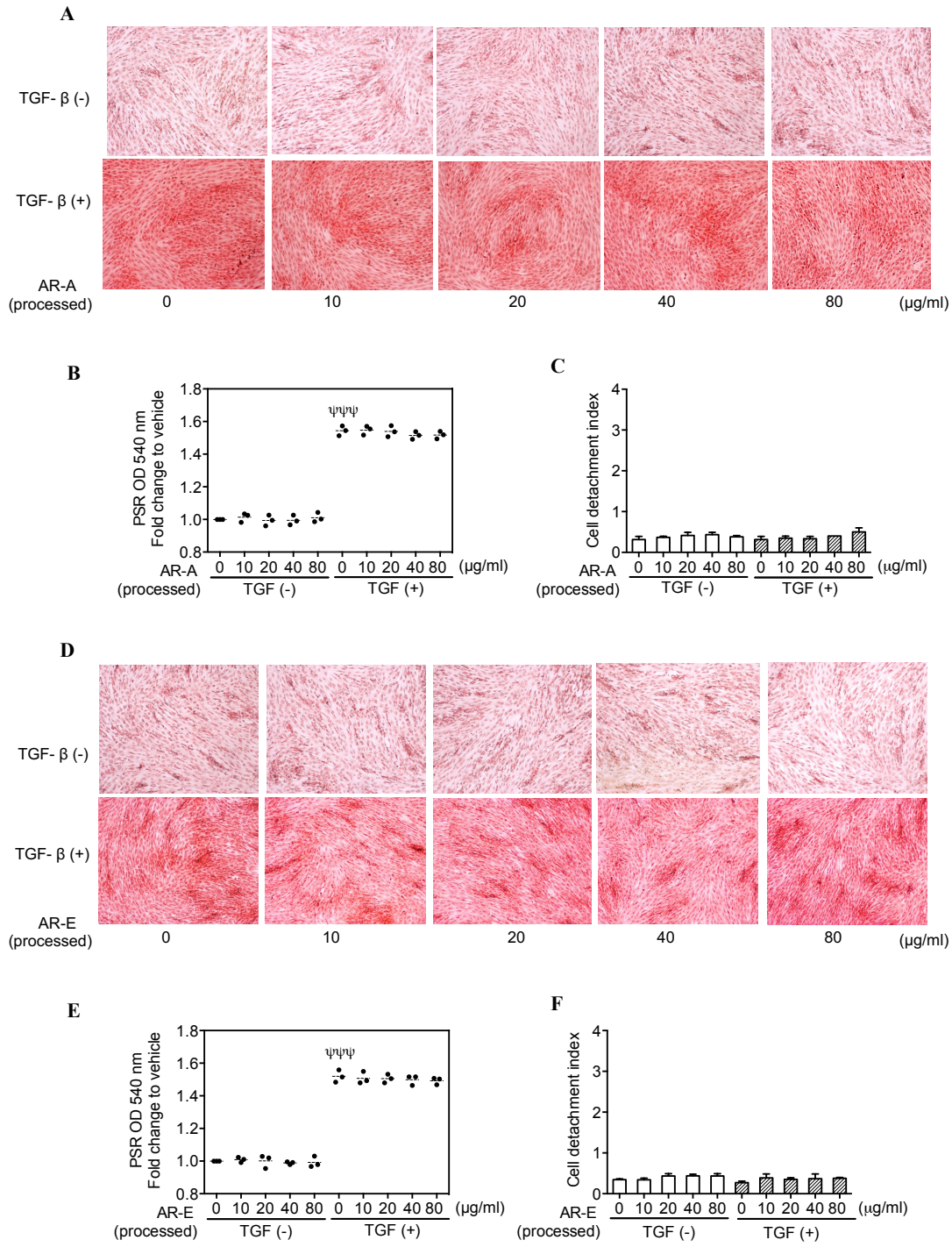

Fig. 3.5. Processed AR aqueous (AR-A) and ethanolic (AR-E) extracts did not affect fibrogenesis. NRK-49F cells were treated with 10-80 μg/mL extracts of processed AR with or without 5 ng/ml TGF-β1 for 48 h. Effects on fibrogenesis were illustrated by representative PSR staining images (A, D), which visualised total collagen deposition in red colour; eluted PSR was quantified by spectrophotometric analysis (B, E) and cytotoxicity was approximated by recording a mean cell detachment index (C, F). Experiments were performed in quadruplicate and repeated three times independently. ψψψ $p < 0.001$ *vs* control group.

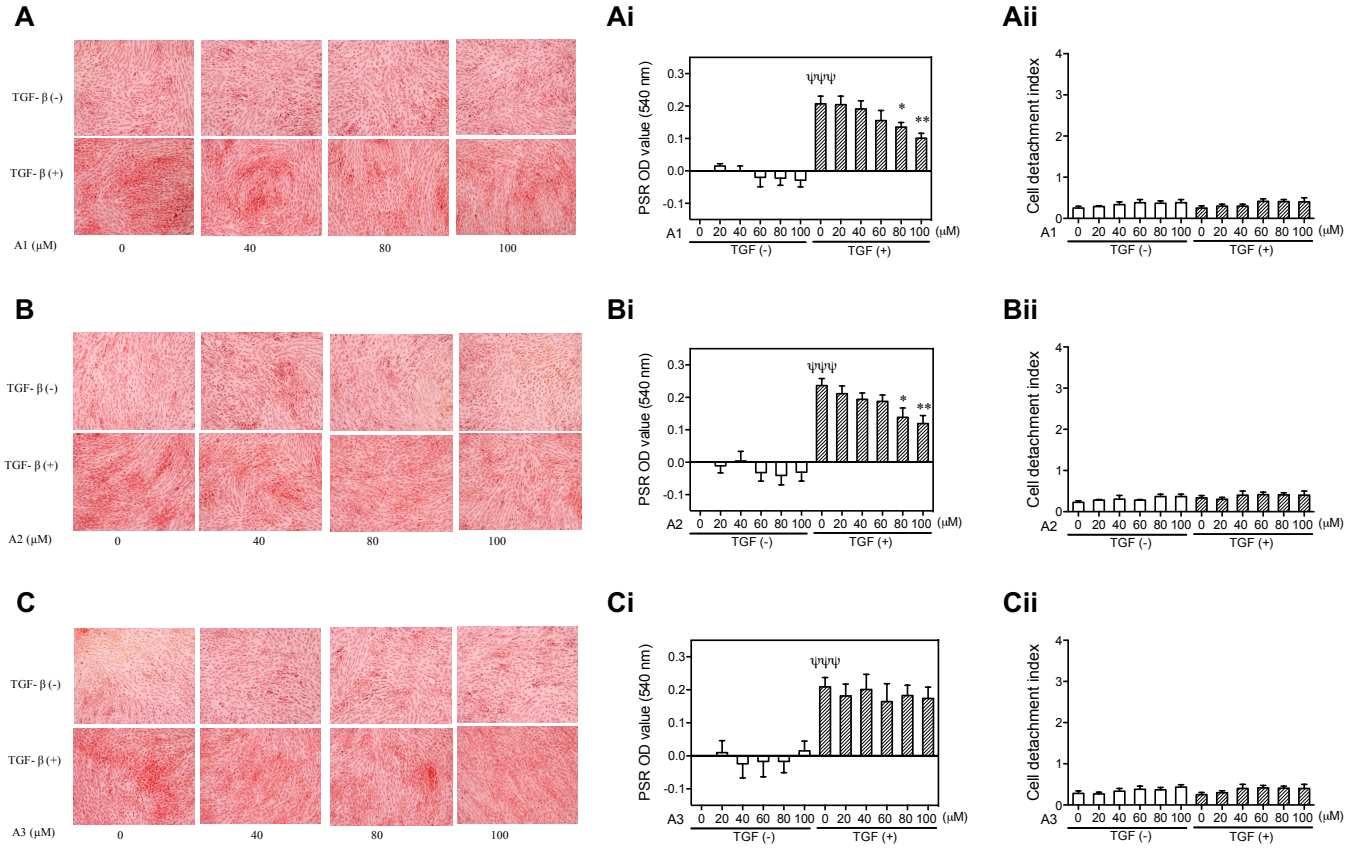

Fig. 3.6a. Alkaloids A1 and A2, but not A3, showed dose-dependent anti-fibrotic activities. NRK-49F cells were treated with 20-100 μM alkaloids (A1-A3) with or without 5 ng/ml TGF-β1 for 48 h. Effects on fibrogenesis were illustrated by representative PSR staining images (A-C), which visualised total collagen deposition in red colour; eluted PSR was quantified by spectrophotometric analysis (Ai-Ci) and cytotoxicity was approximated by recording a mean cell detachment index (Aii-Cii). Experiments were performed in quadruplicate and shown are representative results of two independent experiments with similar results. ψψψ $p < 0.001$ *vs* control group, * $p < 0.05$, ** $p < 0.01$ *vs* TGF-β1 treated group.

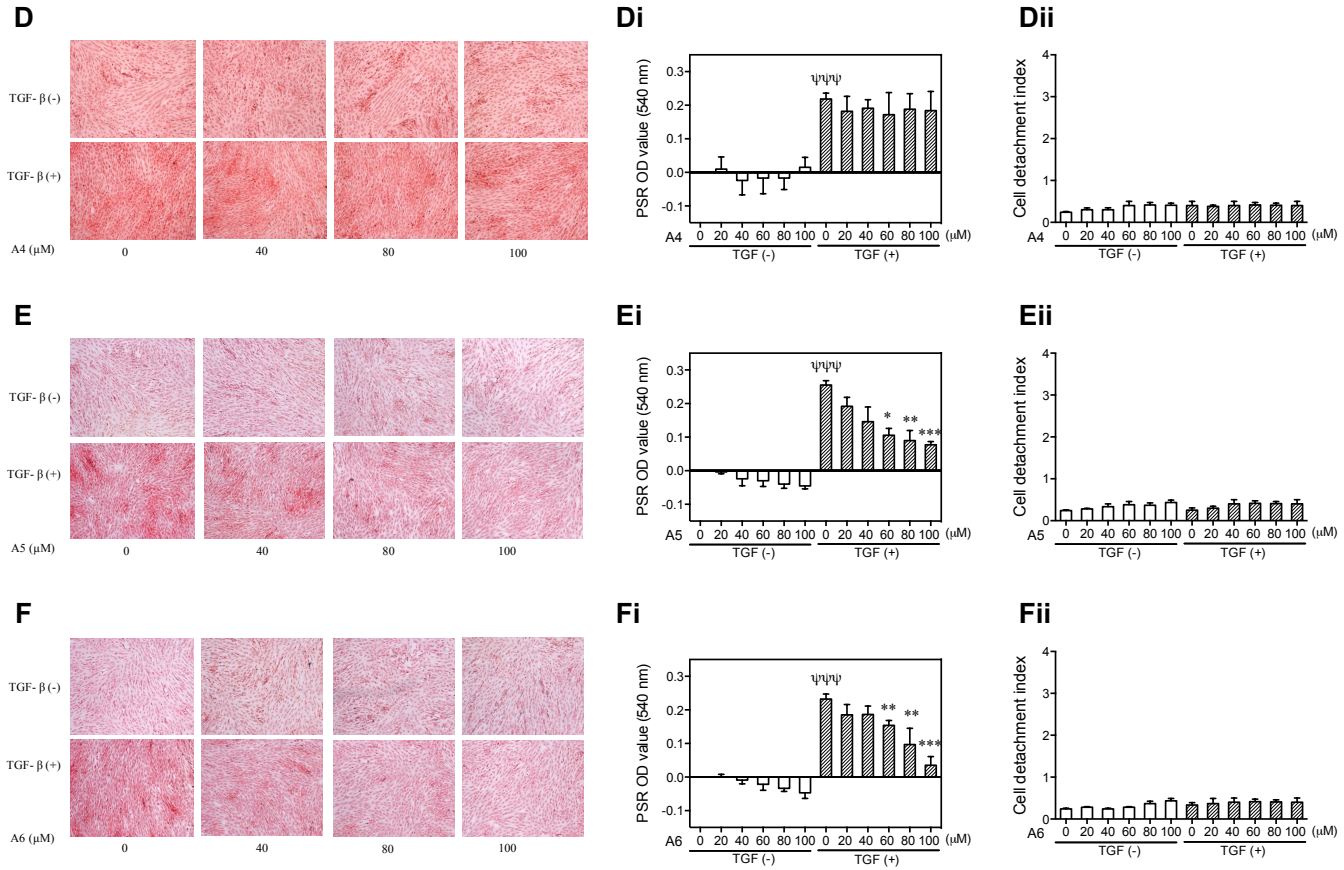

Fig. 3.6b. A5 and A6, but not A4, showed dose-dependent anti-fibrotic activities. NRK-49F cells were treated with 20-100 μM alkaloids (A4-A6) with or without 5 ng/ml TGF-β1 for 48h. Effects on fibrogenesis were illustrated by representative PSR staining images (D-F), which visualised total collagen deposition in red colour; eluted PSR was quantified by spectrophotometric analysis (Di-Fi) and cytotoxicity was approximated by recording a mean cell detachment index (Dii-Fii). Experiments were performed in quadruplicate and shown are representative results of two independent experiments with similar results. ψψψ $p < 0.001$ *vs* control group, * $p < 0.05$, ** $p < 0.01$, *** $p < 0.001$ *vs* TGF-β1 treated group.

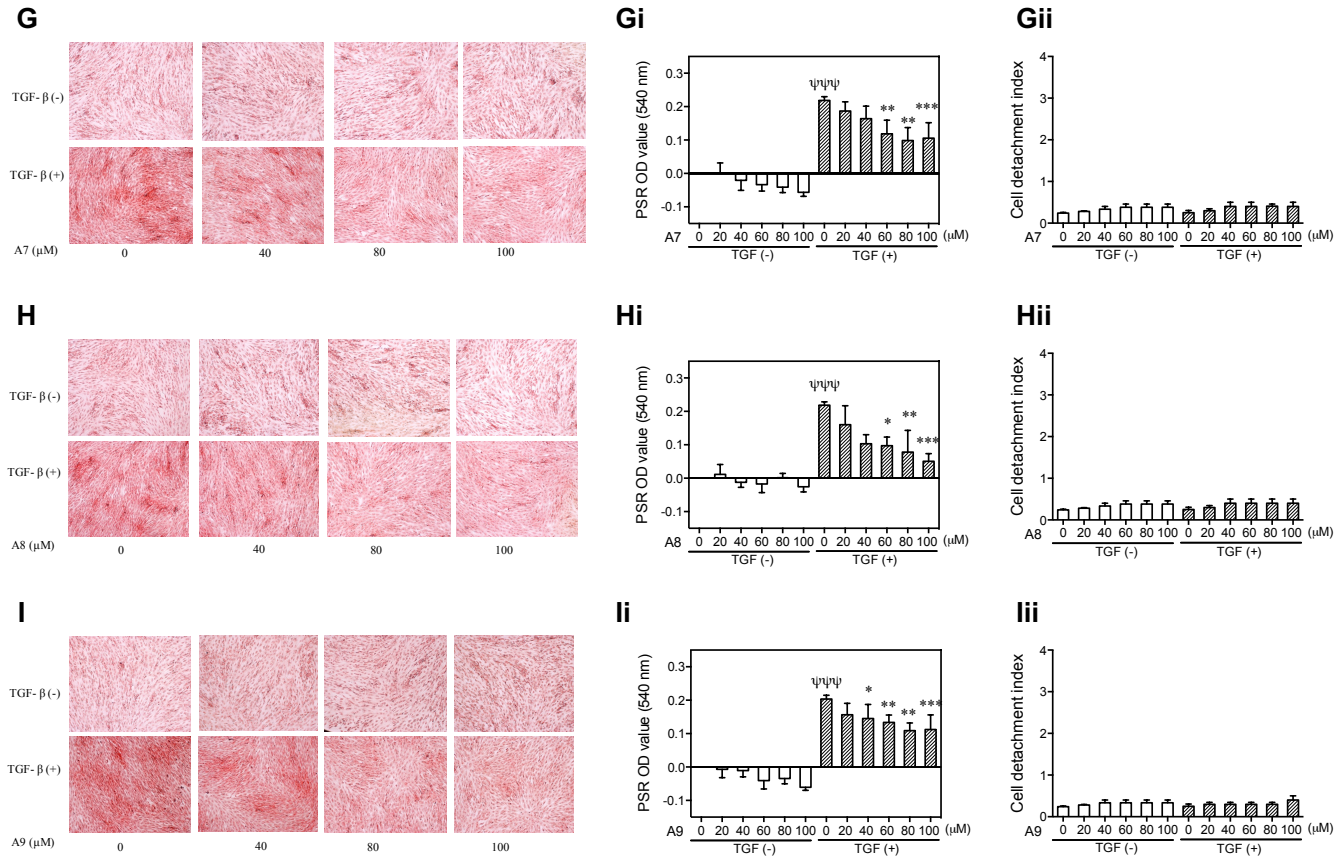

Fig. 3.6c. Alkaloids A7, A8 and A9 showed dose-dependent anti-fibrotic activities. NRK-49F cells were treated with 20-100 μM alkaloids (A7-A9) with or without 5 ng/ml TGF-β1 for 48 h. Effects on fibrogenesis were illustrated by representative PSR staining images (G-I), which visualised total collagen deposition in red colour; eluted PSR was quantified by spectrophotometric analysis (Gi-Ii) and cytotoxicity was approximated by recording a mean cell detachment index (Gii-Iii). Experiments were performed in quadruplicate and shown are representative results of two independent experiments with similar results. ψψψ $p < 0.001$ *vs* control group, * $p < 0.05$, ** $p < 0.01$, *** $p < 0.001$ *vs* TGF-β1 treated group.

3.4. Discussion and Conclusions

In a previous screening study, my supervisor's lab found an ethanolic extract of unprocessed AR was pro-fibrotic in NRK-49F cells in the presence of TGF-β1 (66, 67). In contrast, my data indicated that, in the same *in-vitro* model, aqueous and ethanolic extracts of unprocessed and processed AR, did not affect fibrogenesis, either in presence or absence of TGF-β1. It is in disagreement with the initial expectation that AR is pro-fibrotic. The most likely reason lies in the difference in the two batches of herbs tested, given that the *in-vitro* model of fibrosis used was the same. The quality control of herb AR used before was suboptimal, describing only based on herbal morphology thus less reliable. While the herb AR used in this project has been well authenticated and stringently quality-assured, as described in **Supplementary Fig. 1**. The further validations of these findings are still needed by testing additional well-authenticated batches of the same species and by alternative assays for total collagens and molecular markers of fibrogenesis.

In addition, I found that all these nine aconite alkaloids did not show any pro-fibrotic activities. On the contrary, seven of them, A1, A2, A5, A6, A7, A8 and A9 suppressed TGF-β1 induced fibrogenesis, as shown in **Fig. 3.6**.

Since the main poisonous and bioactive compounds of AR were believed to be aconite alkaloids, which mainly include diester-diterpene alkaloids (DDAs), monoester-diterpene alkaloids (MDAs) and unesterified-diterpene alkaloids (UDAs). Aconite alkaloids are also used as biomarkers to guide toxicological and pharmacological studies, and in quality control (68). The DDAs mainly include A1, A2, and A3, which are the most effective in treating diseases such as rheumatoid arthritis, cardiovascular diseases, tumors, skin wounds and diarrhea (69). However, DDAs also have the highest toxicity to the cardiovascular and nervous system, which limits the safe usage of AR and ALR in clinical therapeutics. DDAs can be firstly transformed into MDAs and then into UDAs through a second hydrolysis during processing as illustrated in **Fig. 1.3**, along with the toxicity is markedly decreased (69). The MDAs mainly comprise A4, A5 and A6, whereas the UDAs mainly include A7,

A8 and A9. In the present study, processing decreased the content of highly toxic A1, A2 and A3 by 92.8, 104.4 and 11.2 times compared to that in unprocessed AR.

Compared to unprocessed ALR, the contents of A1, A2 and A3 decreased 352.5, 617.2 and 155.0 times, 419.2, 970.0 and 1160.8 times, respectively, in two types of processed ALR, HSP and ZFZ. However, the activities of unprocessed and processed ALR extracts have not been tested in *in-vitro* model of fibrosis in the present study yet, because of the results so far do not support my initial hypothesis that the pro-fibrotic activity of AR/ALR could be attributed to aconite alkaloids. There is no report on anti-fibrotic effects of aconite alkaloids, but a school of traditional Chinese medicine (TCM), named "Huoshen Pai", are popular for its extensive but deliberated exploitation of processed ALR to treat deficiency of kidney *Yang*, coldness of the waist and the knees, dropsical limbs, difficulty in micturition, or phlegm and retained fluid (69). This may be explained by TCM theory that ALR has the properties to "warm up" and "resolve" clots and lumps, which are often classified into fibrosis diseases.

Nevertheless, there is ongoing controversy because of the severe toxicity of ALR once used at inappropriate dosages. The poisoning related to the culinary use of AR and ALR also have been reviewed (128). Severe or even fatal aconite alkaloid poisoning can occur after consumption of herbal soups and foods prepared from AR or ALR. Even prolonged boiling time may not be protective if raw preparations and large quantities of AR or ALR are used. It indicated that the public should be warned of the risk of severe poisoning related to the culinary and traditional medicinal uses of AR and ALR.

In conclusion, the present results disagreed with my initial hypothesis that AR is pro-fibrotic as a function of its alkaloids:

- Aqueous and ethanolic extracts of unprocessed and processed AR did not affect fibrogenesis (**Fig. 3.4 and Fig. 3.5**).
- Seven of nine aconite alkaloids showed anti-fibrotic effects (**Fig. 3.6)**.

- Further validation of these results will be needed.

In view that expected pro-fibrotic effects of AR was not reproduced and considering the limited time, I decided to focus on SR and its flavonoids in the rest of my project.

Chapter 4 *In-vitro* anti-fibrotic activities of SR and SR flavonoids

4.1. Quality control of SR extracts

Contents of the five interested flavonoids (F5), i.e. baicalin, baicalein, wogonoside, wogonin and oroxylin-A, in aqueous and methanolic extracts of SR were evaluated by UPLC/Q-TOF-MS and the BPCs and EICs are presented in **Fig. 4.1** and **Fig. 4.2**. It can be found that on the BPCs the mixed standards of the F5 were already well separated with short analysis time (**Fig. 4.1**). For analysis of SRA and SRM, the F5 also reached the baseline separation with high resolution. In addition, due to the high selectivity of UPLC/Q-TOF-MS, the peak areas of F5 can be integrated much simpler and more accurate on the EICs (**Fig. 4.2**).

As a result, the total content of F5 in SRM (22.71%) is 8 times higher than SRA (2.77%). The content of each calculated flavonoid was much more abundant in the SRM than SRA, especially baicalin, which was about 12 times more abundant in SRM. Nevertheless, in both SRA and SRM, baicalin was the most abundant among the F5, followed by wogonoside (**Table 4.1**).

Table 4.1. Percent contents of F5 in SRA and SRM.

Contents (%)	**SRA**	**SRM**	**SRA-F5**	**SRA-F5D**	**SRM-F5**	**SRM-F5D**
Baicalin	1.1283	14.0509	2.7761	0.0330	5.9003	0.0992
Oroxylin-A	0.1400	2.7523	1.0942	0.0781	4.7061	0.0517
Wogonoside	0.8230	3.3455	6.5471	0.1187	3.1387	0.0320
Baicalein	0.5470	2.0571	0.1222	0.0072	0.0294	0.0032
Wogonin	0.1353	0.5007	0.0093	0.0008	0.0078	0.0368
Total (%)	2.7736	22.7065	10.5489	0.2378	13.7823	0.2229

Note: SRA-F5: “F5 fraction” of SRA; SRA-F5D: “F5-depleted fraction” of SRA; SRM-F5: “F5 fraction” of SRM; SRM-F5D: “F5-depleted fraction” of SRM.

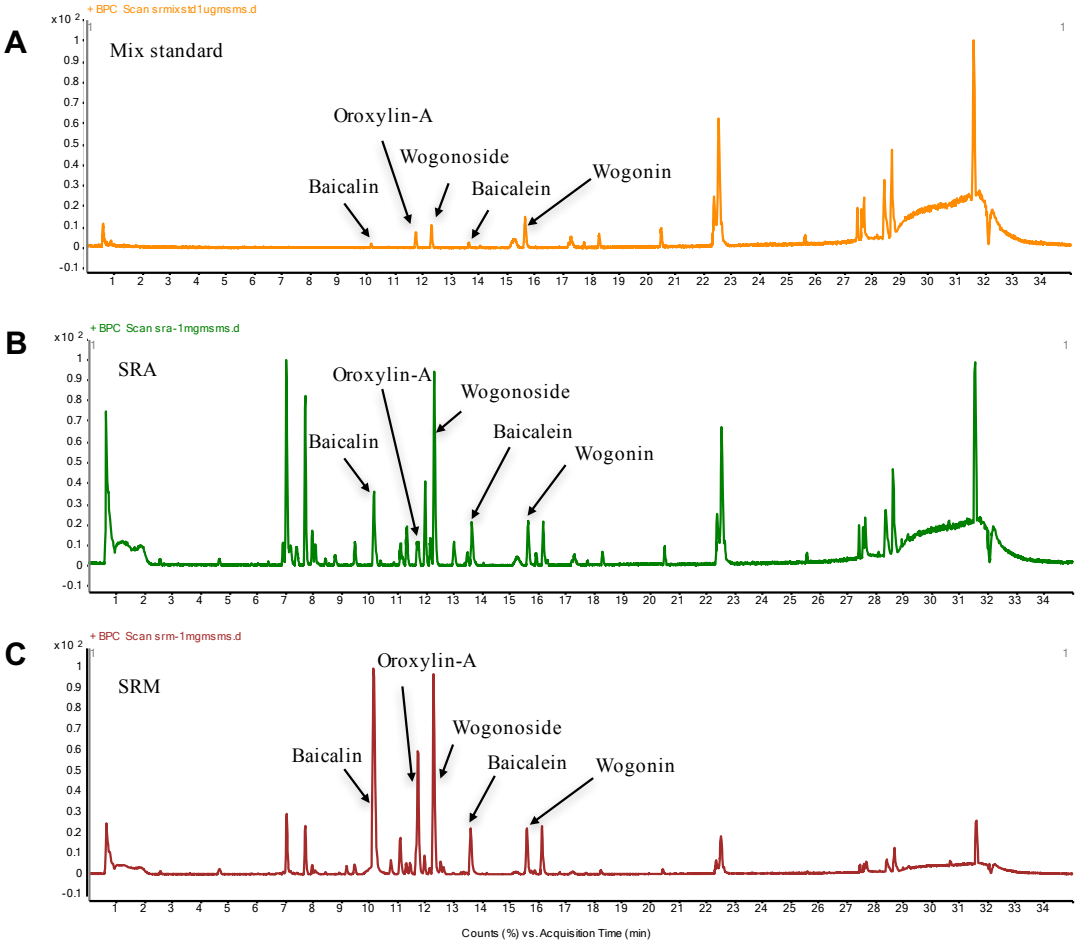

Fig. 4.1. BPCs of SRA and SRM. (A) mixed F5 standards, (B) SRA and (C) SRM. 85 g SR powder was simmered in 600 mL Milli-Q water (for extracting SRA) or 70% methanol (for extracting SRM) for 2 h under reflux on electric heating-jacket, cool and filter. Extracts were dried under vacuum freeze and stored at -20 °C until use. Extracts were dissolved in 100% methanol to 1 mg/mL prior to UPLC-QTOF MS analysis.

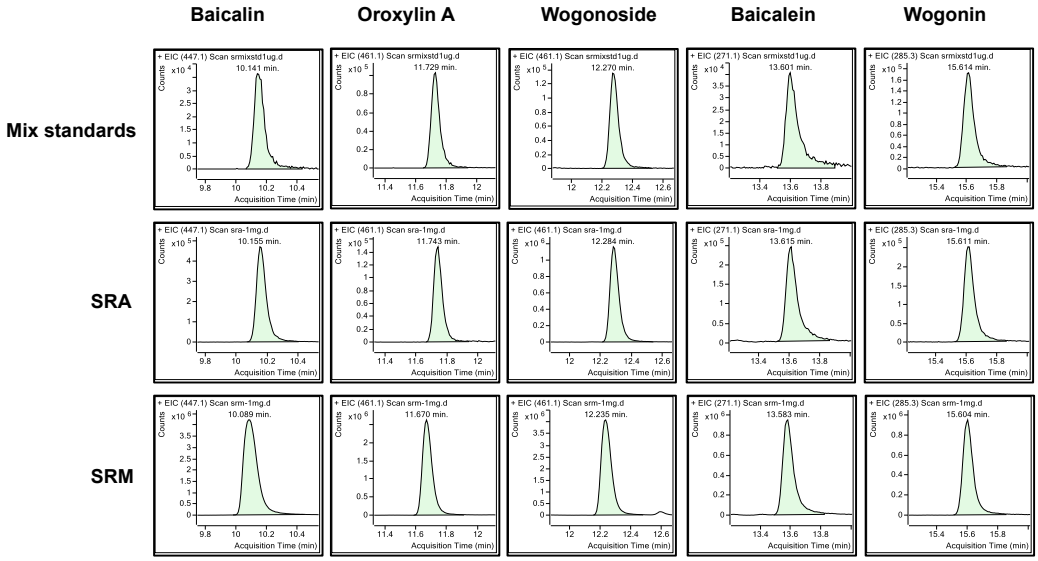

Fig. 4.2. EICs of F5 in SRA and SRM. EICs were generated using exact masse of targeted compounds from positive mode of LC-MS for the quantitation of F5 in SRA and SRM.

Contents of F5 in the "F5 fraction" and the "F5-depleted fraction" from SRA and SRM were evaluated by UPLC-Q/TOF-MS and BPCs are presented in **Fig. 4.3** and **Fig 4.4**. The percent contents of the F5 in the "F5 fraction" and the "F5-depleted fraction" of SRA and SRM are listed in **Table 4.1**. The F5 were separated from both SR extracts and were detected in "F5 fractions" along with several unknown peaks, as shown in **Fig. 4.3 C** and **Fig. 4.4 C**, indicating that the "F5 fractions" separation were not pure. Double isolation and separation of "F5 fractions" were unsuccessful due to current technical difficulties. Thus, the "F5 fractions" and "F5-depleted fractions" will not be used for further tests as they are unable to address the hypothesis whether F5 are the main contributors to the anti-fibrotic activities of SR, given their poor purity.

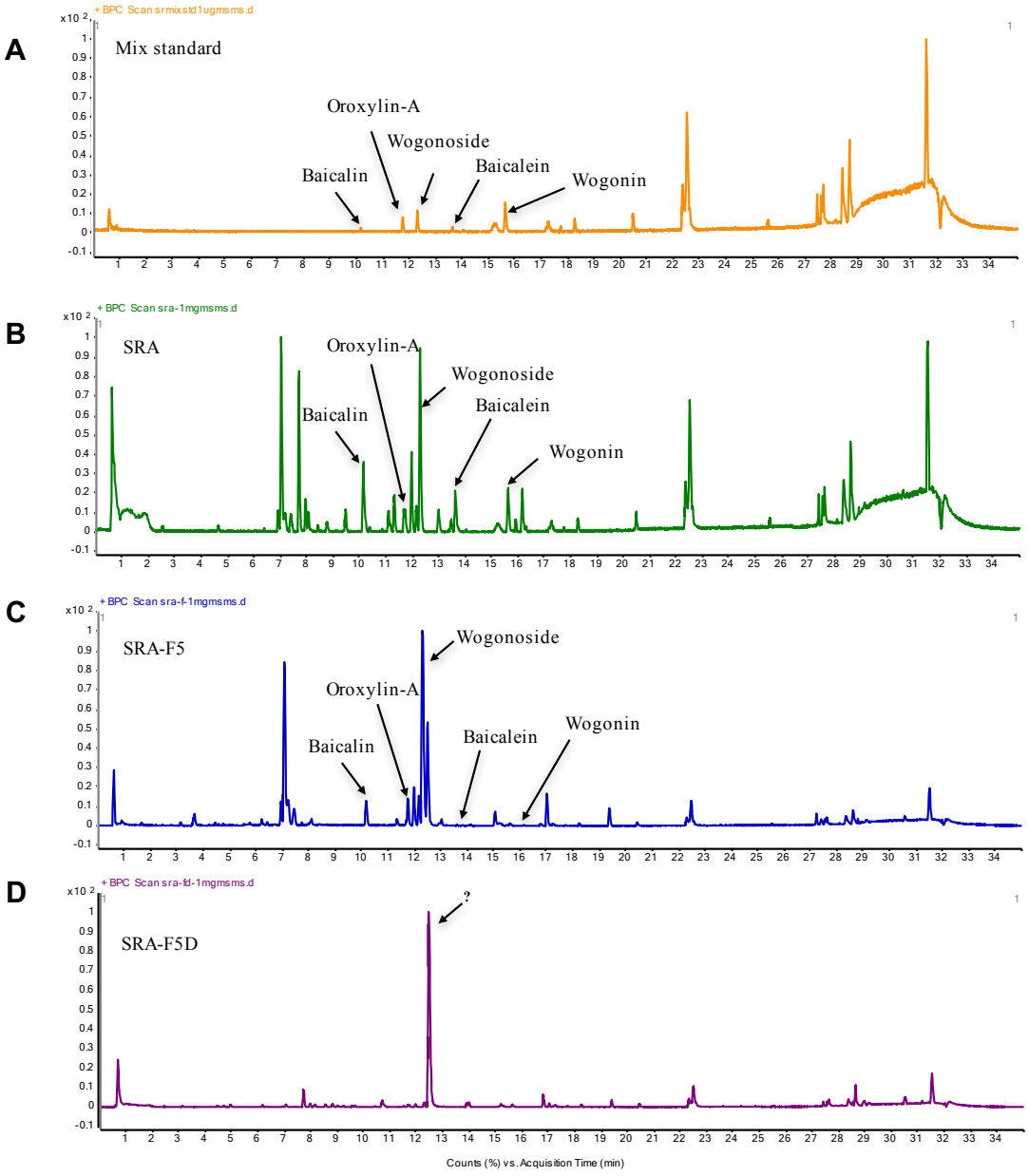

Fig. 4.3. BPCs of the "F5 fraction" (SRA-F5) and "F5-depleted fraction" (SRA-F5D) of SRA. Freeze-dried powder of SRA (110.6 mg) were dissolved in 5 mL methanol and separated by preparative liquid chromatography. Fractions were dried under vacuum freeze and dissolved in methanol to 1 mg/mL prior to UPLC-Q/TOF-MS analysis.

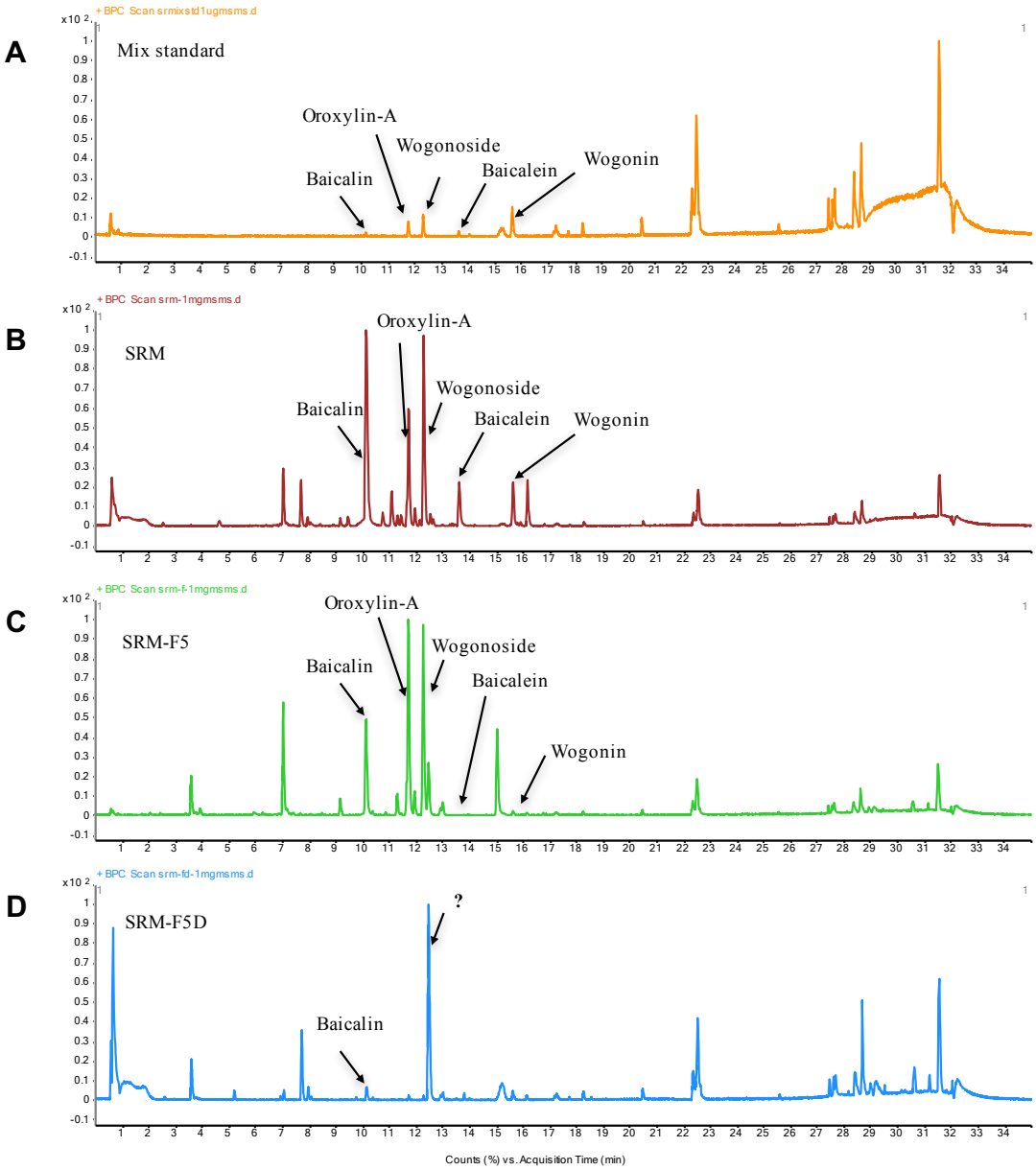

Fig. 4.4. BPCs of the "F5 fraction" (SRM-F5) and the "F5-depleted fraction" (SRM-F5D) of SRM. Freeze-dried powder of SRM (142.4 mg) were dissolved in 5 mL methanol and separated by preparative liquid chromatography. Fractions were dried under vacuum freeze and dissolved in methanol to 1 mg/mL prior to UPLC-Q/TOF-MS analysis.

4.2. Anti-fibrotic activities of SR extracts in an *in-vitro* model of fibrosis

SRA and SRM at concentrations of 20-80 µg/mL were tested in an *in-vitro* model of fibrosis. The concentrations of SR extracts were chosen based on published data (66). As shown in

Fig. 4.5, 80 μg/mL SRA and 40, 60 and 80 μg/mL SRM significantly reduced TGF-β1-induced total collagen deposition as quantified by PSR staining, without significantly increasing cell detachment index (**Fig. 4.5 E, F**).

In view that PSR stain of collagens might not be 100% specific, further validation was put in place by QuickZyme total collagen assays. This is the most common method for evaluating collagen deposition or tissue fibrosis by hydroxyproline quantification. NRK-49F cells were treated with 80 μg/mL SR extracts with 5 ng/ml TGF-β1 for 48 h and the total collagen were indirectly measured through hydroxyproline content from cell lysates. As shown in **Fig. 4.6**, at 80 μg/mL SRM, but not SMA, significantly reduced TGF-β1-induced total collagen accumulation in cell lysates.

To further confirm the anti-fibrotic actives of SR extracts at the molecular level, the effects of 80 μg/mL SRA or SRM on TGF-β1-induced collagen type I, collagen type III, α-SMA and fibronectin was investigated. As expected, immunostaining and high-content imaging analysis revealed that TGF-β1 significantly increased collagen I, collagen III, α-SMA and fibronectin, SRM was more potent in suppressing those molecular markers of fibrogenesis than SRA (**Fig. 4.7**).

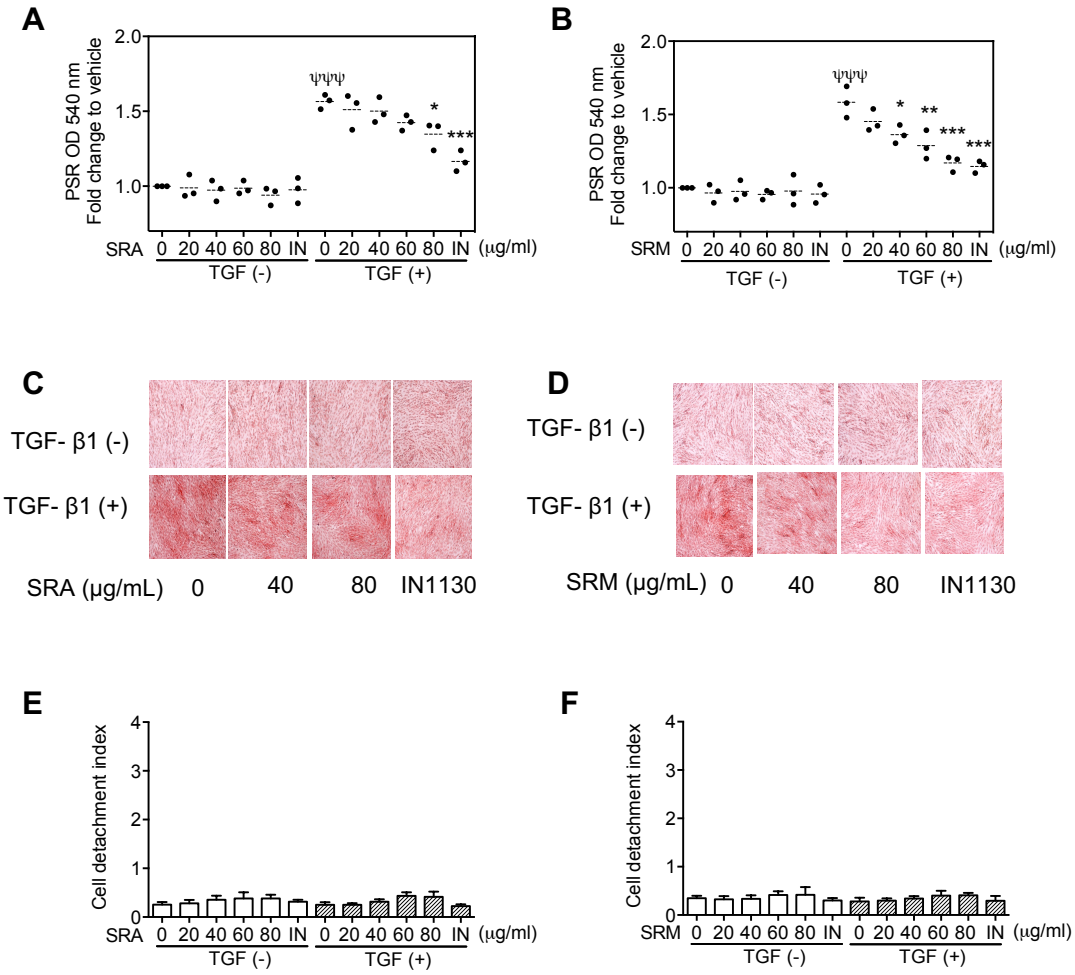

Fig. 4.5. SRA and SRM extracts inhibited fibrogenesis in an in-vitro model of fibrosis induced by TGF-β1. NRK-49F cells were treated with 20-80 μg/mL SR extracts or 1 μM IN1130 (IN) with or without 5 ng/ml TGF-β1 for 48 h. Effects on fibrogenesis were quantified using eluted PSR by spectrophotometric analysis (A, B) and illustrated by representative PSR staining images (C, D), which visualised total collagen deposition in red colour; and cytotoxicity was approximated by recording a mean cell detachment index (E, F). Experiments were performed in quadruplicate and repeated for three times with similar results. ψψψ $p < 0.001$ *vs* control group; * $p < 0.05$, ** $p < 0.01$, *** $p < 0.001$ *vs* TGF-β1 group.

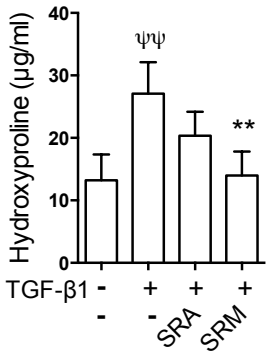

Fig. 4.6. At 80 µg/mL, SRM, but not SRA, significantly inhibited TGF-β1-induced total collagen accumulation in NRK-49F cells. The total collagen in cell lysates was quantified indirectly through hydroxyproline content in NRK-49F cells, which were treated with 80 µg/mL extracts and/or 5 ng/ml TGF-β1 for 48 h. Experiments were performed in quadruplicate (four wells of cells per group). ψψ p <0.01 *vs* control; ** p <0.01 *vs* TGF-β1 treated group.

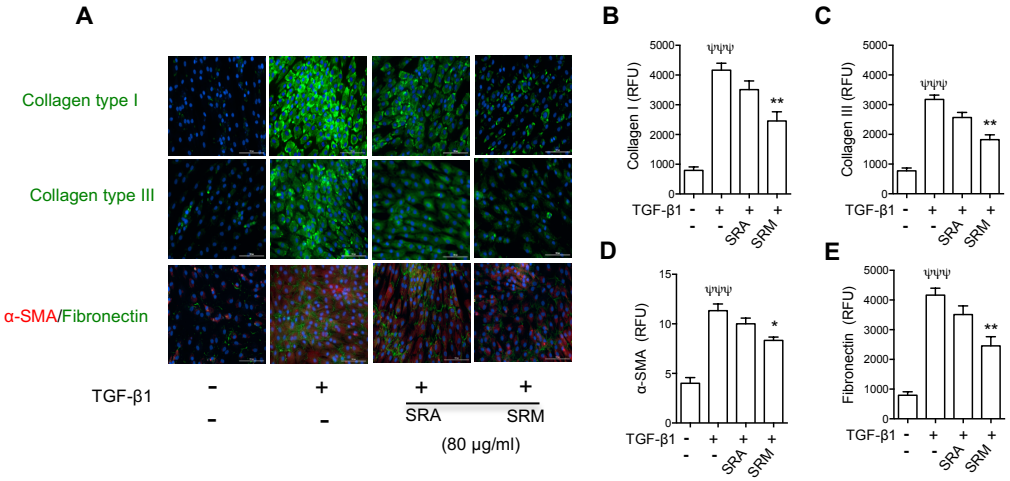

Fig. 4.7. 80 µg/mL SRM, but not SRA, significantly down-regulated TGF-β1-induced collagen type I, collagen type III, α-SMA and fibronectin in NRK-49F cells. Immunocytofluorescence analysis was used to visualise (A) and quantify (B-E) fibrotic makers in cells treated with 80 µg/ml SR extracts in the presence of 5 ng/ml TGF-β1 for 48 h. Fluorescence intensity was measured on a Cytation 5 Multi-mode Reader (BioTek) and expressed in relative fluorescence units (RFU)/well. Experiments were performed in triplicate (three wells of cells per group) and repeated twice with similar results. Shown are representative results of an independent biological study. ψψψ p <0.001 *vs* control; * p <0.05, ** p <0.01 *vs* TGF-β1 treated group.

4.3. Anti-fibrotic activities of SR flavonoids in an *in-vitro* model of fibrosis

As shown in **Fig. 4.8**, baicalin and baicalein showed *in-vitro* anti-fibrotic activities, this confirmed earlier reports from my supervisor's laboratory (66). Also, anti-fibrotic activities of three additional main flavonoids rich in SR, wogonoside, wogonin, and oroxylin-A, were tested but only 80 μM wogonin showed *in-vitro* anti-fibrotic activities, suppressing total collagen deposition (**Fig. 4.8 I)**. While 80 μM baicalin and wogonin showed good anti-fibrotic effects, these concentrations were cytotoxic (**Fig. 4.8 K and N and Fig. 4.9 B)**.

Baicalein appeared to present the best dose-dependent manner as shown in **Fig. 4.8**, showing the best anti-fibrotic activity. Thus, hydroxyproline quantification was further used as a complementary method to measure the total collagen content. NRK-49F cells were treated with 60 μM flavonoids in presence of 5 ng/ml TGF-β1 for 48 h. Cell lysates were harvested for measurement of hydroxyproline content and LDH release, respectively. Baicalein most significantly inhibited total collagen accumulation (**Fig. 4.9 A**), with little cytotoxicity (**Fig. 4.9 B**). However, baicalin and wogonin showed relatively strong LDH release at the concentration of 60 μM, which was consistent with the results of cell detachment index (**Fig. 4.8 K and N)**, suggesting baicalin and wogonin had relatively higher cytotoxicity.

To measure the anti-fibrotic activity of SR flavonoids at the molecular level, further validation was done by image analysis of immunofluorescence staining to quantify molecular makers of fibrogenesis. As shown in **Fig. 4.10**, at the concentration of 60 μM, five SR flavonoids down-regulated TGF-β1-induced collagen type I, collagen type III, α-SMA and fibronectin expression in NRK-49F cells. Among the five flavonoids, baicalein was among the most potent in supressing collagen type I, collagen type III and α-SMA accumulation (**Fig. 4.10A-D**). Interestingly the five flavonoids seemed to have similar effects in supressing fibronectin (**Fig. 4.10E)**.

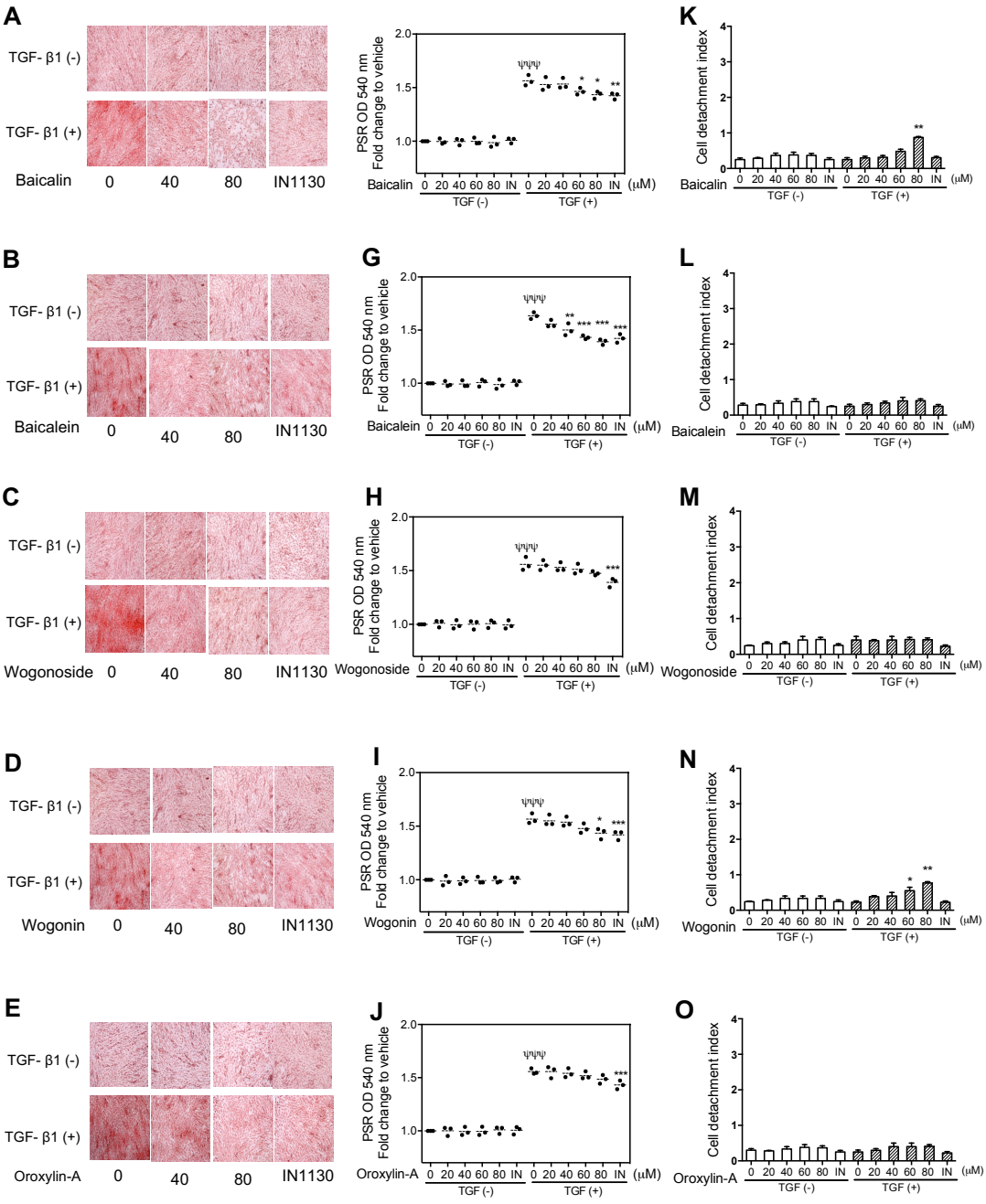

Fig. 4.8. Among F5, baicalin and baicalein were the most potent in inhibiting fibrogenesis in the presence of TGF-β1. NRK-49F cells were treated with 20-80 μM flavonoids or 1μM IN1130 (IN) with or without 5ng/ml TGF-β1 for 48 h. Effects on fibrogenesis were illustrated by representative PSR staining images (A-E), which visualised total collagen deposition in red colour; eluted PSR was quantified by spectrophotometric analysis (F-J) and cytotoxicity was approximated by recording a mean cell detachment index (K-O). Experiments were performed in quadruplicate and repeated three times independently. ψψψ $p < 0.001$ *vs* control group; * $p < 0.05$, ** $p < 0.01$, *** $p < 0.001$ *vs* TGF-β1 treated group.

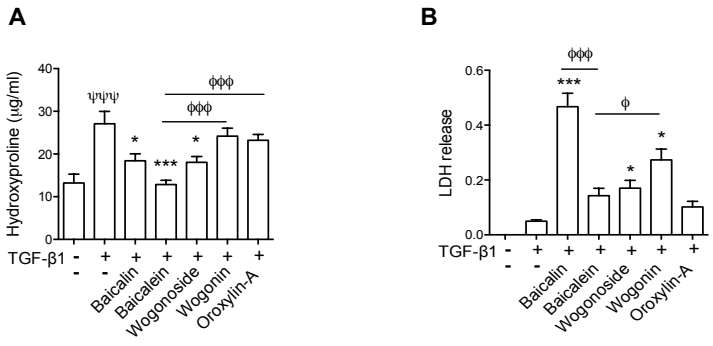

Fig. 4.9. Among 60 μM F5, baicalein showed the best anti-fibrotic activity and little cytotoxicity. NRK-49F cells were treated with 60 μM flavonoids in presence or absence of 5 ng/ml TGF-β1 for 48 h. (A) Total collagen accumulation was quantified indirectly through hydroxyproline content; (B) cytotoxicity was measured by LDH release from cells. Experiments were performed in quadruplicate and repeated for three times with similar results. ψψψ p <0.001 *vs* control group; * p < 0.05, *** p < 0.001 *vs* TGF-β1 treated group, Φ p <0.05, ΦΦΦ p <0.001 *vs* baicalein treated group).

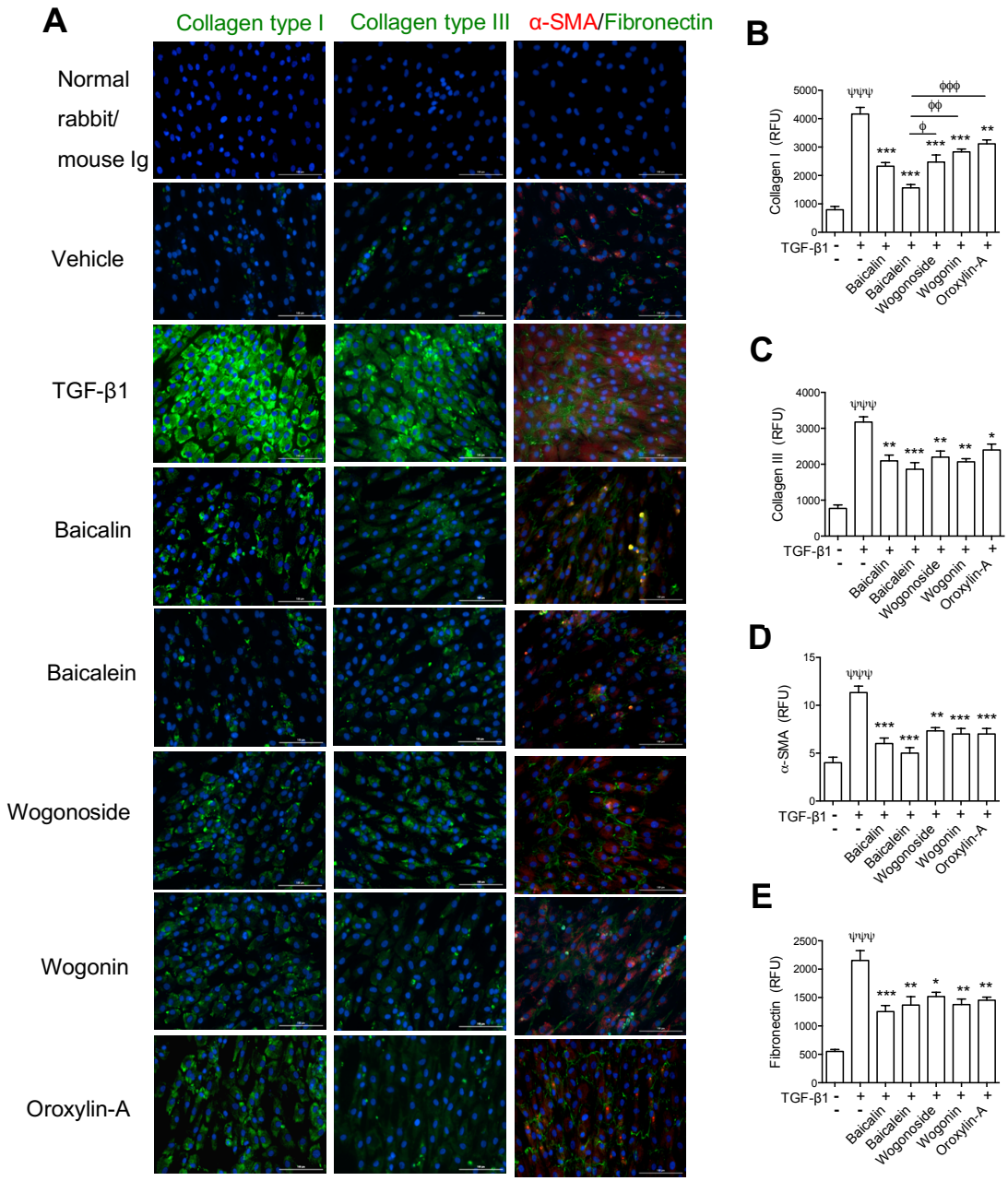

Fig. 4.10. 60 µM F5 down-regulated TGF-β1-induced collagen type I, collagen type III, α-SMA and fibronectin in NRK-49F cells. Immunocytofluorescence analysis was used to visualise (A) and quantify (B-E) fibrotic makers in cells treated with 60 µM flavonoids in the presence of 5 ng/ml TGF-β1 for 48 h. Fluorescence intensity was measured on a Cytation-5 Multi-mode Reader (BioTek) and expressed in relative fluorescence units (RFU)/well. Experiments were performed in triplicate (three wells of cells per group) and repeated twice with similar results. Shown are representative results of an independent biological study. ψψψ $p < 0.001$ *vs* control, * $p < 0.05$, ** $p < 0.01$, *** $p < 0.001$ *vs* TGF-β1 treated group, Φ $p < 0.05$, ΦΦΦ $p < 0.001$ *vs* baicalein treated group).

4.4. Discussions and Conclusions

The reported findings of my supervisor's group that SRM, baicalin and baicalein had *in-vitro* anti-fibrotic activities have been successfully reproduced in the present study. The activities have also been confirmed by others both *in vitro* and *in vivo* (98, 114, 118). I further demonstrated that SRA was less anti-fibrotic than SRM, and the other three members of the F5 (wogonoside, wogonin and oroxylin-A) were less anti-fibrotic than baicalin and baicalein. Although the effects of SRA and oroxylin-A on fibrosis have not been reported previously, some recent reports did show anti-fibrotic effects of wogonoside in a liver fibrosis animal model (119). In addition, wogonin showed anti-fibrotic effects in renal tubular epithelial cell (129).

According to chemical profiling analysis, the total content of F5 in SRM (22.71%) is more than 8 times higher than in SRA (2.77%, **Table 4.1**), and SRM is more potently anti-fibrotic than SRA (**Fig. 4.6 and 4.7**). These results support my hypothesis that flavonoids may mainly contribute to the anti-fibrotic effects of SR. In collaboration with Professor Zhongzhen Zhao's laboratory at Hong Kong Baptist University, we tried to deplete F5 from the SRA and SRM and then determine whether flavonoids-depleted fractions have significantly reduced anti-fibrotic activity. Unfortunately, separation of F5 lacked specificity and efficiency (**Fig 4.3** and **Fig. 4.4**), thus I cannot be certain that non-flavonoids in SRA and SRM do not contribute to their anti-fibrotic activities.

Please note that, this study aimed to identify the most promising SR extract and SR-derived flavonoid for further proteomic studies, taking into consideration of both antifibrotic activities and cytotoxicity at the same concentrations. My data were sufficient to conclude that SRM was better than SRA, while baicalein was the best choice among the F5. I acknowledge that, my current data were not sufficient to reliably quantify the IC50 for SRA, SRM and F5, which will need to test more concentrations for each extract and compound in

non-cytotoxic concentrations. This can be done in the future, but is beyond the scope of this project.

In conclusion, SRM and baicalein have been selected for further proteomics-guided mechanistic studies, which will be described in the next chapters.

Chapter 5 Proteomics of TGF-β1-induced *in-vitro* model of fibrosis

In previous studies, a TGF-β1-induced *in-vitro* model of fibrosis has been established in NRK-49F normal rat kidney fibroblasts in my supervisor's lab (65, 66, 130). The model was characterised by total collagen accumulation and expression of fibrogenic molecular markers. In order to develop an unbiased, holistic view on the mechanism of this TGF-β1-induced *in-vitro* model of fibrosis, quantitative proteomic analysis of this model has been conducted and will be reported in this chapter.

5.1. TGF-β1-induced *in-vitro* model of fibrosis

To establish TGF-β1-induced *in-vitro* model of fibrosis, NRK-49F cells were cultured as described in Materials and Methods (**Section 2.5**) with or without 5 ng/mL TGF-β1. Cell lysates and conditioned media were harvested after 48h. To confirm successful biological experiments, collagen contents in cell lysates and conditioned media were measured by hydroxyproline assay and soluble collagen assay, respectively, as described in Materials and Methods (**Sections 2.10** and **2.11**). As shown in **Fig. 5.1**, TGF-β1 significantly induced total collagen and soluble collagen in cell lysates and conditioned media.

5.2. Proteomic profiling analysis of cell lysates

The cell lysates and conditioned media were trypinised, labelled with TMT reagents and subjected to LC-MS/MS as detailed in Materials and Methods (**Section 2.12**). The MS data were searched using the Proteome Discoverer software and identified proteins were analysed by bioinformatic platforms, including Venn diagram, KEGG pathway and Volcano plot analyses. Proteins of interest were further validated by ELISA.

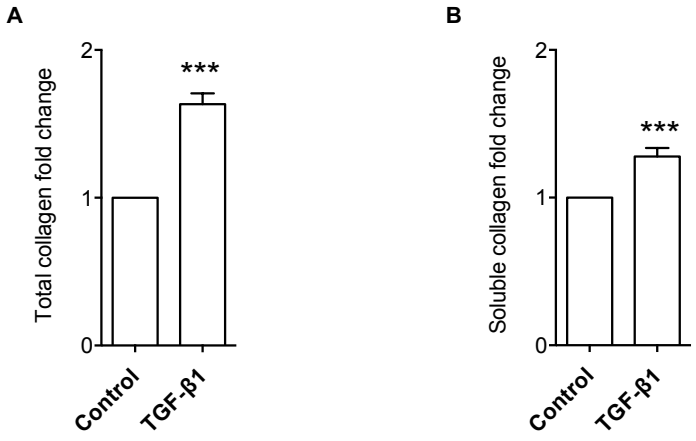

Fig. 5.1. TGF-β1 induced accumulation of total collagen in cell lysates and soluble collagen in conditioned media. NRK-49F cells were cultured in absence and presence of 5 ng/mL TGF-β1 for 48h. Cell lysates and conditioned media were harvested for hydroxyproline assay (A) and soluble collagen assay (B) to quantify total and soluble collagens, respectively. Data represent mean ± SEM of 4 independent cell culture studies. *** $p<0.001$ *vs* control group.

To determine the proteins differentially expressed in NRK-49F cells with and without TGF-β1, four independent pairs of cell lysates from control and TGF-β1-treated groups were subjected to in-solution trypsin-digestion and LC-MS/MS analysis. Peptides were searched against the Proteome Discoverer database and 1438 proteins were identified, with at least 2 unique peptides detected and a 1% false discovery rate (FDR). In particular, 628 proteins were significantly regulated by TGF-β1 (**Supplementary Table 1)**.

Gene Ontology (GO) function enrichment analysis of the 628 proteins significantly changed in TGF-β1 group was performed on the Database for Annotation, Visualization and Integrated Discovery (DAVID; https://david.ncifcrf.gov/). Three ontologies were constructed, including cellular components, biological processes and molecular functions. As shown in **Fig. 5.2**, the enriched cellular component GO terms were grouped into 44 clusters ($p<0.05$), showing that the significantly changed proteins were more enriched in the cytoplasm, extracellular exosome, nucleus, membrane, mitochondrion and cytosol categories. The

enriched biological processes (**Fig. 5.3**) included 24 clusters of proteins and the top five biggest protein clusters were involved in translation, oxidation-reduction process, response to drug, cell-cell adhesion and fatty acid beta-oxidation. As shown in **Fig. 5.4**, 27 enriched molecular function clusters were identified, mainly related to poly(A)RNA binding, protein binding, ATP binding, structural constituent of ribosome, protein homodimerisation activity, etc.

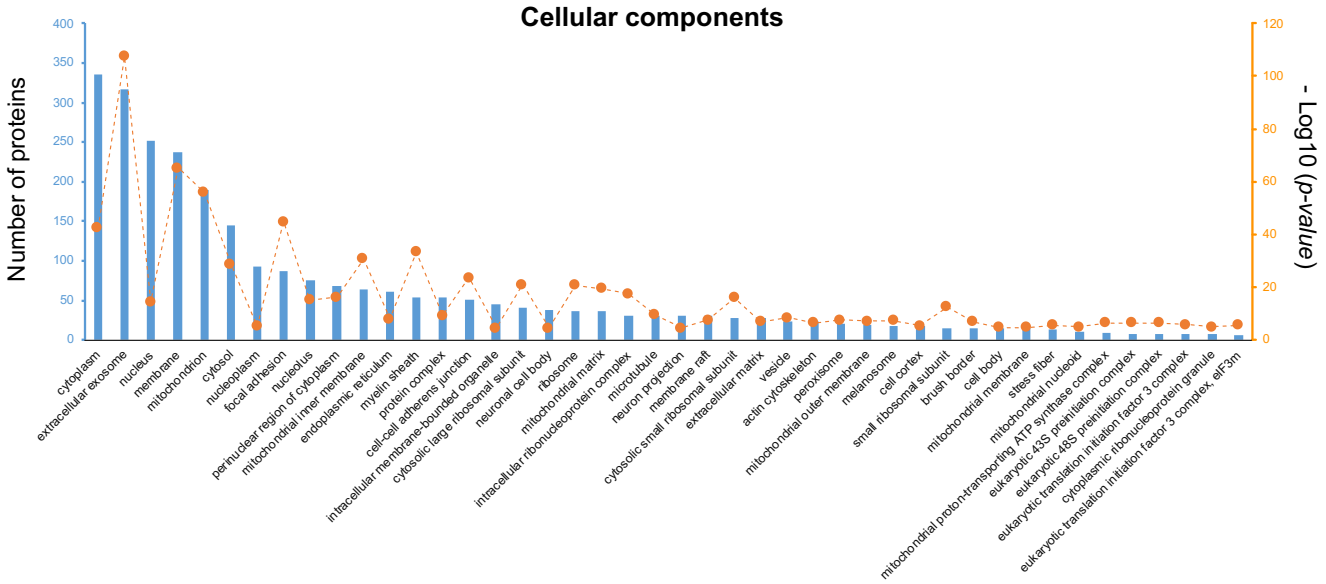

Fig. 5.2. GO cellular component enrichment analysis of the proteins significantly regulated by TGF-β1 in cell lysates. The numbers of involved proteins are indicated by the left y-axis shown as blue bars and the *p*-values (as -Log10 values) are indicated by the right y-axis shown as orange dots, respectively.

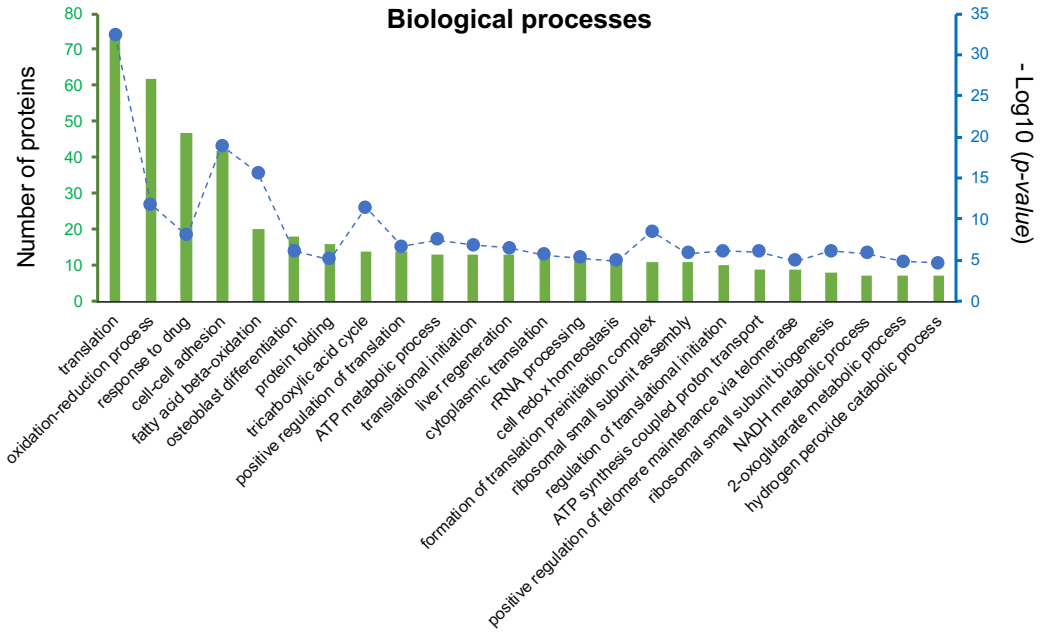

Fig. 5.3. GO biological process enrichment analysis of the proteins significantly regulated by TGF-β1 in cell lysates. The numbers of involved proteins are indicated by the left y-axis shown as green bars and the *p*-values (as -Log10 values) are indicated by the right y-axis shown as blue dots, respectively.

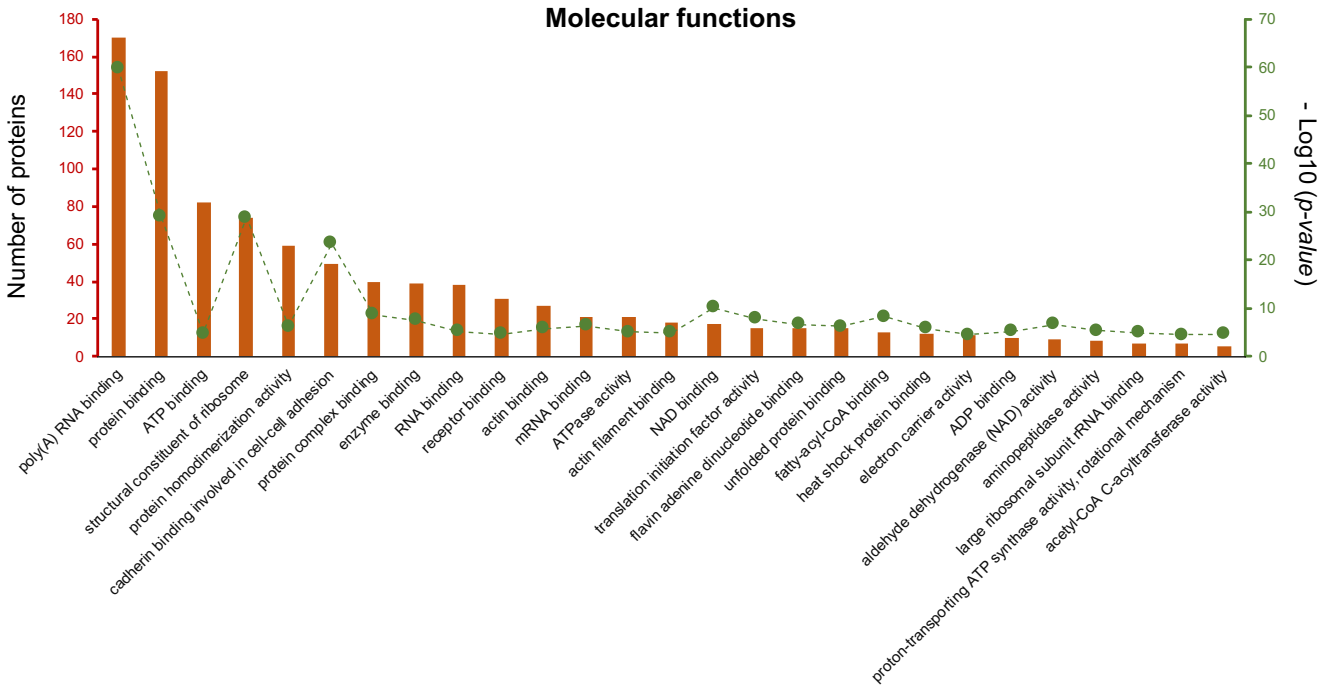

Fig. 5.4. GO molecular function enrichment analysis of the proteins significantly regulated by TGF-β1 in cell lysates. The numbers of involved proteins are indicated by the left y-axis shown as orange bars and the *p*-values (as -Log10 values) are indicated by the right y-axis shown as green dots, respectively.

Biological mechanisms and pathways regulated by TGF-β1 were analysed by the KEGG (https://david.ncifcrf.gov/) and the connections and interactions between these significantly changed proteins were evaluated by STRING analysis (https://string-db.org/). 42 pathways were enriched by KEGG analysis (**Fig. 5.5A**) and the proteins involved in each pathway are listed in **Table 5.1**. Multiple proteins involved in 14 pathways were repressed by TGF-β1, including Citrate cycle (TCA cycle), Pyruvate metabolism, Glyoxylate and dicarboxylate metabolism, Tryptophan metabolism, beta-Alanine metabolism, Propanoate metabolism, Histidine metabolism, Parkinson's disease, Butanoate metabolism, Oxidative phosphorylation, Alzheimer's disease, Fatty acid elongation, Phenylalanine metabolism and Tyrosine metabolism. Other 28 pathways were dysregulated, with some proteins repressed and some others induced by TGF-β1.

The ribosome pathway dysregulated by TGF-β1 was the most significant and involved 68 induced and one repressed proteins (**Table 5.1)**. Ribosome is the cellular translational machinery primarily responsible for protein synthesis from messenger RNAs (131). Eukaryotic ribosomes, known as 80S ribosomes, include two unequal subunits, i.e. the small subunit (40S) and the large subunit (60S), according to their sedimentation coefficients (132, 133). The small ribosomal subunit is responsible for decoding the information encoded in messenger RNA, whereas peptide bond synthesis occurs at the large ribosomal subunit (134). Altogether, eukaryotic ribosomes have 79 ribosomal proteins (135). In the present study, TGF-β1 significantly induced 28 ribosomal proteins of the small subunits (Rps2, Rps3, Rps3a, Rps4X, Rps6, Rps8, Rps9, Rps10, Rps11, Rps13, Rps14, Rps15, Rps15a, Rps16, Rps17, Rps18, Rps19, Rps20, Rps21, Rps23, Rps24, Rps26, Rps27, Rps27l, Rps28, Rps29, Rps30/Fau and Rpsa) and 40 ribosomal proteins of the large subunits (Rpl4, Rpl5, Rpl6, Rpl7, Rpl7a, Rpl8, Rpl9, Rpl10, Rpl10a, Rpl12, Rpl13, Rpl13a, Rpl14, Rpl15, Rpl17, Rpl18, Rpl18A, Rpl19, Rpl21, Rpl22, Rpl23, Rpl23a, Rpl24, Rpl26, Rpl27, Rpl27a, Rpl28, Rpl29, Rpl3, Rpl30, Rpl32, Rpl34, Rpl35, Rpl35a, Rpl36, Rpl36a, Rpl37, Rpl38, Rplp0 and Rplp2). Only one mitochondrial (39S) ribosomal protein L3 (Mrpl3) was suppressed by TGF-β1.

The highest number of proteins significantly regulated by TGF-β1, altogether 121 was involved in multiple metabolic pathways, including 17 proteins up-regulated and 104 down-regulated by TGF-β1 (**Table 5.1**).

STRING analysis illustrated predicted direct (physical) and indirect (functional) associations among proteins significantly regulated by TGF-β1, creating dense interaction networks shown in **Fig. 5.5 B**.

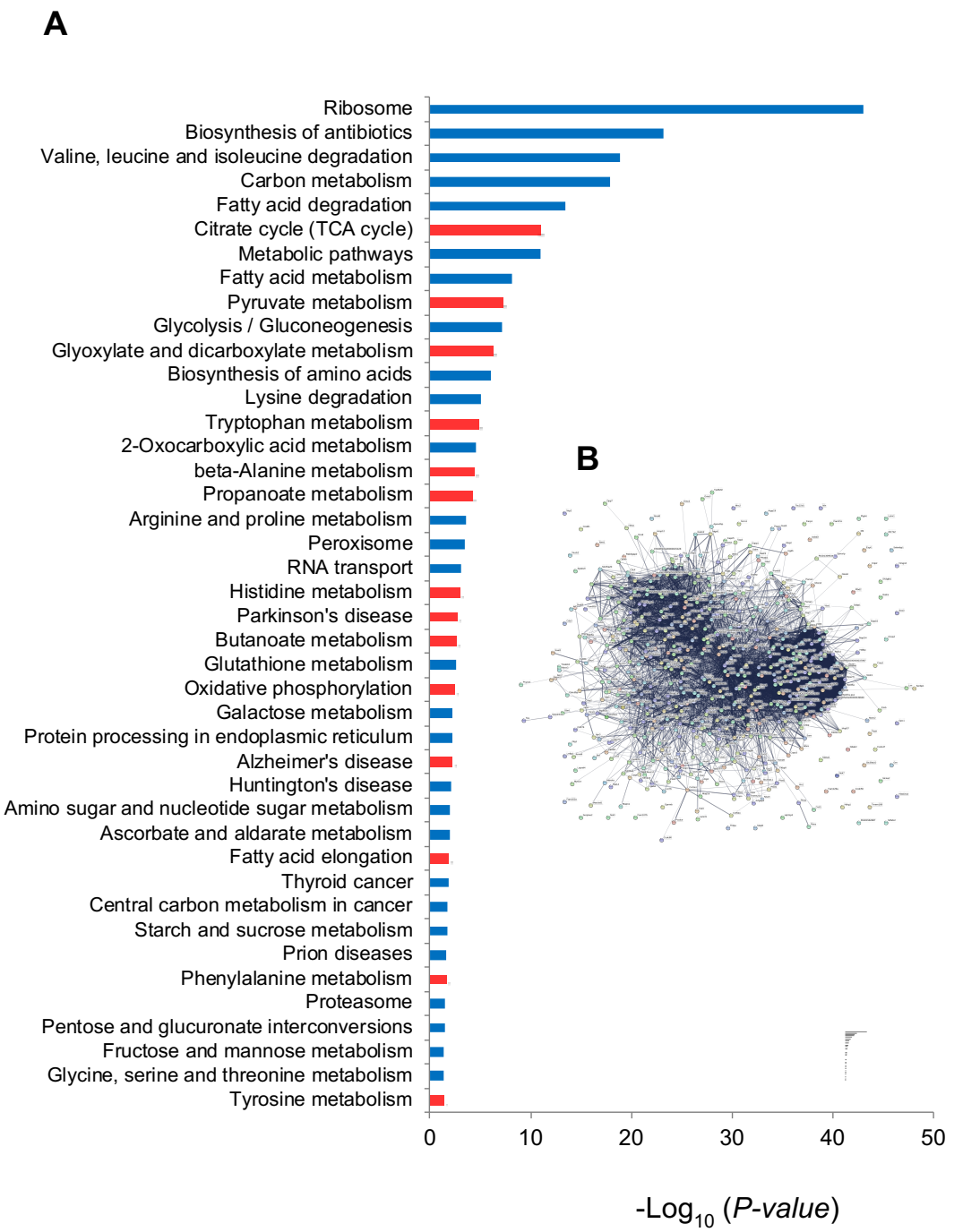

Fig. 5.5. KEGG pathway and STRING network analyses of 628 proteins in cell lysates significantly regulated by TGF-β1. (A) KEGG analysis shows 42 pathways significantly regulated by TGF-β1, among which the most significantly regulated pathway was the ribosome pathway. Y-axis represents significantly enriched KEGG pathway terms and X-axis indicates -Log_{10} *p*-value. (B) STRING analysis illustrates predicted direct (physical) and indirect (functional) associations among proteins significantly regulated by TGF-β1, showing a huge, dense and irregular cluster of proteins.

Table 5.1. Cell-lysate proteins significantly regulated by TGF-β1 are involved in 42 KEGG pathways. Proteins are listed in order of fold-change (TGF-β1 *vs* control) and red fonts indicated the pathways in which proteins were suppressed by TGF-β1.

KEGG pathways	Proteins significantly regulated by TGF-β1 (TGF-β1 *vs* control)
Ribosome (most significant)	Rps30 (2.07), Rpl36a (1.95), Rps23 (1.89), Rpl35a (1.71), Rps24 (1.6), Rpl37 (1.56), Rpl23a (1.56), Rpl27a (1.54), Rps3 (1.52), Rplp0 (1.5), Rps10 (1.5), Rpl35 (1.5), Rps11 (1.47), Rps14 (1.46), Rpl17 (1.45), Rpl27 (1.45), Rpl32 (1.42), Rpsa (1.42), Rpl18A (1.42), Rps16 (1.41), Rps17 (1.41), Rpl22 (1.37), Rps13 (1.36), Rpl18 (1.35), Rps29 (1.34), Rpl26 (1.34), Rps2 (1.33), Rps18 (1.33), Rpl36 (1.33), Rpl6 (1.33), Rps6 (1.33), Rpl13a (1.33), Rps19 (1.32), Rps8 (1.32), Rpl23 (1.32), Rpl13 (1.31), Rps15 (1.31), Rpl38 (1.31), Rpl5 (1.31), Rplp2 (1.3), Rpl10 (1.3), Rpl7 (1.3), Rpl29 (1.3), Rpl15 (1.29), Rps27l (1.29), Rpl12 (1.29), Rps4X (1.28), Rps26 (1.28), Rpl30 (1.27), Rpl3 (1.27), Rpl7a (1.27), Rpl10a (1.27), Rpl21 (1.27), Rps3a (1.26), Rpl34 (1.26), Rpl8 (1.26), Rps20 (1.26), Rpl24 (1.26), Rpl4 (1.25), Rpl9 (1.23), Rps9 (1.23), Rps15a (1.22), Rpl28 (1.22), Rpl19 (1.19), Rpl14 (1.18), Rps27 (1.18), Rps21 (1.17), Rps28 (1.14), Mrpl3 (0.84)
Biosynthesis of antibiotics	Bcat1 (1.94), Psph (1.67), Nme1 (1.64), Nme2 (1.55), Hk2 (1.45), Gfpt1 (1.38), Phgdh (1.26), Ak2 (0.89), Mdh1 (0.88), Galm (0.86), Tpi1 (0.86), Eno2 (0.86), Fh (0.86), Aldh9a1 (0.85), Mdh2 (0.84), Gcsh (0.83), Ldhb (0.82), Got2 (0.82), Pycr2 (0.82), Acat2 (0.82), Bckdha (0.82), Dlat (0.82), Pcyox1 (0.8), Tkt (0.8), Ogdh (0.79), Pfkp (0.79), Acaa1a (0.79), Sdha (0.79), Aco2 (0.78), Aldh7a1 (0.78), Idh3a (0.78), Hk1 (0.77), Dlst (0.77), Cs (0.77), Dld (0.76), Hsd17b10 (0.76), Pgm1 (0.74), Sdhb (0.74), Pdhb (0.73), Echs1 (0.72), Pfkm (0.71), Oat (0.71), Pcca (0.7), Hadhb (0.7), Idh1 (0.7), Hadha (0.69), Idh2 (0.69), Bcat2 (0.68), Ak3 (0.62), Acat1 (0.61), Hadh (0.6), Pccb (0.58), Aldh3a2 (0.58), Acaa2 (0.55), Aldh2 (0.54), Cat (0.47)
Valine, leucine and isoleucine degradation	Bcat1 (1.94), Aldh9a1 (0.85), Bckdha (0.82), Acat2 (0.82), Acaa1a (0.79), Aldh7A1 (0.78), Hsd17b10 (0.76), Mccc2 (0.76), Dld (0.76), Mccc1 (0.73), Acads (0.72), Echs1 (0.72), Hadhb (0.7), Pcca (0.7), Hadha (0.69), Bcat2 (0.68), Hibch (0.65), Acadsb (0.64), Hibadh (0.63), Acat1 (0.61), Ivd (0.61), Hadh (0.6), Aldh3a2 (0.58), Pccb (0.58), Aldh6A1 (0.55), Acaa2 (0.55), Aldh2 (0.54)
Carbon metabolism	Psph (1.67), Hk2 (1.45), Phgdh (1.26), Mdh1 (0.88), Tpi1 (0.86), Eno2 (0.86), Fh (0.86), Mdh2 (0.84), Acat2 (0.82), Got2 (0.82), Dlat (0.82), Tkt (0.8), Ogdh (0.79), Pfkp (0.79), Sdha (0.79), Aco2 (0.78), Idh3a (0.78), Hk1 (0.77), Dlst (0.77), Cs (0.77), Dld (0.76), Sdhb (0.74), Pdhb (0.73), Pc (0.73), Echs1 (0.72), Acads (0.72), Pfkm (0.71), Idh1 (0.7), Pcca (0.7), Hadha (0.69), Idh2 (0.69), Glud1 (0.66), Hibch (0.65), Acat1 (0.61), Pccb (0.58), Aldh6A1 (0.55), Cat (0.47)
Fatty acid degradation	Acsl5 (1.29), Aldh9a1 (0.85), Acat2 (0.82), Acaa1a (0.79), Aldh7A1 (0.78), Cpt1a (0.77), Acadvl (0.74), Acads (0.72), Echs1 (0.72), Acadl (0.7), Hadhb (0.7), Hadha (0.69), Eci1 (0.67), Cpt2 (0.67), Eci2 (0.65), Acadsb (0.64), Acat1 (0.61), Hadh (0.6), Aldh3a2 (0.58), Acaa2 (0.55), Aldh2 (0.54)
Citrate cycle (TCA cycle)	Mdh1 (0.88), Fh (0.86), Mdh2 (0.84), Dlat (0.82), Ogdh (0.79), Sdha (0.79), Aco2 (0.78), Idh3a (0.78), Dlst (0.77), Cs (0.77), Dld (0.76), Sdhb (0.74), Pdhb (0.73), Pc (0.73), Idh1 (0.7), Idh2 (0.69)
Metabolic pathways (involved highest number of proteins)	Enpp1 (3.56), Bcat1 (1.94), Asns (1.85), Psph (1.67), Nme1 (1.64), Impdh2 (1.61), Ggt1 (1.58), Mthfd2l (1.56), Nme2 (1.55), Ugdh (1.46), Hk2 (1.45), Gfpt1 (1.38), Acsl5 (1.29), Fasn (1.26), Phgdh (1.26), Agps (1.21), Ckb (1.21), Atp5c1 (0.89), Ak2 (0.89), Mdh1 (0.88), Gmps (0.88), Galm (0.86), Tpi1 (0.86), Fh (0.86), Eno2 (0.86), Thtpa (0.85), Aldh9a1 (0.85), Atp6v0a1 (0.85), Cmas (0.84), Mdh2 (0.84), Uqcrc1 (0.84), Hexa (0.84), P4ha1 (0.84), Gcsh (0.83), Prdx6 (0.83), Ldhb (0.82), Got2 (0.82), Pycr2 (0.82), Acat2 (0.82), Cmpk1 (0.82), Dlat (0.82), Impa1 (0.82), Atp5l (0.82), Bckdha (0.82), Dhfr (0.81), Gaa (0.81), Tkt (0.8), Atp5f1 (0.8), Ogdh (0.79), Galns (0.79), Atp5j (0.79), Pfkp (0.79), Dhcr7 (0.79), Acaa1a (0.79), Sdha (0.79), Idh3a (0.78), Aco2 (0.78), Aldh7A1 (0.78), Pcyt1a (0.77), Hk1 (0.77), Dlst (0.77), Cs (0.77), Atp5a1 (0.77), Dld (0.76), Hsd17b10 (0.76), Mccc2 (0.76), Atp5o (0.76), Alad (0.74), Pgm1 (0.74), Atp5b (0.74), Acadvl (0.74), Dhrs4 (0.74), Plcd1 (0.74), Sdhb (0.74), Pdhb (0.73), Pc (0.73), Mccc1 (0.73), Mpst (0.72), Atp5d (0.72), Acads (0.72), Echs1 (0.72), Cox4i1 (0.71), Pfkm (0.71), Oat (0.71), Sord (0.71), Pygb (0.71), Cox5a (0.7), Pcca (0.7), Hadhb (0.7), Idh1 (0.7), Aldh4a1 (0.7), Acadl (0.7), Fah (0.69), Hadha (0.69), Idh2 (0.69), Maoa

	(0.69), Uqcrq (0.69), Cox5b (0.68), Atp5j2 (0.68), Bcat2 (0.68), Hsd17b4 (0.67), Glud1 (0.66), Gusb (0.65), Hibch (0.65), Acadsb (0.64), Anpep (0.64), Hibadh (0.63), Aldh3b1 (0.62), Spr (0.61), Acat1 (0.61), Ivd (0.61), Hadh (0.6), Scp2 (0.59), Pccb (0.58), Aldh3a2 (0.58), Bdh2 (0.58), Acaa2 (0.55), Aldh6A1 (0.55), Aldh2 (0.54), Ugt1A6 (0.43), Aldh3a1 (0.22)
Fatty acid metabolism	Acsl5 (1.29), Fasn (1.26), Acat2 (0.82), Acaa1a (0.79), Cpt1a (0.77), Acadvl (0.74), Acads (0.72), Echs1 (0.72), Tecr (0.71), Acadl (0.7), Hadhb (0.7), Hadha (0.69), Cpt2 (0.67), Acadsb (0.64), Acat1 (0.61), Hadh (0.6), Acaa2 (0.55)
Pyruvate metabolism	Mdh1 (0.88), Fh (0.86), Aldh9a1 (0.85), Mdh2 (0.84), Ldhb (0.82), Dlat (0.82), Acat2 (0.82), Aldh7A1 (0.78), Dld (0.76), Pdhb (0.73), Pc (0.73), Acat1 (0.61), Aldh3a2 (0.58), Aldh2 (0.54)
Glycolysis / Gluconeogenesis	Hk2 (1.45), Galm (0.86), Tpi1 (0.86), Eno2 (0.86), Aldh9a1 (0.85), Ldhb (0.82), Dlat (0.82), Pfkp (0.79), Aldh7A1 (0.78), Hk1 (0.77), Dld (0.76), Pgm1 (0.74), Pdhb (0.73), Pfkm (0.71), Aldh3b1 (0.62), Aldh3a2 (0.58), Aldh2 (0.54), Aldh3a1 (0.22)
Glyoxylate and dicarboxylate metabolism	Mdh1 (0.88), Mdh2 (0.84), Gcsh (0.83), Acat2 (0.82), Aco2 (0.78), Cs (0.77), Dld (0.76), Pcca (0.7), Acat1 (0.61), Pccb (0.58), Cat (0.47)
Biosynthesis of amino acids	Bcat1 (1.94), Psph (1.67), Phgdh (1.26), Tpi1 (0.86), Eno2 0.86), Got2 (0.82), Pycr2 (0.82), Tkt (0.8), Pfkp (0.79), Aco2 (0.78), Idh3a (0.78), Aldh7A1 (0.78), Cs (0.77), Pc (0.73), Pfkm (0.71), Idh1 (0.7), Idh2 (0.69), Bcat2 (0.68)
Lysine degradation	Plod2 (1.19), Aldh9a1 (0.85), Acat2 (0.82), Ogdh (0.79), Aldh7A1 (0.78), Dlst (0.77), Echs1 (0.72), Hadha (0.69), Plod1 (0.69), Acat1 (0.61), Hadh (0.6), Aldh3a2 (0.58), Aldh2 (0.54)
Tryptophan metabolism	Aldh9a1 (0.85), Acat2 (0.82), Ogdh (0.79), Aldh7a1 (0.78), Echs1 (0.72), Maoa (0.69), Hadha (0.69), Acat1 (0.61), Hadh (0.6), Aldh3a2 (0.58), Aldh2 (0.54), Cat (0.47)
2-Oxocarboxylic acid metabolism	Bcat1(1.94), Got2(0.82), Aco2(0.78), Idh3a (0.78), Cs (0.77), Idh1(0.7), Idh2(0.69), Bcat2(0.68)
beta-Alanine metabolism	Aldh9a1(0.85), Aldh7A1(0.78), Echs1(0.72), Hadha (0.69), Hibch (0.65), Aldh3b1(0.62), Aldh3a2(0.58), Aldh6a1(0.55), Aldh2(0.54), Aldh3a1(0.22)
Propanoate metabolism	Ldhb (0.82), Acat2 (0.82), Echs1 (0.72), Pcca (0.7), Hadha (0.69), Hibch (0.65), Acat1 (0.61), Pccb (0.58), Aldh6a1 (0.55)
Arginine and proline metabolism	Ckb (1.21), Aldh9a1 (0.85), P4ha1 (0.84), Got2 (0.82), Pycr2 (0.82), Aldh7a1 (0.78), Oat (0.71), Aldh4a1 (0.7), Maoa (0.69), Aldh3a2(0.58), Aldh2(0.54)
Peroxisome	Prdx5 (1.33), Acsl5 (1.29), Agps (1.21), Prdx1 (1.16), Acaa1a (0.79), Crat (0.78), Dhrs4 (0.74), Idh1 (0.7), Idh2 (0.69), Hsd17b4 (0.67), Eci2 (0.65), Scp2 (0.59), Ech1 (0.5), Cat (0.47)
RNA transport	Eif2S3 (1.45), Eif4a2 (1.4), Eif3j (1.36), Eef1a1 (1.33), Eif3h (1.28), Eif3a (1.27), Eif2b1 (1.25), Eif3c (1.24), Strap (1.22), Eif3i (1.21), Eif3d (1.18), Eif3b (1.17), Kpnb1 (1.14), Nup153 (1.13), Pabpc1 (1.13), Tpr (0.91), Nup93 (0.82), Ube2i (0.8) Eif5 (0.79), Sumo2 (0.78)
Histidine metabolism	Aldh9a1 (0.85), Aldh7a1 (0.78), Maoa (0.69), Aldh3b1 (0.62), Aldh3a2 (0.58), Aldh2 (0.54), Aldh3a1 (0.22)
Parkinson's disease	Atp5c1 (0.89), Gnai2 (0.87), Uba1 (0.86), Uqcrc1 (0.84), Vdac1 (0.82), Atp5f1 (0.8), Park7 (0.8), Sdha (0.79), Atp5j (0.79), Atp5a1 (0.77), Atp5o (0.76), Atp5b (0.74), Sdhb (0.74), Atp5d (0.72), Cox4i1 (0.71), Cox5a (0.7), Uqcrq (0.69), Cox5b (0.68)
Butanoate metabolism	Acat2 (0.82), Acads (0.72), Echs1 (0.72), Hadha (0.69), Acat1 (0.61), Hadh (0.6), Bdh2 (0.58)
Glutathione metabolism	Ggt1 (1.58), Oplah (0.79), Gpx1 (0.75), Gstm2 (0.74), Idh1 (0.7), Idh2 (0.69), Gstp1 (0.67), Anpep (0.64), Mgst1 (0.62), Gsta3 (0.59)
Oxidative phosphorylation	Atp5c1 (0.89), Atp6v0a1 (0.85), Uqcrc1 (0.84), Atp5l (0.82), Atp5f1 (0.8), Sdha (0.79), Atp5j (0.79), Atp5a1 (0.77), Atp5o (0.76), Atp5b (0.74), Sdhb (0.74), Atp5d (0.72), Cox4i1 (0.71), Cox5a (0.7), Uqcrq (0.69), Atp5j2 (0.68), Cox5b (0.68)

Galactose metabolism	Hk2 (1.45), Galm (0.86), Gaa (0.81), Pfkp (0.79), Hk1 (0.77), Pgm1 (0.74), Pfkm (0.71)
Protein processing in endoplasmic reticulum	Sec61a1 (1.61), Bax (1.38), Nsfl1C (1.33), Dnajc3 (1.33), Dnaja2 (1.31), Hsp90Ab1 (1.28), Hspa8 (1.26), Hsp90Aa1 (1.21), Hsph1 (1.21), Rad23b (0.95), Dnajb11 (0.92), Vcp (0.9), Pdia6 (0.88), Pdia4 (0.82), Eif2ak2 (0.79), Sel1l (0.78), Capn1 (0.74), Os9 (0.51)
Alzheimer's disease	Atp5c1 (0.89), Uqcrc1 (0.84), Mapk1 (0.84), Itpr3 (0.83), Atp5f1 (0.8), Sdha (0.79), Atp5j (0.79), Atp5a1 (0.77), Hsd17b10 (0.76), Atp5o (0.76), Atp5b (0.74), Capn1 (0.74), Sdhb (0.74), Atp5d (0.72), Cox4i1 (0.71), Cox5a (0.7), Uqcrq (0.69), Cox5b (0.68), Mapk3 (0.64)
Huntington's disease	Bax (1.38), Dctn1 (0.9), Atp5c1 (0.89), Ap2m1 (0.87), Hdac1 (0.85), Uqcrc1 (0.84), Clta (0.82), Vdac1 (0.82), Atp5f1 (0.8), Sdha (0.79), Atp5j (0.79), Atp5a1 (0.77), Atp5o (0.76), Atp5b (0.74), Sdhb (0.74), Atp5d (0.72), Cox4i1 (0.71), Cox5a (0.7), Uqcrq (0.69), Cox5b (0.68)
Amino sugar and nucleotide sugar metabolism	Ugdh (1.46), Hk2 (1.45), Gfpt1 (1.38), Cmas (0.84), Hexa (0.84), Cyb5r3 (0.81), Pgm1 (0.74), Hk1 (0.77)
Ascorbate and aldarate metabolism	Ugdh (1.46), Aldh9a1 (0.85), Aldh7a1 (0.78), Aldh3a2 (0.58), Aldh2 (0.54), Ugt1a6 (0.43)
Fatty acid elongation	Echs1 (0.72), Tecr (0.71), Hadhb (0.70), Hadha (0.69), Hadh (0.60), Acaa2 (0.55)
Thyroid cancer	Map2k1 (1.31), Tpm3 (1.12), Tpr (0.91), Mapk1 (0.84), Mapk3 (0.64), Ctnnb1 (0.56)
Central carbon metabolism in cancer	Slc7a5 (1.51), Hk2 (1.45), Map2k1 (1.31), Mapk1 (0.84), Pfkp (0.79), Hk1 (0.77), Pdhb (0.73), Pfkm (0.71), Mapk3 (0.64)
Starch and sucrose metabolism	Enpp1 (3.56), Hk2 (1.45), Gaa (0.81), Hk1 (0.77), Pgm1 (0.74), Pygb (0.71)
Prion diseases	Bax (1.38), Map2k1 (1.31), Stip1 (1.08), Mapk1 (0.84), Mapk3 (0.64), Ncam1 (0.63)
Phenylalanine metabolism	Got2 (0.82), Mif (0.74), Maoa (0.69), Aldh3b1 (0.62), Aldh3a1 (0.22)
Proteasome	Psmb7 (1.45), Psmb6 (1.28), Psma4 (1.24), Psma1 (1.14), Psmb10 (0.73), Psme1 (0.70), Psmb9 (0.70)
Pentose and glucuronate interconversions	Ugdh (1.46), Sord (0.71), Gusb (0.65), Aldh3a2 (0.58), Aldh2 (0.54), Ugt1A6 (0.43)
Fructose and mannose metabolism	Hk2 (1.45), Tpi1 (0.86), Pfkp (0.79), Hk1 (0.77), Sord (0.71), Pfkm (0.71)
Glycine, serine and threonine metabolism	Psph (1.67), Phgdh (1.26), Gcsh (0.83), Aldh7A1 (0.78), Dld (0.76), Maoa (0.69)
Tyrosine metabolism	Got2 (0.82), Mif (0.74), Maoa (0.69), Fah (0.69), Aldh3b1 (0.62), Aldh3a1 (0.22)

To focus on the proteins more robustly regulated by TGF-β1, a cut-off of fold-changes >1.5 or <0.67 (TGF-β1 *vs* control) was applied. KEGG pathway analysis of those short-listed proteins demonstrated that 22 pathways were significantly regulated by TGF-β1. As shown in **Fig. 5.6**, TGF-β1 suppressed multiple proteins enriched in 16 pathways, including Fatty acid degradation, beta-Alanine metabolism, Tryptophan metabolism, Histidine metabolism, Propanoate metabolism, Metabolism of xenobiotics by cytochrome P450, Drug metabolism - cytochrome P450, Pentose and glucuronate interconversions, Peroxisome, Chemical carcinogenesis, Lysine degradation, Fatty acid metabolism, Ascorbate and aldarate metabolism, Glyoxylate and dicarboxylate metabolism, Butanoate metabolism and Glycolysis/Gluconeogenesis. Besides, TGF-β1 dysregulated 5 pathways, including Valine, leucine and isoleucine degradation, Metabolic pathways, Biosynthesis of antibiotics, Carbon metabolism and Glutathione metabolism. Furthermore, multiple proteins of the Ribosome pathway were significantly induced by TGF-β1.

Focusing on the interaction networks of proteins regulated by TGF-β1 with fold-changes >1.5 or <0.67 (TGF-β1 *vs* control), STRING analysis revealed two major clusters of proteins (a and b) connected by inosine-5'-monophosphate dehydrogenase 2 (Impdh2; **Fig. 5.7A)**. Impdh2, a rate-limiting enzyme mainly involved in guanosine and deoxyguanosine biosynthesis, was induced by TGF-β1 and has been proposed as a druggable target (136). Indeed, non-selective Impdh inhibitors have multiple therapeutic values, including repressing fibrosis (136-139). The accession numbers, fold-changes and *p*-values of proteins involved in clusters a and b are listed in **Table 5.2.** Most proteins in cluster a, except Dpysl3, Slc7a1 and Slc7a5 (which are located at periphery of the cluster), were down-regulated by TGF-β1. In cluster b, TGF-β1 up-regulated most proteins except Ak3, a mitochondrial enzyme located at the periphery of the cluster.

KEGG pathway analysis of proteins in these two clusters indicated that TGF-β1-induced *in-vitro* model of fibrosis is mainly associated with multiple metabolic pathways (cluster a) and

ribosome pathway (cluster b) as highlighted in **Fig. 5.7 B**. There were 18 pathways involved in cluster a and the top 3 with lowest *p-values* were Valine, leucine and isoleucine degradation, Fatty acid degradation and Metabolic pathways. As shown in **Table 5.3**, it is interesting that almost all proteins involved in multiple metabolic pathways were down-regulated by TGF-β1. However, TGF-β1 significantly induced 10 proteins participated in the ribosome pathway, including four small subunits (Rps30, Rps24, Rps23 and Rps3) and six large subunits (Rpl36a, Rpl35a, Rpl23a, Rpl37 Rpl27a and Rplp0, **Table 5.3**). Thus, it suggested that TGF-β1-induced fibrogenesis is associated with a previously unrecognized mismatch of reduced proteins involved in metabolic pathways and increased ribosomal proteins.

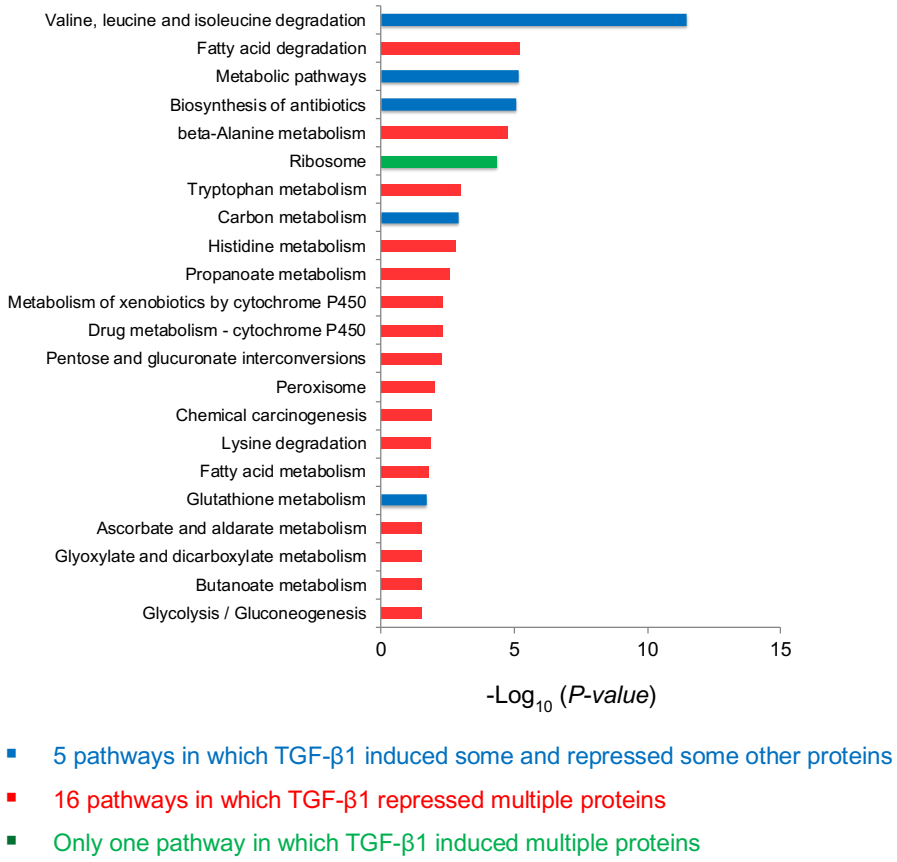

Fig. 5.6. KEGG pathway analysis of 127 proteins in cell lysates significantly regulated by TGF-β1 with fold-change >1.5 or < 0.67 (TGF-β1 vs control). Y-axis represents significantly enriched KEGG pathways and X-axis indicates -Log_{10} *p*-value.

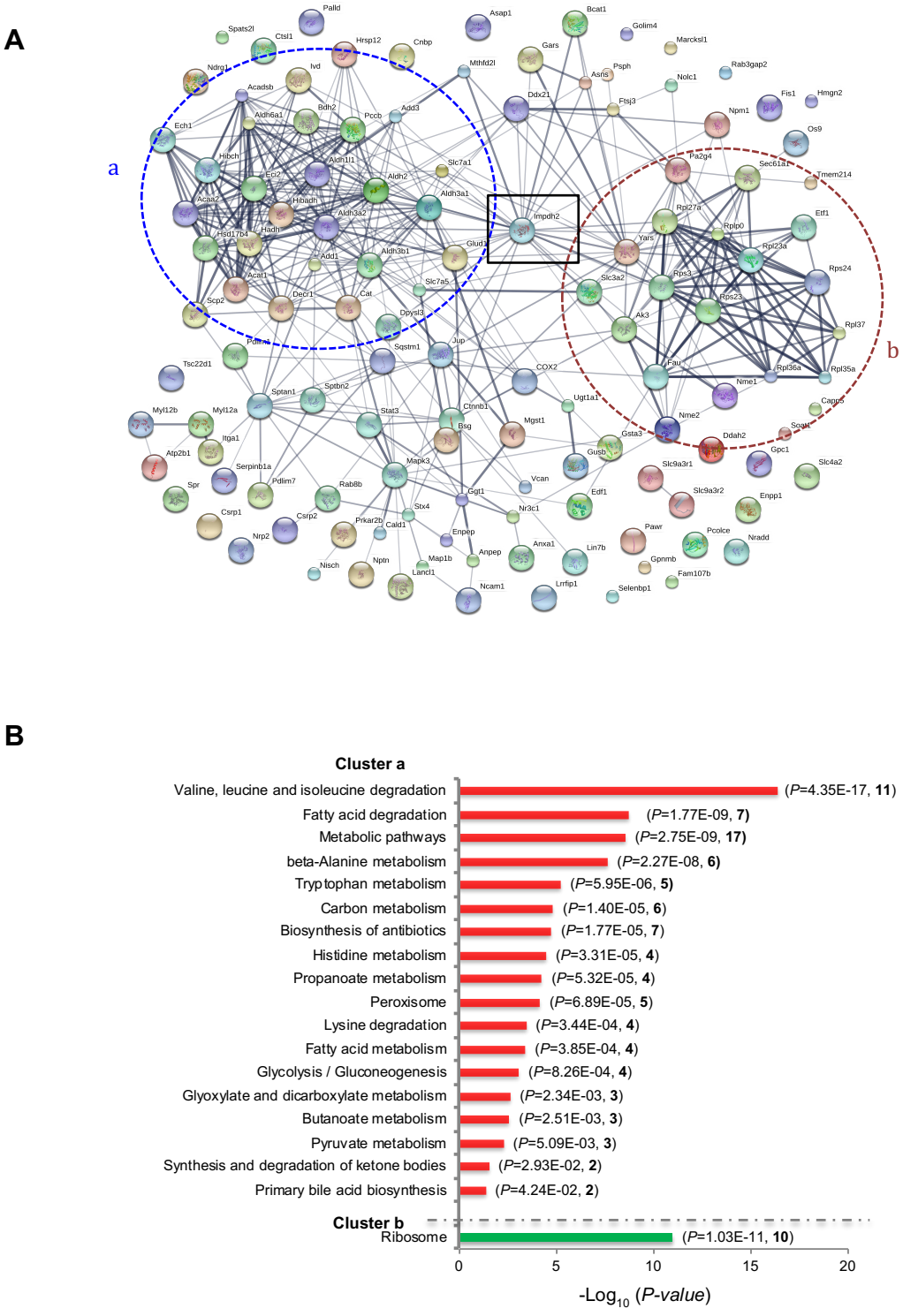

Fig. 5.7. TGF-β1 significantly regulated multiple metabolic pathways and the ribosome pathway, with Impdh2 sitting in between as a possible "middleman". (A) STRING analysis reveals predicted direct (physical) and indirect (functional) associations among proteins significantly regulated by TGF-β1 with fold changes >1.5 or < 0.67. Two major clusters (a and b) were observed which were connected by Impdh2. (B) KEGG pathway analysis of proteins clustered in a and b was performed, respectively. Cluster a contains proteins involved in multiple metabolic pathways; Cluster b is enriched with proteins of the ribosome pathway.

Table 5.2 Proteins in clusters a and b (Fig. 5.7a) listed in order of fold-change (green font: induced by TGF-β1, red font: reduced by TGF-β1, TGF-β1 *vs* control)

Accession	Protein	Description	Fold change	*p-value*
Proteins involved in cluster a				
Q62952	Dpysl3	Dihydropyrimidinase-related protein 3	2.3262	0.000002
P30823	Slc7a1	High affinity cationic amino acid transporter 1	2.0636	0.001813
Q63016	Slc7a5	Large neutral amino acids transporter small subunit 1	1.5106	0.001791
P97852	Hsd17b4	Peroxisomal multifunctional enzyme type 2	0.6697	0.000066
P10860	Glud1	Glutamate dehydrogenase 1, mitochondrial	0.6588	0.000231
P52759	Hrsp12	Ribonuclease UK114	0.6538	0.000871
Q5XIC0	Eci2	Enoyl-CoA delta isomerase 2, mitochondrial	0.6525	0.000008
Q5XIE6	Hibch	3-hydroxyisobutyryl-CoA hydrolase, mitochondrial	0.6522	0.035802
P28037	Aldh1l1	Cytosolic 10-formyltetrahydrofolate dehydrogenase	0.6431	0.010616
P70584	Acadsb	Short/branched chain specific acyl-CoA dehydrogenase, mitochondrial	0.6362	0.000239
P29266	Hibadh	3-hydroxyisobutyrate dehydrogenase, mitochondrial	0.6302	0.000031
Q5XI42	Aldh3b1	Aldehyde dehydrogenase family 3 member B1	0.6198	0.007889
P12007	Ivd	Isovaleryl-CoA dehydrogenase, mitochondrial	0.6106	0.000045
P17764	Acat1	Acetyl-CoA acetyltransferase, mitochondrial	0.6060	0.000974
Q9WVK7	Hadh	Hydroxyacyl-coenzyme A dehydrogenase, mitochondrial	0.5985	0.000007
P11915	Scp2	Non-specific lipid-transfer protein	0.5931	0.000252
P07633	Pccb	Propionyl-CoA carboxylase beta chain, mitochondrial	0.5820	0.000029
D4A1J4	Bdh2	3-hydroxybutyrate dehydrogenase type 2	0.5803	0.009471
P30839	Aldh3a2	Fatty aldehyde dehydrogenase	0.5781	0.000434
P13437	Acaa2	3-ketoacyl-CoA thiolase, mitochondrial	0.5473	0.000061
Q02253	Aldh6a1	Methylmalonate-semialdehyde dehydrogenase [acylating], mitochondrial	0.5472	0.000002
P11884	Aldh2	Aldehyde dehydrogenase, mitochondrial	0.5406	0.000011
Q62651	Ech1	Delta (3,5)-Delta (2,4)-dienoyl-CoA isomerase, mitochondrial	0.4955	0.001429
Q64591	Decr1	2,4-dienoyl-CoA reductase, mitochondrial	0.4932	0.000248
P04762	Cat	Catalase	0.4743	0.000000
Q63028	Add1	Alpha-adducin	0.4357	0.000076
Q62847	Add3	Gamma-adducin	0.3743	0.005222
P11883	Aldh3a1	Aldehyde dehydrogenase, dimeric NADP-preferring	0.2221	0.000007
Proteins involved in cluster b				
P62864	Rps30	40S ribosomal protein S30	2.0675	0.006588
P83883	Rpl36a	60S ribosomal protein L36a	1.9455	0.015902
P62268	Rps23	40S ribosomal protein S23	1.8894	0.000462
P04646	Rpl35a	60S ribosomal protein L35a	1.7115	0.010021
Q4KM49	Yars	Tyrosine-tRNA ligase, cytoplasmic	1.7072	0.000006
Q5U2Q7	Etf1	Eukaryotic peptide chain release factor subunit 1	1.7037	0.006442
Q05982	Nme1	Nucleoside diphosphate kinase A	1.6351	0.018424

P61621	Sec61a1	Protein transport protein Sec61 subunit alpha isoform 1	1.6099	0.049741
P62850	Rps24	40S ribosomal protein S24	1.6045	0.000270
P61928	Rpl37	60S ribosomal protein L37	1.5624	0.003400
P62752	Rpl23a	60S ribosomal protein L23a	1.5556	0.001320
P19804	Nme2	Nucleoside diphosphate kinase B	1.5517	0.024035
P18445	Rpl27a	60S ribosomal protein L27a	1.5435	0.002928
Q6AYD3	Pa2g4	Proliferation-associated protein 2G4	1.5241	0.000058
P62909	Rps3	40S ribosomal protein S3	1.5218	0.002851
Q794F9	Slc3a2	4F2 cell-surface antigen heavy chain	1.5066	0.002933
P19945	Rplp0	60S acidic ribosomal protein P0	1.5003	0.000487
P29411	Ak3	GTP: AMP phosphotransferase AK3, mitochondrial	0.6212	0.000036

Table 5.3 KEGG pathways and the involved proteins significantly regulated by TGF-β1 in clusters a and b. (green font: induced by TGF-β1, red font: reduced by TGF-β1, TGF-β1 *vs* control).

KEGG pathways	**TGF-β1-regulated proteins (fold-change, TGF-β1/control)**
Cluster a	
Valine, leucine and isoleucine degradation	Hibch (0.65), Acadsb (0.64), Hibadh (0.63), Ivd (0.61), Acat1 (0.61), Hadh (0.60), Pccb (0.58), Aldh3a2 (0.58), Acaa2 (0.55), Aldh6a1 (0.55), Aldh2 (0.52)
Fatty acid degradation	Eci2 (0.65), Acadsb (0.64), Acat1(0.61), Hadh (0.60), Aldh3a2 (0.58), Acaa2 (0.55), Aldh2 (0.52)
Metabolic pathways	Hsd17b4 (0.67), Glud1(0.66), Hibch (0.65), Acadsb (0.64), Hibadh (0.63), Aldh3b1(0.62), Ivd (0.61), Acat1(0.61), Hadh (0.60), Scp2 (0.59), Aldh3a2 (0.58), Bdh2 (0.58), Pccb (0.58), Acaa2 (0.55), Aldh6a1(0.55), Aldh2 (0.52), Aldh3a1(0.22)
beta-Alanine metabolism	Hibch (0.65), Aldh3b1 (0.62), Aldh3a2 (0.58), Aldh6a1(0.55), Aldh2 (0.52), Aldh3a1 (0.22)
Tryptophan metabolism	Acat1(0.61), Hadh (0.60), Aldh3a2 (0.58), Aldh2 (0.52), Cat (0.47)
Carbon metabolism	Glud1(0.66), Hibch (0.65), Acat1(0.61), Pccb (0.58), Aldh6a1(0.55), Cat (0.47),
Biosynthesis of antibiotics	Acaa2 (0.55), Aldh2 (0.52), Cat (0.47), Hadh (0.60), Acat1(0.61), Pccb (0.58), Aldh3a2 (0.58)
Histidine metabolism	Aldh3b1 (0.62), Aldh3a2 (0.58), Aldh2 (0.52), Aldh3a1(0.22)
Propanoate metabolism	Hibch (0.65), Acat1(0.61), Pccb (0.58), Aldh6a1(0.55)
Peroxisome	Hsd17b4 (0.67), Eci2 (0.65), Scp2 (0.59), Ech1 (0.50), Cat (0.47)
Lysine degradation	Acat1(0.61), Hadh (0.60), Aldh3a2 (0.58), Aldh2 (0.52)
Fatty acid metabolism	Acadsb (0.64), Acat1(0.61), Hadh (0.60), Acaa2 (0.55)
Glycolysis / Gluconeogenesis	Aldh3b1 (0.62), Aldh3a2 (0.58), Aldh2 (0.52), Aldh3a1 (0.22)
Glyoxylate and dicarboxylate metabolism	Acat1(0.61), Pccb (0.58), Cat (0.47)
Butanoate metabolism	Acat1(0.61), Hadh (0.60), Bdh2 (0.58)
Pyruvate metabolism	Acat1(0.61), Aldh3a2 (0.58), Aldh2 (0.52)
Synthesis and degradation of ketone bodies	Acat1(0.61), Bdh2 (0.58)
Primary bile acid biosynthesis	Hsd17b4 (0.67), Scp2 (0.59)
Cluster b	
Ribosome	Rps30 (2.11), Rpl36a (1.95), Rps23 (1.89), Rpl35a (1.71), Rps24

	(1.60), Rpl23a (1.56), Rpl37 (1.56), Rpl27a (1.54), Rps3 (1.52), Rplp0 (1.50)

A volcano plot with fold change as the X-axis and -Log10 (*p*-value) as the Y-axis was used to demonstrate the overall distribution of differentially expressed proteins (TGF-β1 *vs* control). As shown in **Fig. 5.8**, there are 254 and 374 proteins up- and down-regulated by TGF-β1, respectively ($p<0.05$). These proteins with fold change >2 or <0.5 are listed in **Table 5.4** and **5.5**. Remarkably, TGF-β1 mostly dramatically induced Enpp1 and reduced Aldh3a1 in cell lysates. These two proteins were thus selected for further validation by ELISA.

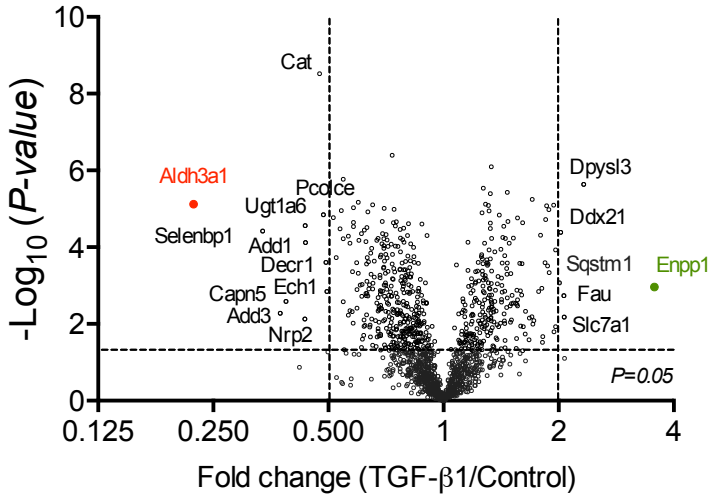

Fig. 5.8. Volcano plot displaying the proteins differentially regulated by TGF-β1. The volcano plot indicates -Log10 (*p*-value, according to *t*-tests) for all identified proteins (Y-axis) plotted against their respective fold change (X-axis). Proteins subjected to ELISA validation are highlighted either in green fonts (induced by TGF-β1) or red fonts (repressed by TGF-β1).

Table 5.4 Cell-lysate proteins most significantly up-regulated by TGF-β1 with fold change>2.

Accession	Protein	Description	Fold change	*p*-value
Q924C3	Enpp1	Ectonucleotide pyrophosphatase/phosphodiesterase family member 1	3.5573	0.001098
Q62952	Dpysl3	Dihydropyrimidinase-related protein 3	2.3262	0.000002
P62864	Fau	40S ribosomal protein S30	2.0675	0.006588
P30823	Slc7a1	High affinity cationic amino acid transporter 1	2.0636	0.001813
Q3B8Q1	Ddx21	Nucleolar RNA helicase 2	2.0255	0.000041
O08623	Sqstm1	Sequestosome-1	2.0113	0.000856

Table 5.5. Cell-lysate proteins most significantly down-regulated by TGF-β1 with fold change <0.5.

Accession	Protein	Description	Fold change	*p*-value
P11883	Aldh3a1	Aldehyde dehydrogenase, dimeric NADP-preferring	0.2221	0.000007
Q8VIF7	Selenbp1	Selenium-binding protein 1	0.3363	0.000038
Q62847	Add3	Gamma-adducin	0.3743	0.005222
Q8R4C0	Capn5	Calpain-5	0.3877	0.002592
O35276	Nrp2	Neuropilin-2	0.4342	0.007414
P08430	Ugt1a6	UDP-glucuronosyltransferase 1-6	0.4348	0.000027
Q63028	Add1	Alpha-adducin	0.4357	0.000076
P04762	Cat	Catalase	0.4743	0.000000
O08628	Pcolce	Procollagen C-endopeptidase enhancer 1	0.4854	0.000014
Q64591	Decr1	2,4-dienoyl-CoA reductase, mitochondrial	0.4932	0.000248
Q62651	Ech1	Delta (3,5)-Delta (2,4)-dienoyl-CoA isomerase, mitochondrial	0.4955	0.001429

5.3. ELISA validation of selected cell-lysate proteins

ELISA assays were performed on three proteins significantly regulated by TGF-β1 in cell lysates samples, including the most up-regulated protein Enpp1, the most down-regulated protein Aldh3a1 (**Fig. 5.8**), and Impdh2, which connected two clusters of TGF-β1-regulted proteins as shown in **Fig. 5.7 A**. Enpp1 and Impdh2 were confirmed to be significantly up-regulated by TGF-β1, whereas the Aldh3a1 was confirmed to be significantly down-regulated (**Fig. 5.9**). Thus, the ELISA results were consistent with the proteomic findings.

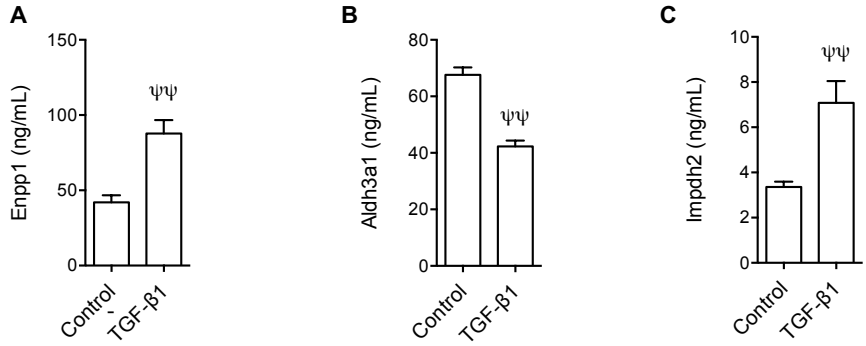

Fig. 5.9. ELISA validation of selected cell-lysate proteins. Expression levels of Enpp1 (A), Aldh3a1 (B) and Impdh2 (C) in cell lysates were analysed by ELISA. n=4, ψψ $p < 0.01$ *vs* control group.

5.4. Effect of Sappanone A, an Impdh2 inhibitor, on TGF-β1-induced fibrogenesis

According to the data of STRING and KEGG pathway analysis **(Fig. 5.7)**, multiple metabolic pathways and the ribosome pathway were linked by Imphd2, which was up-regulated by TGF-β1 and its expression level was confirmed by ELISA (**Fig. 5.9 C**). It is intriguing whether Impdh2 may play an important role in TGF-β1-induced fibrogenesis. The inhibitors of Impdh (including Impdh1 and Impdh2), such as mycophenolic acid (138, 140) and BMS-566419 (137) have been reported to attenuate the progression of renal fibrosis. Sappanone A is known to selectively bind and inactivate Impdh2 but not Impdh1 (136). Thus, I set to address whether the Impdh2 inhibitor sappanone A has an anti-fibrotic effect in this *in-vitro* model of TGF-β1-induced fibrosis.

As shown in **Fig. 5.10**, sappanone A at concentrations of 2-32 μM, did not significantly decrease total collagen accumulation in TGF-β1-induced *in-vitro* model of fibrosis as indicated by PSR-staining assay. Up to 32 μM sappanone A did not increase LDH release from cells and cell detachment index. The lack of anti-fibrotic activity was in contrast to IN1130, a TGF-β type I receptor inhibitor, which significantly inhibited the TGF-β1-induced collagen deposition in the same condition.

The results do not directly support my initial hypothesis that Impdh2 could be a therapeutic target in TGF-β1-induced fibrogenesis. It neither disproves the hypothesis. The quality

control of the commercial Sappanone A and its efficacy in repressing Impdh2 activity at the concentrations used deserve further investigation. Further studies using alternative techniques, such as genetic inhibition of *Impdh2*, are also required to further examine the hypothesis that Impdh2 could be an anti-fibrotic target.

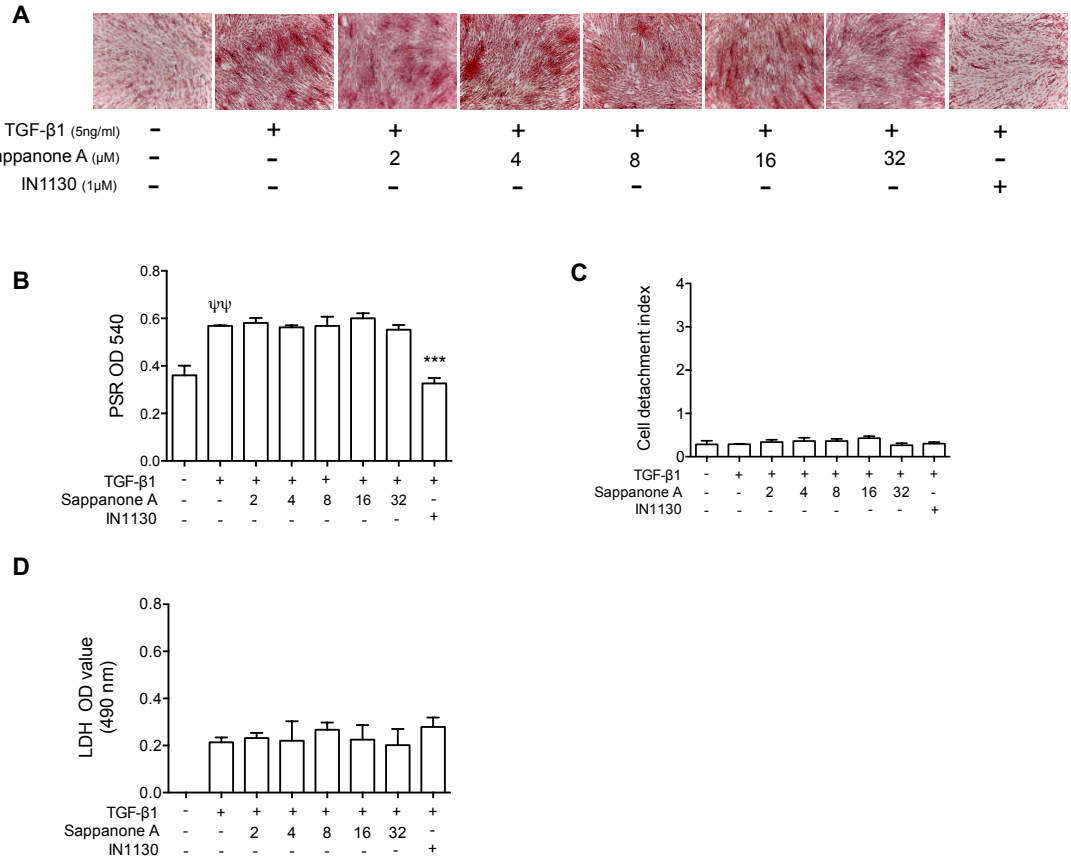

Fig. 5.10. Sappanone A, an Impdh2 inhibitor, did not affect TGF-β1-induced fibrogenesis. NRK-49F cells were treated with 2-32 μM Sappanone A or 1 μM IN1130 in presence of 5 ng/ml TGF-β1 for 48 h. Effects on fibrogenesis were illustrated by representative PSR staining images (A), which visualised total collagen deposition in red colour (×100 magnification); eluted PSR was quantified by spectrophotometric analysis (B) and cytotoxicity was approximated by recording a mean cell detachment index (C) and LDH release assay (D). Experiments were performed in quadruplicate and shown are representative results of two independent experiments with similar results. ψψ $p < 0.01$ *vs* control group, *** $p < 0.001$ *vs* TGF-β1 treated group.

5.5. Proteomic profiling analysis of conditioned media

In total 725 proteins were identified in the conditioned media, of which 62 were significantly regulated by TGF-β1 (**Table 5.6** and **5.7**). No protein was detected only in either control or TGF-β1 group. GO cellular component analysis indicated that in total 20 clusters were generated and the highest number of proteins regulated by TGF-β1 were components of extracellular exosomes, followed by cytoplasm, extracellular space, extracellular region, extracellular matrix, and so on (**Fig. 5.11**). The lists of the proteins involved in enriched GO cellular components are shown in **Table 5.8.** Forty clusters of proteins were identified under GO biological processes. The highest numbers of proteins regulated by TGF-β1 participated in cell adhesion, angiogenesis, proteolysis, cellular response to interleukin-1, positive regulation of ERK1 and ERK2 cascade, etc (**Fig. 5.12**). The lists of the proteins involved in the enriched GO biological processes are shown in **Table 5.9.** As shown in **Fig. 5.13**, GO molecular functions of TGF-β1-regulated proteins in conditioned media were related to bindings with heparin, calciumion, integrin, proteoglycan, insulin-like growth factor, kininogen, CCR2 chemokine receptor. The lists of the proteins involved in enriched GO molecular functions are shown in **Table 5.10**.

Table 5.6. Proteins significantly up-regulated by TGF-β1 in conditioned media.

Accession	Protein	Description	Fold change	*p-value*
P20961	Serpine1 (PAI-1)	Plasminogen activator inhibitor 1	4.41	0.0003
P14844	Ccl2	C-C motif chemokine 2	3.47	0.0012
Q6QMY6	Tsku	Tsukushin	2.60	0.0178
Q9QXY8	Ccl7	C-C motif chemokine 7	2.43	0.0014
Q9ES72	Cyr61	Protein CYR61	2.14	0.0082
Q9R0K8	Stc2	Stanniocalcin-2	1.82	0.0360
Q811A3	Plod2	Procollagen-lysine,2-oxoglutarate 5-dioxygenase 2	1.81	0.0005
O35806	Ltbp2	Latent-transforming growth factor beta-binding protein 2	1.78	0.0310
Q9R1E9	Ctgf	Connective tissue growth factor	1.73	0.0024
P17209	Myl4	Myosin light chain 4	1.68	0.0027

Q9JI03	Col5a1	Collagen alpha-1(V) chain 1	1.56	0.0442
P54690	Bcat1	Branched-chain-amino-acid aminotransferase, cytosolic	1.55	0.0243
Q9WV75	Spon2	Spondin-2	1.54	0.0480
Q9Z0W7	Clic4	Chloride intracellular channel protein 4	1.53	0.0379
Q62736	Cald1	Non-muscle caldesmon	1.49	0.0024
Q4V7E8	Lrrfip2	Leucine-rich repeat flightless-interacting protein 2	1.49	0.0494
Q62908	Csrp2	Cysteine and glycine-rich protein 2	1.46	0.0126
Q3B8Q1	Ddx21	Nucleolar RNA helicase 2	1.35	0.0043
Q2LAP6	Tes	Testin	1.27	0.0231
P39069	Ak1	Adenylate kinase isoenzyme 1	1.27	0.0332
Q9Z2G8	Nap1l1	Nucleosome assembly protein 1-like 1	1.25	0.0421
P23514	Copb1	Coatomer subunit beta	1.21	0.0468
P62752	Rpl23a	60S ribosomal protein L23a	1.19	0.0270
Q6AXS5	Serbp1	Plasminogen activator inhibitor 1 RNA-binding protein	1.15	0.0098
P13084	Npm1	Nucleophosmin	1.14	0.0325

Table 5.7. Proteins significantly down-regulated by TGF-β1 in conditioned media.

Accession	**Protein**	**Description**	**Fold change**	***p-value***
Q9QZQ5	Nov	Protein NOV homolog	0.28	0.0339
B5DFC9	Nid2	Nidogen-2	0.34	0.0393
Q63548	Sema3a	Semaphorin-3A	0.35	0.0412
Q64610	Enpp2	Ectonucleotide pyrophosphatase/phosphodiesterase family member 2	0.36	0.0435
Q6P6T1	C1s	Complement C1s subcomponent	0.39	0.0412
Q6IE64	C1rl	Complement C1r subcomponent-like protein	0.41	0.0487
P03957	Mmp3	Stromelysin-1	0.43	0.0475
Q6P7C7	Gpnmb	Transmembrane glycoprotein NMB	0.49	0.0180
O70513	Lgals3bp	Galectin-3-binding protein	0.5	0.0424
P01322	Ins1	Insulin-1	0.52	0.0122
Q62894	Ecm1	Extracellular matrix protein 1	0.53	0.0372
O55004	Rnase4	Ribonuclease 4	0.54	0.0357
Q08420	Sod3	Extracellular superoxide dismutase [Cu-Zn]	0.55	0.0283
P05964	S100a6	Protein S100-A6	0.56	0.0394
P07092	Serpine2	Glia-derived nexin	0.56	0.0041

P05371	Clu	Clusterin	0.57	0.0342
P52303	Ap1b1	AP-1 complex subunit beta-1	0.58	0.0198
P11883	Aldh3a1	Aldehyde dehydrogenase, dimeric NADP-preferring	0.59	0.0189
O35276	Nrp2	Neuropilin-2	0.59	0.0034
P15087	Cpe	Carboxypeptidase E	0.6	0.0286
P00787	Ctsb	Cathepsin B	0.61	0.0046
P17164	Fuca1	Tissue alpha-L-fucosidase	0.62	0.0006
P97546	Nptn	Neuroplastin	0.63	0.0316
P07154	Ctsl	Cathepsin L1	0.66	0.0420
Q5U4F3	Fam107b	Protein FAM107B	0.67	0.0107
P35053	Gpc1	Glypican-1	0.68	0.0169
B0BNI5	Olfml3	Olfactomedin-like protein 3	0.69	0.0435
Q6P502	Cct3	T-complex protein 1 subunit gamma	0.69	0.0041
Q32KJ6	Galns	N-acetylgalactosamine-6-sulfatase	0.7	0.0175
Q6IRK9	Cpq	Carboxypeptidase Q	0.75	0.0082
Q66H12	Naga	Alpha-N-acetylgalactosaminidase	0.76	0.0276
Q6P7A9	Gaa	Lysosomal alpha-glucosidase	0.78	0.0209
P70615	Lmnb1	Lamin-B1	0.79	0.0250
P28077	Psmb9	Proteasome subunit beta type-9	0.8	0.0180
Q4KM35	Psmb10	Proteasome subunit beta type-10	0.82	0.0341
Q68FP1	Gsn	Gelsolin	0.84	0.0122
O35217	Minpp1	Multiple inositol polyphosphate phosphatase 1	0.85	0.0200

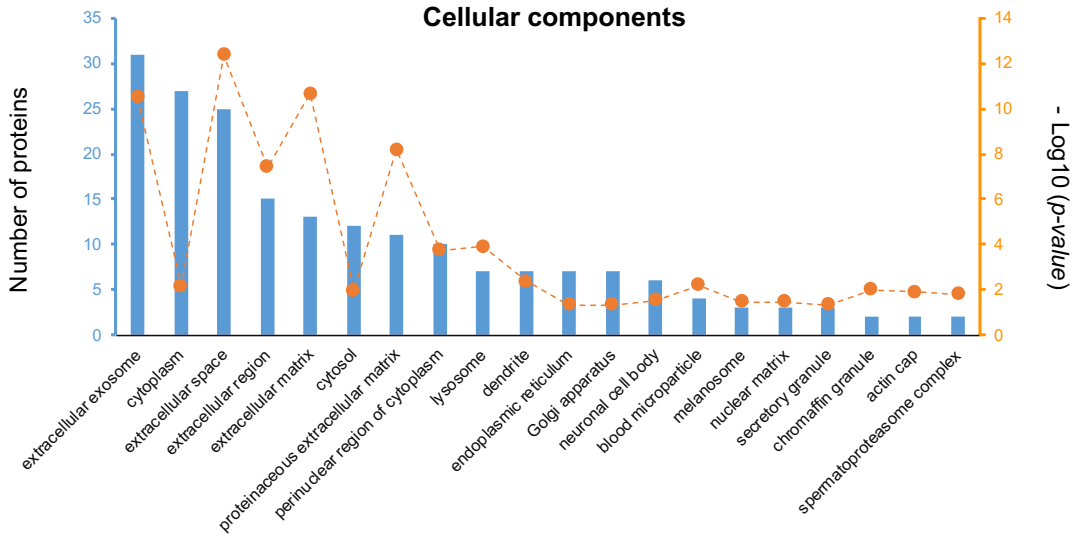

Fig. 5.11. GO cellular component enrichment analysis of the proteins in conditioned media significantly regulated by TGF-β1. The numbers of involved proteins are indicated by the left y-axis shown as blue bars and the *p*-values (as -Log10 values) are indicated by the right y-axis shown as orange dots, respectively.

Table 5.8. GO cellular component analysis of proteins in conditioned media significantly regulated by TGF-β1. ("●": induced by TGF-β1; "●": repressed by TGF-β1).

GO cellular components	Protein (fold change, TGF-β1 *vs* control)
Extracellular exosome	● PAI-1(4.41), Plod2 (1.81), Ltbp2 (1.78), Col5a1 (1.56), Spon2 (1.54), Clic4 (1.53), Ak1 (1.27), Rpl23a (1.19), Serbp1 (1.15) ● Nid2 (0.34), C1s (0.39), C1rl (0.41), Lgals3bp (0.50), Ecm1 (0.53), Rnase4 (0.54), Sod3 (0.55), S100a6 (0.56), Clu (0.57), Cpe (0.60), Ctsb (0.61), Fuca1 (0.62), Ctsl (0.66), Gpc1 (0.68), Cct3 (0.69), Galns (0.70), Cpq (0.75), Naga (0.76), Gaa (0.78), Psmb9 (0.80), Gsn (0.84), Minpp1 (0.85)
Cytoplasm	● PAI-1(4.41), Ccl2 (3.47), Bcat1 (1.55), Clic4 (1.53), Tes (1.27), Ak1 (1.27), Nap1l1 (1.25), Copb1 (1.21), Rpl23a (1.19), Serbp1 (1.15), Npm1 (1.14) ● Nov (0.28), Enpp2 (0.36), Ins1 (0.52), Sod3 (0.55), S100a6 (0.56), Clu (0.57), Aldh3a1 (0.59), Ctsb (0.61), Ctsl (0.66), Cct3 (0.69), Cpq (0.75), Naga (0.76), Lmnb1 (0.79), Psmb9 (0.80), Psmb10 (0.82), Gsn (0.84)
Extracellular space	● PAI-1(4.41), Ccl2 (3.47), Tsku (2.60), Ccl7 (2.43), Stc2 (1.82), Ltbp2 (1.78), Ctgf (1.73), Spon2 (1.54) ● Sema3a (0.35), Enpp2 (0.36), C1rl (0.41), Mmp3 (0.43), Lgals3bp (0.50), Ins1 (0.52), Ecm1 (0.53), Sod3 (0.55), Serpine2 (0.56), Clu (0.57), Aldh3a1 (0.59), Cpe (0.60), Ctsb (0.61), Ctsl (0.66), Gpc1 (0.68), Cpq (0.75), Gsn (0.84)
Extracellular region	● PAI-1(4.41), Ccl2 (3.47), Tsku (2.60), Cyr61 (2.14), Ctgf (1.73) ● Nov (0.28), C1s (0.39), C1rl (0.41), Rnase4 (0.54), Serpine2 (0.56), Clu (0.57), Cpe (0.60), Ctsb (0.61), Olfml3 (0.69), Gsn (0.84)
Extracellular matrix	● PAI-1(4.41), Cyr61 (2.14), Col5a1 (1.56), Spon2 (1.54), Ltbp2 (1.78) ● Nov (0.28), Nid2 (0.34), Mmp3 (0.43), Lgals3bp (0.50), Ecm1 (0.53), Sod3 (0.55), Serpine2 (0.56), Clu (0.57)
Cytosol	● Clic4 (1.53), Ctgf (1.73), Bcat1 (1.55), Npm1 (1.14) ● Mmp3 (0.43), Ins1 (0.52), S100a6 (0.56), Serpine2 (0.56), Clu (0.57), Aldh3a1 (0.59), Psmb9 (0.80), Gsn (0.84)
Proteinaceous extracellular matrix	● Cyr61 (2.14), Ltbp2 (1.78), Ctgf (1.73), Col5a1 (1.56), Spon2 (1.54) ● Nov (0.28), Nid2 (0.34), Mmp3 (0.43), Lgals3bp (0.50), Ecm1 (0.53), Gpc1 (0.68)
Perinuclear region of cytoplasm	● Ccl2 (3.47), Stc2 (1.82), Ctgf (1.73), Clic4 (1.53), Ak1 (1.27), Serbp1 (1.15) ● S100a6 (0.56), Clu (0.57), Ctsb (0.61), Gsn (0.84)
Lysosome	● Ctsb (0.61), Fuca1 (0.62), Ctsl (0.66), Galns (0.70), Cpq (0.75), Naga (0.76), Gaa (0.78)
Dendrite	● Ccl2 (3.47), Cald1 (1.49) ● Nov (0.28), Sema3a (0.35), Mmp3 (0.43), Cpe (0.60), Nptn (0.63)
Endoplasmic reticulum	● Stc2 (1.82), Plod2 (1.81), Clic4 (1.53), Copb1 (1.21) ● Clu (0.57), Aldh3a1 (0.59), Cpq (0.75)
Golgi apparatus	● Stc2 (1.82), Ctgf (1.73), Copb1 (1.21) ● Enpp2 (0.36), Ap1b1 (0.58), Cpe (0.60), Cpq (0.75)
Neuronal cell body	● Ccl2 (3.47), Cald1 (1.49) ● Nov (0.28), Serpine2 (0.56), Cpe (0.60), Gpc1 (0.68)
Blood microparticle	● Gsn (0.84), Clu (0.57), Lgals3bp (0.50), C1s (0.39)
Melanosome	● Nap1l1 (1.25) ● Gpnmb (0.49), Ctsb (0.61)
Nuclear matrix	● Clic4 (1.53), Npm1 (1.14) ● Lmnb1 (0.79)
Secretory granule	● Ctsl (0.66), Cpe (0.60), Ins1 (0.52)

Chromaffin granule	• PAI-1(4.41)
	• Clu (0.57)
Actin cap	• Cald1 (1.49)
	• Gsn (0.84)
Spermatoproteasome complex	• Psmb10 (0.82), Psmb9 (0.80)

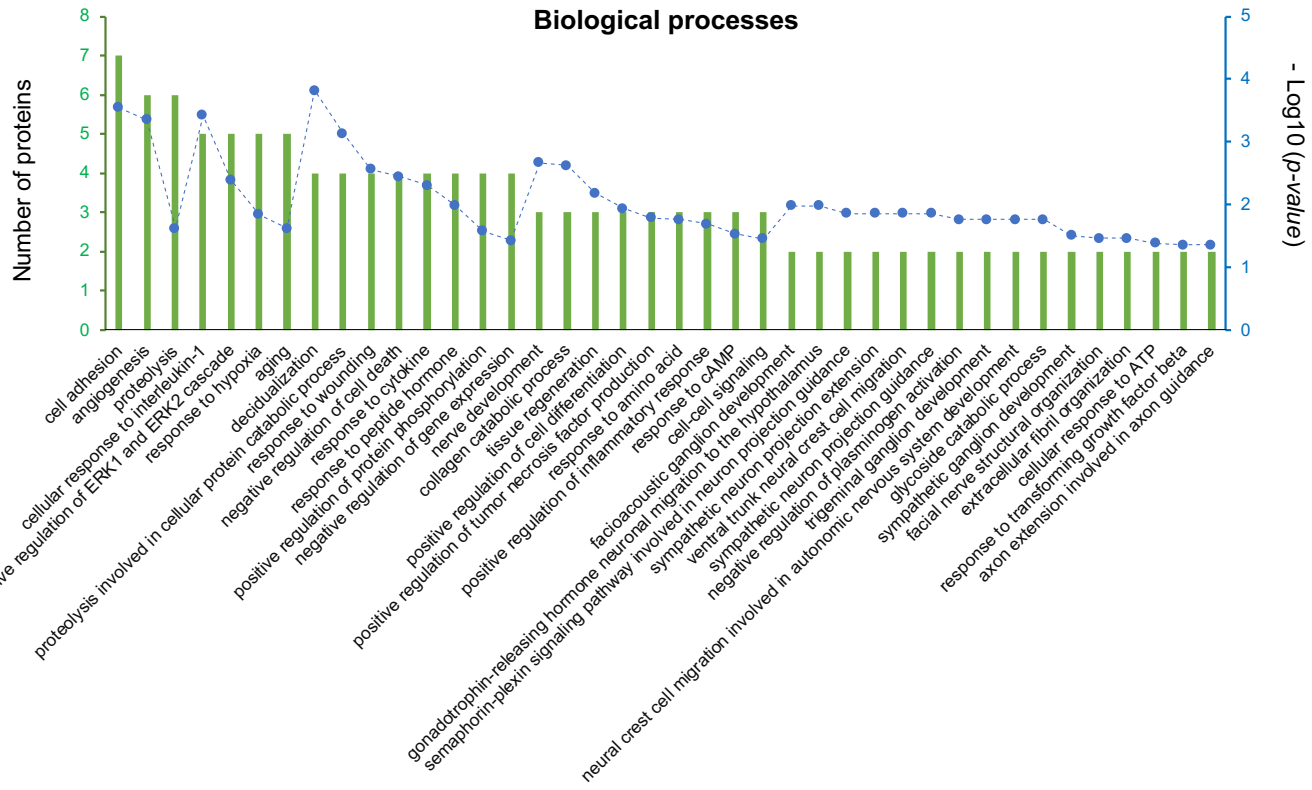

Fig. 5.12. GO biological processe enrichment analysis of the proteins in conditioned media significantly regulated by TGF-β1. The numbers of involved proteins are indicated by the left y-axis shown as green bars and the *p*-values (as -Log10 values) are indicated by the right y-axis shown as blue dots, respectively.

Table 5.9. GO biological process analysis of proteins in conditioned media significantly regulated by TGF-β1. ("●": induced by TGF-β1; "●": repressed by TGF-β1).

GO biological processes	Protein (fold change, TGF-β1 *vs* control)
Cell adhesion	● Cyr61 (2.14), Ctgf (1.73), Col5a1 (1.56), Spon2 (1.54)
	● Nov (0.28), Gpnmb (0.49), Lgals3bp (0.50)
Angiogenesis	● PAI-1(4.41), Ctgf (1.73), Clic4 (1.53)
	● Nov (0.28), Ecm1 (0.53), Nrp2 (0.59)
Proteolysis	● C1s (0.39), C1rl (0.41), Mmp3 (0.43), Ctsb (0.61), Ctsl (0.66), Cpq (0.75)
Cellular response to interleukin-1	● PAI-1(4.41), Ccl2 (3.47), Ccl7 (2.43)
	● Mmp3 (0.43), Psmb9 (0.80)
Positive regulation of ERK1 and ERK2 cascade	● Ccl2 (3.47), Ccl7 (2.43), Ctgf (1.73)
	● Gpnmb (0.49), Nptn (0.63)
Response to hypoxia	● Ccl2 (3.47), Plod2 (1.81)
	● Mmp3 (0.43), Sod3 (0.55), Aldh3a1 (0.59)
Aging	● Ccl2 (3.47), Ctgf (1.73)
	● Clu (0.57), Aldh3a1 (0.59), Gsn (0.84)
Decidualization	● PAI-1(4.41), Stc2 (1.82)
	● Ctsb (0.61), Ctsl (0.66)
Proteolysis involved in cellular protein catabolic process	● Psmb10 (0.82), Psmb9 (0.80), Ctsl (0.66), Ctsb (0.61)
Response to wounding	● Ccl2 (3.47)
	● Serpine2 (0.56), Clu (0.57), Ctsb (0.61)
Negative regulation of cell death	● Cyr61 (2.14), Ctgf (1.73)
	● Nov (0.28), Ctsb (0.61)
Response to cytokine	● PAI-1(4.41)
	● Mmp3 (0.43), Ins1 (0.52), Ctsb (0.61)
Response to peptide hormone	● Stc2 (1.82), Ctgf (1.73)
	● Ins1 (0.52), Ctsb (0.61)
Positive regulation of protein phosphorylation	● Cyr61 (2.14), Ctgf (1.73)
	● Gpnmb (0.49), Nptn (0.63)
Negative regulation of gene expression	● PAI-1(4.41), Stc2 (1.82), Ctgf (1.73), Npm1 (1.14)
Nerve development	● Sema3a (0.35), Nrp2 (0.59), Ctsl (0.66)
Collagen catabolic process	● Mmp3 (0.43), Ctsb (0.61), Ctsl (0.66)
Tissue regeneration	● PAI-1(4.41)
	● Cpq (0.75), Gsn (0.84)
Positive regulation of cell differentiation	● Cyr61 (2.14), Ctgf (1.73)
	● Clu (0.57)
Positive regulation of tumor necrosis factor production	● Ccl2 (3.47), Spon2 (1.54)
	● Clu (0.57)
Response to amino acid	● Ccl2 (3.47), Ctgf (1.73)
	● Mmp3 (0.43)
Positive regulation of inflammatory response	● PAI-1(4.41), Ccl2 (3.47), Ccl7 (2.43)

Response to camp	• Aldh3a1 (0.59), Ins1 (0.52), C1s (0.39)
Cell-cell signalling	• Cyr61 (2.14), Ctgf (1.73)
	• Nov (0.28)
Facioacoustic ganglion development	• Nrp2 (0.59), Sema3a (0.35)
Gonadotrophin-releasing hormone neuronal migration to the hypothalamus	• Nrp2 (0.59), Sema3a (0.35)
Semaphorin-plexin signaling pathway involved in neuron projection guidance	• Nrp2 (0.59), Sema3a (0.35)
Sympathetic neuron projection extension	• Nrp2 (0.59), Sema3a (0.35)
Ventral trunk neural crest cell migration	• Nrp2 (0.59), Sema3a (0.35)
Sympathetic neuron projection guidance	• Nrp2 (0.59), Sema3a (0.35)
Negative regulation of plasminogen activation	• PAI-1(4.41)
	• Serpine2 (0.56)
Trigeminal ganglion development	• Nrp2 (0.59), Sema3a (0.35)
Neural crest cell migration involved in autonomic nervous system development	• Nrp2 (0.59), Sema3a (0.35)
Glycoside catabolic process	• Naga (0.76), Fuca1 (0.62)
Sympathetic ganglion development	• Nrp2 (0.59), Sema3a (0.35)
Facial nerve structural organization	• Nrp2 (0.59), Sema3a (0.35)
Extracellular fibril organization	• Ltbp2 (1.78), Col5a1 (1.56)
Cellular response to ATP	• PAI-1(4.41), Ccl2 (3.47)
Response to transforming growth factor beta	• PAI-1(4.41), Cald1 (1.49)
Axon extension involved in axon guidance	• Nrp2 (0.59), Sema3a (0.35)

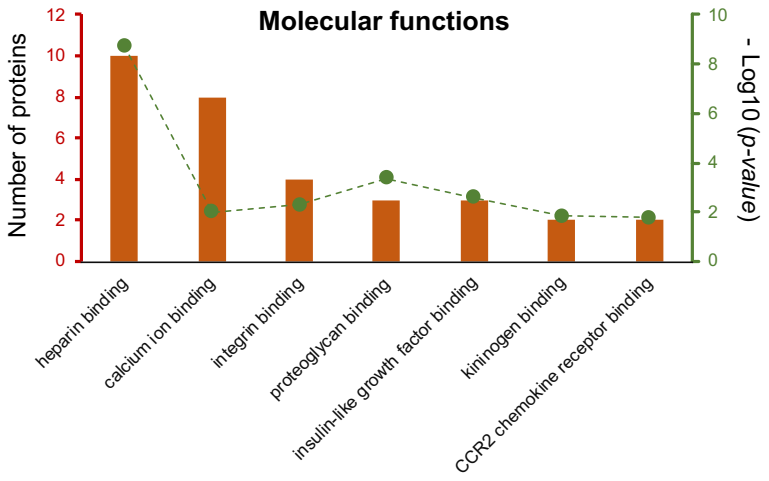

Fig. 5.13. GO molecular function enrichment analysis of the proteins in conditioned media significantly regulated by TGF-β1. The numbers of involved proteins are indicated by the left y-axis shown as orange bars and the *p*-values (as -Log10 values) are indicated by the right y-axis shown as green dots, respectively.

Table 5.10. GO molecular function analysis of proteins in conditioned media significantly regulated by TGF-β1 ("●": induced by TGF-β1; "●": repressed by TGF-β1).

GO molecular functions	**Protein (fold change, TGF-β1 *vs* control)**
Heparin binding	● Ccl2 (3.47), Ccl7 (2.43), Cyr61 (2.14), Ltbp2 (1.78), Ctgf (1.73), Col5a1 (1.56)
	● Nov (0.28), Gpnmb (0.49), Serpine2 (0.56), Nrp2 (0.59)
Calcium ion binding	● Ltbp2 (1.78), Myl4 (1.68)
	● Nid2 (0.34), Enpp2 (0.36), C1s (0.39), Mmp3 (0.43), S100a6 (0.56), Gsn (0.84)
Integrin binding	● Cyr61 (2.14), Ctgf (1.73)
	● Nov (0.28), Gpnmb (0.49)
Proteoglycan binding	● Col5a1 (1.56)
	● Ctsb (0.61), Ctsl (0.66)
Insulin-like growth factor binding	● Cyr61 (2.14), Ctgf (1.73)
	● Nov (0.28)
Kininogen binding	● Ctsb (0.61), Ctsl (0.66)
CCR2 chemokine receptor binding	● Ccl2 (3.47), Ccl7 (2.43)

As shown in **Fig. 5.14**, STRING analysis of the conditioned media reveals that increased PAI-1, a potent inhibitor of collagen degradation, and repressed collagen-degradation enzyme Mmp3, centred the secretomic interaction map of TGF-β1-regulated proteins, suggesting that TGF-β1 repression of collagen degradation might play an important role in TGF-β1 induced fibrogenesis. Also locating at the centre of this secretomic interaction map are TGF-β1-induced chemokines Ccl2 (MCP-1) and Ccl7 (MCP-3), suggesting that TGF-β1-induced fibrogenesis is inherently coupled with inflammation by promoting chemotactic effects. Indeed, PAI-1, Ccl2 and Ccl7 regulation by TGF-β1 is involved in positive regulation of inflammation resonse, according to GO biological process analysis (**Table 5.9**).

KEGG pathway analysis suggested that TGF-β1 regulated the Lysosome and the Rheumatoid arthristis pathways (**Fig. 5.15**). Six proteins were involved in the Lysosome pathway, including Gaa, Naga, Galns, Ctsl, Ctsb and Ap1b1, which were all significantly reduced by TGF-β1. In addition, GO cellular component analysis showed that 7 proteins located in lysosome, including Ctsb, Fuca1, Ctsl, Galns, Cpq, Naga and Gaa, were all reduced by TGF-β1 (**Table 5.8**). In the rheumatoid arthritis pathway, TGF-β1 induced Ccl2 and suppressed Ctsl and Mmp3.

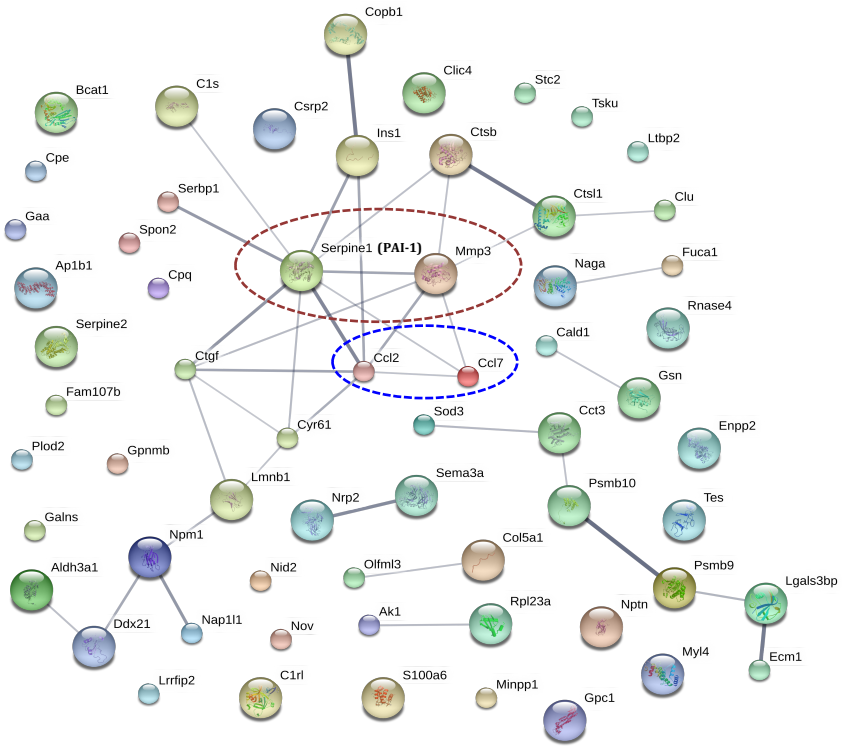

Fig. 5.14. STRING analysis illustrates predicted direct (physical) and indirect (functional) associations among proteins in conditioned media significantly regulated by TGF-β1. TGF-β1-induced PAI-1 and -repressed Mmp3 (red circle) and TGF-β1-induced chemokines Ccl2 and Ccl7 (blue circle) centered the protein interaction network.

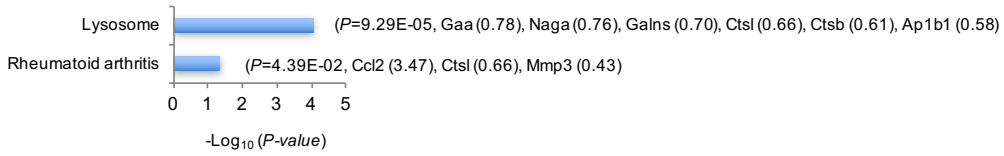

Fig. 5.15. KEGG pathways of proteins in conditioned media regulated by TGF-β1. Y-axis represents significantly enriched KEGG pathway terms and X-axis indicates -Log10 *p*-value. The *p*-value and involved proteins (fold change, TGF-β1 *vs* control) were demonstrated in the brackets.

Volcano plot analysis was applied to demonstrate TGF-β1-induced and -suppressed proteins in conditioned media, including 25 up-regulated and 37 down-regulated proteins. As shown in **Fig. 5.16**, PAI-1 was the most significantly and most dramatically induced by TGF-β1, accompanying up-regulation of chemokines Ccl2 and Ccl7, signalling mediators Cyr61 (Ccn1), Ctgf (Ccn2) and Tsku, and collagen crosslinking enzyme Plod2. In addition, TGF-β1 most dramatically repressed another CCN family member, Nov (Ccn3), and suppressed collagen degradation enzyme Mmp3, among other proteins.

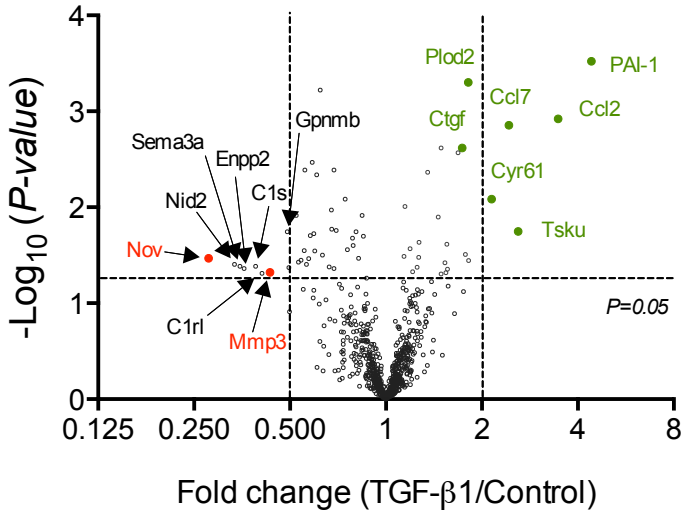

Fig. 5.16. Volcano plot shows the proteins in conditioned media regulated by TGF-β1. Those proteins of interest for further validation are highlighted in green font (induced by TGF-β1) and red font (suppressed by TGF-β1), respectively.

5.6. ELISA validation of selected proteins in conditioned media

Nine proteins in conditioned media were selected for validation by ELISA. They are: (1) five TGF-β1-induced proteins with fold changes>2: PAI-1, Ccl2, Ccl7, Tsku and Cyr61; (2) two TGF-β1-induced proteins with likely relevance to fibrosis: collagen crosslinking enzyme Plod2 and fibrotic mediator Ctgf; (3) the protein most significantly down-regulated by TGF-β1, Nov; and (4) collagen degradation enzyme Mmp3. In agreement with the mass spectrometric data, ELISA assay of PAI-1, Ccl2, Ccl7, Tsku, Plod2, Cyr61 and Ctgf confirmed that they were significantly induced by TGF-β1, Nov and Mmp3 were both significantly lower in TGF-β1 group (**Fig. 5.17**).

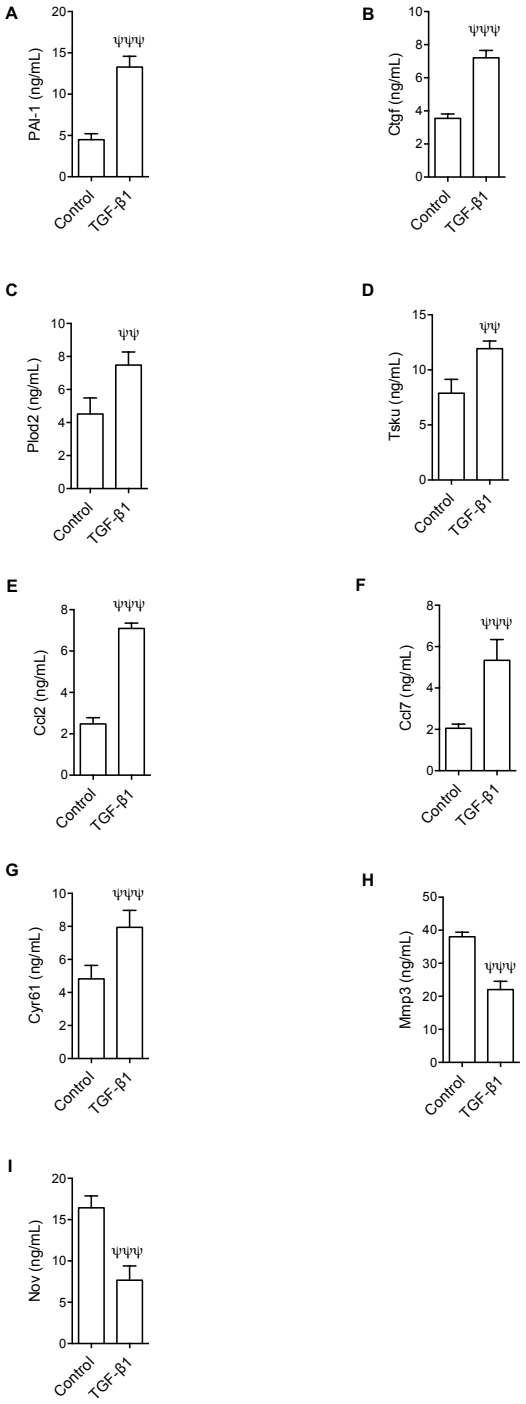

Fig. 5.17. Validation of selected proteins in conditioned media by ELISA. ELISA results of PAI-1(A), Ctgf (B), Plod2 (C), Tsku (D), Ccl2 (E), Ccl7 (F), Cyr61 (G), Mmp3 (H) and Nov (I). n=4, ψψ $p < 0.01$, ψψψ $p < 0.001$ *vs* control group.

5.7. Discussions

5.7.1. Comparison with a proteomic study of TGF-β1-induced fibrogenesis in NRK-49F cells in the literature

As far as I know, there is only one proteomic anlysis of TGF-β1 induced fibrogenesis in NRK-49F cells (and indeed any fibroblasts) in the literature (141). Although the same cell line NRK-49F was used in both studies, different experimental design and technical details resulted in varied findings. The main differences between the two studies are summarised in **Table 5.11**.

Table 5.11. Comparison of proteomic studies of TGF-β1-induced fibrogenesis in NRK-49F cells.

	Reference (141)	Present study
Cell cluture	Cells were grown to 60%-70% confluence in 10%FBS-DMEM for 12h, change to serum-free medium after washing twice.	Cells were grown in DMEM with 2.5% FCS and 2.5% Nu-serum replacement for 3 days, then changed the medium to 1% ITS-DMEM for another 4 days. Cells were washed with serum free, phenol red-free DMEM twice.
Treatment	2 ng/mL TGF-β1 for 6 h	5 ng/mL TGF-β1 for 48 h
Protein extration	• The conditioned media were not collected for proteomics analysis; • Cells lysates were harvested using a buffer containing 5mM EDTA,9.5M urea, 4%v/v CHAPS, 65mM DTT and protease inhibitors for 1 h at 24℃ and subjected to proteomic analysis	• The conditioned media were collected for proteomics analysis; • Cells lysates were harvested using a RIPA buffer with protease and phosphatase inhibitors for 10 min at room temperature, and were subjected to proteomic analysis
Proteomic analysis methodlogy	• 2D-gel electrophoresis and in-gel digestion of selected spots • MALDI-TOF-MS with reference to NCBI and Swiss-Prot databases	• In-solution digestion and TMT-labelling • (nESI) Orbitrap-MS with reference to Protein Discover and Mascot databases

Note: MALDI: matrix assisted laser desorption/ionisation; TOF: time-of-flight; (nESI): nano-electrospray ionisation (nESI).

Kang *et al*. missed all proteins in conditione media. Using a much less sensitive, 2D-gel electrophoresis-based proteomic technology, they only found 74 proteins significantly regulated by TGF-β1 (141). This is in contrast to 628 proteins regulated by TGF-β1 in the present study. As shown in **Fig. 5.18**, there were 13 overlapping proteins and their accession numbers, *p*-values and fold-changes are listed in **Table 5.12**. Among them, TGF-β1 significantly suppressed Gstp1, Oat, Sdhb and Lrpap1 and induced Cald1, Pdlim1, Nme2 and Stip1 in both studies. However, 5 proteins, including Aldh3a1, Icam1, Stmn1, Prdx2 and Ruvbl1, showed different trends after TGF-β1 treatment. In addition, several differentially expressed proteins were highlighted in that study, including PAI-1, peroxisome proliferator-

activated receptor, prohibitin, intercellular adhesion molecule-1, however, they were not detected in the present study. Those descrepanies can be explained by the different experimental designs and methods summarised in **Table 5.10** (142). Of interest, although PAI-1 was induced by TGF-β1 in cell lysates 6 hours (141) after treatment, PAI-1 induced by TGF-β1 48 h after treatment in the present work was only observed in conditioned media, but not in cell lysates.

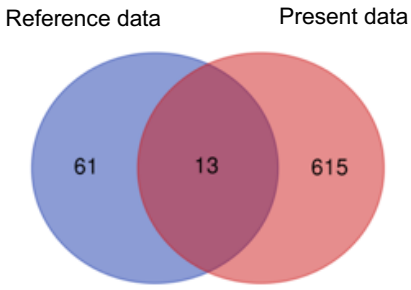

Fig. 5.18. Venn diagram showing similarities and differences between the proteins significantly changed by TGF-β1 in reference data (141) and the proteins detected in present study.

Table 5.12. The overlapping proteins significantly changed by TGF-β1 in reference data and the present study. The fold change columns correspond to the expression of each protein relative to its expression in control cells.

Accession	Protein	Description	Present data		Reference
			t-test	Fold change	Fold change
P11883	Aldh3a1	Aldehyde dehydrogenase, dimeric NADP-preferring	0.000007	−4.5	1.6
Q00238	Icam1	Intercellular adhesion molecule 1	0.000536	−1.5	2.1
P04906	Gstp1	Glutathione S-transferase P	0.013291	−1.5	−2.0
P04182	Oat	Ornithine aminotransferase, mitochondrial	0.004721	−1.4	−2
P21913	Sdhb	Succinate dehydrogenase [ubiquinone] iron-sulfur subunit, mitochondrial	0.020986	−1.4	−2.0
Q99068	Lrpap1	Alpha-2-macroglobulin receptor-associated protein	0.001466	−1.4	−2.5
P13668	Stmn1	Stathmin	0.009580	−1.2	1.2
P35704	Prdx2	Peroxiredoxin-2	0.005688	−1.2	8.6
Q62736	Cald1	Non-muscle caldesmon	0.000117	2.0	3.4
P52944	Pdlim1	PDZ and LIM domain protein 1	0.000008	1.9	3.5

P19804	Nme2	Nucleoside diphosphate kinase B	0.024035	1.6	3.0
P60123	Ruvbl1	RuvB-like 1	0.005566	1.2	−1.2
O35814	Stip1	Stress-induced-phosphoprotein 1	0.000292	1.1	2.2

5.7.2. TGF-β1-induced fibrogenesis may be an intracellular metabolic disorder

TGF-β1-induced fibrogenesis in fibroblasts may be an intracellular metabolic disorder characterised by increased intracellular proteins of the ribosome pathway and reduced proteins of multiple metabolic pathways.

As shown in **Fig. 5.5**, TGF-β1 most significantly regulated the ribosome pathway and induced numerous cytosolic ribosomal proteins, while repressing Mrpl3, a mitochondrial ribosomal protein (**Table 5.1**), suggesting that TGF-β1-induced fibrogenesis may be differentially associated with cytosolic and mitochondrial ribosomal proteins. TGF-β1 is well known to induce cell hypertrophy (143), which is associated with increased protein synthesis through regulation of mTOR, a key kinase involved in protein synthesis and growth (144). mTORC1 positively regulates ribosomal RNA transcription, the synthesis of ribosomal proteins and other components required for ribosome assembly (145, 146). Given the roles of ribosome in protein synthesis, it may not be surprising that the ribosome pathway is induced by TGF-β1. However, to my best knowledge, the functions of those ribosomal proteins in fibrosis remain largely unknown, which deserve further study.

Fig. 5.5 shows mutiple metablic pathways were significantly regulated by TGF-β1 in cell lysates, in particularly, energy metabolism, including the citrate acid (TCA) cycle, fatty acid metabolism/degradation/elongation, glycolysis/gluconeogenesis. The TCA cycle, with the primary responsibility for cellular energy production, is the final common oxidative pathway for fats, carbohydrates and amino acids and is the most important central pathway connecting almost all individual metabolic pathways (145). Addtionally, the TCA cycle has a close relationship with fibrotic diseases. Zhao *et al*. reported that overall decreased TCA cycle metabolites and enzymes in lungs of patients with idiopathic pulmonary fibrosis (147). At the early stage of liver fibrosis in rat, the TCA cycle was slowed by cellular regulation to reduce the natural production of reactive oxygen species (ROS) (148). Similarly, in the present study, the proteins enriched in the TCA cycle were all repressed by TGF-β1 (**Table 5.1**), potentially indicating a down-regulated TCA cycle. Fatty acid metabolism occurs primarily in the mitochondria and is important for generating ATP for energy production and participates in the TCA cycle, ultimately leading to ATP synthesis. In the present study, the proteins invovled in fatty acid degradation (except Acsl5), fatty acid metabolism (except

Acsl5 and Fasn) and fatty acid elongation were reduced by TGF-β1 (**Table 5.1**), suggesting that multiple fatty acid metabolism pathways may participate in TGF-β1-induced fibrosis. Xiong *et al*. demonstrated that endothelial fatty acid oxidation is a critical *in-vitro* and *in-vivo* regulator of TGF-β1-induced endothelial-to-mesenchymal transition (EndoMT). TGF-β1-induced EndoMT is accompanied by an inhibition of fatty acid oxidation (149). In addition, humans and mouse models with tubulointerstitial fibrosis had lower expression of key enzymes and regulators of fatty acid oxidation (150). Togather these studies indicate a potential associassion between fatty acid metabolism and TGF-β1-induced fibrosis in fibroblasts that may merit further evaluation. Almost all the proteins involved in glycolysis/gluconeogenesis pathway were reduced by TGF-β1 (**Table 5.1**), suggesting that glycolysis contributed to energy production by generating ATP and participating in the TCA cycle (151). In addition, amino acid metabolism was regulated by TGF-β1 (**Fig. 5.5**, **Table 5.1**), i.e. valine, leucine, and isoleucine degradation, biosynthesis of amino acids, lysine degradation, tryptophan metabolism, beta-alanine metabolism, arginine and proline metabolism, histidine metabolism, phenylalanine metabolism, glycine, serine and threonine metabolism, tyrosine metabolism. These findings are in keeping with the facts that the ribosome pathway was most significantly regulated by TGF-β1 and that the ribosome mediates the incorporation of amino acids into proteins.

5.7.3. TGF-β1 most significantly induced Enpp1 and repressed Aldh3a1 and Cat

Enpp1, a membrane-bound protein, plays a role in regulating pyrophosphate levels, and functions in bone mineralisation and soft tissue calcification (152). Shimokado *et al*. reported that Enpp1 was decreased at the mRNA, protein and enzymatic acivity levels in Smad3(-/-) vascular smooth muscle cells (vSMCs) compared with Smad3(+/+) vSMCs. Smad3 is a well-known intracellular signalling molecule of TGF-β. In their study, a ChIP assay also revealed that phosphorylated Smad3 directly binds to the promotor region of Enpp1 gene, leading to TGF-β/Smad3 signalling and translation of Enpp1 (153). Xu *et al*. showed that Enpp1 expression was increased when end-plate chondrocytes were exposed to TGF-β1, but decreased after TGF-β knockdown with siRNA. It suggested that expression of Enpp1 is likely dependent on TGF-β1 in end-plate chondrocytes (154, 155). However, no study has examined whether Enpp1 is involved in TGF-β1-induced fibrogenesis in renal fibroblasts yet.

Aldh3a1, a member of the aldehyde dehydrogenase superfamily, protects the ocular tissue from ultraviolet radiation (UVR)-induced oxidative stress through multiple mechanisms including directly absorbing UV light, metabolising toxic aldehydes derived from lipid peroxidation, scavenging reactive oxygen species and producing antioxidant NAD(P)H (156,

157). In particular, Aldh3a1 showed antioxidant activities in stromal fibroblasts *in vitro* (158). However, the importance of dramatic repression of Aldh3a1 in TGF-β1-induced fibrosgenesis is unknown and deserves further investigation. In addition, TGF-β1 most significantly repressed the abundance of catalase (Cat), an important enzyme in protecting the cell from oxidative damage (159). Indeed, Sunami, R. *et al* reported that catalase deficiency promoted tubulointerstitial injury and fibrosis after unilateral ureteral obstruction (160). Furthermore, Kobayashi, M. *et al* demonstrated that catalase deficiency enhanced renal fibrosis in mice (159). These studies support the protective role of catalase in renal fibrosis and suggest catalase repression may play an important role in TGF-β1-induced fibrogenesis.

5.7.4. TGF-β1 triggered pro-fibrotic and anti-fibrotic signals

Fibrosis is characterised by excessive accumulation of ECM, resulting from increased synthesis and/or decreased degradation of ECM. The plasminogen activation system plays an important role in ECM degradation, whereas PAI-1 (serpine 1) is a potent inhibitor of plasminogen activators (161, 162). Accordingly, PAI-1 was most significantly and dramatically induced by TGF-β1 in present study, and a number of studies have established the association of elevated expression of PAI-1 in glomerulosclerosis and kidney fibrosis and PAI-1 deficiency reduced TGF-β1-induced collagen accumulation and kidney fibrosis (163, 164). Thus, PAI-1 is a critical element of the TGF-β network which could be considered as a therapeutic target for fibrosis (165). Of note, in the aforementioned proteomic study by Kang *et .al*, the expression of PAI-1 was induced by TGF-β1 in cell lysates of NRK- 49F cells (141), but in the present study, PAI-1 only can be detected in conditioned media but not in cell lysates.

In addition, the matrix metalloproteinase (MMP) system is also known for their critical role in degradation and remodelling of ECM (166). The results of the present study demonstrated that Mmp3 was decreased after TGF-β1 treatment whereas the possible roles of Mmp3 in the pathogenesis of kidney fibrosis are largely unknown. Additionally, the specific roles of Mmp3 in fibrosis may dependent on diverse organs and cell types. It has been found that the mRNA and protein expression of Mmp3 was upregulated in patients with idiopathic pulmonary fibrosis (167) as well as in bleomycin induced lung fibrosis (168, 169). Moreover, transient adenoviral vector-mediated expression of recombinant Mmp3 in rat lungs resulted in accumulation of myofibroblasts and fibrosis (169). It suggested that Mmp3 may have emerged as a critical player in the pathogenesis of fibrosis.

Collagen cross linking is another important structural modification that can prevent ECM degradation in fibrosis (170). Plod2, a collagen cross-linking enzyme, was increased in fibrogenesis induced by TGF-β1. Plod2 is responsible for the hydroxylation of lysine residues in collagen telopeptides and is essential for collagen pyridinoline cross-link formation (171, 172). The increase in pyridinoline cross-links leads to irreversible accumulation of collagen and difficulty of collagen degradation (170, 173). It is interesting to find out whether Plod2 could be targeted as a viable anti-fibrotic strategy.

Ctgf, also known as Ccn2, a member of the CCN family, is regarded a major pro-fibrotic molecule, acting downstream of TGF-β1 and resulting in ECM accumulation and fibrosis. As an established fibrogenic mediator, Ctgf (Ccn2) is considered a therapeutic target of renal fibrosis (174-176). In contrast to pro-fibrotic Ctgf (Ccn2), two other CCN family members, Cyr61 (Ccn1) and Nov (Ccn3) appear to have anti-fibrotic activities, although through distinct mechanisms. Overexpression of Cyr61 (Ccn1) triggers cellular senescence, which contributes to wound healing (177) and tissue repair (178), where senescent cells can increase expression of ECM-degrading enzymes such as MMPs (179) and downregulation of ECM components such as collagen (180). In addition, Kim *et al*. (178) reported that Cyr61 accumulated in livers of patients with cirrhosis as well as murine models of hepatic injury. Cyr61 acts as a key regulator that triggers cellular senescence through reactive oxygen species-dependent activation of the p53- and $p16^{INK4}$/pRb pathway in activated hepatic stellate cells and portal fibroblasts, thereby limiting fibrogenesis and promoting regression of liver fibrosis induced by carbon tetrachloride intoxication and bile duct ligation. Further, tail vein delivery of purified Cyr61 protein in mice with established fibrosis accelerates fibrosis regression. These findings suggest that activation of the Cyr61-induced senescence pathway may hold therapeutic promise. Furthermore, Nov (Ccn3) acts as a negative regulator of Ctgf (Ccn2) in *in-vitro* (181) and *in-vivo* models (182) with the capacity to limit ECM accumulation and ameliorate fibrosis. Except Ctgf (Ccn2) inhibitors, clinical trials have not been carried out on selectively regulating other CCN proteins, it will be interesting to investigate the full range of CCN members as multiple therapeutic targets in the future (183).

Tsku (Tsukushi), a member of the secreted small leucine-rich repeat proteoglycan (SLRP) family, interact with signalling molecules such as BMP (184), Wnt (185) and TGF-β1 (186). In particular, Tsku can enhance macrophage activation (187), whereas macrophages are critically involved in pro- and anti-fibrotic procedures (188). Tsku also inhibited myofibroblast differentiation by competing with endogenous TGF-β1 (187, 189). Therefore, Tsku may play dual functions in TGF-β1-induced fibrosis and its role as a target for anti-fibrotic therapy may need further investigation.

5.7.5. TGF-β1 induced chemokines Ccl2 and Ccl7

Notably, two chemokines Ccl2 (MCP-1) and Ccl7 (MCP-3) were significantly up-regulated by TGF-β1. Many studies have emphasised that fibrosis is tightly linked with inflammation and chemokines mediate tissue fibrosis of many different organs (190). Especially Ccl2, as a major promoter of inflammation, has been highlighted in renal fibrosis in animal models of UUO (191) and diabetic nephropathy (192). A mouse model of UUO indicated that Ccl2, through its cognate receptor, Ccr2, is responsible for progression of renal fibrosis and that inhibition of Ccl2/Ccr2 signalling may serve a beneficial therapeutic application for renal fibrosis (191). Evidence from animal models of diabetes also suggested that Ccl2 can directly and indirectly promote renal fibrosis. Ccl2-deficient diabetic kidneys showed that a lack of Ccl2 reduces accumulation of interstitial myofibroblasts and deposition of glomerular and interstitial collagen type IV (192). In addition, therapeutic blockade of Ccl2 in type 1 diabetic mice reduced glomerular deposition of TGF-β1 and collagen IV (193). Notably, in each of these studies, a deficiency or blockade of Ccl2 was associated with a marked decline in the number of kidney macrophages, suggesting that Ccl2-mediated macrophage accumulation and activation promotes fibrosis in diabetic nephropathy. Systematic reviews of the literature have identified Ccl2, as well as TGF-β and Mmp2, as promising biomarkers with diagnostic and prognostic potential in patients with renal disease (194, 195).

Ccl7 was overexpressed in dermal fibroblasts in systemic sclerosis and suggested that it may have pro-fibrotic effects (196). Subsequent study showed that Ccl7-induced collagen type I secretion is partially mediated by Smad3-dependent signalling, meanwhile, Ccl7 gene expression was stimulated by recombinant TGF-β1. Comparison of downstream signalling that regulates collagen gene activation by both cytokines confirmed the central role of MAPK pathway activation in mediating the effects of both factors (197). A mouse model of UUO indicated the role of Ccl7 in renal TIF differs depending on the stage of the pathology. In early stages (0-8 days), Ccl7 deficient (Ccl7-KO) mice displayed attenuated TIF potentially involving two mechanisms: an early (0-3 days) decrease of inflammatory cell infiltration followed (3-8 days) by a decrease in tubular ECM production independent of inflammation. In contrast, during later stages of obstruction (10-14 days), Ccl7-KO mice displayed increased TIF which was again associated with reduced inflammation (198). Taken together, targeting chemokines Ccl2/7 or related pathways may be an alternative strategy to attenuate or reverse fibrosis in chronic kidney disease.

5.8. Conclusions

This project has successfully established a proteomic view on an *in-vitro* model of TGF-β1-induced fibrogenesis in NRK-49F cells. Analysis of data on cell lysates and conditioned media has led to complementary insights into TGF-β1-induced fibrosis and related biological mechanisms and contexts (**Fig. 5.19)**.

- It was characterised with increased ribosomal proteins and reduced proteins involved in multiple metabolic pathways. The dysregulated pathways were linked by Impdh2, a druggable target (**Fig. 5.7**).
- It is characterised by most robustly induced Enpp1 and supressed Aldh3a1, although their roles in renal fibrosis are little known (**Fig. 5.8**).
- It is characterised by most significantly repressed expression of catalase, a very important enzyme in protecting the cell from oxidative damage by reactive oxygen species (**Fig. 5.8)**.
- It was mediated by dysregulation of key matrix degradation regulators (PAI-1 and Mmp3), signalling mediators (Cyr61/Ccn1, Ctgf/Ccn2, Nov/Ccn3 and Tsku) and a collagen crosslinker (Plod2), and was inherently coupled with inflammation mediated by chemokines Ccl2 and Ccl7 (**Fig. 5.16**).

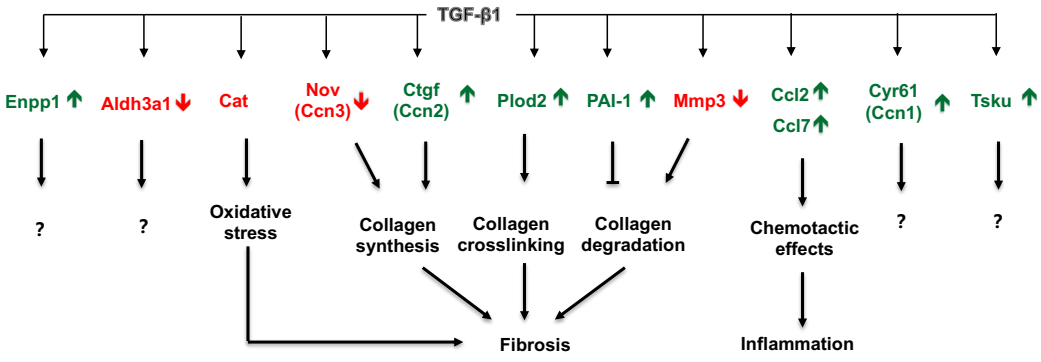

Fig. 5.19. Possible mechanisms and potential therapeutic targets of TGF-β1-induced fibrosis in NRK-49F cells. TGF-β1-induced fibrosis is characterized by dysregulation of key matrix degradation regulators (PAI-1↑ and Mmp3 ↓), signalling mediators (Cyr61/Ccn1 ↑, Ctgf/Ccn2 ↑, Nov/Ccn3 ↓ and Tsku ↑) and a collagen crosslinker (Plod2 ↑), and is coupled with inflammation mediated by chemokines (Ccl2 ↑ and Ccl7 ↑). Induced and repressed proteins by TGF-β1were highlighted in green and red fonts.

Chapter 6: Comparative proteomic analysis of the fibrotic effects of SRM, baicalein and IN1130

In chapter 4, anti-fibrotic activities of two SR extracts (SRA and SRM) and five SR derived-flavonoids commonly used for SR quality control (baicalin, baicalein, wogonoside, wogogin and oroxylin-A) were examined by quantitative analysis of total collagen and fibrogenic molecular markers. SRM, which contained 8-fold more flavonoids than SRA (**Table 4.1)**, had 4-fold higher anti-fibrotic activities (**Fig. 4.5**). Among the five SR flavonoids, baicalein showed the highest anti-fibrotic activity, with little toxicity (**Fig. 4.9**). Accordingly, SRM and baicalein were selected for further proteomic analysis of their mechanisms of action, in parallel with proteomic studies of TGF-β1-induced *in-vitro* model of fibrogenesis (Chapter 5). IN1130 was also studied, both as a positive control for anti-fibrotic activities and as an inhibitor of Alk5, the TGF-β type I recerptor.

6.1. Experimental design and workflow

To explore the anti-fibrotic mechanisms of SRM, baicalein and IN1130, NRK-49F cells were treated with or without 5 ng/mL TGF-β1, in the presence of 5 ng/mL TGF-β1 plus 40 μg/mL SRM, 80 μg/mL SRM, 40 μM baicalein, 80 μM baicalein and 1 μM IN1130, (**Fig. 6.1**). The cell lysates and conditioned media were harvested after 48 h treatment. In order to verify successful biological and pharmacological experiments, collagen contents in cell lysates and conditioned media were measured by hydroxyproline assay and soluble collagen assay, respectively, as described in **Section 2.10** and **2.11**. As shown in **Fig. 6.1B**, TGF-β1 significantly increased total collagen content in cell lysates, which was significantly repressed by both concentrations of SRM and baicalein, as well as 1 μM IN1130. TGF-β1-induced soluble collagen accumulation in conditioned media was significantly reduced by 80 μM baicalein and IN1130, and there were decreasing trends in 80 μg/mL SRM and 40 μM baicalein groups (**Fig. 6.1C)**. Cell lysates and conditioned media were then trypsinised, labelled with TMT reagents and analysed by LC-MS/MS as detailed in **Section 2.12**.

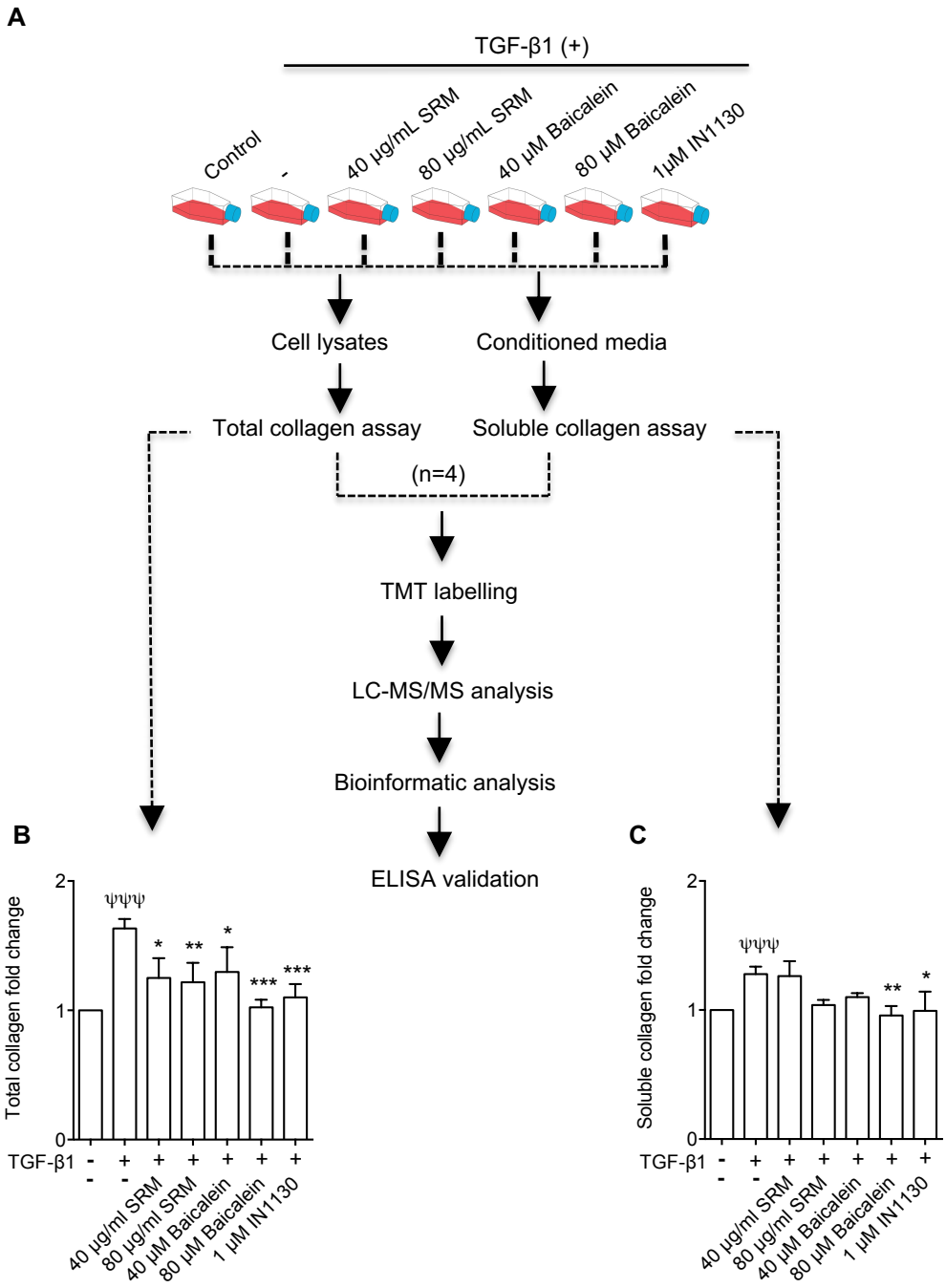

Fig. 6.1. Experimental design, workflow and establishment of TGF-β1-induced *in-vitro* model of fibrogenesis in NRK-49F cells and effects of anti-fibrotic drugs. (A) Experimental design and proteomic workflow. Cells were cultured in absence and presence of 5 ng/mL TGF-β1, and in the presence of 5 ng/mL TGF-β1 plus 40 µg/mL, 80 µg/mL SRM, 40 µM, 80 µM baicalein or 1 µM IN1130 for 48 h. Both cell lysates and conditioned media were harvested for hydroxyproline assay (B), soluble collagen assay (C), proteomic analysis and ELISA. Data represent mean ± SEM of 4 independent cell culture studies. Statistical analysis was performed on transformed data using repeated measures ANOVA. ψψψ $p<0.001$ *vs* control group, * $p<0.05$, ** $p<0.01$, *** $p<0.001$ *vs* TGF-β1 group. The control and TGF-β1 (+) groups are the same as those already reported in **Chapter 5, page 84**.

6.2. Results on cell lysates

6.2.1. Proteomic analysis and data interpretation

Fig. 6.2 shows the numbers of proteins significantly regulated by different treatments, in comparison with TGF-β1 alone group. In total, 72 and 68 proteins were significantly regulated by 40 μg/mL and 80 μg/mL SRM, respectively, with 31 proteins regulated by both concentrations (**Fig. 6.2A**); 122 and 304 proteins were significantly regulated by 40 μM and 80 μM baicalein, respectively, with 94 shared by two groups (**Fig. 6.2B**); of the 297 proteins significantly regulated by IN1130, 155 proteins were only regulated by IN1130, with the rest also regulated by SRM or baicalein (**Fig. 6.2C**).

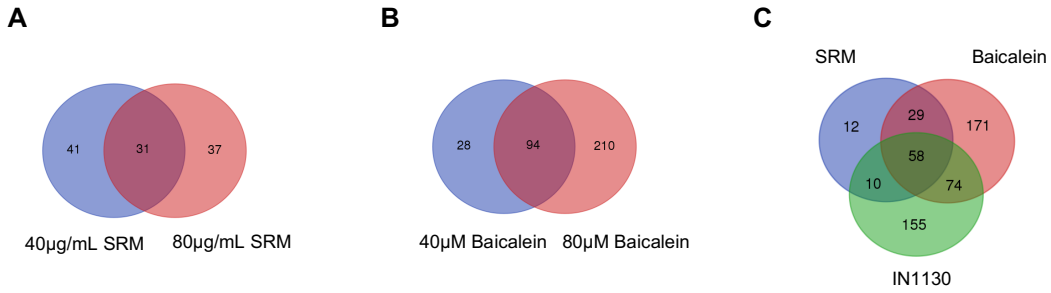

Fig. 6.2. Venn diagram analysis of cell-lysate proteins regulated by SRM, baicalein and IN1130 in TGF-β1-induced *in-vitro* model of fibrosis. Venn diagrams show numbers of proteins significantly regulated by (A) 40 and 80 μg/mL SRM, (B) 40 and 80 μM baicalein, and (C) 1 μM IN1130 and either concentration of SRM or baicalein. (TGF-β1 plus either drug *vs* TGF-β1 alone, $p<0.05$).

To identify the biological pathways regulated by SRM, baicalein and IN1130, proteins significantly changed in each group as suggested by proteomic analysis (**Fig. 6.2**) were analysed by KEGG pathway analysis. In total 49 significantly regulated pathways were enriched, as shown in **Fig. 6.3A**. Overlay of pathways regulated by SRM, baicalein and IN1130 is illustrated in **Fig. 6.3B.** Taken together, comparative pathway analysis of cell lysates indicated the following (green/red/blue fonts indicate up-/down-/dys-regulated proteins of given pathways, listed in order of *p*-value):

- SRM, baicalein and IN1130 all regulated Ribosome (**Table 6.1**) and Focal adhesion pathways (**Supplementary Table 2**);
- SRM and baicalein, but not IN1130, regulated the Lysosome pathway (**Table 6.2**);
- SRM and IN1130, but not baicalein, regulated the Amoebiasis pathway (**Supplementary Table 3**);

- Baicalein and IN1130, but not SRM, regulated 13 pathways, including Drug metabolism- cytochrome P450, Histidine metabolism, Carbon metabolism, Metabolic pathways, Glycolysis/ Gluconeogenesis, Tyrosine metabolism, Glutathione metabolism, Metabolism of xenobiotics by cytochrome P450, Chemical carcinogenesis, Peroxisome, Biosynthesis of antibiotics, Valine, leucine and isoleucine degradation and Glyoxylate and dicarboxylate metabolism (**Supplementary Table 4**);
- Five pathways were regulated by SRM only, including ECM-receptor interaction, Platelet activation, Protein digestion and absorption, PI3K-Akt signalling pathway and Tight junction (**Supplementary Table 5**);
- Eightteen pathways were regulated by baicalein only, including Galactose metabolism, Fructose and mannose metabolism, Cardiac muscle contraction, Dilated cardiomyopathy, Hypertrophic cardiomyopathy (HCM), Adrenergic signaling in cardiomyocytes, Phenylalanine metabolism, Adherens junction, Alzheimer's disease, Parkinson's disease, Biosynthesis of amino acids, Citrate cycle (TCA cycle), Oxidative phosphorylation, Pentose and glucuronate interconversions, Porphyrin and chlorophyll metabolism, Huntington's disease, Arginine and proline metabolism and Folate biosynthesis (**Supplementray Table 6**); and
- Nine pathways were regulated by IN1130 only, including Fatty acid degradation, Fatty acid metabolism, beta-Alanine metabolism, Colorectal cancer, Propanoate metabolism, Fatty acid elongation, Endometrial cancer, Lysine degradation and Prion diseases (**Supplementary Table 7**).

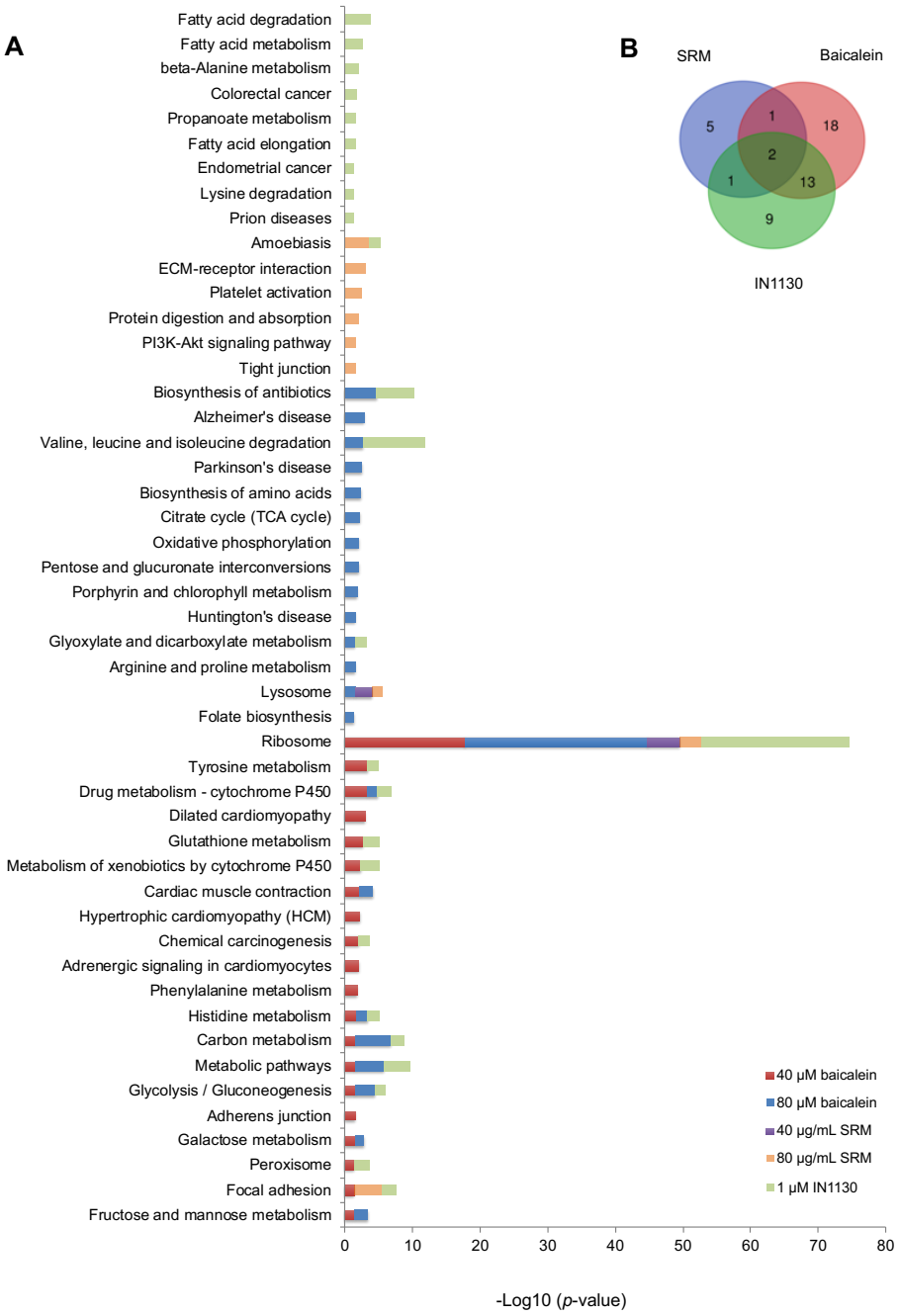

Fig. 6.3. KEGG pathway analysis of cell-lysate proteomics significantly regulated by SRM, baicalein and IN1130. (A) KEGG analysis shows 49 pathways significantly regulated by SRM, baicalein and IN1130, among which the ribosome pathway shows the highest significance. (B) Venn diagram illustrates the similarities and differences of the pathways regulated by SRM, baicalein and IN1130.

As shown in **Fig. 6.3**, the pathway most significantly regulated by all three drugs was the ribosome pathway. 9, 42 and 36 ribosomal proteins of the ribosome pathway were regulated by SRM, baicalein and IN1130, respectively. As shown in **Fig. 6.4** and **Table 6.1**, the 9 ribosomal proteins regulated by SRM were also regulated by both baicalein and IN1130,

including 3 small ribosomal subunits (Rps30, Rps23, Rps3) and 6 large ribosomal subunits (Rpl36a, Rpl35a, Rpl27a, Rplp0, Rpl35, Rpl32). Both baicalein and IN1130 suppressed 18 ribosomal proteins, including 4 small ribosomal subunits (Rps10, Rps11, Rps14 and Rps24) and 14 large ribosomal subunits (Rpl6, Rpl7, Rpl10, Rpl13, Rpl13a, Rpl17, Rpl18, Rpl18a, Rpl21, Rpl22, Rpl23a, Rpl27, Rpl38 and Rplp1). In addition, 13 ribosomal proteins including 2 small ribosomal subunits (Rps2, Rps29), and 11 large ribosomal subunits (Rpl23, Rpl12, Rpl5, Rpl36, Rpl0a, Rpl26, Rpl3, Rpl34, Rpl7a, Rpl15 and Rplp2) were repressed by baicalein only. While Mrpl3 (39S ribosomal protein L3) and Rps27a were induced by baicalein. IN1130 suppressed 9 ribosomal proteins, including 6 small ribosomal subunits (Rps16, Rps8, Rps18, Rps26, Rps13 and Rpsa) and 3 large ribosomal subunits (Rpl37, Rpl30 and Rpl9).

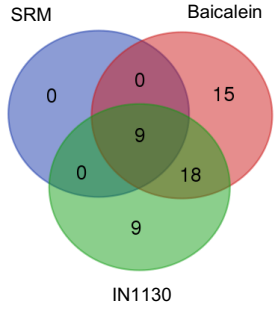

Fig. 6.4. Venn diagram analysis of ribosomal proteins regulated by SRM, baicalein and IN1130 (TGF-β1 plus either drug *vs* TGF-β1 alone, $p<0.05$).

Table 6.1. SRM, baicalein and IN1130 all significantly regulated the proteomic profiling of the ribosome pathway. Shown are mean fold-changes of propteomic abundance versus TGF-β1 group, $p<0.05$, NS: not significantly regulated by drug(s).

Accession	Protein	Control	TGF-β1	TGF-β1				
				40 μg/mL SRM	80 μg/mL SRM	40 μM Baicalein	80 μM Baicalein	IN1130
P62864	Rps30	0.48	1.00	0.76	0.67	0.70	0.71	0.52
P18445	Rpl27a	0.65	1.00	0.80	0.79	0.74	0.42	0.69
P83883	Rpl36a	0.51	1.00	0.70	0.74	0.75	0.46	0.62
P04646	Rpl35a	0.58	1.00	0.70	0.79	0.78	0.50	0.62
P62909	Rps3	0.66	1.00	0.75	0.80	NS	0.61	0.71
P62912	Rpl32	0.70	1.00	0.76	NS	0.78	0.58	0.71
P17078	Rpl35	0.67	1.00	0.81	NS	NS	0.57	0.77
P19945	Rplp0	0.67	1.00	0.80	NS	NS	0.74	0.71
P62268	Rps23	0.53	1.00	NS	0.69	NS	0.78	0.60
P24049	Rpl17	0.69	1.00	NS	NS	0.77	0.64	0.73
P19944	Rplp1	0.82	1.00	NS	NS	0.77	0.86	0.77

P62718	Rpl18a	0.70	1.00	NS	NS	0.78	0.67	0.79
P61354	Rpl27	0.69	1.00	NS	NS	0.78	0.66	0.71
P20280	Rpl21	0.79	1.00	NS	NS	0.79	0.68	0.79
P41123	Rpl13	0.77	1.00	NS	NS	0.79	-	0.76
P63174	Rpl38	0.76	1.00	NS	NS	0.80	0.75	0.78
Q6PDV7	Rpl10	0.77	1.00	NS	NS	0.80	0.67	0.80
P12001	Rpl18	0.74	1.00	NS	NS	0.80	0.78	0.75
P62752	Rpl23a	0.64	1.00	NS	NS	0.80	0.65	0.73
P35427	Rpl13a	0.75	1.00	NS	NS	0.81	0.77	NS
P05426	Rpl7	0.77	1.00	NS	NS	NS	0.70	0.79
P63326	Rps10	0.67	1.00	NS	NS	NS	0.72	0.71
P47198	Rpl22	0.73	1.00	NS	NS	NS	0.72	0.75
P21533	Rpl6	0.75	1.00	NS	NS	NS	0.75	0.78
P62850	Rps24	0.62	1.00	NS	NS	NS	0.76	0.73
P13471	Rps14	0.68	1.00	NS	NS	NS	0.76	0.69
P62282	Rps11	0.68	1.00	NS	NS	NS	0.78	0.74
P23358	Rpl12	0.78	1.00	NS	NS	0.76	0.73	NS
P11250	Rpl34	0.79	1.00	NS	NS	0.77	0.66	NS
P62425	Rpl7a	0.79	1.00	NS	NS	0.78	0.76	NS
P62275	Rps29	0.75	1.00	NS	NS	0.78	NS	NS
P62832	Rpl23	0.76	1.00	NS	NS	0.80	0.68	NS
P62907	Rpl10a	0.79	1.00	NS	NS	0.80	0.76	NS
P21531	Rpl3	0.79	1.00	NS	NS	0.80	0.68	NS
P39032	Rpl36	0.75	1.00	NS	NS	NS	0.66	NS
P61314	Rpl15	0.77	1.00	NS	NS	NS	0.72	NS
P12749	Rpl26	0.75	1.00	NS	NS	NS	0.75	NS
P02401	Rplp2	0.77	1.00	NS	NS	NS	0.76	NS
P27952	Rps2	0.75	1.00	NS	NS	NS	0.76	NS
P09895	Rpl5	0.76	1.00	NS	NS	NS	0.78	NS
P18665	Mrpl3	1.19	1.00	NS	NS	NS	1.35	NS
P62982	Rps27a	0.96	1.00	NS	NS	NS	1.36	NS
P61928	Rpl37	0.64	1.00	NS	NS	NS	NS	0.68
P62243	Rps8	0.76	1.00	NS	NS	NS	NS	0.75
P62856	Rps26	0.78	1.00	NS	NS	NS	NS	0.77
P62278	Rps13	0.73	1.00	NS	NS	NS	NS	0.78
P62890	Rpl30	0.79	1.00	NS	NS	NS	NS	0.78
P62271	Rps18	0.75	1.00	NS	NS	NS	NS	0.78
P62250	Rps16	0.71	1.00	NS	NS	NS	NS	0.78
P38983	Rpsa	0.70	1.00	NS	NS	NS	NS	0.80
P17077	Rpl9	0.81	1.00	NS	NS	NS	NS	0.81

Comparative KEGG pathway analysis of cell lysates indicated that 40, 80 μg/mL SRM and 80 μM baicalein significantly regulated the proteins enriched in the lysosome pathway (**Fig. 6.3)**. As shown in **Table 6.2**, Dnase2 was induced by SRM at both concentrations; both 40 μg/mL SRM and 80 μM baicalein suppressed Ctsb and induced Aga; Ppt1 and Ctsd were induced by 80 μg/mL SRM and 80 μM baicalein; only 40 μg/mL SRM repressed Lamp1 and induced Arsb; Ctsl was induced by 80 μg/mL SRM only; only 80 μM baicalein suppressed Acp2 and Naga and induced Gusb and Atp6v0a1.

Table 6.2. SRM and baicalein, but not IN1130, significantly regulated proteins involved in the lysosome pathway. Shown here are mean fold changes of proteins expression versus TGF-β1 group, $p<0.05$, " NS ": not significantly regulated by drug(s).

Accession	Protein	Control	TGF-β1	TGF-β1		
				40 μg/mL SRM	80 μg/mL SRM	80 μM Baicalein
P14562	Lamp1	0.63	1.00	0.64	NS	NS
P00787	Ctsb	0.82	1.00	0.74	NS	0.65
P50430	Arsb	1.23	1.00	1.24	NS	NS
Q9QZK8	Dnase2	1.18	1.00	1.32	1.49	NS
P30919	Aga	1.90	1.00	1.71	NS	1.86
P07154	Ctsl	1.59	1.00	NS	1.36	NS
P45479	Ppt1	1.24	1.00	NS	1.58	1.44
P24268	Ctsd	1.05	1.00	NS	1.65	1.63
P20611	Acp2	1.07	1.00	NS	NS	0.73
Q66H12	Naga	1.13	1.00	NS	NS	0.77
P06760	Gusb	1.54	1.00	NS	NS	1.28
P25286	Atp6v0a1	1.17	1.00	NS	NS	1.46

The differential expression patterns of proteins in response to treatment conditions were shown as volcano plots. As shown in **Fig. 6.5**, Enpp1, the protein most significantly induced by TGF-β1, was also mostly suppressed by SRM, baicalein and IN1130; Aldh3a1, the protein most repressed by TGF-β1, was also dramatically reversed by IN1130 and 80 μg/mL SRM. TGF-β1-induced Sqstm1 was further induced by 80 μM baicalein. Ccdc80, one of the proteins most induced by SRM, was also induced by 80 μM baicalein. Tfrc was up-regulated by baicalein and 80 μg/mL SRM; Akr1b7 was also induced by both concentrations of baicalein.

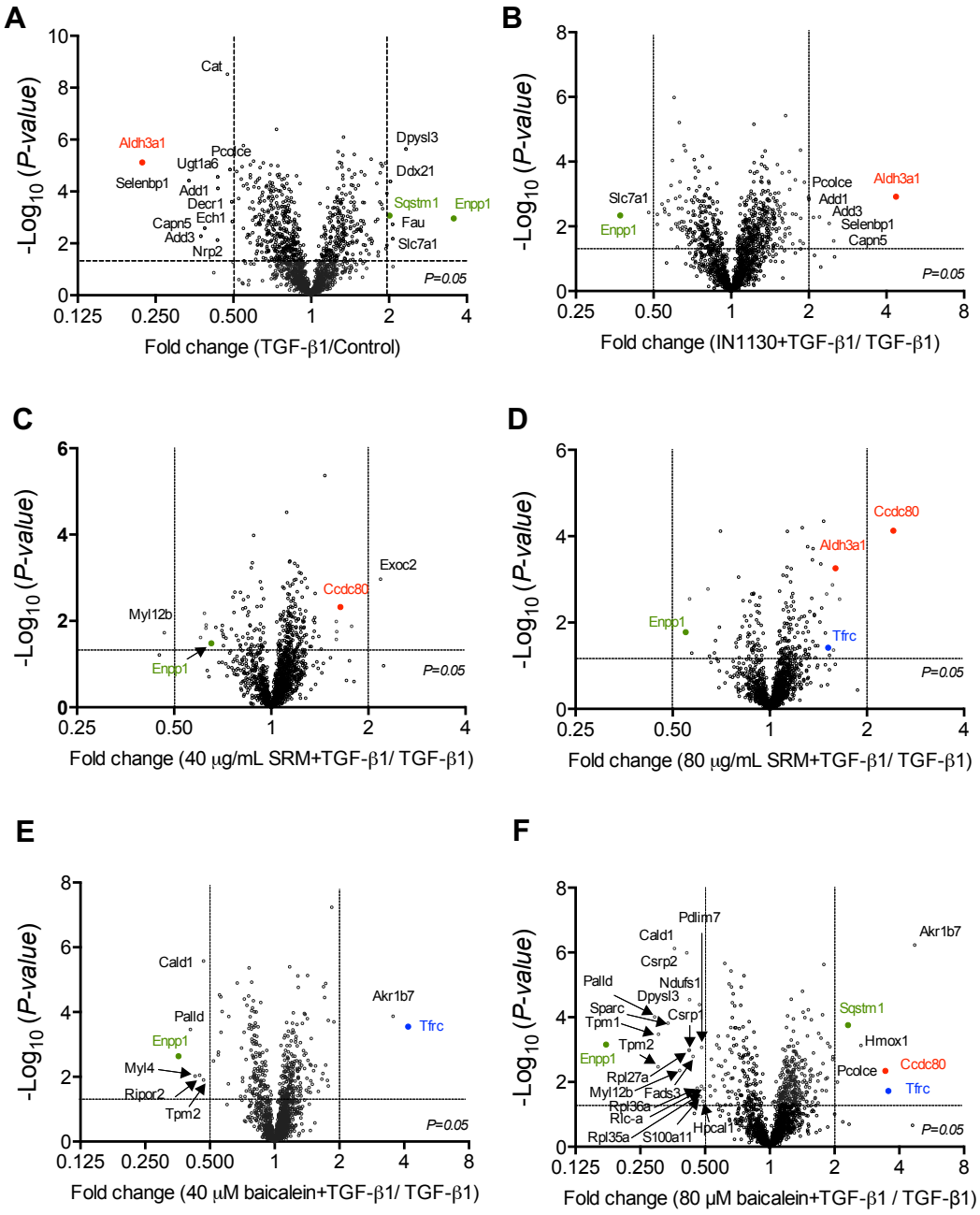

Fig. 6.5. Volcano plots of cell-lysate proteins regulated by SRM, baicalien and IN1130 in TGF-β1-induced *in-vitro* model of fibrosis. Proteins significantly regulated by (A) TGF-β1 (TGF-β1 *vs* control) and (B-F) 1μM IN1130, 40 μg/mL SRM, 80 μg/mL SRM, 40 μM baicalein and 80 μM baicalein, in the presence of TGF-β1. X-axes show fold-change values and Y-axes display the -Log10 (*p*-value, according to *t*-tests). In each plot, proteins above the horizontal dashed line were differentially up-regulated or down-regulated by respective treatments. Proteins subjected to ELISA validation are highlighted either in green fonts (induced by TGF-β1) or red fonts (repressed by TGF-β1) or blue fonts (no significant difference between TGF-β1 and control groups).

6.2.2. ELISA validation

Five proteins, including Enpp1, Aldh3a1, Ccdc80, Tfrc and Sqstm1 were selected for ELISA validation primarily on the basis of large fold-changes induced by different treatments. In addition, Impdh2 was also chosen as a candidate protein because it connected two clusters of TGF-β1-regulted proteins as shown in STRING map (**Fig. 5.7A)**. The changes in abundance of proteins as suggested by ANOVA analysis of proteomics data are shown in **Fig. 6.6 A-F**, with corresponding ELISA results shown in **Fig. 6.6 G-L**. The expression patterns of Enpp1, Aldh3a1, Impdh2 and Trfc were largely validated by ELISA, consistent with proteomic data. Nevertheless, proteomic data showed that Enpp1 was suppressed by baicalein dose dependently (**Fig. 6.6A**), but this dose-dependency was not confirmed by ELISA (**Fig. 6.6G**). According to proteomic data, Ccdc80 was significantly suppressed by TGF-β1 and induced by 80 μg/mL SRM and 80 μM baicalein (**Fig. 6.6D**), while Ccdc80 regulation by TGF-β1 was not significant according to ELISA. Besides, Ccdc80 was induced by both concentrations of SRM and baicalein but the dose-dependency observed in proteomic data were not confirmed by ELISA (**Fig. 6.6J**). Proteomic analysis showed that Sqstm1 was significantly induced by TGF-β1 and further induced by both concentrations of baicalein (**Fig. 6.6F**). ELISA confirmed that TGF-β1 significantly induced Sqstm1 and this was reversed by IN1130, but not by either SRM or baicalein (**Fig. 6.6L)**.

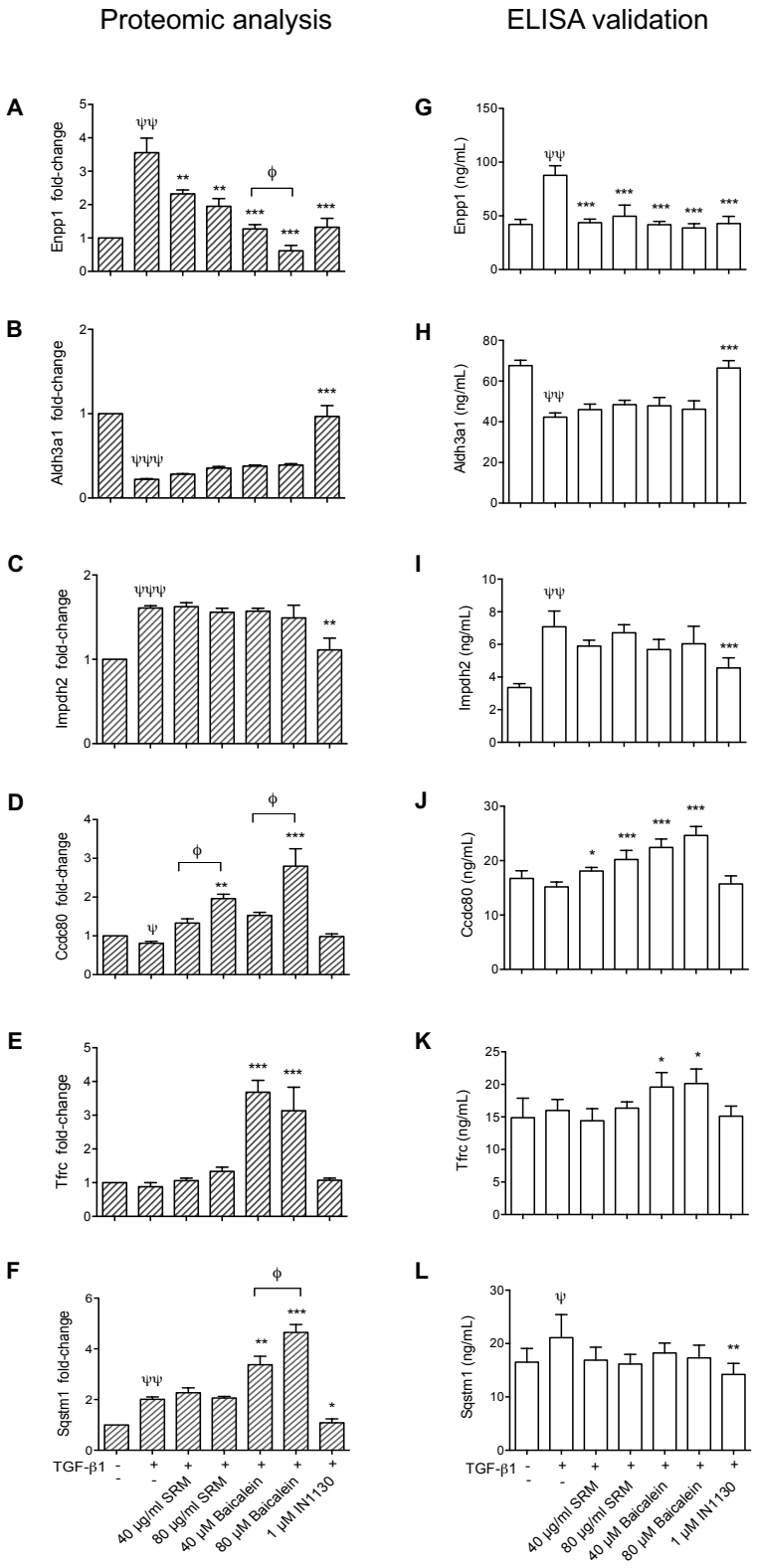

Fig. 6.6. Comparison of proteomoic analysis and ELISA validation of selected cell-lysate proteins regulated by SRM, baicalein and/or IN1130. Shown are relative abundance in proteomic data (left) and ELISA data (right) of Enpp1 (A, G), Aldh3a1 (B, H), Impdh2 (C, I), Ccdc80 (D, J), Tfrc (E, K) and Sqstm1 (F, L). n=4, ψ p<0.05, ψψ p< 0.01, ψψψ p< 0.001 *vs* control group. *p<0.05, **p< 0.01, ***p<0.001 *vs* TGF-β1 group. ϕ p<0.05 between selected groups.

6.3. Results on conditioned media

6.3.1. Proteomic analysis and data interpretation

Proteomic analysis indicated that 95 and 138 proteins were significantly regulated by 40 and 80 µg/mL SRM, respectively. As shown in **Fig. 6.7**, 79 of these proteins were regulated at both concentrations; 86 and 161 proteins were significantly regulated by 40 and 80 µM baicalein, respectively, with 59 regulated by both concentrations; among 46 IN1130-regulated proteins, 11 were regulated by both SRM and baicalein, 16 were uniquely regulated by IN1130, 2 and 17 were regulated by at least one concentration of baicalein and SRM, respectively.

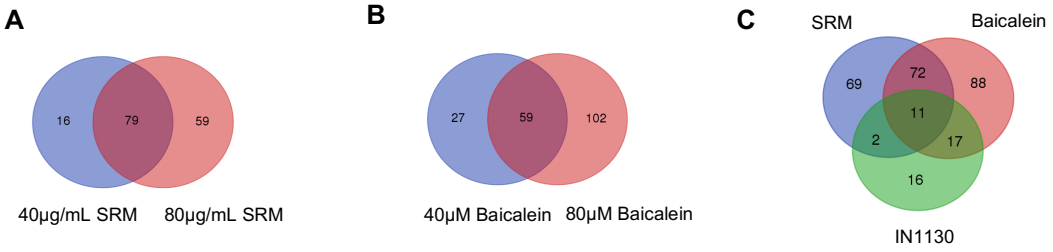

Fig. 6.7. Venn diagram analysis of secreted proteins significantly regulated by SRM, baicalein and IN1130. Proteins regulated by (A) 40 and 80 µg/mL SRM, (B) 40 and 80 µM baicalein, and (C) 1 µM IN1130 and at least one concentration of SRM or baicalein. (TGF-β1 plus either drug *vs* TGF-β1 alone, $p<0.05$).

KEGG pathway analysis of secretomic data was performed to identify biological pathways regulated by SRM, baicalein and IN1130. Results were as illustrated in **Fig. 6.8**:

- Treatment by both concentrations of SRM and the higher concentration of baicalein, but not 40 µM baicalein or 1 µM IN1130, significantly regulated proteins of the Ribosome pathway in conditioned media in TGF-β1-induced *in-vitro* model of fibrosis (**Table 6.3**);
- Only baicalein regulated the proteins enriched in other 10 pathways (**Table 6.4**), including:
    - Both concentrations of baicalein increased proteins increased proteins enriched in the Lysome and Tyosine metabolism pathways and complexly regulated the ECM-receptor interaction pathway;
    - Lower concentration of baicalein selectively up- and down-regulated of proteins enriched in Galactose metabolism and Amoebiasis pathway, respectively;
    - Higher concentration of baicalein selectively up-regulated proteins enriched in Proteasome, Glycolysis / Gluconeogenesis and Insulin signalling pathway; and

dysregulated proteins enriched in Biosynthesis of antibiotics and Lysine degradation pathways.

- No KEGG pathway was enriched among IN1130-regulated proteins;

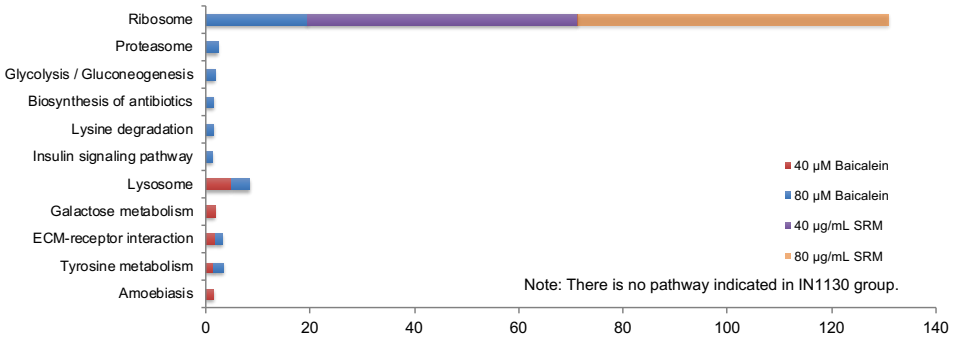

Fig. 6.8. KEGG pathway analysis of proteins in conditioned media significantly regulated by SRM and baicalein in TGF-β1-induced *in-vitro* model of fibrosis. sKEGG analysis shows 11 pathways significantly regulated by SRM and baicalein, among which the ribosome pathway shows the most significance.

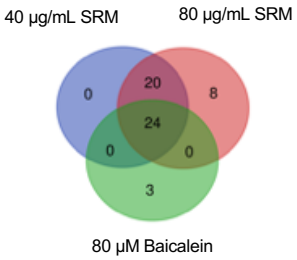

Fig. 6.9. Venn diagram analysis of secreted proteins involved in the ribosome pathway, which were regulated by SRM and/or baicalein. (TGF-β1 plus either drug *vs* TGF-β1 alone, $p<0.05$).

Comparative analyses of conditioned media indicated that both concentrations of SRM and 80 μM baicalein, but not IN1130, significantly regulated the ribosome pathway. Of note, 44, 52, and 27 ribosomal proteins were respectively regulated by 40 μg/mL SRM, 80 μg/mL SRM and 80 μM baicalein (**Fig. 6.9**). As shown in **Table 6.3**, both concentrations of SRM and 80 μM baicalein increased 21 small ribosomal subunits (Rps2, Rps3, Rps3a, Rps4x, Rps5, Rps6, Rps7, Rps8, Rps9, Rps13, Rps15, Rps16, Rps17, Rps18, Rps19, Rps23, Rps24, Rps25, Rps26, Rps30 and Rpsa) and 3 large ribosomal subunits (Rpl26, Rpl31, Rpl37); both concentrations of SRM increased 20 large ribosomal subunits (Rpl3, Rpl4, Rpl7a, Rpl8, Rpl10, Rpl11, Rpl13, Rpl13a, Rpl14, Rpl15, Rpl17, Rpl18, Rpl18a, Rpl19, Rpl29, Rpl30, Rpl32, Rpl34, Rpl36a, Rplp1); only 80 μg/mL SRM increased 3 small ribosomal subunits

(Rps11, Rps15a and Rps20) and 5 large ribosomal subunits (Rpl6, Rpl24, Rpl27, Rpl28 and Rpl35a); only 80 μM baicalein increased one small ribosomal subunit Rps14 and slightly suppressed two large ribosomal subunits (Rpl38 and Rpl9).

Table 6.3. Both concentrations of SRM and 80 μM baicalein regulated proteins in conditioned media enriched in the ribosome pathway. Shown here are mean fold changes of proteins expression versus TGF-β1 group, $p<0.05$, " NS ": not significantly regulated by drug(s).

Accession	Protein	Control	TGF-β1	TGF-β1		
				40 μg/mL SRM	80 μg/mL SRM	80 μM Baicalein
P62909	Rps3	0.90	1.00	1.56	1.78	1.60
P61928	Rpl37	0.94	1.00	1.95	1.81	1.86
P38983	Rpsa	0.96	1.00	1.87	1.87	1.66
P62864	Rps30	0.98	1.00	1.41	1.79	1.55
P62083	Rps7	1.02	1.00	2.06	2.84	2.00
P29314	Rps9	1.03	1.00	1.74	1.98	1.80
P62268	Rps23	1.04	1.00	1.71	2.10	1.87
P62755	Rps6	1.04	1.00	1.82	2.14	1.89
P27952	Rps2	1.07	1.00	2.07	2.69	2.33
P62856	Rps26	1.09	1.00	1.73	2.17	2.09
P62250	Rps16	1.09	1.00	1.78	2.14	1.91
P24050	Rps5	1.11	1.00	2.10	2.44	2.11
P04644	Rps17	1.12	1.00	2.14	2.74	2.20
P62243	Rps8	1.15	1.00	2.10	2.32	1.97
P17074	Rps19	1.16	1.00	1.60	2.10	1.82
P62902	Rpl31	1.21	1.00	2.16	3.23	2.15
P12749	Rpl26	1.21	1.00	2.00	2.38	1.86
P62853	Rps25	1.23	1.00	2.18	2.80	2.49
P49242	Rps3a	1.27	1.00	2.21	2.79	2.70
P62845	Rps15	1.37	1.00	2.94	3.29	3.54
P62271	Rps18	1.38	1.00	1.99	2.54	2.22
P62850	Rps24	1.40	1.00	3.25	4.07	3.59
P62703	Rps4x	1.45	1.00	2.77	3.46	3.16
P62278	Rps13	1.65	1.00	3.40	4.46	3.70
P61314	Rpl15	0.76	1.00	1.66	2.16	NS
P84100	Rpl19	0.76	1.00	1.73	2.08	NS
Q6PDV7	Rpl10	0.83	1.00	1.48	2.05	NS
P62890	Rpl30	0.83	1.00	1.67	2.38	NS
P62425	Rpl7a	0.89	1.00	1.58	2.20	NS
P24049	Rpl17	0.89	1.00	1.68	2.00	NS
P62919	Rpl8	0.90	1.00	1.67	2.10	NS

P62718	Rpl18a	0.90	1.00	1.71	2.20	NS
P12001	Rpl18	0.91	1.00	1.67	2.28	NS
P50878	Rpl4	0.93	1.00	1.73	2.20	NS
Q63507	Rpl14	0.94	1.00	1.81	2.37	NS
P21531	Rpl3	0.95	1.00	1.70	1.95	NS
P19944	Rplp1	0.95	1.00	1.36	1.34	NS
P35427	Rpl13a	0.96	1.00	2.09	2.58	NS
P11250	Rpl34	0.97	1.00	1.64	2.32	NS
P62912	Rpl32	0.97	1.00	1.81	2.30	NS
P62914	Rpl11	0.98	1.00	1.61	2.02	NS
P83883	Rpl36a	1.04	1.00	1.56	1.45	NS
P25886	Rpl29	1.05	1.00	1.64	2.04	NS
P41123	Rpl13	1.33	1.00	1.57	1.94	NS
P04646	Rpl35a	0.82	1.00	NS	1.58	NS
P83732	Rpl24	0.86	1.00	NS	1.82	NS
P21533	Rpl6	0.86	1.00	NS	1.79	NS
P62246	Rps15a	0.89	1.00	NS	1.75	NS
P60868	Rps20	0.93	1.00	NS	1.74	NS
P61354	Rpl27	0.94	1.00	NS	1.64	NS
P62282	Rps11	1.09	1.00	NS	2.12	NS
P17702	Rpl28	1.24	1.00	NS	1.91	NS
P63174	Rpl38	0.88	1.00	NS	NS	0.47
P17077	Rpl9	0.95	1.00	NS	NS	0.60
P13471	Rps14	1.28	1.00	NS	NS	2.35

Table 6.4. Baicalein significantly regulated proteins in conditioned media enriched in 10 KEGG pathways. Shown here are mean fold-changes of protein abundance in conditioned media versus TGF-β1 group, $p<0.05$, " NS ": not significantly regulated by 40 μM or 80 μM Baicalein.

Accession	**Protein**	**Control**	**TGF-β1**	**TGF-β1**	
				40 μM Baicalein	**80 μM Baicalein**
Lysosome					
O54715	Atp6ap1	1.02	1.00	1.44	1.64
Q6P7A9	Gaa	1.27	1.00	1.53	1.61
P30919	Aga	1.35	1.00	1.97	2.35
Q9R0J8	Lgmn	1.35	1.00	1.80	1.98
P24268	Ctsd	1.36	1.00	1.92	2.28
P10960	Psap	1.36	1.00	2.10	2.72
P00787	Ctsb	1.65	1.00	2.11	2.42
Q32KJ6	Galns	1.43	1.00	1.49	NS

P08081	Clta	0.99	1.00	NS	0.60
P08082	Cltb	1.00	1.00	NS	0.56
ECM-receptor interaction					
Q9JI03	Col5a1	0.64	1.00	0.48	0.33
P02466	Col1a2	0.71	1.00	0.36	0.24
P02454	Col1a1	0.95	1.00	0.55	0.60
P04937	Fn1	0.96	1.00	0.40	0.29
P34901	Sdc4	1.13	1.00	NS	3.02
Tyrosine metabolism					
P30904	Mif	1.28	1.00	1.59	1.94
P25093	Fah	1.36	1.00	1.47	1.51
P11883	Aldh3a1	1.68	1.00	1.67	NS
P12711	Adh5	0.95	1.00	NS	1.82
P22734	Comt	1.05	1.00	NS	1.56
Proteasome					
P17220	Psma2	1.06	1.00	NS	1.64
P62193	Psmc1	1.09	1.00	NS	1.44
Q63347	Psmc2	1.13	1.00	NS	1.64
Q4KM35	Psmb10	1.22	1.00	NS	1.61
P28077	Psmb9	1.24	1.00	NS	1.54
Glycolysis / Gluconeogenesis					
P12711	Adh5	0.95	1.00	NS	1.82
P04797	Gapdh	0.96	1.00	NS	2.32
Q9JLJ3	Aldh9a1	1.03	1.00	NS	1.77
P11884	Aldh2	1.17	1.00	NS	1.64
P47860	Pfkp	1.51	1.00	NS	1.66
Biosynthesis of antibiotics					
P39069	Ak1	0.79	1.00	NS	0.67
P12711	Adh5	0.95	1.00	NS	1.48
P04797	Gapdh	0.96	1.00	NS	1.82
Q9JLJ3	Aldh9a1	1.03	1.00	NS	2.32
Q8VHF5	Cs	1.05	1.00	NS	1.77
P11884	Aldh2	1.17	1.00	NS	1.54
P04762	Cat	1.22	1.00	NS	1.64
P47860	Pfkp	1.51	1.00	NS	1.66
Lysine degradation					
Q811A3	Plod2	0.55	1.00	NS	1.59
Q9JLJ3	Aldh9a1	1.03	1.00	NS	0.75
P11884	Aldh2	1.17	1.00	NS	1.77
Q63321	Plod1	1.24	1.00	NS	1.66
Insulin signalling pathway					
P53534	Pygb	0.95	1.00	NS	1.46

P63074	Eif4e	0.99	1.00	NS	1.57
P62755	Rps6	1.04	1.00	NS	1.89
P12369	Prkar2b	1.10	1.00	NS	1.79
P62161	Calm1	1.36	1.00	NS	2.30
P01322	Ins1	1.91	1.00	NS	1.53
Galactose metabolism					
Q5RJP0	Akr1b7	0.99	1.00	1.67	NS
Q6P7A9	Gaa	1.27	1.00	1.53	NS
P47860	Pfkp	1.51	1.00	2.17	NS
Amoebiasis					
P02466	Col1a2	0.71	1.00	0.36	NS
P02454	Col1a1	0.95	1.00	0.55	NS
Q9JI03	Col5a1	0.64	1.00	0.48	NS
P04937	Fn1	0.96	1.00	0.40	NS

Volcano plots are used to illustrate the proteins in conditioned media regulated by SRM, baicalein and IN1130. As shown in **Fig. 6.10 A&B**, TGF-β1-regulated PAI-1, Ccl2, Ccl7, Tsku, Cyr61 and Nov were dramatically reversed by IN1130. This suggests that expression of these proteins may be Alk5-dependent, and further confirmation experiments are warranted. More proteins were increased than reduced in SRM groups, especially the ribosomal proteins such as Rps13, Rps15, Rps24, Rps4x. Csrp1 was mostly reduced by both concentrations of SRM **(Fig. 6.10 C&D)**. Baicalein most repressed the expression of PAI-1, Ccl2 and Ccl7, which among the most induced by TGF-β1. TGF-β1-repressed Mmp3, however, was not reversed by IN1130 or SRM, but was reversed by both concentrations of baicalein, suggesting TGF-β1 and baicalein regulation of Mmp3 was Alk5-independent (**Fig. 6.10 E&F)**.

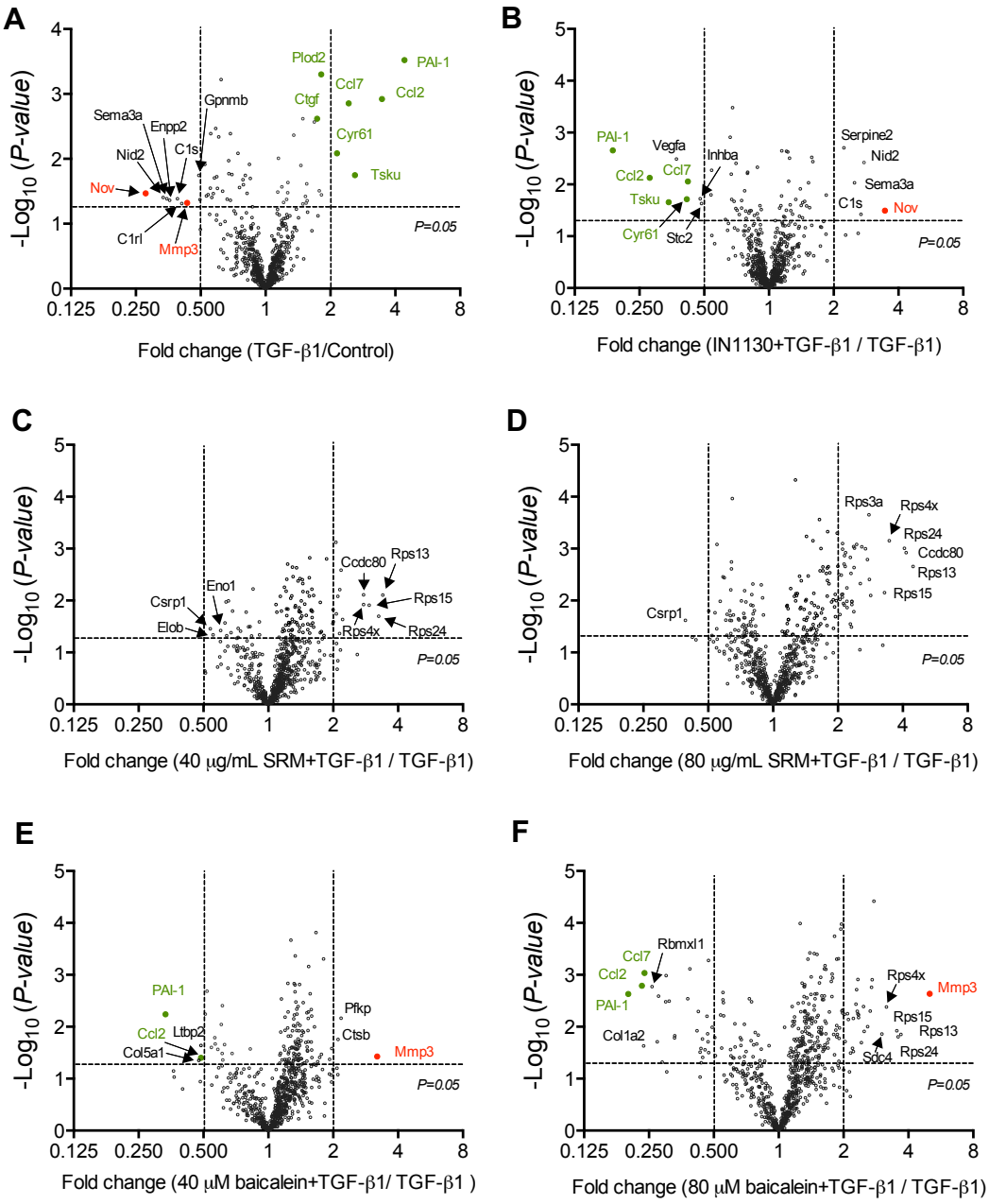

Fig. 6.10. Volcano-plot analysis of SRM, baicalien and IN1130 effects on proteomics of conditioned media in TGF-β1-induced *in-vitro* model of fibrosis. Proteins significantly regulated by (A) TGF-β1 (TGF-β1 *vs* control); (B-F) 1 μM IN1130, 40 μg/mL SRM, 80 μg/mL SRM, 40 μM baicalein and 80 μM baicalein, in the presence of TGF-β1. In each plot, proteins above the horizontal dashed line were differentially increased or reduced by respective treatments. Proteins subjected to ELISA validation are highlighted either in green fonts (induced by TGF-β1) or red fonts (repressed by TGF-β1).

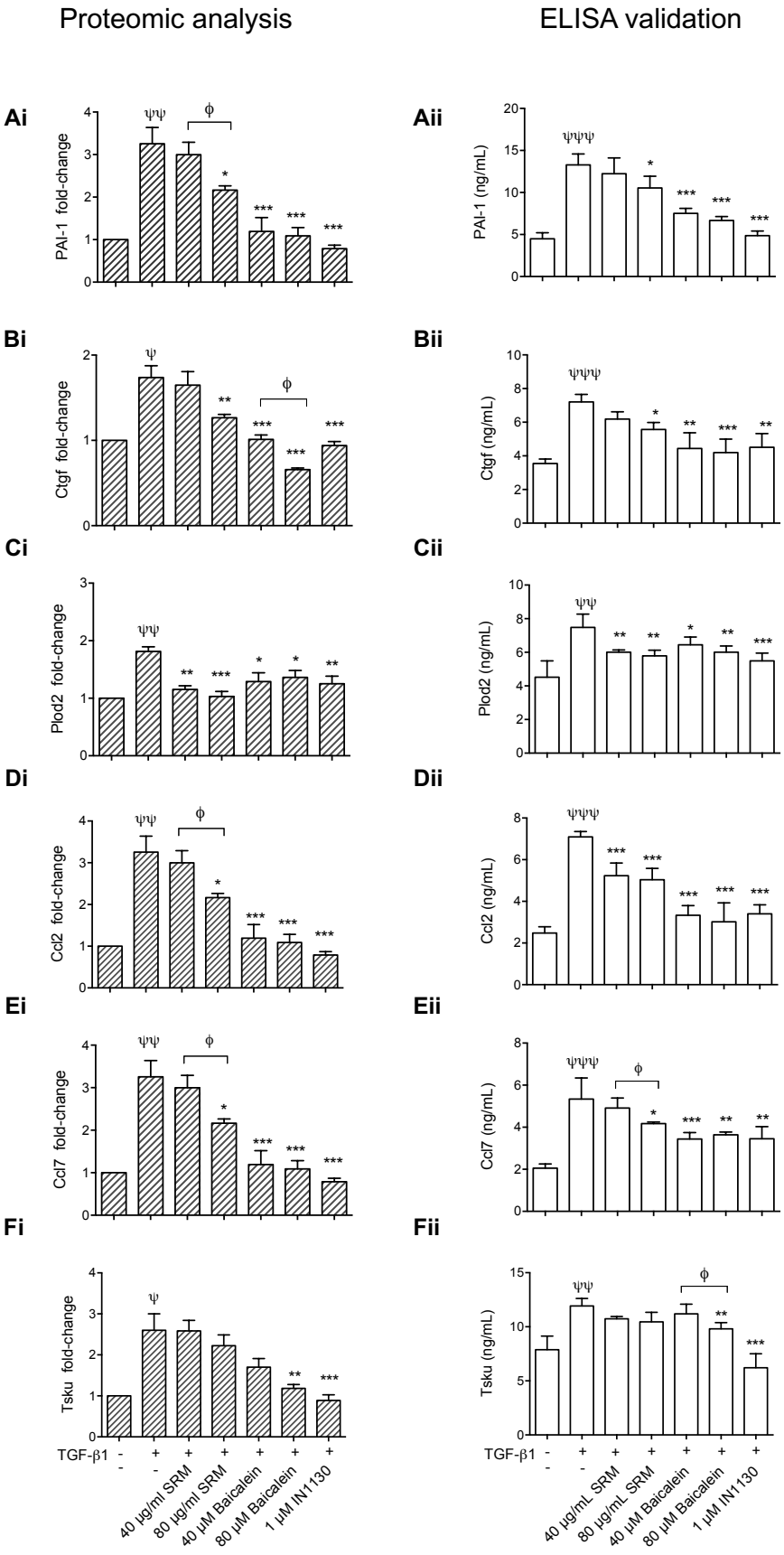

(Legend see next page)

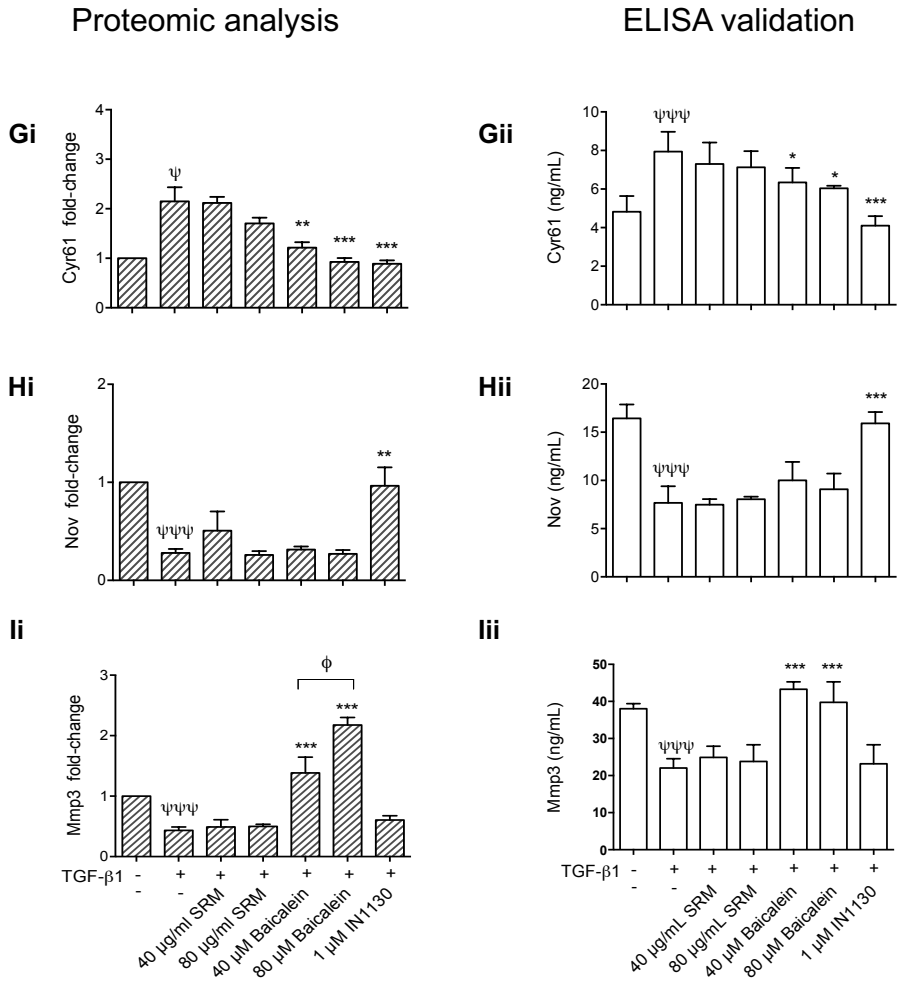

Fig. 6.11. Comparison of proteomic analysis and ELISA validation of selected proteins in conditioned media regulated by SRM, baicalein and IN1130. The relative abundance in proteomic data (left) and ELISA data (right) of PAI-1 (Ai, Aii), Ctgf (Bi, Bii), Plod2 (Ci, Cii), Ccl2 (Di, Dii), Ccl7 (Ei, Eii), Tsku (Fi, Fii), Cyr61 (Gi, Gii), Nov (Hi, Hii) and Mmp3 (Ii, Iii). n=4, ψ p<0.05, ψψ p< 0.01, ψψψ p< 0.001 *vs* control group. *p<0.05, **p< 0.01, ***p<0.001 *vs* TGF-β1 group. ϕ p<0.05, according to one-way ANOVA analysis.

6.3.2. ELISA validation

Based on fold-changes induced by TGF-β1 and the published literature on relevance to fibrosis, nine proteins in conditioned media, including PAI-1, Ctgf, Plod2, Ccl2, Ccl7, Tsku, Cyr61, Nov and Mmp3, were selected for validation by ELISA. The changes in abundance of proteins as suggested by proteomic analysis are shown in **Fig. 6.11Ai-Ii**, with corresponding ELISA results shown in **Fig. 6.11Aii-Iii**. The effects of TGF-β1 as well as antifibrotic SRM, baicalein and IN1130 on Plod2, Ccl7, Tsku, Cyr61 and Nov as suggested by LC-MS/MS-based protteomic data were fully validated by ELISA (**Fig. 6.11C, E, F, G and H**). Although the proteomic data showed that PAI-1 and Ccl2 were suppressed by SRM

dose dependently (**Fig. 6.11Ai and Di**), ELISA results only confirmed that they were suppressed by SRM but not in a dose-dependent manner (**Fig. 6.11Aii and Dii**). Similarly, baicalein were suggested to dose dependently suppressed Ctgf and Mmp3 (**Fig. 6.11Bi and Ii**), whereas ELISA data showed that they were suppressed by baicalein, but not dose-dependently (**Fig. 6.11Bii and Iii**).

6.4. Discussions

6.4.1. Discussion on cell-lysate results

Based on ELISA results, the effects of TGF-β1 and three drugs on cell-lysate proteins are summarised in **Fig. 6.8.**

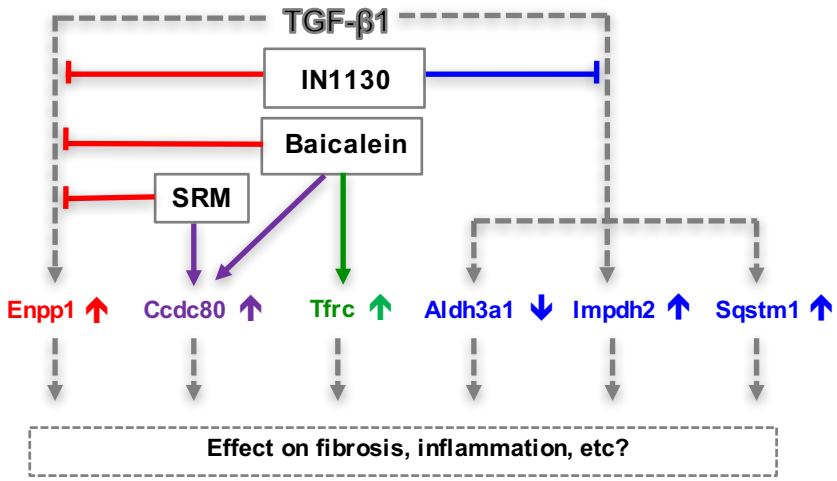

Fig. 6.12. Effect of SRM, baicalein and IN1130 on proteins of interest in cell lysates of TGF-β1-induced fibrosis. TGF-β1-induced Enpp1 was reversed by SRM, baicalein and IN1130 (marked in red); Ccdc80 was induced by SRM & baicalein, but not IN1130 (marked in purple); Tfrc was only induced by baicalein (marked in green); TGF-β1-induced Impdh2 & Sqstm1 and -repressed Aldh3a1 was only reversed by IN1130 (marked in blue). Arrow after protein names refer to induction (↑) and suppression (↓).

Enpp1 was most induced by TGF-β1 (**Fig. 6.5A** and **Fig. 6.6A**) and most supressed by SRM, baicalein and IN1130 (**Fig. 6.5B-F** and **Fig. 6.6G**), raising a possibility that all three anti-fibrotic drugs may be anti-fibrotic by suppressing the induction of Enpp1 by TGF-β1. However, the precise role for Enpp1 in TGF-β1-induced fibrosis and inflammation remain unclear (**Chapter 5, page 122**) and how SRM, baicalein and IN1130 decrease the Enpp1 also deserve further investigation.

Ccdc80, also known as steroid-sensitive gene-1, DRO1 or URB, is a secreted protein that binds to ECM proteins and promotes cell adhesion (199). Ccdc80 was not significantly regulated by TGF-β1 but was induced by both SRM and bacalein, rather than IN1130 (**Fig. 6.6J**). IN1130 acts as an established TGF-β type I receptor kinase (ALK5) inhibitor and suppresses renal fibrosis (200), suggesting SRM and baicalein may share ALK5-independent mechanisms. Brennan *et al.* reported that the gene expression of Ccdc80 in human renal

epithelial cells were significantly up-regulated by TGF-β1 (201), however, the role of Ccdc80 in fibrosis and inflammation is little known.

Tfrc was not significantly regulated by TGF-β1 but was only induced by baicalein (**Fig. 6.6K**). Tfrc, a transmembrane glycoprotein that binds to iron-bound transferrin and mediates extracellular iron delivery into cells (202, 203). Tfrc is widely believed to be important for iron acquisition by all mammalian cells (204). Shpyleva *et al*. reported that non-alcoholic fatty liver disease-associated fibrogenesis was correlated with a marked increase in Tfrc expression (205). Soluble Tfrc in urine has been considered a potential biomarker for IgA nephropathy (IgAN) and Henoch-Schönlein purpura nephritis (HSPN) as significant higher urinary Tfrc was detected in IgAN and HSPN patients (206). Thus, whether baicalein-induced Trfc can contribute to therapeutic deserve further studies.

Akr1b7, also known as MVDP or Akr1b14, is a member of the Aldo-keto reductase superfamily (207), which is characterised by catalysing reduced nicotinamide adenine dinucleotide (phosphate) (NAD(P)H)-dependent oxido-reduction of carbonyl groups (208, 209). The proteomic data indicated that Akr1b7 was induced by baicalein with fold change>2 (**Fig. 6.5 E&F**), but it was not subjected to ELISA validation in view that this protein is not conserved in human species. The rat Akr1b7 has 87% amino-acid sequence identity to the corresponding mouse Akr1b7 (210, 211). Akr1b1, another AKR1 subfamily member, is conserved in human (209) and was significantly induced by baicalein according to proteomic data. Lu *et al*. reported that the expression of Akr1b1 was decreased in cell culture-induced senescent human primary proximal tubule epithelial cells (212). Akr1b1 variants have been shown to be associated with diabetic neuropathy and nephropathy (213). Thus, roles of Akr1b7 and Akr1b1 in mediating therapeutic effects may deserve further investifation.

Aldh3a1 was mostly repressed by TGF-β1, and mostly reversed by IN1130 but not SRM or baicalein (**Fig. 6.6H**), suggesting that IN1130 may play anti-fibrotic role in reversing TGF-β1-repressed Aldh3a1. As dicussed in **Chapter 5 (page 122),** the functions of Aldh3a1 in TGF-β1-induced fibrosis remain unclear and how IN1130 increase the Aldh3a1 also deserve further study.

Impdh2 was induced by TGF-β1, and only reversed by IN1130 but not SRM or baicalein (**Fig. 6.6I**), suggesting that IN1130 may play anti-fibrotic role by repressing TGF-β1-induced Impdh2. As discussed in **Chapter 5 (page 95, 102-103**), Impdh2 could be an anti-fibrotic target and how IN1130 suppresses Impdh2 also deserves further study.

TGF-β1-induced Sqstm1 was only suppressed by IN1130 in the present study, suggesting that their expression may be Alk5-dependent (**Fig. 6.6L**). Sqstm1, also called p62, is a ubiquitin - binding scaffold protein, acting as an adapter protein in multiple signalling pathways (214, 215). Because its degradation is dependent on autophagy, accumulation of Sqstm1 has been used as a marker for inhibition of autophagy or defects in autophagic degradation (216, 217). Several studies have discussed the roles of autophagy in renal fibrosis (218-221). Livingston *et al*. recently reported that persistent activation of autophagy in kidney proximal tubules promotes renal interstitial fibrosis during UUO. The pro-fibrotic function of autophagy is related to the regulation on tubular cell death, interstitial inflammation, and the production of pro-fibrotic factors (221). In contrast, Ding *et al*. suggested an anti-fibrotic role of autophagy in kidneys by regulating the degradation of mature TGF-β1 (219). Given that the conflicting evidence aforementioned, it will be essential to examine in this particular *in-vitro* model that the role of Sqstm1 in autophagy and TGF-β1-induced fibrosis and whether IN1130 plays an anti-fibrotic role, at least in part, by repressing TGF-β1-induced Sqstm1.

6.4.2. Discussion on condition-media results

The possible roles of validated proteins in conditioned media are illustrated in **Fig. 6.13.**

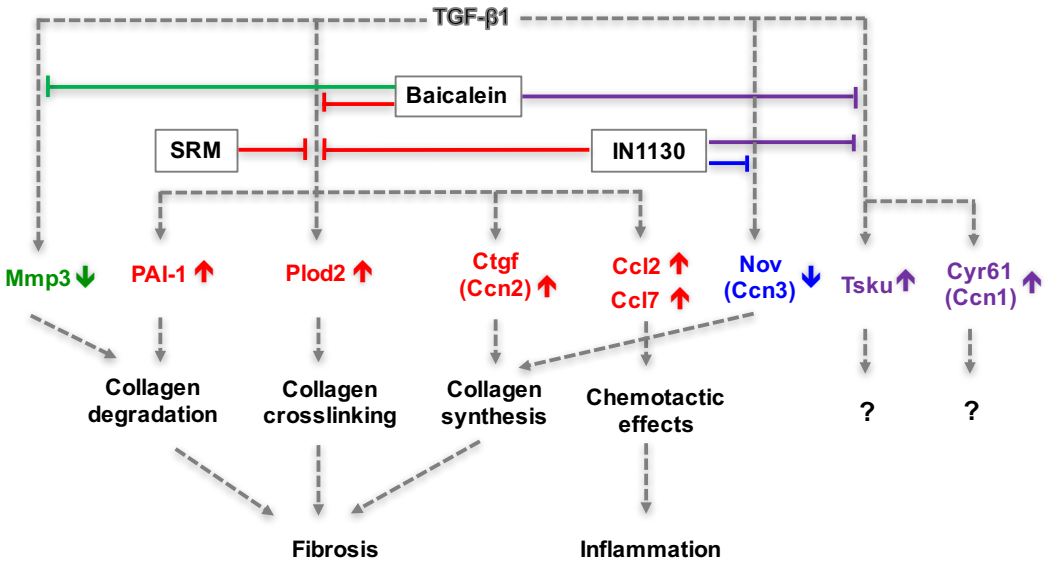

Fig. 6.13. Effects of TGF-β1, SRM, baicalein and IN1130 on proteins in conditioned media and their possible roles in fibrosis and inflammation. TGF-β1-induced PAI-1, Ctgf (Ccn2), Plod2, Ccl2 (MCP-1) and Ccl7 (MCP-3) were reversed by SRM, baicalein and IN1130 (marked in red); TGF-β1-induced Ccn1 (Cyr61) and Tsku were reversed by baicalein & IN1130, but not SRM (marked in purple); TGF-β1 repression of Ccn3 was only reversed by IN1130 (marked in blue); and TGF-β1 repression of Mmp3 was only reversed by baicalein (marked in green).

SRM, baicalein and IN1130 all suppressed TGF-β1-induced PAI-1, Plod2 and Ctgf (**Fig. 6.11Aii, Bii and Cii**), suggesting that SRM, baicalein and IN1130 may share similar anti-fibrotic mechanisms by regulating collagen synthesis, crosslinking and degradation in this *in-vitro* model of fibrosis. The balance of collagen synthesis and degradation is crucial to maintain the normal tissue structure (222). In renal fibrosis, collagen degradation does not keep pace with collagen synthesis, resulting in increased accumulation of collagens, which prevents the tissue repair and remodelling and leads to renal failure (46). The plasminogen activation system has an established role in degrading ECM components (165, 222, 223). PAI-1 is a major inhibitor of urokinase plasminogen activator (uPA) and tissue plasminogen activator (tPA), which cleave plasminogen into active plasmin (161, 162). The role of PAI-1 in kidney fibrosis has been well described (223, 224). PAI-1 is a critical element of the TGF-β network which could be considered as a therapeutic option for fibrosis (165). Collagen cross-linking is another important structural modification that can prevent degradation in fibrosis (170). Pold2 acts as a collagen cross-linker (173) and is responsible for the hydroxylation of lysine residues in collagen telopeptides (172), although its role in fibrosis has been little studied. Ctgf (Ccn2), a downstream of TGF-β1 and an established fibrogenic mediator, were thought to account for extracellular matrix accumulation and renal fibrosis, and has been proposed an anti-fibrotic target (174-176). In the present study, SRM and baicalein, similar to IN1130, have shown promises to be developed further as antifibrotics, by repressing TGF-β1-induced PAI-1, Plod2 and Ctgf.

SRM, baicalein and IN1130 suppressed TGF-β1-induced chemokines Ccl2 and Ccl7 (**Fig. 6.11Dii&Eii**), suggesting that they may alleviate TGF-β1-induced inflammation in inflammatory fibrotic disorders. Indeed, Wang *et al*. found that baicalein inhibited Ccl2 release and ECM accumulation and concluded that the anti-fibrotic mechanism of baicalein may involve its anti-inflammatory effects via inactivation of the NF-κB and MAPK signal pathways in UUO mice model (98). In addition, an increasing number of studies demonstrated that the anti-inflammatory effects of baicalein in renal fibrosis is associated with inhibition of EMT process, which is induced by TGF-β1 through activation of NF-κB in fibrotic kidney (207). The activated NF-κB mediated expression of inflammatory cytokines such as Ccl2, TNF-α and IL-1β (225, 226). Therefore, these findings indicate that suppression of inflammatory responses could contribute to the therapeutic of effects of baicalein, SRM and IN1130, and may play an anti-inflammatory role in renal fibrosis and could be considered as a therapeutic candidate against kidney diseases.

Baicalein, similar to IN1130, suppressed TGF-β1-induced Tsku and Cyr61 (**Fig. 6.11 Fii&Gii**). It suggested that the anti-fibrotic activity of baicalein may be associated with supressing the expression of Tsku and Cyr61, in an Alk5-dependent manner. As discussed in

Chapter 5 (page 123), the functions of Tsku and Cyr61 in fibrosis remain to be fully established, thus the potential values of them as anti-fibrotic and/or anti-inflammatory targets and their roles in the therapeutic of baicalein deserve further investigation.

Only baicalein reversed TGF-β1-suppressed Mmp3 (**Fig. 6.11Iii**), suggesting that anti-fibrotic mechanism of baicalein may differ from both SRM and IN1130 by increasing Mmp3 accumulation in conditioned media. MMPs has major roles in degrading ECM components (166, 224), indicating that Mmp3 may contribute to the pathogenesis of fibrosis. As discussed in **Chapter 5 (page 122)**, current data on roles of Mmp3 in fibrosis and anti-fibrotic therapies are limited. Thus, the roles of Mmp3 in the antifibrotic effect of baicalein deserve further study.

Only IN1130 reversed TGF-β1-suppressed Nov (**Fig. 6.11Hii**). Given the reported anti-fibrotic properties of Nov, this finding suggests that the anti-fibrotic property of IN1130 may be at least in part mediated by increasing Nov. Interestingly, although TGF-β1-induced PAI-1, Plod2, Ctgf, Ccl2 and Ccl7, which were repressed by IN1130 and thus likely Alk5-depedent, were also repressed by SRM and baicalein. While TGF-β1-induced Tsku and Cyr61 were repressed by both baicalein and IN1130, TGF-β1-repressed Nov was only repressed by IN1130, but not SRM and baicalein. It's important to find out if IN1130-reduced Nov was due to repression of Alk5, and if so, why baicalein and SRM failed to repress this but not other Alk5-dependent proteins.

6.4.3. Discussion on integrated analysis of findings on cell-lysate and condition-media proteins

In cell lysates, SRM, baicalein and IN1130 more or less reversed TGF-β1-induced ribosomal proteins. Increasing evidence suggests that eukaryotic 80S ribosome is a viable target for anti-cancer drugs (227) and alternative therapeutic treatment of cardiovascular diseases (228). Functions of ribosomal proteins in fibrosis and in effects of SRM, baicalein and IN1130 remain largely unknown and deserve further investigation. The ribosomal protein S6 kinase (S6K) is a crucial effector of the mechanistic target of rapamycin (mTOR) signalling (229, 230). mTORC1 activates downstream target S6K, whose first identified substrate was ribosomal protein S6 (Rps6), a component of the 40S ribosome (229). mTOR activation was demonstrated to increase phosphorylation of S6K in albumin-treated primary proximal tubular epithelial cells (231) and mesangial cells exposed to high glucose (232). In an *in vivo* model of aldosterone-induced tubulointerstitial fibrosis, western blot analysis for phosphorylated S6K and mTOR in kidney tissues revealed that high expression in fibrotic samples compared with controls (233). These findings indicated the mTORC-S6K pathway

was activated in several *in vitro* and *in vivo* models of fibrosis, emphasising the importance to develop a greater understanding on the relevance of the mTORC-S6K pathway, and indeed ribosomal proteins, in kidney fibrosis. In present the study, the proteomic abundance of Rps6 in cell lysates was significantly increased in TGF-β1 group (**Table 5.1**), but was not further changed by either SRM, baicalein or IN1130 treatment; in contrast, the proteomic abundance of Rps6 in conditioned media was not affected by TGF-β1, but it was significantly increased in both 40 μM and 80 μM SRM groups, as well as in the 80 μM baicalein group (**Table 6.3**). These results need further validation by alternative methods. In view that Rps6 can be phosphorylated by S6K, it raises that questions whether other ribosoal problems could be modified post-translationally. This could mean that proteomic abundance could be due to changes in post-translational modifications, which change the visibility of the proteins by MS rather than by real changes of protein abundance.

In addition, given that the ribosome is an intracellular organelle, the reduced proteins involved in the ribosome pathway in cell lysates may suggest that all the three drugs repressed the intracellular ribosome pathway, while the ribosomal proteins involved in the ribosome pathway in conditioned media induced by SRM and baicalein may suggest that they increased release of intracellular proteins into media, possibly due to cytotoxic effects, although other possibilities unrelated to toxicity can not be ruled out.

Comparative KEGG pathway analyses of cell lysate indicated that SRM and baicalein significantly regulated proteins enriched in the lysosome pathway. Lysosomes are membrane-bound organelles responsible for macromolecule degradation and recycling, and involved in various cellular processes, including secretion, plasma membrane repair, cell signalling and energy metabolism (234). For example, collagen fragments are mainly degraded by lysosome (222, 235). In addition, lysosomal proteases cathepsins are implicated in multiple cellular processes, such as regulation of cell cycle, cell death and autophagy (236). Cathepsins, originally found in the lysosomes, also have been detected in cytosol, nucleus as well as extracellular space, and multiple specific functions have been assigned to individual cathepsins (237). To date, 15 cathepsins have been identified and classified into three families: serine (cathepsin A and G), aspartate (cathepsins D and E), or cysteine (cathepsin B, C, F, H, K, L, O, S, V, X, and W) proteases (238). In the present study, cathepsin B, D and L (Ctsb, Ctsd and Ctsl) were detected in cell lysates. Ctsb was induced by TGF-β1 and reversed by 40 μg/mL SRM and 40 μM baicalein, in contrast, both Ctsd and Ctsl were reduced by TGF-β1 and increased after SRM and baicalein administration (**Table. 6.2**).

Several studies have demonstrated the critical role of cathepsins in kidney disease development and progression, especially cathepsin B, D and L (238-244). It has been

demonstrated that Ctsb may promote glomerular inflammation and other cell damages resulting into glomerular injury and end-stage renal disease by activating inflammasome, a complex of proteins containing NOD-like receptor with pyrin domain 3 (NLRP3), which drives production of pro-inflammatory cytokines in response to infection and tissue injury (245). Increasing knowledge has implicated that inflammasomes are involved in the pathogenesis of AKI and CKD (246, 247). Therefore, NLRP3 has been considered a potential target for the treatment of progressive CKD (248). Fox *et al*. reported that the expression of Ctsb was increased in UUO mouse model (242). In addition, Ctsb was overexpressed in various models of liver injury and patients with chronic liver diseases, suggesting its potential as diagnostic biomarkers for chronic liver diseases (249). Ctsd was highly expressed in damaged tubular cells in nephrotoxic and ischaemia reperfusion-induced AKI (241). Inhibition of Ctsd by Pepstatin A resulted in a reduction in apoptosis and a decrease in tubular cell damage, suggesting a possible contribution of Ctsd in apoptosis during AKI. Up-regulation of Ctsd has been detected in a panel of human CKD renal biopsies and two mouse CKD models (UUO and chronic ischaemia reperfusion injury) (242). Ctsd inhibition using Pepstatin A in CKD models led to reduction in kidney fibrosis via increasing collagenolytic activity and extracellular protease activity of urokinase-type plasminogen activator (uPA). uPA processes plasminogen into plasmin, which participate in ECM degradation (250). In CKD patients, Ctsd serum levels were significantly higher and correlated with endothelial dysfunction (251). Induction of Ctsl expression in podocytes contributed to the development of proteinuria in streptozotocin-induced diabetic nephropathy (252). Sever *et al*. showed that mRNA levels of Ctsl were increased in renal biopsy samples of patients with proteinuric kidney diseases, including membranous glomerulonephritis, focal segmental glomerulosclerosis, and diabetic nephropathy (253). In addition, serum Ctsl activity was markedly elevated in CKD patients and these levels were positively correlated with the severity of proteinuria (254). An increased risk of mortality and morbidity in patients with CKD is associated with higher levels of proteinuria (255). Urinary excretion of Ctsl was higher in children with type I diabetes, suggesting the value of Ctsl as potential predictors for early diabetic kidney disease (256). In summary, Ctsb, Ctsd and Ctsl have been reported to mediate extracellular matrix homeostasis (242), inflammation (245), apoptosis (242) in kidney disease, whereas the functions of Lamp1, Acp2, Naga, Arsb, Dnase2, Aga, Ppt1, Gusb and Atp6v0a1 in fibrotic diseases are little understood. In view of that potential role of cathepsins in renal fibrosis, further validation of their expression and related mechanisms may deserve consideration in the future.

In conditioned media, only baicalein significantly regulated secreted proteins enriched in the lysosome pathway. Atp6ap1, Gaa, Aga, Lgmn, Ctsd, Psap and Ctsb and were all increased

by baicalein at both concentrations; Galns was induced by 40 μM baicalein; while Clta and Cltb were reduced by 80 μM baicalein (**Table 6.4)**. The functions of those lysosomal proteins have been rarely reported in fibrosis diseases. Lgmn, or legumain, a cysteine peptidase that specifically hydrolyses asparaginyl bonds, is known to exist in many organs and is particularly abundant in the kidney (257). Lgmn is mainly expressed in proximal tubules of the rat (258) and mouse (259) kidney. It has been found that fibronectin was degraded by Lgmn in cultured renal proximal tubular cells and the accumulation of fibronectin in the renal tubulointerstitial area was significantly increased in UUO kidneys from Lgmn-deficient mice (260). These findings indicated that Lgmn may regulate extracellular matrix remodelling by mediating fibronectin degradation. In addition, the processing of lysosomal cathepsins (Ctsb, Ctsh and Ctsl), from single-chain forms into two-chain forms, was completely defective in Lgmn-deficient mice, suggesting that Lgmn may play a role in lysosomal degradation system (259). Given that the lysosome is an intracellular organelle, the changed proteins involved in the lysosome pathway in cell lysates may suggest that SRM and baicalein regulated the intracellular lysosome pathway, while the increased proteins involved in the lysosome pathway in conditioned media induced by baicalein may suggest that baicalein increased release of intracellular proteins into media, either due to cytotoxic effects, i.e. by increase cell death, or by other unknown mechanisms, such as exosomes and other multivesicular bodies (261).

6.5. Conclusions

In this chapter, proteomic analysis has uncovered shared, dose-dependent and drug-specific mechanisms of three antifibrotics, SRM, baicalein and IN1130:

- SRM, baicalein and IN1130 have shared anti-fibrotic and anti-inflammatory mechanisms, involving repressing TGF-β1-indeuced PAI-1, Plod2, Ctgf, Ccl2 and Ccl7.
- SRM, baicalein and IN1130 differed in regulating proteins such as Nov and Mmp3.
- Roles for Aldh3a1, Enpp1, Cyr61, Tsku, Impdh2, Ccdc80 and Tfrc in fibrogenesis and anti-fibrotic therapy deserve further studies.
- SRM, baicalein and IN1130 all repressed the intracellular ribosome pathway, while they differed in regulating ribosomal proteins in conditioned media. The pharmacological and toxicological implications of these findings deserve further studies.
- SRM and baicalein, but not IN1130, regulated the intracellular lysosome pathway, while they differentially regulated multiple metabolism pathways. The importance of those pathways in anti-fibrotic therapeutics deserve further studies.

Chapter 7. General discussion and future work

7.1. General discussion

7.1.1. Quality control of materials and methods

Authentication and quality control of research materials are fundamental for safeguarding integrity of scientific research and to boost reproducibility of research findings (262, 263). In this project, identities of SR, AR and ALR were thoroughly examined by morphological, genetic and chemical criteria to ensure that they were derived from the correct species and met the legal standards in terms of general characteristics, macroscopic and microscopic morphology, bioactive constituents and contaminants, e.g. heavy metals and pesticides. The voucher samples have been deposited in our own lab and at Royal Botanical Gardens Kew and will be made available upon request to facilitate independent comparison of results with the international community in the future. These stringent procedures have ensured that our research materials met good practice guidelines (264, 265). Through a collaboration with Kew, I have learnt that, from a botanist point of view, the scientific value of voucher samples would be significantly improved if herbarium specimens (i.e. dried and flattened aerial parts of each of the corresponding plant species from the same crop) had been included. This would, of course, require even closer collaborations with botanists when harvesting the medicinal plants in future projects. Herbs were procured from regions known for producing geo-authentic herbs of these species. In the future, it will be desirable to harvest from Good Agricultural Practice (GAP)-certified farms, if there are any.

AR and ALR have to be processed to meet pharmacopoeial standards to be used as legal materia medica. Although there are legal standards for quality control of processed herbs, there are no standard operating procedures for processing these herbs in China and internationally. I have collaborated with experts at the frontiers leading the development of national guidelines (264), and we have also confirmed that the processed AR and ALR met legal requirements according to pharmacopoeias. With respect to the herbal extracts, chemical analysis of each extraction was undertaken using HPLC, although selectively enriching and depleting certain groups of compounds failed due to the complexity of the compositions and limitations of the existing chemical separation technology.

To avoid mislabelling, misidentification and impurity of herbal compounds, molecular weights of all compounds used in the project were validated by HPLC-MS/MS.

Similarly, antibodies cannot be taken for granted as specific (266). In this project, for all antibodies used for cytoimmunostaining, non-immune IgGs, positive and negative control cells have been used to confirm specificity.

Misidentification of cell cultures is another major pitfall that affects reproducibility and the integrity of scientific research (267, 268). In a cellular model-based project, it is crucial to ensure that cells used are authenticated. Following the current best practice, NRK-49F cell line has been successfully authenticated as a normal rat kidney fibroblast-like cells; this supports the use of this cell line to model fibrosis for the discovery of anti-fibrotic and pro-fibrotic activities, which can be further validated *in-vivo* in rodent models. However, to establish human relevance, it is desirable to confirm findings in human kidney fibroblast cell lines (269, 270), but unfortunately, we found that two cell lines expected to be derived from human kidneys were proven to be misidentified. This did highlight the necessity to authenticate cells for this project.

7.1.2. Choice of cellular model and *in-vitro* model of fibrosis

NRK-49F cell line was chosen as a suitable renal fibroblast cell model in my work. NRK-49F cells are derived from normal rat kidneys and are morphologically and behaviourally similar to fibroblasts. In the past, NRK-49F cells have been widely used in fibrogenesis studies, especially those induced by TGF-β1(271, 272). Furthermore, the NRK-49F cell culture conditions to minimise cell proliferation and maximise the fibrogenic response to TGF-β have already been established (272). The initial plan was to use two human renal fibroblasts "TK173" and "TK188" cells to validate findings in NRK-49F cells to establish human relevance of findings. Unexpectedly, these cells were proven to be of mouse origin, as shown in **Fig.2.3** and **Fig.2.4**. In interest of time, I decided to stick to NRK-49F cells only in present work.

The *in-vitro* model of fibrosis represents as a reproducible cell model of fibrosis currently available and uses the dye PSR to visualise total collagen protein deposition, which can be further quantified by spectrophotometric analysis of eluted stain (65). However, this model has its limitations. Firstly, it cannot be used if TGF-β1-treated cells do not produce enough collagen for the change to be detected by PSR staining. Indeed, this model provide unsuitable for a variety of cell types that are known to be important in TIF and glomerulosclerosis (data not shown). Secondly, as PSR stains for collagen, relevant changes in non-collagenous ECM components will be overlooked in this model. Finally, this model relies on an intact cell monolayer and disruption of this monolayer or contraction of cells could affect the readout. To address this limitation, additional parameters, hydroxyproline assay and immunoassays of selected ECM proteins, were used to further validate key results in this study, as shown in **Fig. 4.6, 4.7, 4.9 and 4.10**. Moreover, as reported by Qureshi et.al. (37), an immunofluorescence-based method would also be considered in the future, because

it allows us to focus directly on the mature deposited ECM by stripping the cellular component and only imaging the remaining ECM.

In addition, cytotoxicity might contribute towards anti-fibrotic activity. The *in-vitro* model of fibrosis relies on cells remaining in the culturing system for reliable data on total collagen accumulation. It is important to know how many viable cells are remaining at the end of the experiment. Thus, throughout the whole study, I monitored cell attachment to control the credibility of the assays. Furthermore, LDH assay were applied to further examine the cytotoxitiy (**Fig. 4.9B**). However, I don't exclude the possibility of herbal compounds/extracts playing anti-fibrotic roles by growth arrest or lowered cell metabolism. Additional cytotoxicity assays, such as MTT assay, Presto blue or trypan blue, would be provided in the further (273).

In order to evaluate the reproducibility of anti-fibrotic activities of SRM and balcalein reported previously by my supervisor's lab (65), same *in-vitro* model, timing and dose of treatments were chosen in this work. Indeed, it presents good reproducibility but it also has limitations by choosing a late time point, some immediate early genes and signal transductions responsible for progressive fibrosis may have been missed out. Nonetheless, by focusing on sustainable changes of proteomic profiling, signalling and pathways (274, 275), findings of the present study might open a broad avenue for developing new strategies to target sustainable events responsible for refractory fibrosis and progressive CKD. In the future, it would be desirable to examine whether findings in NRK-49F cells are comparable to those in human renal fibroblast cell lines, rat and human renal fibroblast primary cultures, as well as in *in-vivo* models and in CKD patients.

7.1.3. Toxicity of SR and SR flavonoids

Previous studies have demonstrated that SR and their flavonoids posscess a variety of biological activities mainly including anti-inflammatory (276), antioxidant (91), anti-cancer (81, 277) and anti-fibrotic effects (118). There have been few reports about their safety and toxicity. In the present study, *in-vitro* cytotoxicity was assessed by an approximated cell detachment index and a LDH release assay. Up to 80 μg/mL SR methanolic extract and 80 μM baicalein did not significantly increased cell detachment, while 60 μM baicalin and wogonin increased LDH release in keeping with results of cell detachment index, suggesting baicalin and wogonin had higher cytotoxicity.

The cytotoxicity of SR methanolic extracts has been hardly reported before. The cytotoxicity of a SR aqueous extract, however, has been investigated in human corneal epithelial cells by trypan blue staining, MTT assay and flow cytometry. SR aqueous extract showed no evidence of cytotoxicity at 5% (approximately 50 mg/mL) concentration for 5 min exposure

(278). In another toxicological study, SR aqueous extract did not induce any dermal irritation/corrosion in rabbits or skin sensitisation in guinea pigs (279). Recently, a Phase I, randomised, double-blinded trial of a single ascending dose (100-2800 mg) of baicalein chewable tablets was carried out in 72 healthy Chinese subjects (6-8 subjects per group). 11 mild treatment-related adverse events were observed and resolved without any treatment, including two cases of abdominal distention, blurred vision and decreased plasma fibrinogen levels, and a single case of hyperactive bowel sounds, constipation, dizziness, somnolence and decreased blood leukocyte dcount, respectively. No serious adverse event occurred and clinical laboratory assessments showed no signs of liver or kidney toxicity. Importantly, much of the ingested bacalein appeared in the circulation in the form of its metabolite baicalin (280), thus the anti-fibrotioc activity and cytotoxicity of baicalin observed in my project urge to take *in-vivo* metabolism into consideration when considering the efficacy and toxicity of baicalein as a therapy. It may worth mentioning that Cai *et al*. have even reported kidney injury and fibrosis induced by oral administration of high doses of baicalin (400, 800 and 1600 mg/kg) for 8 days in SD rats (281).

Furthermore, cases of hepatotoxicity of Move Free ® arthritis supplement have been attributed to SR (282-284). In all cases, SR was proposed to have caused liver injury confirmed by liver histology and in one case it was also proposed that this supplement caused pulmonary complications (283). Moreover, laboratory studies of SR flavonoids *in vivo* have also revealed toxic effects. The acute and sub-chronic toxicity of wogonin was examined in B6 albino mice and Sprague-Dawley (SD) rats (285), revealing that a long period of treatment with high dose of wogonin (120 mg/kg) could induce reversible heart injury in rats. Sub-chronic toxicity of wogonin was further examined in Beagle dog at dosages of 60, 30 and 15 mg/kg per day for 90 days via intravenous administration (286). Typical adverse effects such as hyperptyalism, somatasthenia, swollen snout accompanied with the scratching and the discontinuity urine dripping were observed especially in high-dose group.

7.1.4. Proteomic approach to guide mechanistic studies

Proteomic methodology is a powerful tool for unbiased global analysis of biological systems and also has enormous potential to complement targeted studies. In the present study, besides known druggable targets e.g. PAI-1 and Ccn2/Ctgf, potential roles for Aldh3a1, Enpp1, Impdh2, Ccn1/Cyr61, Ccn3/Nov, Mmp3, Plod2 and Tsku, as well as the ribosome, lysosome and metabolic pathways in fibrogensis and as anti-fibrotic targets have been highlighted as being deserving further investigation. However, some common fibrotic makers and mediators (e.g. α-SMA and IL-11R/IL-11(287)) could not be detected, while

others presented unexpected results. For example, fibronectin and vimentin did not change significantly in both cell lysates and conditioned media in TGF-β1-treated group; Col1a1, Col1a2, and Col5a1 significantly decreased after TGF-β1 treatment in cell lysate samples, while there was no significant change in conditioned media. While the expression of α-SMA, fibronectin, collengen I&III were successfully measured by immunofluorescence and/or hydorxyproline assays or soluble collagen assays, as shown in **Fig. 4.7 & 4.10 and Fig. 6.1**, presenting significantly difference in TGF-β1 treatment groups. The most possible reason is protein post-translational modification (PTMs). PTMs present analytical difficulties to proteomic strategies due to their complexity and particular biochemical properties. To date, over 300 different PTMs have been described and the most common PTMs include phosphorylation, crosslinking, acetylation and glycosylation, etc (288). PTMs massively increase the complexity of organismal proteomes and have a wide array of functions during the cellular processes, e.g., altering protein structure and localisation, causing protein-protein interactions to activate or inactivate a protein. In particular, ECM proteins interact with many other proteins and are often highly covalently crosslinked resulting in low solubility. Fibronectin, for example, consists of a series of repeating modules (type I, II and III fibronectin repeats), several of which serve as binding sites for other ECM components, such as heparin, fibrin and collagens (289). Hence, proteomic approaches face the difficult to detect and quantify these modifications and many strategies incorporating various isolation, enrichment or fractionation methodologies are required to increase the signal-noise ratio and enable the detection of a wide range of molecule concentrations (290, 291).

Currently the key technology used in proteomics is mass spectrometry, which ionises sample molecules and separates the ions according to their mass-to-charge ratio and measures the signal intensity of the ions. Tandem MS results in the fragmentation of peptide ions to provide structural information about the ions, which enables the determination of their amino acid sequence. Tandem MS is the core technology used in “bottom-up” proteomics, in which proteins are extracted from the sample of interest then enzymatically digested into peptides prior to analysis (292). Thus, it is an essential step to enrich the modified peptides by depleting the bulk of non-modified peptides that hamper PTMs analysis (293, 294).

To address some of the aforementioned problems, specific technical innovation is needed. Techniques firstly include improving extract and lysis performance either with ammonium hydroxide to remove the cells effectively from 2D cell cultures (295), or with hypotonic buffers to extract proteins preserving the architecture and bioactivity of the protein scaffold (296), or combining ammonium hydroxide and detergent extraction and DNase treatment to remove nuclei (297). Secondly, the strategies target either PTMs structure, such as affinity chromatography (298, 299), or physicochemical characteristics of the modified peptides, for

example, resulting in specific retention characteristics in reversed phase (300) or hydrophilic interaction chromatography (301). Strong cation exchange chromatography can be used to selectively enrich charge-reduced peptides, e.g., phosphopeptides, glycopeptides, N-terminally acetylated peptides (302). In order to increase specificity and additionally fractionate complex samples, two and more enrichment methods are commonly combined, such as combining affinity chromatography and hydrophilic interaction chromatography for the selective enrichment of phosphopeptides (303). Phosphorylation is the most well-studied PTMs, the improvement in purification of phosphorylated proteins and peptides and current proteomic strategies used to qualitatively and quantitatively probe these enriched phosphoproteomes have been developed and exploited (293, 304).

Another major challenge when performing proteomic analysis is extracting important information from these large datasets. Here, to pursue a better understanding of the holistic view of TGF-β1-induced fibrogenesis and the mechanism of the anti-fibrotic activities of three drugs, STRING network and KEGG pathway analysis were performed in **Chapters 5** and **6**. Analysis of interaction networks based on previously reported protein-protein interactions, could provide insights into the functional roles of the identified proteins. For example, as shown in **Fig. 5.7A**, STRING analysis has led to the emergence of two major clusters (a and b), indicating that proteins in network with many common interaction partners are more likely to function together. Indeed, KEGG pathway analysis has shown that the proteins in these two clusters were mainly associated with multiple metabolic pathways and the ribosome pathway (**Fig. 5.7B**). However, how to identify and validate those pathways and functions regulated by TGF-β1 and three antifibtotics is another task.

7.2. Future work

7.2.1. Confirmation of the effects of AR/ALR on fibrogenesis

One of the issues remains unsolved in this project is the effect of AR/ALR on fibrogenesis. As described in **Chapter 3**, the pro-fibrotic activity of AR identified by a screening studies of my Supervisor's lab was not reproduced in my project. To draw solid conclusions, the activities of AR in TGF-β1-induced fibrogenesis should be further examined using additional batches of well-authenticated AR, preferably also using alternative assays for total collagens (e.g. hydroxyproline assay) and fibrotic molecular markers (e. g. collagen type I & III). In addition, processed and unprocessed ALR extracts have been produced and their quality control conducted in the present study, however, their effects on fibrogenesis have not been tested due to the limited time. The next studies should thus examine the effects of processed and unprocessed ALR on TGF-β1-induced fibrogenesis.

7.2.2. Anti-fibrotic activities of synthetic baicalein derivatives

Flavonoids are known for their numerous biological activities, such as anti-fibrotic (118, 305), anti-inflammatory (207), antioxidant (306), anti-cancer (277), cardiovasculoprotective (95) and neuroprotective activities (307). Like other flavonoids, one major concern in the clinical application of baicalein is its low aqueous solubility, which leads to poor oral bioavailability. After oral administration, baicalein undergoes extensive first-pass metabolism in intestine and liver in human and rats, and it is quickly metabolised to baicalin in the blood (308-310). To improve the bioavailability of baicalein, various strategies have been developed, e.g. nanocrystal (311) and self-microemulsifying drug delivery system (312). Modification of baicalein molecules to create analogs is another strategy. A series of synthetic derivatives of baicalein (**Fig. 7.1**) have been synthesised and gifted by Prof. Yung-Chi Cheng's laboratory at Yale University (313). In total, 27 synthetic baicalein derivatives were received and examined by HRMS to validate their molecular weights. As shown in **Supplementary Table 8**, all synthetic baicalein derivatives, except S2 and S3, were found with the expected molecular weights. In the present study, baicalein showed most potent *in-vitro* efficacy, with little cytotoxicity. However, its efficacy is still relatively moderate (IC50 =38.2±2.7 μM). To address those problems, it is desirable to examine if better anti-fibrotic and less toxic bacalein derivatives can be discovered and if any structure-activity relationship can be explored by using these structural analogs.

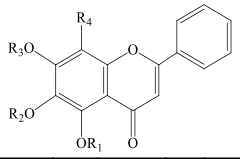

Compound	R_1	R_2	R_3	R_4
S2	H	Ac	H	H
S3	H	Ac	Ac	H
S5	Me	Ac	Me	H
S6	Me	Me	Me	H
S7	Me	Ac	Ac	H
S8	H	Me	Me	H
S9	Bn	Ac	Ac	H
S10	H	Bn	Ac	H
S14	Ac	Ac	Bn	H
S15	H	Bn	H	H
S24	H	Ac	Ac	Br
S25	H	H	H	Br
S32	H	CH_2CH_3	H	H
S38	H	CH_2CH_3	Me	H

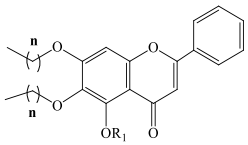

Compound	R_1	n
S18	H	2
S23	Me	2
S33	H	1
S34	H	7
S40	H	4
S41	Me	4
S42	H	5
S43	Me	5
S45	H	3
S46	Me	3

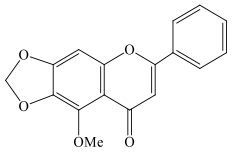

S20

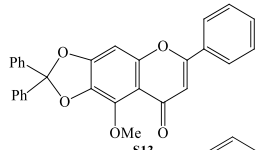

S13

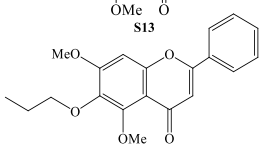

S22

Fig. 7.1. Structures of synthetic baicalein derivatives.

7.2.3. Further validation

Given the limitations of proteomic approach discussed in section **7.1.4**, further validation of proteomic findings on any candidate proteins in cell lysates and conditioned media presents the first step towards understanding their possible roles in TGF-β1-induced fibrogenesis and mechanisms of the anti-fibrotic activities of SRM, baicalein and IN1130. In the next step, it is imperative to perform further studies focusing on two major aspects. Firstly, in view that the ribosome pathway was most significantly regulated in this *in-vitro* system, validation of ribosomal proteins should be done. Rps13, Rps15, Rps24 and Rps4x, which were most significantly regulated by SRM and baicalein (**Fig. 6.10**), could be planned for validation by ELISA or western blot experiments. Secondly, in view that Impdh2 connected two clusters of TGF-β1-regulted proteins as shown in STRING map (**Fig. 5.7A)**, and it has also been reported as a druggable target to attenuate the progression of renal fibrosis (138, 140). In the present study, sappanone A (an Impdh2 inhibitor), up to concentrations 32 μM, did not significantly decrease total collagen accumulation in TGF-β1-induced *in-vitro* model of fibrosis **(Fig. 5.10)**. However, the quality control of the commercial sappanone A and its efficacy in repressing Impdh2 activity at the concentrations used deserve further investigation. The effects of Sappanone A and/or genetic inhibitors of Impdh2 (e.g. Impdh2 siRNA or gene delation) on TGF-β1-induced fibrogenesis should be examined in *in vitro* and *in vivo* work in the future to establish whether Impdh2 could be an anti-fibrotic target.

7.2.4. Integrating proteomics and metabolomics

This work has focused on the proteomic analysis of TGF-β1-induced fibrogenesis and mechanisms of the anti-fibrotic activities of SRM, baicalein and IN1130. The proteomic data have highlighted important changes in metabolic pathways in TGF-β1-induced fibrogenesis and in SRM, baicalein and IN1130 effects on fibrogenesis, thus justifying further studies using a metabolomic analysis, another unbiased means to identify and quantify changes of metabolites, which are the end products of cellular processes (314). Therefore, to take this work further, the remaining cell lysates and conditioned media samples of this project have been sent to Dr. Jonathan Swann's laboratory at Imperial College London and will be further analysed in a metabolomic approach. Integration of proteomics and metabolomics may further advance the understanding of TGF-β1-induced fibrogenesis and the mechanism of three antifibrotics, but it may also pose bioinformatic challenges.

Chapter 8 Bibliography

1. Webster AC, Nagler EV, Morton RL, Masson P. Chronic Kidney Disease. Lancet (London, England). 2017;389(10075):1238-52.

2. Levey AS, Eckardt KU, Tsukamoto Y, Levin A, Coresh J, Rossert J, et al. Definition and classification of chronic kidney disease: a position statement from Kidney Disease: Improving Global Outcomes (KDIGO). Kidney international. 2005;67(6):2089-100.

3. Levey AS, de Jong PE, Coresh J, El Nahas M, Astor BC, Matsushita K, et al. The definition, classification, and prognosis of chronic kidney disease: a KDIGO Controversies Conference report. Kidney international. 2011;80(1):17-28.

4. Djudjaj S, Boor P. Cellular and molecular mechanisms of kidney fibrosis. Molecular aspects of medicine. 2018.

5. Woo KT, Choong HL, Wong KS, Tan HB, Chan CM. The contribution of chronic kidney disease to the global burden of major noncommunicable diseases. Kidney international. 2012;81(10):1044-5.

6. Andrassy KM. Comments on 'KDIGO 2012 Clinical Practice Guideline for the Evaluation and Management of Chronic Kidney Disease'. Kidney international. 2013;84(3):622-3.

7. Stevens PE, Levin A. Evaluation and management of chronic kidney disease: synopsis of the kidney disease: improving global outcomes 2012 clinical practice guideline. Annals of internal medicine. 2013;158(11):825-30.

8. Mende CW. Application of direct renin inhibition to chronic kidney disease. Cardiovascular drugs and therapy. 2010;24(2):139-49.

9. Turgut F, Bolton WK. Potential new therapeutic agents for diabetic kidney disease. American journal of kidney diseases : the official journal of the National Kidney Foundation. 2010;55(5):928-40.

10. Akhurst RJ, Hata A. Targeting the TGFbeta signalling pathway in disease. Nature reviews Drug discovery. 2012;11(10):790-811.

11. Reeves WB, Rawal BB, Abdel-Rahman EM, Awad AS. Therapeutic Modalities in Diabetic Nephropathy: Future Approaches. Open journal of nephrology. 2012;2(2):5-18.

12. Voelker J, Berg PH, Sheetz M, Duffin K, Shen T, Moser B, et al. Anti-TGF-beta1 Antibody Therapy in Patients with Diabetic Nephropathy. Journal of the American Society of Nephrology : JASN. 2017;28(3):953-62.

13. Sharma K, Ix JH, Mathew AV, Cho M, Pflueger A, Dunn SR, et al. Pirfenidone for diabetic nephropathy. Journal of the American Society of Nephrology : JASN. 2011;22(6):1144-51.

14. Adler SG, Schwartz S, Williams ME, Arauz-Pacheco C, Bolton WK, Lee T, et al. Phase 1 study of anti-CTGF monoclonal antibody in patients with diabetes and microalbuminuria. Clinical journal of the American Society of Nephrology : CJASN. 2010;5(8):1420-8.

15. Mann JF, Green D, Jamerson K, Ruilope LM, Kuranoff SJ, Littke T, et al. Avosentan for overt diabetic nephropathy. Journal of the American Society of Nephrology : JASN. 2010;21(3):527-35.

16. Kohan DE, Lambers Heerspink HJ, Coll B, Andress D, Brennan JJ, Kitzman DW, et al. Predictors of Atrasentan-Associated Fluid Retention and Change in Albuminuria in

Patients with Diabetic Nephropathy. Clinical journal of the American Society of Nephrology : CJASN. 2015;10(9):1568-74.

17. de Zeeuw D, Coll B, Andress D, Brennan JJ, Tang H, Houser M, et al. The endothelin antagonist atrasentan lowers residual albuminuria in patients with type 2 diabetic nephropathy. Journal of the American Society of Nephrology : JASN. 2014;25(5):1083-93.

18. Wenzel RR, Littke T, Kuranoff S, Jurgens C, Bruck H, Ritz E, et al. Avosentan reduces albumin excretion in diabetics with macroalbuminuria. Journal of the American Society of Nephrology : JASN. 2009;20(3):655-64.

19. Dhaun N, Ferro CJ, Davenport AP, Haynes WG, Goddard J, Webb DJ. Haemodynamic and renal effects of endothelin receptor antagonism in patients with chronic kidney disease. Nephrology, dialysis, transplantation : official publication of the European Dialysis and Transplant Association - European Renal Association. 2007;22(11):3228-34.

20. Menne J, Eulberg D, Beyer D, Baumann M, Saudek F, Valkusz Z, et al. C-C motif-ligand 2 inhibition with emapticap pegol (NOX-E36) in type 2 diabetic patients with albuminuria. Nephrology, dialysis, transplantation : official publication of the European Dialysis and Transplant Association - European Renal Association. 2017;32(2):307-15.

21. de Zeeuw D, Bekker P, Henkel E, Hasslacher C, Gouni-Berthold I, Mehling H, et al. The effect of CCR2 inhibitor CCX140-B on residual albuminuria in patients with type 2 diabetes and nephropathy: a randomised trial. The lancet Diabetes & endocrinology. 2015;3(9):687-96.

22. Ansquer JC, Foucher C, Rattier S, Taskinen MR, Steiner G. Fenofibrate reduces progression to microalbuminuria over 3 years in a placebo-controlled study in type 2 diabetes: results from the Diabetes Atherosclerosis Intervention Study (DAIS). American journal of kidney diseases : the official journal of the National Kidney Foundation. 2005;45(3):485-93.

23. Lachin JM, Viberti G, Zinman B, Haffner SM, Aftring RP, Paul G, et al. Renal function in type 2 diabetes with rosiglitazone, metformin, and glyburide monotherapy. Clinical journal of the American Society of Nephrology : CJASN. 2011;6(5):1032-40.

24. Bolignano D, Zoccali C. Glitazones in chronic kidney disease: potential and concerns. Nutrition, metabolism, and cardiovascular diseases : NMCD. 2012;22(3):167-75.

25. Reisman SA, Chertow GM, Hebbar S, Vaziri ND, Ward KW, Meyer CJ. Bardoxolone methyl decreases megalin and activates nrf2 in the kidney. Journal of the American Society of Nephrology : JASN. 2012;23(10):1663-73.

26. Pergola PE, Krauth M, Huff JW, Ferguson DA, Ruiz S, Meyer CJ, et al. Effect of bardoxolone methyl on kidney function in patients with T2D and Stage 3b-4 CKD. American journal of nephrology. 2011;33(5):469-76.

27. de Zeeuw D, Akizawa T, Audhya P, Bakris GL, Chin M, Christ-Schmidt H, et al. Bardoxolone methyl in type 2 diabetes and stage 4 chronic kidney disease. The New England journal of medicine. 2013;369(26):2492-503.

28. Tumlin JA, Galphin CM, Rovin BH. Advanced diabetic nephropathy with nephrotic range proteinuria: a pilot study of the long-term efficacy of subcutaneous ACTH gel on proteinuria, progression of CKD, and urinary levels of VEGF and MCP-1. Journal of diabetes research. 2013;2013:489869.

29. Brosius FC, Tuttle KR, Kretzler M. JAK inhibition in the treatment of diabetic kidney disease. Diabetologia. 2016;59(8):1624-7.

30. Pergola PE. Weekly Doses of GCS-100, a Galectin-3 Antagonist, Resulted in Significant Improvement in eGFR in Patients With CKD in a Randomized. 2014.

31. Duffield JS. Cellular and molecular mechanisms in kidney fibrosis. The Journal of clinical investigation. 2014;124(6):2299-306.

32. Hewitson TD. Renal tubulointerstitial fibrosis: common but never simple. American journal of physiology Renal physiology. 2009;296(6):F1239-44.

33. Ishibe S, Cantley LG. Epithelial-mesenchymal-epithelial cycling in kidney repair. Current opinion in nephrology and hypertension. 2008;17(4):379-85.

34. Grgic I, Campanholle G, Bijol V, Wang C, Sabbisetti VS, Ichimura T, et al. Targeted proximal tubule injury triggers interstitial fibrosis and glomerulosclerosis. Kidney international. 2012;82(2):172-83.

35. Li J, Qu X, Bertram JF. Endothelial-myofibroblast transition contributes to the early development of diabetic renal interstitial fibrosis in streptozotocin-induced diabetic mice. The American journal of pathology. 2009;175(4):1380-8.

36. Humphreys BD, Lin SL, Kobayashi A, Hudson TE, Nowlin BT, Bonventre JV, et al. Fate tracing reveals the pericyte and not epithelial origin of myofibroblasts in kidney fibrosis. The American journal of pathology. 2010;176(1):85-97.

37. Qureshi OS, Bon H, Twomey B, Holdsworth G, Ford K, Bergin M, et al. An immunofluorescence assay for extracellular matrix components highlights the role of epithelial cells in producing a stable, fibrillar extracellular matrix. Biology open. 2017;6(10):1423-33.

38. Strutz F, Zeisberg M, Renziehausen A, Raschke B, Becker V, van Kooten C, et al. TGF-beta 1 induces proliferation in human renal fibroblasts via induction of basic fibroblast growth factor (FGF-2). Kidney international. 2001;59(2):579-92.

39. Stenvinkel P, Ketteler M, Johnson RJ, Lindholm B, Pecoits-Filho R, Riella M, et al. IL-10, IL-6, and TNF-alpha: central factors in the altered cytokine network of uremia--the good, the bad, and the ugly. Kidney international. 2005;67(4):1216-33.

40. Norman JT, Clark IM, Garcia PL. Hypoxia promotes fibrogenesis in human renal fibroblasts. Kidney international. 2000;58(6):2351-66.

41. Meran S, Steadman R. Fibroblasts and myofibroblasts in renal fibrosis. International journal of experimental pathology. 2011;92(3):158-67.

42. Liu Y. Renal fibrosis: new insights into the pathogenesis and therapeutics. Kidney international. 2006;69(2):213-7.

43. Wada T, Sakai N, Sakai Y, Matsushima K, Kaneko S, Furuichi K. Involvement of bone-marrow-derived cells in kidney fibrosis. Clinical and experimental nephrology. 2011;15(1):8-13.

44. Niedermeier M, Reich B, Rodriguez Gomez M, Denzel A, Schmidbauer K, Gobel N, et al. CD4+ T cells control the differentiation of Gr1+ monocytes into fibrocytes. Proceedings of the National Academy of Sciences of the United States of America. 2009;106(42):17892-7.

45. Gewin L, Zent R, Pozzi A. Progression of chronic kidney disease: too much cellular talk causes damage. Kidney international. 2017;91(3):552-60.

46. Liu Y. Cellular and molecular mechanisms of renal fibrosis. Nat Rev Nephrol. 2011;7(12):684-96.

47. Hutchison N, Fligny C, Duffield JS. Resident mesenchymal cells and fibrosis. Biochimica et biophysica acta. 2013;1832(7):962-71.

48. Loeffler I, Wolf G. Epithelial-to-Mesenchymal Transition in Diabetic Nephropathy: Fact or Fiction? Cells. 2015;4(4):631-52.

49. Lan HY, Chung AC. TGF-beta/Smad signaling in kidney disease. Seminars in nephrology. 2012;32(3):236-43.

50. Iwano M, Plieth D, Danoff TM, Xue C, Okada H, Neilson EG. Evidence that fibroblasts derive from epithelium during tissue fibrosis. The Journal of clinical investigation. 2002;110(3):341-50.

51. Bottinger EP. TGF-beta in renal injury and disease. Seminars in nephrology. 2007;27(3):309-20.

52. Lan HY. Diverse roles of TGF-beta/Smads in renal fibrosis and inflammation. International journal of biological sciences. 2011;7(7):1056-67.

53. Bottinger EP, Kopp JB. Lessons from TGF-beta transgenic mice. Mineral and electrolyte metabolism. 1998;24(2-3):154-60.

54. Ziyadeh FN, Hoffman BB, Han DC, Iglesias-De La Cruz MC, Hong SW, Isono M, et al. Long-term prevention of renal insufficiency, excess matrix gene expression, and glomerular mesangial matrix expansion by treatment with monoclonal antitransforming growth factor-beta antibody in db/db diabetic mice. Proceedings of the National Academy of Sciences of the United States of America. 2000;97(14):8015-20.

55. Bitzer M, Sterzel RB, Bottinger EP. Transforming growth factor-beta in renal disease. Kidney & blood pressure research. 1998;21(1):1-12.

56. Maarouf OH, Aravamudhan A, Rangarajan D, Kusaba T, Zhang V, Welborn J, et al. Paracrine Wnt1 Drives Interstitial Fibrosis without Inflammation by Tubulointerstitial Cross-Talk. Journal of the American Society of Nephrology : JASN. 2016;27(3):781-90.

57. Furukawa F, Matsuzaki K, Mori S, Tahashi Y, Yoshida K, Sugano Y, et al. p38 MAPK mediates fibrogenic signal through Smad3 phosphorylation in rat myofibroblasts. Hepatology (Baltimore, Md). 2003;38(4):879-89.

58. Zhong Y, Menon MC, Deng Y, Chen Y, He JC. Recent Advances in Traditional Chinese Medicine for Kidney Disease. American journal of kidney diseases : the official journal of the National Kidney Foundation. 2015;66(3):513-22.

59. Zhang L, Schuppan D. Traditional Chinese Medicine (TCM) for fibrotic liver disease: hope and hype. Journal of hepatology. 2014;61(1):166-8.

60. Zhao C-q, Zhou Y, Ping J, Xu L-m. Traditional Chinese medicine for treatment of liver diseases: progress, challenges and opportunities. Journal of Integrative Medicine. 2014;12(5):401-8.

61. Chen SR, Chen XP, Lu JJ, Wang Y, Wang YT. Potent natural products and herbal medicines for treating liver fibrosis. Chinese medicine. 2015;10:7.

62. Xu Q. FY, Duez P., Hendry B. M., Hylands P. J. . The hunt for anti-fibrotic and pro-fibrotic botanicals. Science. 2014;346 (6216 Suppl):S19-S20.

63. Ai J, Nie J, He J, Guo Q, Li M, Lei Y, et al. GQ5 Hinders Renal Fibrosis in Obstructive Nephropathy by Selectively Inhibiting TGF-beta-Induced Smad3 Phosphorylation. Journal of the American Society of Nephrology : JASN. 2015;26(8):1827-38.

64. Debelle FD, Vanherweghem JL, Nortier JL. Aristolochic acid nephropathy: a worldwide problem. Kidney international. 2008;74(2):158-69.

65. Xu Q, Norman JT, Shrivastav S, Lucio-Cazana J, Kopp JB. In vitro models of TGF-beta-induced fibrosis suitable for high-throughput screening of antifibrotic agents. American journal of physiology Renal physiology. 2007;293(2):F631-40.

66. Hu Q, Noor M, Wong YF, Hylands PJ, Simmonds MS, Xu Q, et al. In vitro anti-

fibrotic activities of herbal compounds and herbs. Nephrology, dialysis, transplantation : official publication of the European Dialysis and Transplant Association - European Renal Association. 2009;24(10):3033-41.

67. Wong YF QS, Kong Q, Zhang XL, Liang XM, Hu Q, Noor M, Hendry BM, Xu Q. Knowledge-based discovery of anti-fibrotic and pro-fibrotic activities from Chinese materia medica. In Kuang X, ed. Recent Advances in Theories and Practice of Chinese Medicine, Intech, 2012, pp337-352.

68. Singhuber J, Zhu M, Prinz S, Kopp B. Aconitum in traditional Chinese medicine: a valuable drug or an unpredictable risk? Journal of ethnopharmacology. 2009;126(1):18-30.

69. Zhou G, Tang L, Zhou X, Wang T, Kou Z, Wang Z. A review on phytochemistry and pharmacological activities of the processed lateral root of Aconitum carmichaelii Debeaux. Journal of ethnopharmacology. 2015;160:173-93.

70. Bisset NG. Arrow poisons in China. Part II. Aconitum--botany, chemistry, and pharmacology. Journal of ethnopharmacology. 1981;4(3):247-336.

71. Liu S, Li F, Li Y, Li W, Xu J, Du H. A review of traditional and current methods used to potentially reduce toxicity of Aconitum roots in Traditional Chinese Medicine. Journal of ethnopharmacology. 2017;207:237-50.

72. Zhao Z, Liang Z, Chan K, Lu G, Lee EL, Chen H, et al. A unique issue in the standardization of Chinese materia medica: processing. Planta medica. 2010;76(17):1975-86.

73. Chen JH, Lee CY, Liau BC, Lee MR, Jong TT, Chiang ST. Determination of aconitine-type alkaloids as markers in fuzi (Aconitum carmichaeli) by LC/(+)ESI/MS(3). Journal of pharmaceutical and biomedical analysis. 2008;48(4):1105-11.

74. Gao T, Bi H, Ma S, Lu J. The antitumor and immunostimulating activities of water soluble polysaccharides from Radix Aconiti, Radix Aconiti Lateralis and Radix Aconiti Kusnezoffii. Natural product communications. 2010;5(3):447-55.

75. Xu Q, Wong YF, Qu S, Kong Q, Zhang X-L, Liang X-M, et al. Knowledge-based discovery of anti-fibrotic and pro-fibrotic activities from Chinese materia medica. Recent Advances in Theories and Practice of Chinese Medicine, Prof Haixue Kuang (Ed), InTech. 2012:337-52.

76. Chinese herbal medicine kidney damage and its Chinese medicine treatment. Beijing; People’s Health Publishing Press; 2004: pp230. Beijing; People’s Health Publishing Press. 2004:230.

77. MHRA warns of the dangers of taking unlicensed herbal medicines containing aconite. 16 April, 2013.

78. Pharmacopoeia of the People’s Republic of China 2010. Beijing Chemical Industry Press. .

79. Wang M, Franz G. The Role of the European Pharmacopoeia (Ph Eur) in Quality Control of Traditional Chinese Herbal Medicine in European Member States. World J Tradit Chin Med. 2015;1(1):5-16.

80. American Herbal Pharmacopoeia: Botanical Pharmacognosy - Microscopic Characterization of Botanical Medicines 2011: Chemical Rubber Company press.

81. Li-Weber M. New therapeutic aspects of flavones: the anticancer properties of Scutellaria and its main active constituents Wogonin, Baicalein and Baicalin. Cancer Treat Rev. 2009;35(1):57-68.

82. Martin J, Dusek J. [The Baikal scullcap (Scutellaria baicalensis Georgi)--a potential source of new drugs]. Ceska a Slovenska farmacie : casopis Ceske farmaceuticke spolecnosti a Slovenske farmaceuticke spolecnosti. 2002;51(6):277-83.

83. Chung H, Choi HS, Seo EK, Kang DH, Oh ES. Baicalin and baicalein inhibit transforming growth factor-beta1-mediated epithelial-mesenchymal transition in human breast epithelial cells. Biochemical and biophysical research communications. 2015;458(3):707-13.

84. Chen HJ, Liang TM, Lee IJ, Huang YT, Lin YL. Scutellariae radix suppresses LPS-induced liver endothelial cell activation and inhibits hepatic stellate cell migration. Journal of ethnopharmacology. 2013;150(3):835-42.

85. Huang HL, Wang YJ, Zhang QY, Liu B, Wang FY, Li JJ, et al. Hepatoprotective effects of baicalein against CCl(4)-induced acute liver injury in mice. World journal of gastroenterology : WJG. 2012;18(45):6605-13.

86. Liu H, Sun W, Wan YG, Tu Y, Yu BY, Hu H. [Regulatory mechanism of NF-kappaB signaling pathway on renal tissue inflammation in chronic kidney disease and interventional effect of traditional Chinese medicine]. Zhongguo Zhong yao za zhi = Zhongguo zhongyao zazhi = China journal of Chinese materia medica. 2013;38(24):4246-51.

87. Sohn SH, Lee H, Nam JY, Kim SH, Jung HJ, Kim Y, et al. Screening of herbal medicines for the recovery of cisplatin-induced nephrotoxicity. Environmental toxicology and pharmacology. 2009;28(2):206-12.

88. Han J, Ye M, Xu M, Sun J, Wang B, Guo D. Characterization of flavonoids in the traditional Chinese herbal medicine-Huangqin by liquid chromatography coupled with electrospray ionization mass spectrometry. Journal of chromatography B, Analytical technologies in the biomedical and life sciences. 2007;848(2):355-62.

89. Middleton E, Jr., Kandaswami C, Theoharides TC. The effects of plant flavonoids on mammalian cells: implications for inflammation, heart disease, and cancer. Pharmacological reviews. 2000;52(4):673-751.

90. Havsteen BH. The biochemistry and medical significance of the flavonoids. Pharmacology & therapeutics. 2002;96(2-3):67-202.

91. Wozniak D, Drys A, Matkowski A. Antiradical and antioxidant activity of flavones from Scutellariae baicalensis radix. Nat Prod Res. 2015;29(16):1567-70.

92. Chen Y, Zhu J. Anti-HBV effect of individual traditional Chinese herbal medicine in vitro and in vivo: an analytic review. Journal of viral hepatitis. 2013;20(7):445-52.

93. Lin M, Li L, Li L, Pokhrel G, Qi G, Rong R, et al. The protective effect of baicalin against renal ischemia-reperfusion injury through inhibition of inflammation and apoptosis. BMC complementary and alternative medicine. 2014;14:19.

94. Kim EH, Shim B, Kang S, Jeong G, Lee JS, Yu YB, et al. Anti-inflammatory effects of Scutellaria baicalensis extract via suppression of immune modulators and MAP kinase signaling molecules. Journal of ethnopharmacology. 2009;126(2):320-31.

95. Huang Y, Tsang SY, Yao X, Chen ZY. Biological properties of baicalein in cardiovascular system. Current drug targets Cardiovascular & haematological disorders. 2005;5(2):177-84.

96. Shang X, He X, He X, Li M, Zhang R, Fan P, et al. The genus Scutellaria an ethnopharmacological and phytochemical review. Journal of ethnopharmacology. 2010;128(2):279-313.

97. Zhang YF, Zhou SZ, Cheng XY, Yi B, Shan SZ, Wang J, et al. Baicalein attenuates hypertrophic scar formation via inhibiting TGF-beta/Smad2/3 signaling pathway. The British journal of dermatology. 2015.

98. Wang W, Zhou PH, Xu CG, Zhou XJ, Hu W, Zhang J. Baicalein attenuates renal fibrosis by inhibiting inflammation via down-regulating NF-kappaB and MAPK signal

pathways. Journal of molecular histology. 2015;46(3):283-90.

99. Wang Q, Wen R, Lin Q, Wang N, Lu P, Zhu X. Wogonoside Shows Antifibrotic Effects in an Experimental Regression Model of Hepatic Fibrosis. Digestive diseases and sciences. 2015.

100. Sahu BD, Mahesh Kumar J, Sistla R. Baicalein, a Bioflavonoid, Prevents Cisplatin-Induced Acute Kidney Injury by Up-Regulating Antioxidant Defenses and Down-Regulating the MAPKs and NF-kappaB Pathways. PloS one. 2015;10(7):e0134139.

101. Pan TL, Wang PW, Huang CH, Leu YL, Wu TH, Wu YR, et al. Herbal formula, Scutellariae radix and Rhei rhizoma attenuate dimethylnitrosamine-induced liver fibrosis in a rat model. Scientific reports. 2015;5:11734.

102. Nan JX, Park EJ, Kim YC, Ko G, Sohn DH. Scutellaria baicalensis inhibits liver fibrosis induced by bile duct ligation or carbon tetrachloride in rats. The Journal of pharmacy and pharmacology. 2002;54(4):555-63.

103. Latella G, Sferra R, Vetuschi A, Zanninelli G, D'Angelo A, Catitti V, et al. Prevention of colonic fibrosis by Boswellia and Scutellaria extracts in rats with colitis induced by 2,4,5-trinitrobenzene sulphonic acid. European journal of clinical investigation. 2008;38(6):410-20.

104. Yang MD, Chiang YM, Higashiyama R, Asahina K, Mann DA, Mann J, et al. Rosmarinic acid and baicalin epigenetically derepress peroxisomal proliferator-activated receptor gamma in hepatic stellate cells for their antifibrotic effect. Hepatology (Baltimore, Md). 2012;55(4):1271-81.

105. Qiao H, Han H, Hong D, Ren Z, Chen Y, Zhou C. Protective effects of baicalin on carbon tetrachloride induced liver injury by activating PPARgamma and inhibiting TGFbeta1. Pharmaceutical biology. 2011;49(1):38-45.

106. Peng XD, Dai LL, Huang CQ, He CM, Chen LJ. Correlation between anti-fibrotic effect of baicalin and serum cytokines in rat hepatic fibrosis. World journal of gastroenterology. 2009;15(37):4720-5.

107. Liu T, Dai W, Li C, Liu F, Chen Y, Weng D, et al. Baicalin Alleviates Silica-Induced Lung Inflammation and Fibrosis by Inhibiting the Th17 Response in C57BL/6 Mice. Journal of natural products. 2015;78(12):3049-57.

108. Tan YJ, Zhu CL, Mao HX. Therapeutic effect of baicalin in treatment of renal interstitial fibrosis in rats with unliateral ureteral obstruction and related mechanisms. Zhongguo dang dai er ke za zhi = Chinese journal of contemporary pediatrics. 2016;18(4):365-71.

109. Shimizu I, Ma YR, Mizobuchi Y, Liu F, Miura T, Nakai Y, et al. Effects of Sho-saiko-to, a Japanese herbal medicine, on hepatic fibrosis in rats. Hepatology (Baltimore, Md). 1999;29(1):149-60.

110. Shimizu I. Sho-saiko-to: Japanese herbal medicine for protection against hepatic fibrosis and carcinoma. Journal of gastroenterology and hepatology. 2000;15 Suppl:D84-90.

111. Gao Y, Lu J, Zhang Y, Chen Y, Gu Z, Jiang X. Baicalein attenuates bleomycin-induced pulmonary fibrosis in rats through inhibition of miR-21. Pulmonary pharmacology & therapeutics. 2013;26(6):649-54.

112. Zhao F, Fu L, Yang W, Dong Y, Yang J, Sun S, et al. Cardioprotective effects of baicalein on heart failure via modulation of Ca(2+) handling proteins in vivo and in vitro. Life sciences. 2016;145:213-23.

113. Zong J, Zhang DP, Zhou H, Bian ZY, Deng W, Dai J, et al. Baicalein protects against cardiac hypertrophy through blocking MEK-ERK1/2 signaling. Journal of cellular

biochemistry. 2013;114(5):1058-65.

114. Kong EK, Yu S, Sanderson JE, Chen KB, Huang Y, Yu CM. A novel anti-fibrotic agent, baicalein, for the treatment of myocardial fibrosis in spontaneously hypertensive rats. European journal of pharmacology. 2011;658(2-3):175-81.

115. Kong EK, Huang Y, Sanderson JE, Chan KB, Yu S, Yu CM. Baicalein and Wogonin inhibit collagen deposition in SHR and WKY cardiac fibroblast cultures. BMB reports. 2010;43(4):297-303.

116. Sun H, Che QM, Zhao X, Pu XP. Antifibrotic effects of chronic baicalein administration in a CCl4 liver fibrosis model in rats. European journal of pharmacology. 2010;631(1-3):53-60.

117. Inoue T, Jackson EK. Strong antiproliferative effects of baicalein in cultured rat hepatic stellate cells. European journal of pharmacology. 1999;378(1):129-35.

118. Wang W, Zhou PH, Xu CG, Zhou XJ, Hu W, Zhang J. Baicalein ameliorates renal interstitial fibrosis by inducing myofibroblast apoptosis in vivo and in vitro. BJU international. 2016;118(1):145-52.

119. Wang Q, Wen R, Lin Q, Wang N, Lu P, Zhu X. Wogonoside Shows Antifibrotic Effects in an Experimental Regression Model of Hepatic Fibrosis. Digestive diseases and sciences. 2015;60(11):3329-39.

120. Khan S, Zhang D, Zhang Y, Li M, Wang C. Wogonin attenuates diabetic cardiomyopathy through its anti-inflammatory and anti-oxidative properties. Molecular and cellular endocrinology. 2016;428:101-8.

121. Pan TL, Wang PW, Leu YL, Wu TH, Wu TS. Inhibitory effects of Scutellaria baicalensis extract on hepatic stellate cells through inducing G2/M cell cycle arrest and activating ERK-dependent apoptosis via Bax and caspase pathway. Journal of ethnopharmacology. 2012;139(3):829-37.

122. Li X, Peng XD, Zhang WL, Dai LL. Inhibiting effects of denshensu, baicalin, astragalus and Panax notoginseng saponins on hepatic fibrosis and their possible mechanisms. Zhonghua gan zang bing za zhi = Zhonghua ganzangbing zazhi = Chinese journal of hepatology. 2008;16(3):193-7.

123. Parodi B, Aresu O, Bini D, Lorenzini R, Schena F, Visconti P, et al. Species identification and confirmation of human and animal cell lines: a PCR-based method. BioTechniques. 2002;32(2):432-4, 6, 8-40.

124. Prockop DJ, Udenfriend S. A specific method for the analysis of hydroxyproline in tissues and urine. Analytical biochemistry. 1960;1:228-39.

125. Chan TY. Aconitum alkaloid content and the high toxicity of aconite tincture. Forensic Sci Int. 2012;222(1-3):1-3.

126. Qin Y, Wang JB, Zhao YL, Shan LM, Li BC, Fang F, et al. Establishment of a bioassay for the toxicity evaluation and quality control of Aconitum herbs. J Hazard Mater. 2012;199-200:350-7.

127. Lin CC, Chan TY, Deng JF. Clinical features and management of herb-induced aconitine poisoning. Ann Emerg Med. 2004;43(5):574-9.

128. Chan TY. Aconitum alkaloid poisoning related to the culinary uses of aconite roots. Toxins (Basel). 2014;6(9):2605-11.

129. Meng XM, Ren GL, Gao L, Li HD, Wu WF, Li XF, et al. Anti-fibrotic effect of wogonin in renal tubular epithelial cells via Smad3-dependent mechanisms. European journal of pharmacology. 2016;789:134-43.

130. Rankin AC, Hendry BM, Corcoran JP, Xu Q. An in vitro model for the pro-fibrotic effects of retinoids: mechanisms of action. Br J Pharmacol. 2013;170(6):1177-89.

131. Wilson DN, Doudna Cate JH. The structure and function of the eukaryotic ribosome. Cold Spring Harb Perspect Biol. 2012;4(5).

132. Rabl J, Leibundgut M, Ataide SF, Haag A, Ban N. Crystal structure of the eukaryotic 40S ribosomal subunit in complex with initiation factor 1. Science (New York, NY). 2011;331(6018):730-6.

133. Klinge S, Voigts-Hoffmann F, Leibundgut M, Arpagaus S, Ban N. Crystal structure of the eukaryotic 60S ribosomal subunit in complex with initiation factor 6. Science (New York, NY). 2011;334(6058):941-8.

134. Schmeing TM, Ramakrishnan V. What recent ribosome structures have revealed about the mechanism of translation. Nature. 2009;461(7268):1234-42.

135. Zhou X, Liao WJ, Liao JM, Liao P, Lu H. Ribosomal proteins: functions beyond the ribosome. Journal of molecular cell biology. 2015;7(2):92-104.

136. Liao LX, Song XM, Wang LC, Lv HN, Chen JF, Liu D, et al. Highly selective inhibition of IMPDH2 provides the basis of antineuroinflammation therapy. Proceedings of the National Academy of Sciences of the United States of America. 2017;114(29):E5986-E94.

137. Nakanishi T, Morokata T, Noto T, Kubo K, Umeno H, Kinugasa F, et al. Effect of the inosine 5'-monophosphate dehydrogenase inhibitor BMS-566419 on renal fibrosis in unilateral ureteral obstruction in rats. International immunopharmacology. 2010;10(11):1434-9.

138. Petrova DT, Brandhorst G, Brehmer F, Gross O, Oellerich M, Armstrong VW. Mycophenolic acid displays IMPDH-dependent and IMPDH-independent effects on renal fibroblast proliferation and function. Therapeutic drug monitoring. 2010;32(4):405-12.

139. Zimmermann AG, Gu JJ, Laliberte J, Mitchell BS. Inosine-5'-monophosphate dehydrogenase: regulation of expression and role in cellular proliferation and T lymphocyte activation. Progress in nucleic acid research and molecular biology. 1998;61:181-209.

140. Morath C, Schwenger V, Beimler J, Mehrabi A, Schmidt J, Zeier M, et al. Antifibrotic actions of mycophenolic acid. Clinical transplantation. 2006;20 Suppl 17:25-9.

141. Kang JH, Cho HJ, Lee IS, Kim M, Lee IK, Chang YC. Comparative proteome analysis of TGF-beta1-induced fibrosis processes in normal rat kidney interstitial fibroblast cells in response to ascofuranone. Proteomics. 2009;9(19):4445-56.

142. Choksawangkarn W, Edwards N, Wang Y, Gutierrez P, Fenselau C. Comparative study of workflows optimized for in-gel, in-solution, and on-filter proteolysis in the analysis of plasma membrane proteins. Journal of proteome research. 2012;11(5):3030-4.

143. Loeffler I, Wolf G. Transforming growth factor-beta and the progression of renal disease. Nephrology, dialysis, transplantation : official publication of the European Dialysis and Transplant Association - European Renal Association. 2014;29 Suppl 1:i37-i45.

144. Proud CG. mTORC1 regulates the efficiency and cellular capacity for protein synthesis. Biochemical Society transactions. 2013;41(4):923-6.

145. Iadevaia V, Liu R, Proud CG. mTORC1 signaling controls multiple steps in ribosome biogenesis. Seminars in cell & developmental biology. 2014;36:113-20.

146. Wang X, Proud CG. The mTOR pathway in the control of protein synthesis. Physiology (Bethesda, Md). 2006;21:362-9.

147. Zhao YD, Yin L, Archer S, Lu C, Zhao G, Yao Y, et al. Metabolic heterogeneity of

idiopathic pulmonary fibrosis: a metabolomic study. BMJ open respiratory research. 2017;4(1):e000183.

148. Jiang H, Song JM, Gao PF, Qin XJ, Xu SZ, Zhang JF. Metabolic characterization of the early stage of hepatic fibrosis in rat using GC-TOF/MS and multivariate data analyses. Biomedical chromatography : BMC. 2017;31(6).

149. Xiong J, Kawagishi H, Yan Y, Liu J, Wells QS, Edmunds LR, et al. A Metabolic Basis for Endothelial-to-Mesenchymal Transition. Molecular cell. 2018;69(4):689-98.e7.

150. Kang HM, Ahn SH, Choi P, Ko YA, Han SH, Chinga F, et al. Defective fatty acid oxidation in renal tubular epithelial cells has a key role in kidney fibrosis development. Nature medicine. 2015;21(1):37-46.

151. Kim JW, Tchernyshyov I, Semenza GL, Dang CV. HIF-1-mediated expression of pyruvate dehydrogenase kinase: a metabolic switch required for cellular adaptation to hypoxia. Cell metabolism. 2006;3(3):177-85.

152. Goding JW, Grobben B, Slegers H. Physiological and pathophysiological functions of the ecto-nucleotide pyrophosphatase/phosphodiesterase family. Biochimica et biophysica acta. 2003;1638(1):1-19.

153. Shimokado A, Sun Y, Nakanishi M, Sato F, Oikawa K, Akasaka T, et al. Smad3 plays an inhibitory role in phosphate-induced vascular smooth muscle cell calcification. Exp Mol Pathol. 2014;97(3):458-64.

154. Xu HG, Li ZR, Wang H, Liu P, Xiang SN, Wang CD, et al. Expression of ectonucleotide pyrophosphatase-1 in end-plate chondrocytes with transforming growth factor beta 1 siRNA interference by cyclic mechanical tension. Chin Med J (Engl). 2013;126(20):3886-90.

155. Xu HG, Li ZR, Wang H, Liu P, Xiang SN, Wang CD, et al. Intermittent cyclic mechanical tension-induced down-regulation of ectonucleotide pyrophosphatase phosphodiesterase 1 gene expression is mainly dependent on TGF-beta1 in end-plate chondrocytes. Orthop Surg. 2013;5(1):40-5.

156. Stagos D, Chen Y, Cantore M, Jester JV, Vasiliou V. Corneal aldehyde dehydrogenases: multiple functions and novel nuclear localization. Brain Res Bull. 2010;81(2-3):211-8.

157. Jester JV, Brown D, Pappa A, Vasiliou V. Myofibroblast differentiation modulates keratocyte crystallin protein expression, concentration, and cellular light scattering. Invest Ophthalmol Vis Sci. 2012;53(2):770-8.

158. Lassen N, Pappa A, Black WJ, Jester JV, Day BJ, Min E, et al. Antioxidant function of corneal ALDH3A1 in cultured stromal fibroblasts. Free Radic Biol Med. 2006;41(9):1459-69.

159. Kobayashi M, Sugiyama H, Wang DH, Toda N, Maeshima Y, Yamasaki Y, et al. Catalase deficiency renders remnant kidneys more susceptible to oxidant tissue injury and renal fibrosis in mice. Kidney international. 2005;68(3):1018-31.

160. Sunami R, Sugiyama H, Wang DH, Kobayashi M, Maeshima Y, Yamasaki Y, et al. Acatalasemia sensitizes renal tubular epithelial cells to apoptosis and exacerbates renal fibrosis after unilateral ureteral obstruction. American journal of physiology Renal physiology. 2004;286(6):F1030-8.

161. Sprengers ED, Kluft C. Plasminogen activator inhibitors. Blood. 1987;69(2):381-7.

162. Hu K, Mars WM, Liu Y. Novel actions of tissue-type plasminogen activator in chronic kidney disease. Front Biosci. 2008;13:5174-86.

163. Ghosh AK, Vaughan DE. PAI-1 in tissue fibrosis. J Cell Physiol. 2012;227(2):493-

507.

164. Ma LJ, Fogo AB. PAI-1 and kidney fibrosis. Front Biosci (Landmark Ed). 2009;14:2028-41.

165. Rabieian R, Boshtam M, Zareei M, Kouhpayeh S, Masoudifar A, Mirzaei H. Plasminogen Activator Inhibitor Type-1 as a Regulator of Fibrosis. Journal of cellular biochemistry. 2018;119(1):17-27.

166. Zhao H, Dong Y, Tian X, Tan TK, Liu Z, Zhao Y, et al. Matrix metalloproteinases contribute to kidney fibrosis in chronic kidney diseases. World journal of nephrology. 2013;2(3):84-9.

167. Pardo A, Cabrera S, Maldonado M, Selman M. Role of matrix metalloproteinases in the pathogenesis of idiopathic pulmonary fibrosis. Respir Res. 2016;17:23.

168. Cabrera S, Selman M, Lonzano-Bolanos A, Konishi K, Richards TJ, Kaminski N, et al. Gene expression profiles reveal molecular mechanisms involved in the progression and resolution of bleomycin-induced lung fibrosis. American journal of physiology Lung cellular and molecular physiology. 2013;304(9):L593-601.

169. Yamashita CM, Dolgonos L, Zemans RL, Young SK, Robertson J, Briones N, et al. Matrix metalloproteinase 3 is a mediator of pulmonary fibrosis. The American journal of pathology. 2011;179(4):1733-45.

170. van der Slot-Verhoeven AJ, van Dura EA, Attema J, Blauw B, Degroot J, Huizinga TW, et al. The type of collagen cross-link determines the reversibility of experimental skin fibrosis. Biochimica et biophysica acta. 2005;1740(1):60-7.

171. van der Slot AJ, Zuurmond AM, van den Bogaerdt AJ, Ulrich MM, Middelkoop E, Boers W, et al. Increased formation of pyridinoline cross-links due to higher telopeptide lysyl hydroxylase levels is a general fibrotic phenomenon. Matrix Biol. 2004;23(4):251-7.

172. van der Slot AJ, Zuurmond AM, Bardoel AF, Wijmenga C, Pruijs HE, Sillence DO, et al. Identification of PLOD2 as telopeptide lysyl hydroxylase, an important enzyme in fibrosis. The Journal of biological chemistry. 2003;278(42):40967-72.

173. Gjaltema RA, de Rond S, Rots MG, Bank RA. Procollagen Lysyl Hydroxylase 2 Expression Is Regulated by an Alternative Downstream Transforming Growth Factor beta-1 Activation Mechanism. The Journal of biological chemistry. 2015;290(47):28465-76.

174. Phanish MK, Winn SK, Dockrell ME. Connective tissue growth factor-(CTGF, CCN2)--a marker, mediator and therapeutic target for renal fibrosis. Nephron Exp Nephrol. 2010;114(3):e83-92.

175. Lipson KE, Wong C, Teng Y, Spong S. CTGF is a central mediator of tissue remodeling and fibrosis and its inhibition can reverse the process of fibrosis. Fibrogenesis Tissue Repair. 2012;5(Suppl 1):S24.

176. Sanchez-Lopez E, Rodrigues Diez R, Rodriguez Vita J, Rayego Mateos S, Rodrigues Diez RR, Rodriguez Garcia E, et al. [Connective tissue growth factor (CTGF): a key factor in the onset and progression of kidney damage]. Nefrologia. 2009;29(5):382-91.

177. Jun JI, Lau LF. Cellular senescence controls fibrosis in wound healing. Aging (Albany NY). 2010;2(9):627-31.

178. Kim KH, Chen CC, Monzon RI, Lau LF. Matricellular protein CCN1 promotes regression of liver fibrosis through induction of cellular senescence in hepatic myofibroblasts. Molecular and cellular biology. 2013;33(10):2078-90.

179. Pitiyage GN, Slijepcevic P, Gabrani A, Chianea YG, Lim KP, Prime SS, et al. Senescent mesenchymal cells accumulate in human fibrosis by a telomere-independent mechanism and ameliorate fibrosis through matrix metalloproteinases. J Pathol.

2011;223(5):604-17.

180. Jun JI, Lau LF. The matricellular protein CCN1 induces fibroblast senescence and restricts fibrosis in cutaneous wound healing. Nat Cell Biol. 2010;12(7):676-85.

181. Riser BL, Najmabadi F, Perbal B, Peterson DR, Rambow JA, Riser ML, et al. CCN3 (NOV) is a negative regulator of CCN2 (CTGF) and a novel endogenous inhibitor of the fibrotic pathway in an in vitro model of renal disease. The American journal of pathology. 2009;174(5):1725-34.

182. Riser BL, Najmabadi F, Perbal B, Rambow JA, Riser ML, Sukowski E, et al. CCN3/CCN2 regulation and the fibrosis of diabetic renal disease. J Cell Commun Signal. 2010;4(1):39-50.

183. Jun JI, Lau LF. Taking aim at the extracellular matrix: CCN proteins as emerging therapeutic targets. Nature reviews Drug discovery. 2011;10(12):945-63.

184. Ohta K, Lupo G, Kuriyama S, Keynes R, Holt CE, Harris WA, et al. Tsukushi functions as an organizer inducer by inhibition of BMP activity in cooperation with chordin. Dev Cell. 2004;7(3):347-58.

185. Ohta K, Ito A, Kuriyama S, Lupo G, Kosaka M, Ohnuma S, et al. Tsukushi functions as a Wnt signaling inhibitor by competing with Wnt2b for binding to transmembrane protein Frizzled4. Proceedings of the National Academy of Sciences of the United States of America. 2011;108(36):14962-7.

186. Niimori D, Kawano R, Felemban A, Niimori-Kita K, Tanaka H, Ihn H, et al. Tsukushi controls the hair cycle by regulating TGF-beta1 signaling. Dev Biol. 2012;372(1):81-7.

187. Niimori D, Kawano R, Niimori-Kita K, Ihn H, Ohta K. Tsukushi is involved in the wound healing by regulating the expression of cytokines and growth factors. J Cell Commun Signal. 2014;8(3):173-7.

188. Wynn TA, Barron L. Macrophages: master regulators of inflammation and fibrosis. Semin Liver Dis. 2010;30(3):245-57.

189. Ahmad SAI, Anam MB, Ito N, Ohta K. Involvement of Tsukushi in diverse developmental processes. J Cell Commun Signal. 2018.

190. Sahin H, Wasmuth HE. Chemokines in tissue fibrosis. Biochimica et biophysica acta. 2013;1832(7):1041-8.

191. Wada T, Furuichi K, Sakai N, Iwata Y, Kitagawa K, Ishida Y, et al. Gene therapy via blockade of monocyte chemoattractant protein-1 for renal fibrosis. Journal of the American Society of Nephrology : JASN. 2004;15(4):940-8.

192. Chow FY, Nikolic-Paterson DJ, Ozols E, Atkins RC, Rollin BJ, Tesch GH. Monocyte chemoattractant protein-1 promotes the development of diabetic renal injury in streptozotocin-treated mice. Kidney international. 2006;69(1):73-80.

193. Kanamori H, Matsubara T, Mima A, Sumi E, Nagai K, Takahashi T, et al. Inhibition of MCP-1/CCR2 pathway ameliorates the development of diabetic nephropathy. Biochemical and biophysical research communications. 2007;360(4):772-7.

194. Mansour SG, Puthumana J, Coca SG, Gentry M, Parikh CR. Biomarkers for the detection of renal fibrosis and prediction of renal outcomes: a systematic review. BMC Nephrol. 2017;18(1):72.

195. Tesch GH. MCP-1/CCL2: a new diagnostic marker and therapeutic target for progressive renal injury in diabetic nephropathy. American journal of physiology Renal physiology. 2008;294(4):F697-701.

196. Ong VH, Evans LA, Shiwen X, Fisher IB, Rajkumar V, Abraham DJ, et al. Monocyte chemoattractant protein 3 as a mediator of fibrosis: Overexpression in systemic sclerosis and the type 1 tight-skin mouse. Arthritis Rheum. 2003;48(7):1979-91.

197. Ong VH, Carulli MT, Xu S, Khan K, Lindahl G, Abraham DJ, et al. Cross-talk between MCP-3 and TGFbeta promotes fibroblast collagen biosynthesis. Exp Cell Res. 2009;315(2):151-61.

198. Gonzalez J, Mouttalib S, Delage C, Calise D, Maoret JJ, Pradere JP, et al. Dual effect of chemokine CCL7/MCP-3 in the development of renal tubulointerstitial fibrosis. Biochemical and biophysical research communications. 2013;438(2):257-63.

199. Manabe R, Tsutsui K, Yamada T, Kimura M, Nakano I, Shimono C, et al. Transcriptome-based systematic identification of extracellular matrix proteins. Proceedings of the National Academy of Sciences of the United States of America. 2008;105(35):12849-54.

200. Moon JA, Kim HT, Cho IS, Sheen YY, Kim DK. IN-1130, a novel transforming growth factor-beta type I receptor kinase (ALK5) inhibitor, suppresses renal fibrosis in obstructive nephropathy. Kidney international. 2006;70(7):1234-43.

201. Brennan EP, Morine MJ, Walsh DW, Roxburgh SA, Lindenmeyer MT, Brazil DP, et al. Next-generation sequencing identifies TGF-beta1-associated gene expression profiles in renal epithelial cells reiterated in human diabetic nephropathy. Biochimica et biophysica acta. 2012;1822(4):589-99.

202. Aisen P. Transferrin receptor 1. Int J Biochem Cell Biol. 2004;36(11):2137-43.

203. Ponka P, Lok CN. The transferrin receptor: role in health and disease. Int J Biochem Cell Biol. 1999;31(10):1111-37.

204. Gammella E, Buratti P, Cairo G, Recalcati S. The transferrin receptor: the cellular iron gate. Metallomics. 2017;9(10):1367-75.

205. Shpyleva S, Pogribna M, Cozart C, Bryant MS, Muskhelishvili L, Tryndyak VP, et al. Interstrain differences in the progression of nonalcoholic steatohepatitis to fibrosis in mice are associated with altered hepatic iron metabolism. J Nutr Biochem. 2014;25(12):1235-42.

206. Delanghe SE, Speeckaert MM, Segers H, Desmet K, Vande Walle J, Laecke SV, et al. Soluble transferrin receptor in urine, a new biomarker for IgA nephropathy and Henoch-Schonlein purpura nephritis. Clin Biochem. 2013;46(7-8):591-7.

207. Dinda B, Dinda S, DasSharma S, Banik R, Chakraborty A, Dinda M. Therapeutic potentials of baicalin and its aglycone, baicalein against inflammatory disorders. European journal of medicinal chemistry. 2017;131:68-80.

208. Liu MJ, Takahashi Y, Wada T, He J, Gao J, Tian Y, et al. The aldo-keto reductase Akr1b7 gene is a common transcriptional target of xenobiotic receptors pregnane X receptor and constitutive androstane receptor. Mol Pharmacol. 2009;76(3):604-11.

209. Mindnich RD, Penning TM. Aldo-keto reductase (AKR) superfamily: genomics and annotation. Hum Genomics. 2009;3(4):362-70.

210. Sundaram K, Endo S, Matsunaga T, Tanaka N, Hara A, El-Kabbani O. Structure of the His269Arg mutant of the rat aldose reductase-like protein AKR1B14 complexed with NADPH. Acta Crystallogr Sect F Struct Biol Cryst Commun. 2012;68(Pt 4):400-3.

211. Val P, Martinez A, Sahut-Barnola I, Jean C, Veyssiere G, Lefrancois-Martinez AM. A 77-base pair LINE-like sequence elicits androgen-dependent mvdp/akr1-b7 expression in mouse vas deferens, but is dispensable for adrenal expression in rats. Endocrinology. 2002;143(9):3435-48.

212. Lu Y, Wang J, Dapeng C, Wu D, Cai G, Chen X. Bioinformatics analysis of proteomics profiles in senescent human primary proximal tubule epithelial cells. BMC Nephrol. 2016;17:39.

213. Prasad P, Tiwari AK, Kumar KM, Ammini AC, Gupta A, Gupta R, et al. Association analysis of ADPRT1, AKR1B1, RAGE, GFPT2 and PAI-1 gene polymorphisms with chronic renal insufficiency among Asian Indians with type-2 diabetes. BMC Med Genet. 2010;11:52.

214. Liu WJ, Ye L, Huang WF, Guo LJ, Xu ZG, Wu HL, et al. p62 links the autophagy pathway and the ubiqutin-proteasome system upon ubiquitinated protein degradation. Cell Mol Biol Lett. 2016;21:29.

215. Komatsu M, Ichimura Y. Physiological significance of selective degradation of p62 by autophagy. FEBS Lett. 2010;584(7):1374-8.

216. Bjorkoy G, Lamark T, Pankiv S, Overvatn A, Brech A, Johansen T. Monitoring autophagic degradation of p62/SQSTM1. Methods Enzymol. 2009;452:181-97.

217. Bjorkoy G, Lamark T, Brech A, Outzen H, Perander M, Overvatn A, et al. p62/SQSTM1 forms protein aggregates degraded by autophagy and has a protective effect on huntingtin-induced cell death. J Cell Biol. 2005;171(4):603-14.

218. Kim WY, Nam SA, Song HC, Ko JS, Park SH, Kim HL, et al. The role of autophagy in unilateral ureteral obstruction rat model. Nephrology (Carlton). 2012;17(2):148-59.

219. Ding Y, Kim S, Lee SY, Koo JK, Wang Z, Choi ME. Autophagy regulates TGF-beta expression and suppresses kidney fibrosis induced by unilateral ureteral obstruction. Journal of the American Society of Nephrology : JASN. 2014;25(12):2835-46.

220. Kim SI, Na HJ, Ding Y, Wang Z, Lee SJ, Choi ME. Autophagy promotes intracellular degradation of type I collagen induced by transforming growth factor (TGF)-beta1. The Journal of biological chemistry. 2012;287(15):11677-88.

221. Livingston MJ, Ding HF, Huang S, Hill JA, Yin XM, Dong Z. Persistent activation of autophagy in kidney tubular cells promotes renal interstitial fibrosis during unilateral ureteral obstruction. Autophagy. 2016;12(6):976-98.

222. McKleroy W, Lee TH, Atabai K. Always cleave up your mess: targeting collagen degradation to treat tissue fibrosis. American journal of physiology Lung cellular and molecular physiology. 2013;304(11):L709-21.

223. Rerolle JP, Hertig A, Nguyen G, Sraer JD, Rondeau EP. Plasminogen activator inhibitor type 1 is a potential target in renal fibrogenesis. Kidney international. 2000;58(5):1841-50.

224. Malgorzewicz S, Skrzypczak-Jankun E, Jankun J. Plasminogen activator inhibitor-1 in kidney pathology (Review). Int J Mol Med. 2013;31(3):503-10.

225. Tashiro K, Tamada S, Kuwabara N, Komiya T, Takekida K, Asai T, et al. Attenuation of renal fibrosis by proteasome inhibition in rat obstructive nephropathy: possible role of nuclear factor kappaB. Int J Mol Med. 2003;12(4):587-92.

226. Lopez-Novoa JM, Nieto MA. Inflammation and EMT: an alliance towards organ fibrosis and cancer progression. EMBO Mol Med. 2009;1(6-7):303-14.

227. Prokhorova IV, Akulich KA, Makeeva DS, Osterman IA, Skvortsov DA, Sergiev PV, et al. Amicoumacin A induces cancer cell death by targeting the eukaryotic ribosome. Scientific reports. 2016;6:27720.

228. Pellegrino S, Yusupova G. Eukaryotic Ribosome as a Target for Cardiovascular Disease. Cell chemical biology. 2016;23(11):1319-21.

229. Magnuson B, Ekim B, Fingar DC. Regulation and function of ribosomal protein S6

kinase (S6K) within mTOR signalling networks. Biochem J. 2012;441(1):1-21.

230. Andreoli A, Ruf MT, Itin P, Pluschke G, Schmid P. Phosphorylation of the ribosomal protein S6, a marker of mTOR (mammalian target of rapamycin) pathway activation, is strongly increased in hypertrophic scars and keloids. Br J Dermatol. 2015;172(5):1415-7.

231. Nolin AC, Mulhern RM, Panchenko MV, Pisarek-Horowitz A, Wang Z, Shirihai O, et al. Proteinuria causes dysfunctional autophagy in the proximal tubule. American journal of physiology Renal physiology. 2016;311(6):F1271-f9.

232. Fang F, Bae EH, Hu A, Liu GC, Zhou X, Williams V, et al. Deletion of the gene for adiponectin accelerates diabetic nephropathy in the Ins2 (+/C96Y) mouse. Diabetologia. 2015;58(7):1668-78.

233. Wang B, Ding W, Zhang M, Li H, Gu Y. Rapamycin attenuates aldosterone-induced tubulointerstitial inflammation and fibrosis. Cell Physiol Biochem. 2015;35(1):116-25.

234. Settembre C, Fraldi A, Medina DL, Ballabio A. Signals from the lysosome: a control centre for cellular clearance and energy metabolism. Nat Rev Mol Cell Biol. 2013;14(5):283-96.

235. Glasser SW, Hagood JS, Wong S, Taype CA, Madala SK, Hardie WD. Mechanisms of Lung Fibrosis Resolution. The American journal of pathology. 2016;186(5):1066-77.

236. Ciechanover A. Intracellular protein degradation: from a vague idea, through the lysosome and the ubiquitin-proteasome system, and onto human diseases and drug targeting (Nobel lecture). Angew Chem Int Ed Engl. 2005;44(37):5944-67.

237. Brix K, Dunkhorst A, Mayer K, Jordans S. Cysteine cathepsins: cellular roadmap to different functions. Biochimie. 2008;90(2):194-207.

238. Cocchiaro P, De Pasquale V, Della Morte R, Tafuri S, Avallone L, Pizard A, et al. The Multifaceted Role of the Lysosomal Protease Cathepsins in Kidney Disease. Front Cell Dev Biol. 2017;5:114.

239. Svara T, Pogacnik M, Juntes P. Distribution and amount of cathepsin B in gentamicin-induced acute kidney injury in rats. Pol J Vet Sci. 2010;13(1):75-82.

240. Moallem SA, Nazemian F, Eliasi S, Alamdaran SA, Shamsara J, Mohammadpour AH. Correlation between cathepsin D serum concentration and carotid intima-media thickness in hemodialysis patients. Int Urol Nephrol. 2011;43(3):841-8.

241. Cocchiaro P, Fox C, Tregidgo NW, Howarth R, Wood KM, Situmorang GR, et al. Lysosomal protease cathepsin D; a new driver of apoptosis during acute kidney injury. Scientific reports. 2016;6:27112.

242. Fox C, Cocchiaro P, Oakley F, Howarth R, Callaghan K, Leslie J, et al. Inhibition of lysosomal protease cathepsin D reduces renal fibrosis in murine chronic kidney disease. Scientific reports. 2016;6:20101.

243. Yamamoto-Nonaka K, Koike M, Asanuma K, Takagi M, Oliva Trejo JA, Seki T, et al. Cathepsin D in Podocytes Is Important in the Pathogenesis of Proteinuria and CKD. Journal of the American Society of Nephrology : JASN. 2016;27(9):2685-700.

244. Surendran K, Vitiello SP, Pearce DA. Lysosome dysfunction in the pathogenesis of kidney diseases. Pediatr Nephrol. 2014;29(12):2253-61.

245. Conley SM, Abais JM, Boini KM, Li PL. Inflammasome Activation in Chronic Glomerular Diseases. Curr Drug Targets. 2017;18(9):1019-29.

246. Anders HJ, Muruve DA. The inflammasomes in kidney disease. Journal of the American Society of Nephrology : JASN. 2011;22(6):1007-18.

247. Masood H, Che R, Zhang A. Inflammasomes in the Pathophysiology of Kidney

Diseases. Kidney Dis (Basel). 2015;1(3):187-93.

248. Scarpioni R, Ricardi M, Albertazzi V. Secondary amyloidosis in autoinflammatory diseases and the role of inflammation in renal damage. World journal of nephrology. 2016;5(1):66-75.

249. Manchanda M, Das P, Gahlot GPS, Singh R, Roeb E, Roderfeld M, et al. Cathepsin L and B as Potential Markers for Liver Fibrosis: Insights From Patients and Experimental Models. Clin Transl Gastroenterol. 2017;8(6):e99.

250. Lu P, Takai K, Weaver VM, Werb Z. Extracellular matrix degradation and remodeling in development and disease. Cold Spring Harb Perspect Biol. 2011;3(12).

251. Ozkayar N, Piskinpasa S, Akyel F, Turgut D, Bulut M, Turhan T, et al. Relation between serum cathepsin D levels and endothelial dysfunction in patients with chronic kidney disease. Nefrologia. 2015;35(1):72-9.

252. Garsen M, Rops AL, Dijkman H, Willemsen B, van Kuppevelt TH, Russel FG, et al. Cathepsin L is crucial for the development of early experimental diabetic nephropathy. Kidney international. 2016;90(5):1012-22.

253. Sever S, Altintas MM, Nankoe SR, Moller CC, Ko D, Wei C, et al. Proteolytic processing of dynamin by cytoplasmic cathepsin L is a mechanism for proteinuric kidney disease. The Journal of clinical investigation. 2007;117(8):2095-104.

254. Cao Y, Liu X, Li Y, Lu Y, Zhong H, Jiang W, et al. Cathepsin L activity correlates with proteinuria in chronic kidney disease in humans. Int Urol Nephrol. 2017;49(8):1409-17.

255. Hemmelgarn BR, Manns BJ, Lloyd A, James MT, Klarenbach S, Quinn RR, et al. Relation between kidney function, proteinuria, and adverse outcomes. Jama. 2010;303(5):423-9.

256. Soltysiak J, Skowronska B, Fichna P, Stankiewicz W, Lewandowska-Stachowiak M, Ostalska-Nowicka D, et al. Neutrophil gelatinase-associated lipocalin and Cathepsin L as early predictors of kidney dysfunction in children with type 1 diabetes. Endokrynol Pol. 2014;65(6):479-84.

257. Chen JM, Dando PM, Stevens RA, Fortunato M, Barrett AJ. Cloning and expression of mouse legumain, a lysosomal endopeptidase. Biochem J. 1998;335 (Pt 1):111-7.

258. Yamane T, Takeuchi K, Yamamoto Y, Li YH, Fujiwara M, Nishi K, et al. Legumain from bovine kidney: its purification, molecular cloning, immunohistochemical localization and degradation of annexin II and vitamin D-binding protein. Biochimica et biophysica acta. 2002;1596(1):108-20.

259. Shirahama-Noda K, Yamamoto A, Sugihara K, Hashimoto N, Asano M, Nishimura M, et al. Biosynthetic processing of cathepsins and lysosomal degradation are abolished in asparaginyl endopeptidase-deficient mice. The Journal of biological chemistry. 2003;278(35):33194-9.

260. Morita Y, Araki H, Sugimoto T, Takeuchi K, Yamane T, Maeda T, et al. Legumain/asparaginyl endopeptidase controls extracellular matrix remodeling through the degradation of fibronectin in mouse renal proximal tubular cells. FEBS Lett. 2007;581(7):1417-24.

261. Raposo G, Vidal M, H HG. Secretory Lysosomes and the Production of Exosomes. In: Unusual Secretory Pathways: From Bacteria to Man. Berlin, Heidelberg: Springer; 1997. 161-84 p.

262. Buck S. Solving reproducibility. Science (New York, NY). 2015;348(6242):1403.

263. Alberts B, Cicerone RJ, Fienberg SE, Kamb A, McNutt M, Nerem RM, et al. SCIENTIFIC INTEGRITY. Self-correction in science at work. Science (New York, NY).

2015;348(6242):1420-2.

264. Zhao Z, Hu Y, Liang Z, Yuen JP, Jiang Z, Leung KS. Authentication is fundamental for standardization of Chinese medicines. Planta medica. 2006;72(10):865-74.

265. Chan K, Shaw D, Simmonds MS, Leon CJ, Xu Q, Lu A, et al. Good practice in reviewing and publishing studies on herbal medicine, with special emphasis on traditional Chinese medicine and Chinese materia medica. Journal of ethnopharmacology. 2012;140(3):469-75.

266. Baker M. Reproducibility crisis: Blame it on the antibodies. Nature. 2015;521(7552):274-6.

267. Freedman LP, Gibson MC, Ethier SP, Soule HR, Neve RM, Reid YA. Reproducibility: changing the policies and culture of cell line authentication. Nature methods. 2015;12(6):493-7.

268. Yu M, Selvaraj SK, Liang-Chu MM, Aghajani S, Busse M, Yuan J, et al. A resource for cell line authentication, annotation and quality control. Nature. 2015;520(7547):307-11.

269. Muller GA, Frank J, Rodemann HP, Engler-Blum G. Human renal fibroblast cell lines (tFKIF and tNKF) are new tools to investigate pathophysiologic mechanisms of renal interstitial fibrosis. Experimental nephrology. 1995;3(2):127-33.

270. Heeg MH, Koziolek MJ, Vasko R, Schaefer L, Sharma K, Muller GA, et al. The antifibrotic effects of relaxin in human renal fibroblasts are mediated in part by inhibition of the Smad2 pathway. Kidney international. 2005;68(1):96-109.

271. Roberts AB, Sporn MB, Assoian RK, Smith JM, Roche NS, Wakefield LM, et al. Transforming growth factor type beta: rapid induction of fibrosis and angiogenesis in vivo and stimulation of collagen formation in vitro. Proceedings of the National Academy of Sciences of the United States of America. 1986;83(12):4167-71.

272. Grotendorst GR, Rahmanie H, Duncan MR. Combinatorial signaling pathways determine fibroblast proliferation and myofibroblast differentiation. FASEB journal : official publication of the Federation of American Societies for Experimental Biology. 2004;18(3):469-79.

273. Adan A, Kiraz Y, Baran Y. Cell Proliferation and Cytotoxicity Assays. Current pharmaceutical biotechnology. 2016;17(14):1213-21.

274. Tampe B, Tampe D, Zeisberg EM, Muller GA, Bechtel-Walz W, Koziolek M, et al. Induction of Tet3-dependent Epigenetic Remodeling by Low-dose Hydralazine Attenuates Progression of Chronic Kidney Disease. EBioMedicine. 2015;2(1):19-36.

275. Xiao L, Zhou D, Tan RJ, Fu H, Zhou L, Hou FF, et al. Sustained Activation of Wnt/beta-Catenin Signaling Drives AKI to CKD Progression. Journal of the American Society of Nephrology : JASN. 2015.

276. Shimizu T, Shibuya N, Narukawa Y, Oshima N, Hada N, Kiuchi F. Synergistic effect of baicalein, wogonin and oroxylin A mixture: multistep inhibition of the NF-kappaB signalling pathway contributes to an anti-inflammatory effect of Scutellaria root flavonoids. J Nat Med. 2018;72(1):181-91.

277. Gao Y, Snyder SA, Smith JN, Chen YC. Anticancer properties of baicalein: a review. Med Chem Res. 2016;25(8):1515-23.

278. Boost M, Yau P, Yap M, Cho P. Determination of cytotoxicity of traditional Chinese medicine herbs, Rhizoma coptidis, Radix scutellariae, and Cortex phellodendri, by three methods. Cont Lens Anterior Eye. 2016;39(2):128-32.

279. Kim TW, Song IB, Lee HK, Kim MS, Ham SH, Cho JH, et al. Assessment of dermal safety of Scutellaria baicalensis aqueous extract topical application on skin hypersensitivity.

Planta medica. 2013;79(11):959-62.

280. Li M, Shi A, Pang H, Xue W, Li Y, Cao G, et al. Safety, tolerability, and pharmacokinetics of a single ascending dose of baicalein chewable tablets in healthy subjects. Journal of ethnopharmacology. 2014;156:210-5.

281. Cai Y, Ma W, Xiao Y, Wu B, Li X, Liu F, et al. High doses of baicalin induces kidney injury and fibrosis through regulating TGF-beta/Smad signaling pathway. Toxicol Appl Pharmacol. 2017;333:1-9.

282. Yang L, Aronsohn A, Hart J, Jensen D. Herbal hepatoxicity from Chinese skullcap: A case report. World J Hepatol. 2012;4(7):231-3.

283. Dhanasekaran R, Owens V, Sanchez W. Chinese skullcap in move free arthritis supplement causes drug induced liver injury and pulmonary infiltrates. Case Reports Hepatol. 2013;2013:965092.

284. Linnebur SA, Rapacchietta OC, Vejar M. Hepatotoxicity associated with chinese skullcap contained in Move Free Advanced dietary supplement: two case reports and review of the literature. Pharmacotherapy. 2010;30(7):750, 258e-62e.

285. Qi Q, Peng J, Liu W, You Q, Yang Y, Lu N, et al. Toxicological studies of wogonin in experimental animals. Phytother Res. 2009;23(3):417-22.

286. Peng J, Qi Q, You Q, Hu R, Liu W, Feng F, et al. Subchronic toxicity and plasma pharmacokinetic studies on wogonin, a natural flavonoid, in Beagle dogs. Journal of ethnopharmacology. 2009;124(2):257-62.

287. Yin T, Miyazawa K, Yang YC. Characterization of interleukin-11 receptor and protein tyrosine phosphorylation induced by interleukin-11 in mouse 3T3-L1 cells. The Journal of biological chemistry. 1992;267(12):8347-51.

288. Witze ES, Old WM, Resing KA, Ahn NG. Mapping protein post-translational modifications with mass spectrometry. Nature methods. 2007;4(10):798-806.

289. Singh P, Carraher C, Schwarzbauer JE. Assembly of fibronectin extracellular matrix. Annual review of cell and developmental biology. 2010;26:397-419.

290. Mertins P, Qiao JW, Patel J, Udeshi ND, Clauser KR, Mani DR, et al. Integrated proteomic analysis of post-translational modifications by serial enrichment. Nature methods. 2013;10(7):634-7.

291. Doll S, Burlingame AL. Mass spectrometry-based detection and assignment of protein posttranslational modifications. ACS chemical biology. 2015;10(1):63-71.

292. Burkhart JM, Schumbrutzki C, Wortelkamp S, Sickmann A, Zahedi RP. Systematic and quantitative comparison of digest efficiency and specificity reveals the impact of trypsin quality on MS-based proteomics. Journal of proteomics. 2012;75(4):1454-62.

293. Mann M, Jensen ON. Proteomic analysis of post-translational modifications. Nature biotechnology. 2003;21(3):255-61.

294. Swaney DL, Villen J. Proteomic Analysis of Protein Posttranslational Modifications by Mass Spectrometry. Cold Spring Harbor protocols. 2016;2016(3):pdb.top077743.

295. Hellewell AL, Rosini S, Adams JC. A Rapid, Scalable Method for the Isolation, Functional Study, and Analysis of Cell-derived Extracellular Matrix. Journal of visualized experiments : JoVE. 2017(119).

296. Escobedo-Lucea C, Ayuso-Sacido A, Xiong C, Prado-Lopez S, del Pino MS, Melguizo D, et al. Development of a human extracellular matrix for applications related with stem cells and tissue engineering. Stem cell reviews. 2012;8(1):170-83.

297. Franco-Barraza J, Beacham DA, Amatangelo MD, Cukierman E. Preparation of

Extracellular Matrices Produced by Cultured and Primary Fibroblasts. Current protocols in cell biology. 2016;71:10.9.1-.9.34.

298. Pinkse MW, Uitto PM, Hilhorst MJ, Ooms B, Heck AJ. Selective isolation at the femtomole level of phosphopeptides from proteolytic digests using 2D-NanoLC-ESI-MS/MS and titanium oxide precolumns. Analytical chemistry. 2004;76(14):3935-43.

299. Azarkan M, Huet J, Baeyens-Volant D, Looze Y, Vandenbussche G. Affinity chromatography: a useful tool in proteomics studies. Journal of chromatography B, Analytical technologies in the biomedical and life sciences. 2007;849(1-2):81-90.

300. Batth TS, Francavilla C, Olsen JV. Off-line high-pH reversed-phase fractionation for in-depth phosphoproteomics. Journal of proteome research. 2014;13(12):6176-86.

301. Parker BL, Thaysen-Andersen M, Solis N, Scott NE, Larsen MR, Graham ME, et al. Site-specific glycan-peptide analysis for determination of N-glycoproteome heterogeneity. Journal of proteome research. 2013;12(12):5791-800.

302. Edelmann MJ. Strong cation exchange chromatography in analysis of posttranslational modifications: innovations and perspectives. Journal of biomedicine & biotechnology. 2011;2011:936508.

303. Engholm-Keller K, Birck P, Storling J, Pociot F, Mandrup-Poulsen T, Larsen MR. TiSH--a robust and sensitive global phosphoproteomics strategy employing a combination of TiO2, SIMAC, and HILIC. Journal of proteomics. 2012;75(18):5749-61.

304. Collins MO, Yu L, Choudhary JS. Analysis of protein phosphorylation on a proteome-scale. Proteomics. 2007;7(16):2751-68.

305. Hu Q, Gao L, Peng B, Liu X. Baicalin and baicalein attenuate renal fibrosis in vitro via inhibition of the TGF-beta1 signaling pathway. Experimental and therapeutic medicine. 2017;14(4):3074-80.

306. Gao Z, Huang K, Yang X, Xu H. Free radical scavenging and antioxidant activities of flavonoids extracted from the radix of Scutellaria baicalensis Georgi. Biochimica et biophysica acta. 1999;1472(3):643-50.

307. Sowndhararajan K, Deepa P, Kim M, Park SJ, Kim S. Baicalein as a potent neuroprotective agent: A review. Biomedicine & pharmacotherapy = Biomedecine & pharmacotherapie. 2017;95:1021-32.

308. Zhang L, Lin G, Chang Q, Zuo Z. Role of intestinal first-pass metabolism of baicalein in its absorption process. Pharmaceutical research. 2005;22(7):1050-8.

309. Li C, Lin G, Zuo Z. Pharmacological effects and pharmacokinetics properties of Radix Scutellariae and its bioactive flavones. Biopharmaceutics & drug disposition. 2011;32(8):427-45.

310. Zhang L, Li C, Lin G, Krajcsi P, Zuo Z. Hepatic metabolism and disposition of baicalein via the coupling of conjugation enzymes and transporters-in vitro and in vivo evidences. The AAPS journal. 2011;13(3):378-89.

311. Zhang J, Lv H, Jiang K, Gao Y. Enhanced bioavailability after oral and pulmonary administration of baicalein nanocrystal. International journal of pharmaceutics. 2011;420(1):180-8.

312. Liu W, Tian R, Hu W, Jia Y, Jiang H, Zhang J, et al. Preparation and evaluation of self-microemulsifying drug delivery system of baicalein. Fitoterapia. 2012;83(8):1532-9.

313. Lee Y, Yeo H, Liu SH, Jiang Z, Savizky RM, Austin DJ, et al. Increased anti-P-glycoprotein activity of baicalein by alkylation on the A ring. Journal of medicinal chemistry. 2004;47(22):5555-66.

314. Rhee EP. Metabolomics and renal disease. Current opinion in nephrology and hypertension. 2015;24(4):371-9.

Chapter 9 Appendix

Supplementary Fig. 1. Authentication of AR.

PuraPharm培力

‘Birth Certificate’ of Radix Aconiti Research Material

PuraPharm

Code: R-CW20130622 | ‘Birth Certificate’ of Radix Aconiti Research Material

SECTION 1- Tested Items and Results

Test Items	Reference Methods	Results
1. Size	The Pharmacopoeia of the People’s Republic of China 2010, Vol.1, p36 & Appendix II B.	Complied with the criteria.
2. Texture		
3. Colour	The Pharmacopoeia of the People’s Republic of China 2010, Vol.1, p177; Method for the test of Colur, Odour and Taste, PuraPharm Pharmaceuticals Co. Ltd internal standard.	
4. Odour		
5. Taste		
6. Identification		
6.1 Microscopic identification	The Pharmacopoeia of the People’s Republic of China 2010, Vol.1, p36.	Complied with the criteria.
6.2 Identification of DNA sequence	1.CBOL Plant Working Group (2009) A DNA barcode for land plants. *Proc Natl Acad Sci U S.* 2. Identification of the medicinal plants in Aconitum L. by DNA barcoding technique. *Planta Med.*	Complied with the criteria.
6.3 TLC Identification	The Pharmacopoeia of the People’s Republic of China 2010, Vol.1, p36.	Complied with the criteria.
7. Exams		
7.1 Moisture	The Pharmacopoeia of the People’s Republic of China 2010, Vol.1, Appendix IX H.	Complied with the criteria.
7.2.Heavy Metals	The Pharmacopoeia of the People’s Republic of China 2010, Vol.1, Appendix IX B；ICP-MS.	Complied with the criteria.
7.3 Pesticides Residues	The Pharmacopoeia of the People’s Republic of China 2010, Vol.1, Appendix VI E & IX Q.	Complied with the criteria.
7.4 Sulfur Dioxide Residue	The Pharmacopoeia of the People’s Republic of China 2010, Vol.1, Appendix IX U.	Complied with the criteria.
7.5 Aflatoxin	The Pharmacopoeia of the People’s Republic of China 2010, Vol.1, Appendix IX V.	Complied with the criteria.
8. Assay	The Pharmacopoeia of the People’s Republic of China 2010, Vol.1, p36-37.	0.083%
9. Finger Print	PuraPharm Pharmaceuticals Co. Ltd internal standard	Complied with the criteria.

1

Authorized by: Date:

Code: R-CW20130622 | ‘Birth Certificate’ of Radix Aconiti Research Material

SECTION 2- Basic Information

1 Batch Number

D1303110

2 Origin

The dried parent root of *Aconitum carmichaelii* Debx.

3 Region of growth

Jiangyou, Sichuan Province, China

4 Year of Growth

1 year.

5 Harvest Season

Late June to early August

6 Pre-process Information

Removed daughter root, rootlet and mud

Sundried

7 Picture

8 Packaging Information

Vacuum-packed, 200g/package

2

Code: R-CW20130622 | ‘Birth Certificate’ of Radix Aconiti Research Material

SECTION 3- Certificate of Analysis

1. Size

Length 3.5~6cm

Diameter 1.5~2.5cm

2. Texture

Compact

Solid

3. Colour

	Description	PuraPharm Code
Surface	Clear brown grey	B^1G^14
Section	Bright grayish-yellow	B^1H^15

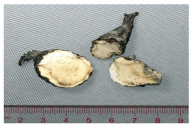

4. Odour

Description	PuraPharm Code
Slight fishy	E1

5. Taste

Description	PuraPharm Code
Strong spicy& Slight numb	E3 &F1

3

6. Identification

6.1 Microscopic identification

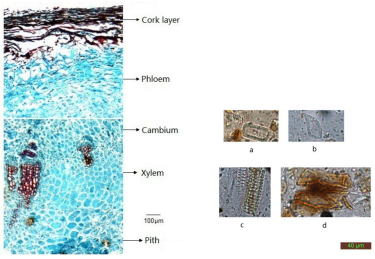

Microscopic identification of Chuanwu
Left-Microscopic characters of transverse section, cork layer, phloem, cambium, xylem and the pith
Right-Microscopic characters of powder. a. square stone cells b. Polygonal stone cells c. Vessel d. Metaderm cells

6.2 Identification of DNA sequence

7. The specific chloroplastic DNA psbA-trnH sequence is determined and compared to DNA database of NCBI, the similarity is >99%. The specific DNA sequence is showed as below:

TGGCTGCTGTTGAAGTTCCATCCACAAATGGCTAAGATTTAGGTCTTGG
TGCATGTCTGGCTTAGTGTATATGAGTCATTGAAGTTGCAGGAGCAAT
ACCCAGCCTCTTAACAGAACAAGAAATTGGGTATTGCTCCTGCATTTTT
TTGTATTAAGTAAAAATTTGACTTTAACAGATTGGTGTTGGTTTGGTGA
ATTCTAGATTATTAGACTATTATGATTATATGATTATGTTCCTC

7.1 TLC Identification

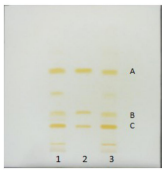

The TLC identification of Chuanwu
1--Test solution
2--Reference mixture
3--Test solution

A-Hypaconitine
B-Aconitine
C-Mesaconitine

8. Exams

8.1 **Moisture**

12%.

8.2 Heavy Metals

Result	Cu	8.375	(ppm)
	As	0.636	(ppm)
	Cd	0.5597	(ppm)
	Pb	1.477	(ppm)
	Hg	0.0107	(ppm)

8.3 Pesticide Residue

Result	Organochlorine pesticide	Content (ppm)	Limit (g/ml)

	DDT (p,p'-DDT、o,p'-DDT、p,p'-DDE、p,p'-DDD)	p,p'-DDT	Not detected	1.4×10^{-14}
		o,p'-DDT	Not detected	1.52×10^{-14}
		p,p'-DDE	Not detected	7.8×10^{-14}
		p,p'-DDD	Not detected	1.09×10^{-14}
		Total	Not detected	——
	BHC(α、β、δ、γ-BHC)	α- BHC	Not detected	6.75×10^{-15}
		β- BHC	Not detected	7.30×10^{-14}
		δ- BHC	Not detected	8.47×10^{-15}
		γ- BHC	5.30×10^{-2}	7.81×10^{-15}
		Total	5.30×10^{-2}	——
	PCNB	PCNB	0	8.75×10^{-15}

8.4 Sulfur Dioxide Residue

7.8mg/kg.

8.5 Aflatoxin

No.	Items	Unit	Result
1	AflatoxinB_1	μg/kg	<0.13*
2	Total amount of Aflatoxin G_2, G_1, B_2, B_1	μg/kg	<0.69*

* is the detecting limit

8. Assay

The amount of Mesaconine ($C_{33}H_{45}NO_{10}$), Aconitine ($C_{34}H_{47}NO_{11}$) and Hypaconitine ($C_{33}H_{45}NO_{10}$) is 0.083%.

Marker Components	Content (%)
Mesaconine	0.0422
Aconitine	0.0078
Hypaconitine	0.0325
Total	0.0825

Mixed reference substance

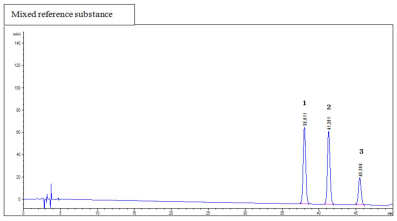

Sample

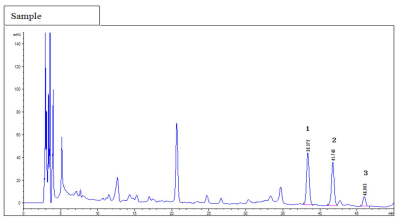

Chromatogram of HPLC
1- Mesaconine , 2- Aconitine , 3- Hypaconitine

9. Fingerprint

Chromatographic system and system suitability: use octadecylsilane bonded silica gel as the stationary phase, acetonitrile as the mobile phase A, and 0.04M ammonium acetate (pH 10.0) as the mobile phase B, elute in gradient as the

following:

Time (min)	A (%)	B (%)
0	26	74
15	26	74
45	60	40
60	60	40
61	90	10
70	90	10
71	26	74
90	26	74

The UV detector is set at 235 nm, temperature of the column is 30°C, and amount of injection is 10 μL. The number of theoretical plate of the column is no less than 3000, calculate with reference to the peak of mesaconitine

Reference Solution: take appropriate amount of Benzoylmesaconine, Benzoylaconine and Benzoylhypaconine, accurately weighed; add 0.01M hydrochloric acid to make the reference solution with the concentration of 50μg/ml. Take appropriate amount of Benzoylmesaconine, Benzoylaconine and Benzoylhypaconine, accurately weighed; add the mixture of N,N- dimethyl formamide-methanol(8:2) to make the reference solution with the concentration of 50μg/ml.

Preparation of the test solution: take 2g of the sample powder, accurately weighed; add 20 mL of 0.05M hydrochloric acid, ultrasonic processing (220W 50-60kHz) for 30mins, then centrifuge (4500 r/mins) for 10 mins, take the supernatant. Re-extract the left over once, gather the supernatant, adjust the pH to 10.0 with concentrated ammonia, then extract 5 times with acetic ether, 20 ml each times; gather the acetic ether and evaporate to dryness, dissolve the residual with N,N- dimethylfomamide - methanol (8:2) and transfer in to a 2 mL volumetric flask and make to the mark with N,N- dimethylfomamide - methanol (8:2), as test solution.

Procedure: Inject accurately 10 μl of the reference solution and the test solution respectively into the column, and calculate the content. Theoretically there should

be 6 peaks shown on the finger print chromatogram, calculate the retention time of the characteristic peaks and S peak, it should be in the rang of a certain value (±5%) 0.270 ~ 0.298 (peak 1), 0.419 ~ 0.463 (peak 2), 0.480 ~ 0.530 (peak 3), 0.724 ~ 0.800 (peak 4), 0.845 ~ 0.935 (peak 5), 1.000 (peak 6).

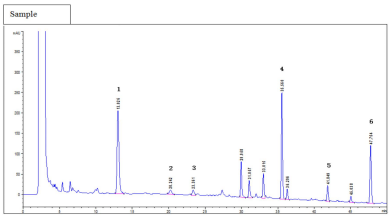

Chromatogram of Fingerprint
1-Benzoylmesaconine, 2-Benzoylaconitine 3-Benzoylhypaconitine, 4-Mesaconine, 5-Aconitine, 6- Hypaconitine (reference peak)

SECTION 4- Storage

1. **Storage**

Ideal Conditions

Temperature <30℃,

Relative humidity < 70%.

Ideal Moisture of Product

<13%

Best Use Before (YYYY-MM)

2015-08

Remarks

Toxic

Individually Packed

Prepared by:

Ms. LAN Xiaoqing

Manager, Department of Quality R&D

Endorsed by:

Dr. WEN Qingwei

Vice Director of R&D Centre

Officer of CNAS Testing Lab

Supplementary Fig. 2. Authentication of ALR.

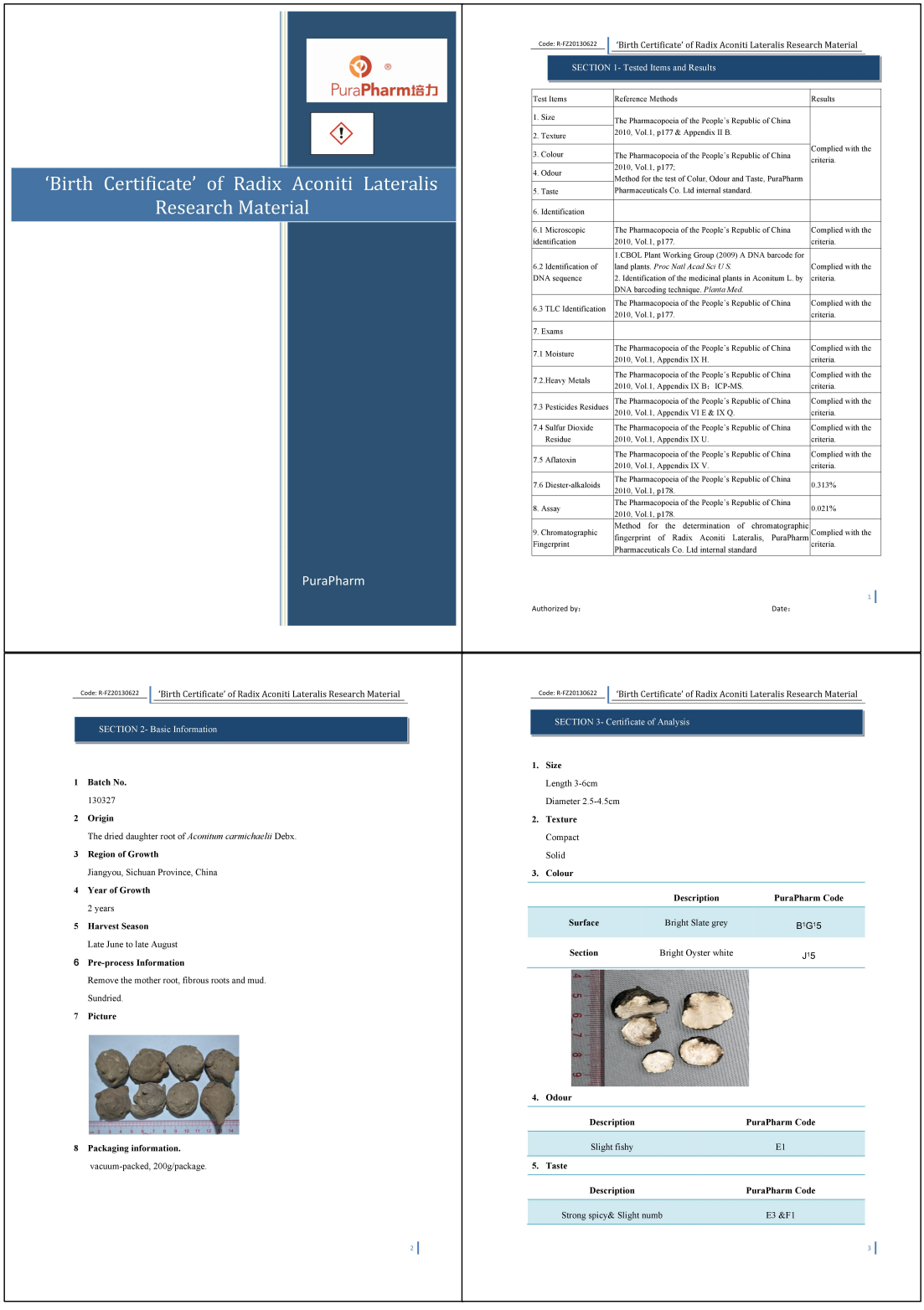

‘Birth Certificate’ of Radix Aconiti Lateralis Research Material

PuraPharm

Code: R-FZ20130622 ‘Birth Certificate’ of Radix Aconiti Lateralis Research Material

SECTION 1- Tested Items and Results

Test Items	Reference Methods	Results
1. Size	The Pharmacopoeia of the People’s Republic of China 2010, Vol.1, p177 & Appendix II B.	Complied with the criteria.
2. Texture		
3. Colour	The Pharmacopoeia of the People’s Republic of China 2010, Vol.1, p177; Method for the test of Colur, Odour and Taste, PuraPharm Pharmaceuticals Co. Ltd internal standard.	
4. Odour		
5. Taste		
6. Identification		
6.1 Microscopic identification	The Pharmacopoeia of the People’s Republic of China 2010, Vol.1, p177.	Complied with the criteria.
6.2 Identification of DNA sequence	1.CBOL Plant Working Group (2009) A DNA barcode for land plants. *Proc Natl Acad Sci U S.* 2. Identification of the medicinal plants in Aconitum L. by DNA barcoding technique. *Planta Med.*	Complied with the criteria.
6.3 TLC Identification	The Pharmacopoeia of the People’s Republic of China 2010, Vol.1, p177.	Complied with the criteria.
7. Exams		
7.1 Moisture	The Pharmacopoeia of the People’s Republic of China 2010, Vol.1, Appendix IX H.	Complied with the criteria.
7.2.Heavy Metals	The Pharmacopoeia of the People’s Republic of China 2010, Vol.1, Appendix IX B；ICP-MS.	Complied with the criteria.
7.3 Pesticides Residues	The Pharmacopoeia of the People’s Republic of China 2010, Vol.1, Appendix VI E & IX Q.	Complied with the criteria.
7.4 Sulfur Dioxide Residue	The Pharmacopoeia of the People’s Republic of China 2010, Vol.1, Appendix IX U.	Complied with the criteria.
7.5 Aflatoxin	The Pharmacopoeia of the People’s Republic of China 2010, Vol.1, Appendix IX V.	Complied with the criteria.
7.6 Diester-alkaloids	The Pharmacopoeia of the People’s Republic of China 2010, Vol.1, p178.	0.313%
8. Assay	The Pharmacopoeia of the People’s Republic of China 2010, Vol.1, p178.	0.021%
9. Chromatographic Fingerprint	Method for the determination of chromatographic fingerprint of Radix Aconiti Lateralis, PuraPharm Pharmaceuticals Co. Ltd internal standard	Complied with the criteria.

Authorized by: Date:

Code: R-FZ20130622 ‘Birth Certificate’ of Radix Aconiti Lateralis Research Material

SECTION 2- Basic Information

1 **Batch No.**

130327

2 **Origin**

The dried daughter root of *Aconitum carmichaelii* Debx.

3 **Region of Growth**

Jiangyou, Sichuan Province, China

4 **Year of Growth**

2 years

5 **Harvest Season**

Late June to late August

6 **Pre-process Information**

Remove the mother root, fibrous roots and mud.

Sundried.

7 **Picture**

8 **Packaging information.**

vacuum-packed, 200g/package.

Code: R-FZ20130622 ‘Birth Certificate’ of Radix Aconiti Lateralis Research Material

SECTION 3- Certificate of Analysis

1. **Size**

Length 3-6cm

Diameter 2.5-4.5cm

2. **Texture**

Compact

Solid

3. **Colour**

	Description	PuraPharm Code
Surface	Bright Slate grey	B^{1}G^{1}5
Section	Bright Oyster white	J^{1}5

4. **Odour**

Description	PuraPharm Code
Slight fishy	E1

5. **Taste**

Description	PuraPharm Code
Strong spicy& Slight numb	E3 &F1

6. Identification

6.1 Microscopic Identification

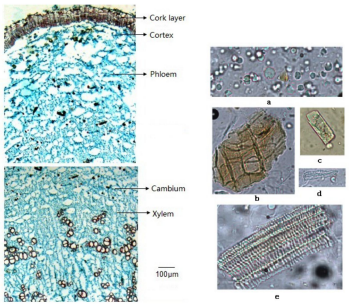

Microscopic identification of Fuzi
Left-Microscopic characters of transverse section: cork layer, cortex, phloem, cambium and xylem. Right-Microscopic identification of powder: a. starch granule b. Metaderm cells c. Square stone cells d. Oblong stone cells e. Bordered pitted vessel

6.2 Identification of DNA sequence

The specific chloroplastic DNA psbA-trnH sequence is determined and compared to DNA database of NCBI, the similarity is >99%. The specific DNA sequence is showed as below:

TGGCTGCTGTTGAAGTTCCATCCACAAATGGCTAAGATTTAGGTCTTG
GTGCATGTCTGGCTTAGTGTATATGAGTCATTGAAGTTGCAGGAGCAA

TACCCAGCCTCTTAACAGAACAAGAAATTGGGTATTGCTCCTGCATTT
TTTTGTATTAAGTAAAAATTTGACTTTAACAGATTGGTGTTGGTTTGG
TGAATTCTAGATTATTAGACTATTATGATTATATGATTATGTTCCTC.

6.3 TLC Identification

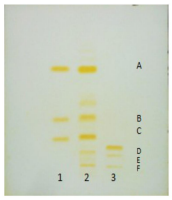

The TLC identification of Fuzi
1--Mixed reference solution 1
2--Test solution
3--Mixed reference solution 2
A--Hypaconitine
B--Aconitine
C--Mesaconitine
D--Benzoylaconine
E--Benzoylhypaconine
F--Benzoylmesaconine

7. Exam

7.1 Moisture

14.4%

7.2 Heavy Metals

Result	Cu	6.387	(ppm)
	As	0.147	(ppm)
	Cd	0.157	(ppm)
	Pb	0.221	(ppm)
	Hg	0.003	(ppm)

7.3 Pesticide Residue

	Organochlorine pesticide		Content (ppm)	Limit (g/ml)
Result	DDT (p,p'-DDT、o,p'-DDT、p,p'-DDE、o,p'-DDT、p,p'-DDD)	p,p'-DDT	Not detected	1.4×10^{-14}
		o,p'-DDT	Not detected	1.52×10^{-14}
		p,p'-DDE	Not detected	7.8×10^{-14}
		p,p'-DDD	Not detected	1.09×10^{-14}
		Total	Not detected	——

	p,p'-DDE、p,p'-DDD)			
	BHC (α、β、δ、γ-BHC)	α-BHC	Not detected	6.75×10^{-15}
		β-BHC	Not detected	7.30×10^{-14}
		δ-BHC	Not detected	8.47×10^{-15}
		γ-BHC	Not detected	7.81×10^{-15}
		Total	Not detected	——
	PCNB	PCNB	Not detected	8.75×10^{-15}

7.4 Sulfur Dioxide Residue

6.4mg/kg.

7.5 Aflatoxin

No.	Items	Unit	Result
1	AflatoxinB_1	μg/kg	<0.13*
2	Total amount of Aflatoxin G_2, G_1, B_2, B_1	μg/kg	<0.69*

* is the detecting limit of method

7.6 Diester-alkaloids

The amount of Mesaconine ($C_{33}H_{45}NO_{10}$), Aconitine ($C_{34}H_{47}NO_{11}$) and Hypaconitine ($C_{33}H_{45}NO_{10}$) is not more than 0.020%.

Marker Components	Content (%)
Mesaconine	0.081
Aconitine	0.092
Hypaconitine	0.140
Total	0.313

8. Assay

The amount of Benzoylmesaconine ($C_{31}H_{43}NO_{10}$), Benzoylaconine ($C_{32}H_{45}NO_{10}$) and Benzoylhypaconine ($C_{31}H_{43}NO_9$) is 0.021%.

Marker Components	Content (%)
Benzoylmesaconine	-
Benzoylaconine	0.0134
Benzoylhypaconine	0.0076
Total	0.0210

Reference solution

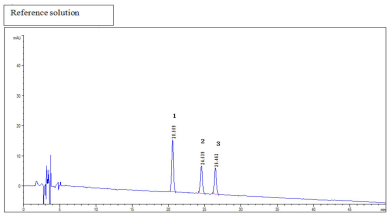

Sample

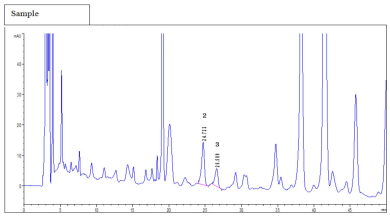

Chromatogram of Assay
1-Benzoylmesaconine , 2-Benzoylaconine , 3-Benzoylhypaconine

9. Fingerprint

Chromatographic system and system suitability: use octadecylsilane bonded silica gel as the stationary phase; acetonitrile as the mobile phase A, and 0.04 M ammonium acetate (PH 10.0) as the mobile phase B. Perform gradient elution as following chart. The detection wavelength is set at 232 nm. Column temperature is 30℃ amount of injection is 10μl.The theoretical plates of the column are no less than 3000, calculated with the reference to the peak of Benzoylmesaconine.

Time(min)	A(%)	B(%)
0	26	74
15	26	74
45	60	40
60	60	40
61	90	10
70	90	10
71	26	74
90	26	74

Reference Solution: Take appropriate amount of Benzoylmesaconine, Benzoylaconine and Benzoylhypaconine, accurately weighed; add 0.01M hydrochloric acid to make the reference solution with the concentration of 50 μg/ml. Take appropriate amount of Benzoylmesaconine, Benzoylaconine and Benzoylhypaconine, accurately weighed; add the mixture of N,N- dimethyl formamide-methanol (8:2) to make the reference solution with the concentration of 50μg/ml.

Preparation of the test solution: take 2 g of the sample powder, accurately weighed; add 20 mL of 0.05M hydrochloric acid, ultrasonic processing(220W 50-60kHz) for 30 mins, then centrifuge (4500r/mins) for 10 mins, take the supernatant. Re-extract the left over once, gather the supernatant, adjust the pH to

10.0 with concentrated ammonia, then extract 5 times with acetic ether, 20ml each times; gather the acetic ether and evaporate to dryness, dissolve the residual with N,N- dimethylfomamide - methanol (8:2) and transfer in to a 2mL volumetric flask and make to the mark with N,N- dimethylfomamide - methanol (8:2), as test solution.

Procedure: respectively inject 10μl of the reference and test solution, run the test under the chromatographic system, record the chromatogram. Theoretically there should be 6 peaks shown on the finger print chromatogram, calculate the retention time of the characteristic peaks and S peak, it should be in the rang of the certain value (±5%), 0.270 ~ 0.298 (peak 1), 0.419 ~ 0.463 (peak 2), 0.480 ~ 0.530 (peak 3), 0.724 ~ 0.800 (peak 4), 0.845 ~ 0.935 (peak 5), 1.000 (peak 6).

Reference solution

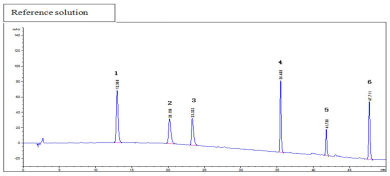

Sample

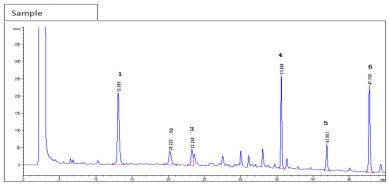

Chromatogram of Fingerprint
1-Benzoylmesaconine, 2-Benzoylaconine, 3-Benzoylhypaconine, 4-Mesaconitine, 5- Aconitine, 6-Hypaconitine (s)

SECTION 4- Storage

1. **Storage**

Ideal Conditions

Temperature <30°C

Relative humidity < 70%

Ideal Moisture of Product

<15%

Best Use Before (YYYY-MM)

2015-08

Remarks

Toxic

Individually Packed

Prepared by:

Ms. LAN Xiaoqing

Manager, Department of Quality R&D

Endorsed by:

Dr. WEN Qingwei

Vice Director of R&D Centre

Officer of CNAS Testing Lab

Supplementary Fig. 3. Authentication of SR.

PuraPharm培力

'Birth Certificate' of Huangqin Research Material

PuraPharm

SECTION 1- Tested Items and Results

Test Items	Reference Methods	Results
1. Size	The Pharmacopoeia of the People's Republic of China 2010, Vol.1, p283 & Appendix II B.	Complied with the criteria.
2. Texture		
3. Colour	The Pharmacopoeia of the People's Republic of China 2010, Vol.1, p283; Method for the test of Colur, Odour and Taste, PuraPharm Pharmaceuticals Co. Ltd internal standard.	
4. Odour		
5. Taste		
6. Identification		
6.1 Microscopic identification	The Pharmacopoeia of the People's Republic of China 2010, Vol.1, p283.	Complied with the criteria.
6.2 Identification of DNA sequence	1.CBOL Plant Working Group (2009) A DNA barcode for land plants. *Proc Natl Acad Sci U S.* 2. Identification of the medicinal plants in Aconitum L. by DNA barcoding technique. *Planta Med.*	Complied with the criteria.
6.3 TLC Identification	The Pharmacopoeia of the People's Republic of China 2010, Vol.1, p283.	Complied with the criteria.
7. Exams		
7.1 Moisture	The Pharmacopoeia of the People's Republic of China 2010, Vol.1, p283 & AppendixIX H.	4.4%
7.2 Heavy Metals	The Pharmacopoeia of the People's Republic of China 2010, Vol.1, Appendix IX B；ICP-MS.	Complied with the criteria.
7.3 Pesticides Residues	The Pharmacopoeia of the People's Republic of China 2010, Vol.1, Appendix VI E & IX Q.	Complied with the criteria.
7.4 Sulfur Dioxide Residue	The Pharmacopoeia of the People's Republic of China 2010, Vol.1, Appendix IX U.	Complied with the criteria.
7.5 Aflatoxin	The Pharmacopoeia of the People's Republic of China 2010, Vol.1, Appendix IX V.	Complied with the criteria.
8. Extractives		
8.1 Ethanol-soluble Extractives	The Pharmacopoeia of the People's Republic of China 2010, Vol.1, p283 & Appendix X A.	69.4%
9. Assay	The Pharmacopoeia of the People's Republic of China 2010, Vol.1, p283.	14.35%
10. Chromatographic Fingerprint	Method for the determination of chromatographic fingerprint of Huangqin, PuraPharm Pharmaceuticals Co. Ltd internal standard.	Complied with the criteria.

SECTION 2- Basic Information

1 Batch Number

130416

2 Origin

Baical Skullcap Root is the dried root of Scutellaria baicalensis Georgi (Fam, Labiatae).

3 Region of Growth

Chengxian, Shanxi Province, China

4 Year of Growth

2～3 years

5 Pre-process Information

Removed rootlet, mud and bark

Sundried

6 Sample Picture

(NO. 130416)

7 Packaging Information

vacuum-packed, 200g/package.

SECTION 3- Certificate of Analysis

1. Size

Length 8-25cm

Diameter 1-3cm

2. Texture

Hard and fragile

3. Colour

	Description	PuraPharm Code
Surface	Medium brown beige	$B^2G^1/3$
Section	Clear green beige	$A^2J^1/4$

4. Odour

Description	PuraPharm Code
Woody, Beany	E1

5. Taste

Description	PuraPharm Code
Strong Bitter	A4

6. Identification

6.1 Microscopic Identification

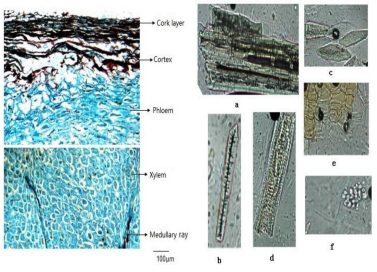

Microscopic identification of Huangqin
Left-Microscopic characters of transverse section: The cork layer, cortex, phloem, xylem, medullary ray
Right-Microscopic characteristics of Huangqin powder: a. Xylon, b. Bast fibre, c. Stone cell, d. Reticulate vessel, e. Cork cell, f. Starch grain

6.2 Identification of DNA sequence

The specific chloroplastic DNA psbA-trnH sequence is determined and compared to DNA database of NCBI, the similarity is >99%. The specific DNA sequence determination is showed as below.

GACTTGTTCTTAGTGTCGAGGAGTTTTTGAATAGATAAATAGAAGGAGCA
ATAAACTCTTTCTTGTTCTATCAAGAGGGGTTATTGCTCCTTTATTTTCTTT
TCAATTAGTAGTCTTTCCTAGACTTATTTCTTTCCATTAAGAATAAATAAA
GAGGATAAAAAATGATTGAAATTCCATTTTTTATCTTATTTTATCTTACAA
GTTCTAAAAAATTAAAATTGAAAAATCGAATTCGTAAATGTAAATTCAAT
ATTCACATCAAAAAAAATATTTAATTTTAAAGTAATTCTAGTAGAGGGGC

GGATGTAGCCAAGTGGATCAAGGCAGTCAGT

6.3 TLC Identification

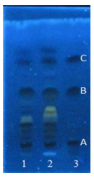

The TLC Identification of Huangqin
1-Tested Sample
2-Reference herb

A-Baicalin
B-Baicalein
C-Wogonin

7. Exams

7.1 Moisture

4.4%

7.2 Heavy Metals

Result	Cu	6.598	(ppm)
	As	0.046	(ppm)
	Cd	0.0224	(ppm)
	Pb	0.184	(ppm)
	Hg	0.0029	(ppm)

7.3 Pesticide Residue

	Organochlorine pesticide		Content（ppm）	Limit（g/ml）
Result	DDT（p,p'-DDT、o,p'-DDT、o,p'-DDT、p,p'-DDE、p,p'-DDD）	p,p'-DDT	Not detected	1.4×10^{-14}
		o,p'-DDT	Not detected	1.52×10^{-14}
		p,p'-DDE	Not detected	7.8×10^{-14}
		p,p'-DDD	Not detected	1.09×10^{-14}
		Total	Not detected	——
	BHC（α、β、δ、γ-BHC）	α- BHC	Not detected	6.75×10^{-15}
		β- BHC	Not detected	7.30×10^{-14}
		δ- BHC	Not detected	8.47×10^{-15}
		γ- BHC	Not detected	7.81×10^{-15}
		Total	Not detected	——
	PCNB	PCNB	Not detected	8.75×10^{-15}

7.4 Sulfur Dioxide Residue

6.4 mg/kg。

7.5 Aflatoxin

No.	Items	Unit	Result
1	AflatoxinB_1	μg/kg	<0.13*
2	Total amount of Aflatoxin G_2, G_1, B_2, B_1	μg/kg	<0.69*

* is the detecting limit of the method

8. Extractive

8.1 Ethanol-soluble Extractive

69.4%

9. Assay

It contains 14.35% of Baicalin ($C_{21}H_{18}O_{11}$).

Baicalin

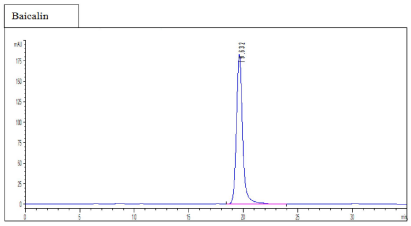

Sample

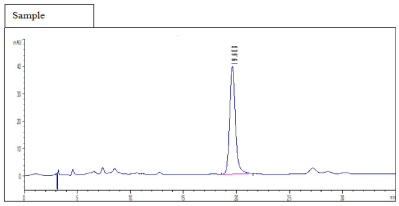

Chromatogram of Assay

10. Fingerprint

Chromatographic system and system suitability: Use octadecylsilane bonded silica gel as the stationary phase and acetonitrile as the mobile phase A, 0.2% phosphoric acid solution as the mobile phase B, perform gradient elution as following chart. The detection wavelength is set at 280 nm. Volume of injection is 5 μl, the theoretical plates of the column is no less than 2000, calculated with the reference to the peak of baicalin.

Time(min)	A（%）	B（%）
0	20	80
20	30	70
35	51	49
40	20	80

Preparation of the reference solution: Accurately weight appropriate amount of baicalin CRS, baicalein CRS and wogonin CRS, dissolve with 70% ethanol to produce the mixture solution contains 110 μg of baicalin, 20 μg of baicalein, and 10 μg of wogonin per ml as the reference solution.

Preparation of the test solution: Accurately weight about 0.1 g of the granule, grind into fine powder, transfer into flask with stopper, add in 25 ml of 70% ethanol, weight, and ultrasonic process for 30 mins, take out allow to cool down, make up the weight loss with 70% ethanol, mix well, filter. Accurately transfer 2 ml of the filtrate into 10 ml volumetric flask, make up to the volume with 70% ethanol, mix well, filter through the 0.45 μm microporous filtering film as the test solution.

Procedure: respectively inject 5μl of the reference and test solution, run the test under the chromatographic system, record the chromatogram. Theoretically there should be 7 peaks shown on the finger print chromatogram, calculate the retention time of the characteristic peaks and S peak, it should be in the rang of the certain value (±5%), 0.44 (peak 1), 1.00 (peak 2), 1.20 (peak 3), 1.33 (peak 4), 1.48(peak 5), 1.89 (peak 6), 2.35(peak 7).

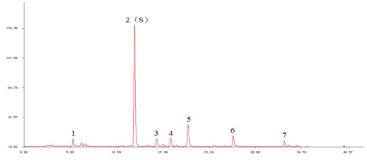

Chromatogram of Fingerprint
2- Baicalin 5- Wogonoside 6-Baicalein 7- Wogonin

SECTION 4- Storage

Storage:

Ideal Conditions

Temperature < 30℃

Relative humidity <60%

Ideal Moisture of Product

<12%

Best Use Before (YYYY-MM)

2015-08

Prepared by:	Endorsed by:
Ms. LAN Xiaoqing	Dr. WEN Qingwei
Manager, Department of Quality R&D	Vice Director of R&D Centre
	Officer of CNAS Testing Lab

Supplementary Table. 1. Cell-lysate proteins significantly regulated by TGF-β1. (listed in the **order of fold change** (TGF-β1/control).

No.	Accession	To	Description	TGF/control	t-test
1	Q924C3	Enpp1	Ectonucleotide pyroph phatase/ph phodiesterase family member 1	3.56	0.001098
2	Q62952	Dpysl3	Dihydropyrimidinase-related protein 3	2.33	0.000002
3	P62864	Fau	40S ribomal protein S30	2.07	0.006588
4	P30823	Slc7a1	High affinity cationic amino acid transporter 1	2.06	0.001813
5	Q3B8Q1	Ddx21	Nucleolar RNA helicase 2	2.03	0.000041
6	O08623	Sqstm1	Sequest ome-1	2.01	0.000856
7	Q5U1Z0	Rab3gap2	Rab3 GTPase-activating protein non-catalytic subunit	1.96	0.011780
8	Q62736	Cald1	Non-muscle caldesmon	1.96	0.000117
9	P83883	Rpl36a	60S ribomal protein L36a	1.95	0.015902
10	P54690	Bcat1	Branched-chain-amino-acid aminotransferase, cytolic	1.94	0.000008
11	P62268	Rps23	40S ribomal protein S23	1.89	0.000462
12	Q62908	Csrp2	Cysteine and glycine-rich protein 2	1.89	0.000010
13	P15205	Map1b	Microtubule-associated protein 1B	1.87	0.000310
14	P52944	Pdlim1	PDZ and LIM domain protein 1	1.86	0.000008
15	P49088	Asns	Asparagine synthetase [glutamine-hydrolyzing]	1.85	0.000019
16	Q9Z1Z9	Pdlim7	PDZ and LIM domain protein 7	1.84	0.000252
17	P18666	Myl12b	Myosin regulatory light chain 12B	1.82	0.021371
18	Q7TP54	Ripor2	Protein FAM65B	1.82	0.029861
19	P69736	Edf1	Endothelial differentiation-related factor 1	1.81	0.001183
20	P41777	Nolc1	Nucleolar and coiled-body ph phoprotein 1	1.79	0.000048
21	P0C5E3	Palld	Palladin (Fragment)	1.77	0.0014380
22	P47875	Csrp1	Cysteine and glycine-rich protein 1	1.72	0.0082442
23	P04646	Rpl35a	60S ribomal protein L35a	1.71	0.0100208
24	Q4KM49	Yars	Tyr ine--tRNA ligase, cytoplasmic	1.71	0.0000057
25	Q5U2Q7	Etf1	Eukaryotic peptide chain release factor subunit 1	1.70	0.0064419
26	A1L1L2	Tmem214	Transmembrane protein 214	1.68	0.0070073
27	Q5M819	Psph	Ph ph erine ph phatase	1.67	0.0258053
28	Q5RJT2	Ftsj3	pre-rRNA processing protein FTSJ3	1.64	0.0046964
29	Q05982	Nme1	Nucle ide diph phate kinase A	1.64	0.0184238
30	P62501	Tsc22d1	TSC22 domain family protein 1	1.62	0.0117020
31	P61621	Sec61a1	Protein transport protein Sec61 subunit alpha isoform 1	1.61	0.0497411
32	E9PU28	Impdh2	In ine-5'-monoph phate dehydrogenase 2	1.61	0.0000230
33	P62850	Rps24	40S ribomal protein S24	1.60	0.0002702
34	P62634	Cnbp	Cellular nucleic acid-binding protein	1.60	0.0017603
35	O70536	Soat1	Sterol O-acyltransferase 1	1.59	0.0114370
36	P13084	Npm1	Nucleoph min	1.59	0.0013604
37	P07314	Ggt1	Gamma-glutamyltranspeptidase 1	1.58	0.0002644
38	P61928	Rpl37	60S ribomal protein L37	1.56	0.0034004

39	Q5I0G4	Gars	Glycine--tRNA ligase (Fragment)	1.56	0.0000174
40	D3ZUA0	Mthfd2l	Probable bifunctional methylenetetrahydrofolate dehydrogenase/cyclohydrolase 2	1.56	0.0023511
41	P62752	Rpl23a	60S ribomal protein L23a	1.56	0.0013196
42	P23347	Slc4a2	Anion exchange protein 2	1.55	0.0030767
43	P19804	Nme2	Nucle ide diph phate kinase B	1.55	0.0240352
44	P13832	Rlc-a	Myosin regulatory light chain RLC-A	1.55	0.0432235
45	P18445	Rpl27a	60S ribomal protein L27a	1.54	0.0029282
46	Q6AYD3	Pa2g4	Proliferation-associated protein 2G4	1.52	0.0000577
47	P62909	Rps3	40S ribomal protein S3	1.52	0.0028506
48	Q63016	Slc7a5	Large neutral amino acids transporter small subunit 1	1.51	0.0017910
49	Q794F9	Slc3a2	4F2 cell-surface antigen heavy chain	1.51	0.0029327
50	Q66HF9	Lrrfip1	Leucine-rich repeat flightless-interacting protein 1	1.50	0.0079293
51	P19945	Rplp0	60S acidic ribomal protein P0	1.50	0.0004868
52	P63326	Rps10	40S ribomal protein S10	1.50	0.0090580
53	P17078	Rpl35	60S ribomal protein L35	1.50	0.0033750
54	O35821	Mybbp1a	Myb-binding protein 1A	1.48	0.0000782
55	Q6P799	Sars	Serine--tRNA ligase, cytoplasmic	1.47	0.0000214
56	Q62920	Pdlim5	PDZ and LIM domain protein 5	1.47	0.0000037
57	P61515	Rpl37a-ps1	Putative 60S ribomal protein L37a	1.47	0.0002564
58	P62282	Rps11	40S ribomal protein S11	1.47	0.0021085
59	O70199	Ugdh	UDP-gluc e 6-dehydrogenase	1.46	0.0005065
60	P63029	Tpt1	Translationally-controlled tumor protein	1.46	0.0003560
61	P13471	Rps14	40S ribomal protein S14	1.46	0.0037187
62	P61354	Rpl27	60S ribomal protein L27	1.45	0.0000590
63	Q9JHW0	Psmb7	Proteasome subunit beta type-7	1.45	0.0266744
64	P81795	Eif2s3	Eukaryotic translation initiation factor 2 subunit 3	1.45	0.0417285
65	P27881	Hk2	Hexokinase-2	1.45	0.0014123
66	Q9Z0W7	Clic4	Chloride intracellular channel protein 4	1.45	0.0001658
67	P24049	Rpl17	60S ribomal protein L17	1.45	0.0098013
68	Q3KRD8	Eif6	Eukaryotic translation initiation factor 6	1.44	0.0083137
69	Q5U216	Ddx39a	ATP-dependent RNA helicase DDX39A	1.44	0.0055149
70	P13383	Ncl	Nucleolin	1.44	0.0000286
71	O35763	Msn	Moesin	1.43	0.0000559
72	P62718	Rpl18a	60S ribomal protein L18a	1.42	0.0002582
73	P06762	Hmox1	Heme oxygenase 1	1.42	0.0014895
74	P38983	Rpsa	40S ribomal protein SA	1.42	0.0009925
75	P62912	Rpl32	60S ribomal protein L32	1.42	0.0026946
76	Q9Z1P2	Actn1	Alpha-actinin-1	1.42	0.0006346
77	Q1RP77	Nop16	Nucleolar protein 16	1.42	0.0023185
78	Q5U318	Pea15	Astrocytic ph phoprotein PEA-15	1.41	0.0440684
79	P62250	Rps16	40S ribomal protein S16	1.41	0.0001128

80	Q6P7B0	Wars	Tryptophan--tRNA ligase, cytoplasmic	1.41	0.0095567
81	Q5RKI1	Eif4a2	Eukaryotic initiation factor 4A-II	1.40	0.0000144
82	P62963	Pfn1	Profilin-1	1.39	0.0116613
83	Q9QXQ0	Actn4	Alpha-actinin-4	1.39	0.0005752
84	Q7TP47	Syncrip	Heterogeneous nuclear ribonucleoprotein Q	1.38	0.0009017
85	Q63690	Bax	Apopt is regulator BAX	1.38	0.0105709
86	P82808	Gfpt1	Glutamine--fruct e-6-ph phate aminotransferase [isomerizing] 1	1.38	0.0252299
87	P63245	Rack1	Guanine nucleotide-binding protein subunit beta-2-like 1	1.37	0.0045998
88	Q05175	Basp1	Brain acid soluble protein 1	1.37	0.0230789
89	P47198	Rpl22	60S ribomal protein L22	1.37	0.0013333
90	Q63560	Map6	Microtubule-associated protein 6	1.37	0.0497353
91	P62278	Rps13	40S ribomal protein S13	1.36	0.0001329
92	A0JPM9	Eif3j	Eukaryotic translation initiation factor 3 subunit J	1.36	0.0025824
93	Q9ES21	Sacm1l	Ph phatidylin itide ph phatase SAC1	1.36	0.0088705
94	Q5U2X6	Ccdc47	Coiled-coil domain-containing protein 47	1.35	0.0395551
95	P12001	Rpl18	60S ribomal protein L18	1.35	0.0041345
96	Q712U5	Arpp19	cAMP-regulated ph phoprotein 19	1.35	0.0048518
97	P11762	Lgals1	Galectin-1	1.35	0.0372277
98	Q63525	Nudc	Nuclear migration protein nudC	1.34	0.0124122
99	Q641X8	Eif3e	Eukaryotic translation initiation factor 3 subunit E	1.34	0.0035566
100	P62961	Ybx1	Nuclease-sensitive element-binding protein 1	1.34	0.0029660
101	Q68FR6	Eef1g	Elongation factor 1-gamma	1.34	0.0000589
102	Q8K1Q0	Nmt1	Glycylpeptide N-tetradecanoyltransferase 1	1.34	0.0004197
103	P62275	Rps29	40S ribomal protein S29	1.34	0.0475435
104	P12749	Rpl26	60S ribomal protein L26	1.34	0.0017594
105	O35987	Nsfl1c	NSFL1 cofactor p47	1.33	0.0026978
106	P62755	Rps6	40S ribomal protein S6	1.33	0.0008892
107	P21533	Rpl6	60S ribomal protein L6	1.33	0.0000008
108	P62271	Rps18	40S ribomal protein S18	1.33	0.0036672
109	Q63692	Cdc37	Hsp90 co-chaperone Cdc37	1.33	0.0083535
110	Q9R0T3	Dnajc3	DnaJ homolog subfamily C member 3	1.33	0.0051897
111	Q9QVC8	Fkbp4	Peptidyl-prolyl cis-trans isomerase FKBP4	1.33	0.0024050
112	D4A4T9	Chordc1	Cysteine and histidine-rich domain-containing protein 1	1.33	0.0147319
113	Q6IRE4	Tsg101	Tumor susceptibility gene 101 protein	1.33	0.0066914
114	P39032	Rpl36	60S ribomal protein L36	1.33	0.0071969
115	Q9R063	Prdx5	Peroxiredoxin-5, mitochondrial	1.33	0.0002008
116	P62630	Eef1a1	Elongation factor 1-alpha 1	1.33	0.0000234
117	P27952	Rps2	40S ribomal protein S2	1.33	0.0000325
118	P35427	Rpl13a	60S ribomal protein L13a	1.33	0.0000040
119	P69682	Necap1	Adaptin ear-binding coat-associated protein 1	1.33	0.0173329
120	P61480	Wdr12	Ribome biogenesis protein WDR12	1.32	0.0012276

121	P62832	Rpl23	60S ribomal protein L23	1.32	0.0038515
122	P17074	Rps19	40S ribomal protein S19	1.32	0.0017947
123	Q62658	Fkbp1a	Peptidyl-prolyl cis-trans isomerase FKBP1A	1.32	0.0011745
124	P62243	Rps8	40S ribomal protein S8	1.32	0.0000114
125	P05197	Eef2	Elongation factor 2	1.32	0.0001188
126	G3V9R8	Hnrnpc	Heterogeneous nuclear ribonucleoprotein C	1.31	0.0077468
127	O35824	Dnaja2	DnaJ homolog subfamily A member 2	1.31	0.0008499
128	P62845	Rps15	40S ribomal protein S15	1.31	0.0043307
129	Q01986	Map2k1	Dual specificity mitogen-activated protein kinase kinase 1	1.31	0.0075095
130	P09895	Rpl5	60S ribomal protein L5	1.31	0.0000082
131	P63174	Rpl38	60S ribomal protein L38	1.31	0.0020781
132	Q68FR9	Eef1d	Elongation factor 1-delta	1.31	0.0002742
133	P41123	Rpl13	60S ribomal protein L13	1.31	0.0200022
134	Q6PDV7	Rpl10	60S ribomal protein L10	1.30	0.0002967
135	P05426	Rpl7	60S ribomal protein L7	1.30	0.0002517
136	P02401	Rplp2	60S acidic ribomal protein P2	1.30	0.0159066
137	Q9QZ86	Nop58	Nucleolar protein 58	1.30	0.0002125
138	P25886	Rpl29	60S ribomal protein L29	1.30	0.0104309
139	P61314	Rpl15	60S ribomal protein L15	1.29	0.0006893
140	O88813	Acsl5	Long-chain-fatty-acid--CoA ligase 5	1.29	0.0066855
141	P23358	Rpl12	60S ribomal protein L12	1.29	0.0000076
142	Q6AYZ1	Tuba1c	Tubulin alpha-1C chain	1.29	0.0116303
143	Q71TY3	Rps27	40S ribomal protein S27	1.29	0.0005498
144	Q3T1J1	Eif5a	Eukaryotic translation initiation factor 5A-1	1.28	0.0058972
145	P28073	Psmb6	Proteasome subunit beta type-6	1.28	0.0006328
146	P34058	Hsp90ab1	Heat shock protein HSP 90-beta	1.28	0.0091371
147	Q6P9U8	Eif3h	Eukaryotic translation initiation factor 3 subunit H	1.28	0.0000794
148	P62856	Rps26	40S ribomal protein S26	1.28	0.0023543
149	P62703	Rps4x	40S ribomal protein S4, X isoform	1.28	0.0015485
150	P22509	Fbl	rRNA 2'-O-methyltransferase fibrillarin	1.28	0.0133284
151	Q641Y8	Ddx1	ATP-dependent RNA helicase DDX1	1.27	0.0281427
152	P20280	Rpl21	60S ribomal protein L21	1.27	0.0007097
153	Q5M7W5	Map4	Microtubule-associated protein 4	1.27	0.0014243
154	Q1JU68	Eif3a	Eukaryotic translation initiation factor 3 subunit A	1.27	0.0000029
155	P62425	Rpl7a	60S ribomal protein L7a	1.27	0.0002663
156	P21531	Rpl3	60S ribomal protein L3	1.27	0.0010299
157	P62907	Rpl10a	60S ri omal protein L10a	1.27	0.0030049
158	P62890	Rpl30	60S ribomal protein L30	1.27	0.0005207
159	P62919	Rpl8	60S ribomal protein L8	1.26	0.0048897
160	Q6VV72	Eif1a	Eukaryotic translation initiation factor 1A	1.26	0.0079177
161	P11250	Rpl34	60S ribomal protein L34	1.26	0.0004188
162	P63018	Hspa8	Heat shock cognate 71 kDa protein	1.26	0.0002032

163	Q5XIP1	Pelo	Protein pelota homolog	1.26	0.0036600
164	P22062	Pcmt1	Protein-L-isoaspartate(D-aspartate) O-methyltransferase	1.26	0.0465209
165	O08651	Phgdh	D-3-ph phoglycerate dehydrogenase	1.26	0.0123408
166	P12785	Fasn	Fatty acid synthase	1.26	0.0000126
167	P49242	Rps3a	40S ribomal protein S3a	1.26	0.0001581
168	P83732	Rpl24	60S ribomal protein L24	1.26	0.0322061
169	P60868	Rps20	40S ribomal protein S20	1.26	0.0001764
170	Q6AZ50	Atg3	Ubiquitin-like-conjugating enzyme ATG3	1.26	0.0368564
171	D3ZBE5	Nek7	Serine/threonine-protein kinase Nek7	1.25	0.0101863
172	Q5RJR8	Lrrc59	Leucine-rich repeat-containing protein 59	1.25	0.0095242
173	B1WC88	N/A	UPF0729 protein C18orf32 homolog	1.25	0.0309817
174	Q64270	Eif2b1	Translation initiation factor eIF-2B subunit alpha	1.25	0.0287751
175	P50878	Rpl4	60S ribomal protein L4	1.25	0.0057550
176	Q9R1T1	Banf1	Barrier-to-autointegration factor	1.25	0.0167957
177	P21670	Psma4	Proteasome subunit alpha type-4	1.24	0.0483779
178	P43245	Abcb1	Multidrug resistance protein 1	1.24	0.0028145
179	B5DFC8	Eif3c	Eukaryotic translation initiation factor 3 subunit C	1.24	0.0007518
180	Q9JMJ4	Prpf19	Pre-mRNA-processing factor 19	1.23	0.0082776
181	P17077	Rpl9	60S ribomal protein L9	1.23	0.0002490
182	Q5XIM5	Cdv3	Protein CDV3 homolog	1.23	0.0449842
183	P38062	Metap2	Methionine aminopeptidase 2	1.23	0.0340740
184	P29314	Rps9	40S ribomal protein S9	1.23	0.0004207
185	Q9WVB1	Rab6a	Ras-related protein Rab-6A	1.23	0.0372107
186	P62246	Rps15a	40S ribomal protein S15a	1.22	0.0133251
187	P17702	Rpl28	60S ribomal protein L28	1.22	0.0023717
188	Q63356	Myo1e	Unconventional myosin-Ie	1.22	0.0236681
189	P82995	Hsp90aa1	Heat shock protein HSP 90-alpha	1.21	0.0004333
190	F1LYQ8	Farp1	FERM, RhoGEF and pleckstrin domain-containing protein 1	1.21	0.0008080
191	Q66HA8	Hsph1	Heat shock protein 105 kDa	1.21	0.0021275
192	B0BNA7	Eif3i	Eukaryotic translation initiation factor 3 subunit I	1.21	0.0008732
193	P07335	Ckb	Creatine kinase B-type	1.21	0.0312553
194	Q9EQR2	Agps	Alkyldihydroxyacetoneph phate synthase, peroxisomal	1.21	0.0257579
195	P37397	Cnn3	Calponin-3	1.20	0.0026069
196	P04644	Rps17	40S ribomal protein S17	1.20	0.0185435
197	O89049	Txnrd1	Thioredoxin reductase 1, cytoplasmic	1.20	0.0058558
198	Q5XHY5	Tars	Threonine--tRNA ligase, cytoplasmic	1.19	0.0013528
199	Q7TNY6	Acbd3	Golgi resident protein GCP60	1.19	0.0208809
200	Q811A3	Plod2	Procollagen-lysine,2-oxoglutarate 5-dioxygenase 2	1.19	0.0426380
201	P60123	Ruvbl1	RuvB-like 1	1.19	0.0055658
202	Q5RJR2	Twf1	Twinfilin-1	1.19	0.0497102
203	P84100	Rpl19	60S ribomal protein L19	1.19	0.0189263
204	P68035	Actc1	Actin, alpha cardiac muscle 1	1.19	0.0085285

205	Q2PQA9	Kif5b	Kinesin-1 heavy chain	1.19	0.0034128
206	P38656	Ssb	Lupus La protein homolog	1.19	0.0344342
207	P24051	Rps27l	40S ribomal protein S27-like	1.18	0.0006568
208	Q5U312	Rai14	Ankycorbin	1.18	0.0009869
209	Q62881	Nol3	Nucleolar protein 3	1.18	0.0301995
210	P40615	Dkc1	H/ACA ribonucleoprotein complex subunit 4	1.18	0.0466678
211	Q6AYK8	Eif3d	Eukaryotic translation initiation factor 3 subunit D	1.18	0.0060480
212	Q63507	Rpl14	60S ribomal protein L14	1.18	0.0178203
213	Q9Z270	Vapa	Vesicle-associated membrane protein-associated protein A	1.18	0.0101869
214	Q9Z1A6	Hdlbp	Vigilin	1.18	0.0015655
215	Q9JIH7	Wnk1	Serine/threonine-protein kinase WNK1	1.17	0.0284400
216	P05765	Rps21	40S ribomal protein S21	1.17	0.0208823
217	Q4G061	Eif3b	Eukaryotic translation initiation factor 3 subunit B	1.17	0.0178759
218	Q63228	Gmfb	Glia maturation factor beta	1.17	0.0371693
219	Q63716	Prdx1	Peroxiredoxin-1	1.16	0.0010450
220	Q66HR2	Mapre1	Microtubule-associated protein RP/EB family member 1	1.16	0.0000741
221	Q68FQ0	Cct5	T-complex protein 1 subunit epsilon	1.16	0.0004009
222	P45592	Cfl1	Cofilin-1	1.15	0.0199921
223	Q66HL2	Cttn	Src substrate cortactin	1.15	0.0188479
224	P28480	Tcp1	T-complex protein 1 subunit alpha	1.15	0.0165744
225	P43138	Apex1	DNA- (apurinic or apyrimidinic site) lyase	1.15	0.0129767
226	P30427	Plec	Plectin	1.15	0.0098421
227	Q62812	Myh9	Myosin-9	1.15	0.0269145
228	P52296	Kpnb1	Importin subunit beta-1	1.14	0.0218246
229	P18420	Psma1	Proteasome subunit alpha type-1	1.14	0.0195399
230	Q6AXS5	Serbp1	Plasminogen activator inhibitor 1 RNA-binding protein	1.14	0.0303913
231	Q9QZA2	Pdcd6ip	Programmed cell death 6-interacting protein	1.14	0.0032095
232	Q04462	Vars	Valine--tRNA ligase	1.14	0.0417600
233	P62859	Rps28	40S ribomal protein S28	1.14	0.0445586
234	P24155	Thop1	Thimet oligopeptidase	1.14	0.0046095
235	Q9Z269	Vapb	Vesicle-associated membrane protein-associated protein B	1.14	0.0065536
236	P37285	Klc1	Kinesin light chain 1	1.14	0.0289927
237	Q5EGY4	Ykt6	Synaptobrevin homolog YKT6	1.13	0.0308115
238	P49791	Nup153	Nuclear pore complex protein Nup153	1.13	0.0043654
239	Q9EPH8	Pabpc1	Polyadenylate-binding protein 1	1.13	0.0026369
240	Q6P502	Cct3	T-complex protein 1 subunit gamma	1.12	0.0021966
241	Q63610	Tpm3	Tropomy in alpha-3 chain	1.12	0.0050609
242	Q5XIG8	Strap	Serine-threonine kinase receptor-associated protein	1.12	0.0154925
243	Q5HZY0	Ubxn4	UBX domain-containing protein 4	1.11	0.0188267
244	D3ZTX0	Tmed7	Transmembrane emp24 domain-containing protein 7	1.11	0.0338770
245	P35281	Rab10	Ras-related protein Rab-10	1.11	0.0449360
246	Q08163	Cap1	Adenylyl cyclase-associated protein 1	1.11	0.0309408

247	Q6MG08	Abcf1	ATP-binding cassette sub-family F member 1	1.10	0.0284181
248	P40329	Rars	Arginine--tRNA ligase, cytoplasmic	1.10	0.0318503
249	Q5XIM9	Cct2	T-complex protein 1 subunit beta	1.10	0.0055078
250	Q794E4	Hnrnpf	Heterogeneous nuclear ribonucleoprotein F	1.10	0.0265802
251	O35814	Stip1	Stress-induced-ph phoprotein 1	1.08	0.0002923
252	Q07266	Dbn1	Drebrin	1.08	0.0466116
253	P05712	Rab2a	Ras-related protein Rab-2A	1.07	0.0127148
254	Q66H80	Arcn1	Coatomer subunit delta	1.05	0.0461805
255	Q4KMA2	Rad23b	UV excision repair protein RAD23 homolog B	0.95	0.0287152
256	Q9Z1X1	Esyt1	Extended synaptotagmin-1	0.93	0.0115308
257	Q64560	Tpp2	Tripeptidyl-peptidase 2	0.93	0.0356649
258	Q6TUG0	Dnajb11	DnaJ homolog subfamily B member 11	0.92	0.0200398
259	Q9WVC0	Sept7	Septin-7	0.92	0.0450362
260	Q00438	Ptbp1	Polypyrimidine tract-binding protein 1	0.91	0.0354257
261	B0BNG0	Emc2	ER membrane protein complex subunit 2	0.91	0.0251889
262	O08629	Trim28	Transcription intermediary factor 1-beta	0.91	0.0122504
263	F1MA98	Tpr	Nucleoprotein TPR	0.91	0.0376338
264	P31977	Ezr	Ezrin	0.91	0.0263836
265	P61980	Hnrnpk	Heterogeneous nuclear ribonucleoprotein K	0.91	0.0000497
266	P15791	Camk2d	Calcium/calmodulin-dependent protein kinase type II subunit delta	0.91	0.0443771
267	Q9JIL3	Ilf3	Interleukin enhancer-binding factor 3	0.90	0.0028383
268	Q63355	Myo1c	Unconventional my in-Ic	0.90	0.0029042
269	P46462	Vcp	Transitional endoplasmic reticulum ATPase	0.90	0.0027992
270	P28023	Dctn1	Dynactin subunit 1	0.90	0.0166048
271	O54975	Xpnpep1	Xaa-Pro aminopeptidase 1	0.90	0.0008480
272	Q91Y78	Uchl3	Ubiquitin carboxyl-terminal hydrolase isozyme L3	0.89	0.0227242
273	P35435	Atp5c1	ATP synthase subunit gamma, mitochondrial	0.89	0.0434718
274	Q6IUR5	Nenf	Neudesin	0.89	0.0087244
275	P16036	Slc25a3	Ph phate carrier protein, mitochondrial	0.89	0.0054680
276	P63331	Ppp2ca	Serine/threonine-protein ph phatase 2A catalytic subunit alpha isoform	0.89	0.0095396
277	P29410	Ak2	Adenylate kinase 2, mitochondrial	0.89	0.0384143
278	Q91Y81	Sept2	Septin-2	0.89	0.0028444
279	O88989	Mdh1	Malate dehydrogenase, cytoplasmic	0.88	0.0024969
280	Q4V7C6	Gmps	GMP synthase [glutamine-hydrolyzing]	0.88	0.0216074
281	P00388	Por	NADPH--cytochrome P450 reductase	0.88	0.0276875
282	O88370	Pip4k2c	Ph phatidylin itol 5-ph phate 4-kinase type-2 gamma	0.88	0.0000250
283	Q63081	Pdia6	Protein disulfide-isomerase A6	0.88	0.0043397
284	Q4FZT0	Stoml2	Stomatin-like protein 2, mitochondrial	0.88	0.0099038
285	P06685	Atp1a1	Sodium/potassium-transporting ATPase subunit alpha-1	0.88	0.0017899
286	P37996	Arl3	ADP-ribylation factor-like protein 3	0.88	0.0291822
287	P84092	Ap2m1	AP-2 complex subunit mu	0.87	0.0171178

288	Q6AY23	Pycr2	Pyrroline-5-carboxylate reductase 2	0.87	0.0169387
289	Q9JK72	Ccs	Copper chaperone for superoxide dismutase	0.87	0.0006857
290	P10111	Ppia	Peptidyl-prolyl cis-trans isomerase A	0.87	0.0107640
291	P04897	Gnai2	Guanine nucleotide-binding protein G(i) subunit alpha-2	0.87	0.0178793
292	Q68FW9	Cops3	COP9 signal ome complex subunit 3	0.87	0.0113669
293	O08839	Bin1	Myc box-dependent-interacting protein 1	0.87	0.0091920
294	Q5U211	Snx3	Sorting nexin-3	0.86	0.0052603
295	Q5SGE0	Lrpprc	Leucine-rich PPR motif-containing protein, mitochondrial	0.86	0.0014064
296	P48500	Tpi1	Tri eph phate isomerase	0.86	0.0471810
297	Q6AY09	Hnrnph2	Heterogeneous nuclear ribonucleoprotein H2	0.86	0.0011837
298	Q66HG4	Galm	Ald e 1-epimerase	0.86	0.0260616
299	Q5U300	Uba1	Ubiquitin-like modifier-activating enzyme 1	0.86	0.0082328
300	Q66H94	Fkbp9	Peptidyl-prolyl cis-trans isomerase FKBP9	0.86	0.0036294
301	Q3MIE4	Vat1	Synaptic vesicle membrane protein VAT-1 homolog	0.86	0.0293934
302	P14408	Fh	Fumarate hydratase, mitochondrial	0.86	0.0449060
303	Q5XIH7	Phb2	Prohibitin-2	0.86	0.0002638
304	Q2LAP6	Tes	Testin	0.86	0.0060924
305	P04550	Ptms	Parathym in	0.86	0.0173610
306	P63312	Tmsb10	Thym in beta-10	0.86	0.0272058
307	P16636	Lox	Protein-lysine 6-oxidase	0.86	0.0083618
308	Q5XIN6	Letm1	LETM1 and EF-hand domain-containing protein 1, mitochondrial	0.86	0.0107029
309	P07323	Eno2	Gamma-enolase	0.86	0.0178061
310	P85515	Actr1a	Alpha-centractin	0.86	0.0014028
311	Q3KR86	Immt	MIC complex subunit Mic60 (Fragment)	0.86	0.0284774
312	Q5U2U0	Clpx	ATP-dependent Clp protease ATP-binding subunit clpX-like, mitochondrial	0.85	0.0090503
313	Q4QQW4	Hdac1	Histone deacetylase 1	0.85	0.0026765
314	Q9JLJ3	Aldh9a1	4-trimethylaminobutyraldehyde dehydrogenase	0.85	0.0019633
315	Q505J8	Farsa	Phenylalanine--tRNA ligase alpha subunit	0.85	0.0429945
316	O35094	Timm44	Mitochondrial import inner membrane translocase subunit TIM44	0.85	0.0304649
317	P25286	Atp6v0a1	V-type proton ATPase 116 kDa subunit a isoform 1	0.85	0.0359705
318	P35704	Prdx2	Peroxiredoxin-2	0.85	0.0056877
319	Q4QQW8	Plbd2	Putative ph pholipase B-like 2	0.85	0.0034790
320	Q8CGV7	Thtpa	Thiamine-triph phatase	0.85	0.0159680
321	P43244	Matr3	Matrin-3	0.85	0.0295578
322	Q80X08	Washc2	WASH complex subunit FAM21	0.85	0.0044541
323	Q62991	Scfd1	Sec1 family domain-containing protein 1	0.85	0.0106231
324	Q9JM53	Aifm1	Apopt is-inducing factor 1, mitochondrial	0.85	0.0071194
325	P69060	Cmas	N-acylneuraminate cytidylyltransferase	0.84	0.0291077
326	Q6PCT3	Tpd52l2	Tumor protein D54	0.84	0.0422336
327	Q68FY0	Uqcrc1	Cytochrome b-c1 complex subunit 1, mitochondrial	0.84	0.0172724
328	P27615	Scarb2	Lys ome membrane protein 2	0.84	0.0128804

329	P54001	P4ha1	Prolyl 4-hydroxylase subunit alpha-1	0.84	0.0211830
330	P18665	Mrpl3	39S ribomal protein L3, mitochondrial	0.84	0.0186807
331	Q641X3	Hexa	Beta-hex aminidase subunit alpha	0.84	0.0055643
332	P04636	Mdh2	Malate dehydrogenase, mitochondrial	0.84	0.0331004
333	P63086	Mapk1	Mitogen-activated protein kinase 1	0.84	0.0002483
334	P97629	Lnpep	Leucyl-cystinyl aminopeptidase	0.84	0.0001766
335	Q5U2Z3	Nap1l4	Nucle ome assembly protein 1-like 4	0.84	0.0067304
336	O35244	Prdx6	Peroxiredoxin-6	0.83	0.0001017
337	Q62636	Rap1b	Ras-related protein Rap-1b	0.83	0.0115236
338	P13668	Stmn1	Stathmin	0.83	0.0095801
339	Q5I0P2	Gcsh	Glycine cleavage system H protein, mitochondrial	0.83	0.0213464
340	Q4KLH4	Pspc1	Paraspeckle component 1	0.83	0.0014221
341	Q63269	Itpr3	In itol 1,4,5-trisph phate receptor type 3	0.83	0.0493230
342	Q62826	Hnrnpm	Heterogeneous nuclear ribonucleoprotein M	0.83	0.0041922
343	Q9Z2L0	Vdac1	Voltage-dependent anion-selective channel protein 1	0.82	0.0131790
344	Q4KM73	Cmpk1	UMP-CMP kinase	0.82	0.0126134
345	Q4KLN7	Arfgap3	ADP-ribylation factor GTPase-activating protein 3	0.82	0.0004936
346	B0BNM1	Naxe	NAD(P)H-hydrate epimerase	0.82	0.0151538
347	Q66HC5	Nup93	Nuclear pore complex protein Nup93	0.82	0.0010450
348	P42123	Ldhb	L-lactate dehydrogenase B chain	0.82	0.0000820
349	P08081	Clta	Clathrin light chain A	0.82	0.0006031
350	Q9WUC4	Atox1	Copper transport protein ATOX1	0.82	0.0353984
351	P97697	Impa1	In itol monoph phatase 1	0.82	0.0126210
352	Q9JI03	Col5a1	Collagen alpha-1(V) chain	0.82	0.0415892
353	Q5XI22	Acat2	Acetyl-CoA acetyltransferase, cyt olic	0.82	0.0002279
354	P06302	Ptma	Prothym in alpha	0.82	0.0014951
355	P11960	Bckdha	2-oxoisovalerate dehydrogenase subunit alpha, mitochondrial (Fragment)	0.82	0.0132905
356	P38659	Pdia4	Protein disulfide-isomerase A4	0.82	0.0144377
357	P20069	Pmpca	Mitochondrial-processing peptidase subunit alpha	0.82	0.0074923
358	P00507	Got2	Aspartate aminotransferase, mitochondrial	0.82	0.0005887
359	Q6PDU7	Atp5l	ATP synthase subunit g, mitochondrial	0.82	0.0003393
360	P08461	Dlat	Dihydrolipoyllysine-residue acetyltransferase component of pyruvate dehydrogenase complex, mitochondrial	0.82	0.0183297
361	Q9ESN0	Fam129a	Protein Niban	0.81	0.0016023
362	P70615	Lmnb1	Lamin-B1	0.81	0.0067297
363	P80254	Ddt	D-dopachrome decarboxylase	0.81	0.0324687
364	Q6QD51	Ccdc80	Coiled-coil domain-containing protein 80	0.81	0.0155696
365	Q6P7A9	Gaa	Lys omal alpha-gluc idase	0.81	0.0009507
366	Q5I0D1	Glod4	Glyoxalase domain-containing protein 4	0.81	0.0000244
367	P17046	Lamp2	Lys ome-associated membrane glycoprotein 2	0.81	0.0183831
368	Q5XHZ0	Trap1	Heat shock protein 75 kDa, mitochondrial	0.81	0.0004147
369	Q62868	Rock2	Rho-associated protein kinase 2	0.81	0.0136241

370	Q810U0	Ccdc50	Coiled-coil domain-containing protein 50	0.81	0.0329995
371	Q07936	Anxa2	Annexin A2	0.81	0.0001686
372	P09456	Prkar1a	cAMP-dependent protein kinase type I-alpha regulatory subunit	0.81	0.0091928
373	Q920D2	Dhfr	Dihydrofolate reductase	0.81	0.0468536
374	Q5XFX0	Tagln2	Transgelin-2	0.81	0.0035694
375	P20070	Cyb5r3	NADH-cytochrome b5 reductase 3	0.81	0.0014827
376	P19511	Atp5f1	ATP synthase F(0) complex subunit B1, mitochondrial	0.80	0.0000492
377	Q99ML5	Pcyox1	Prenylcysteine oxidase	0.80	0.0125499
378	Q9QXU8	Dync1li1	Cytoplasmic dynein 1 light intermediate chain 1	0.80	0.0005829
379	Q62733	Tmpo	Lamina-associated polypeptide 2, isoform beta	0.80	0.0059960
380	Q9EPB1	Dpp7	Dipeptidyl peptidase 2	0.80	0.0029135
381	O88994	Marc2	Mitochondrial amidoxime reducing component 2	0.80	0.0202140
382	Q8CG09	Abcc1	Multidrug resistance-associated protein 1	0.80	0.0316521
383	P50137	Tkt	Transketolase	0.80	0.0033514
384	Q64375	P3h4	Synaptonemal complex protein SC65 (Fragment)	0.80	0.0130969
385	O88767	Park7	Protein deglycase DJ-1	0.80	0.0005405
386	P63281	Ube2i	SUMO-conjugating enzyme UBC9	0.80	0.0002356
387	Q9JLT0	Myh10	My in-10	0.80	0.0074501
388	O35303	Dnm1l	Dynamin-1-like protein	0.79	0.0007290
389	Q642C0	Dnajc8	DnaJ homolog subfamily C member 8	0.79	0.0003905
390	Q07205	Eif5	Eukaryotic translation initiation factor 5	0.79	0.0072797
391	P49911	Anp32a	Acidic leucine-rich nuclear ph phoprotein 32 family member A	0.79	0.0006473
392	Q6AXT0	Mrpl37	39S ribomal protein L37, mitochondrial	0.79	0.0252430
393	Q5XIG0	Nudt9	ADP-ribe pyroph phatase, mitochondrial	0.79	0.0349921
394	P85972	Vcl	Vinculin	0.79	0.0417693
395	P21571	Atp5j	ATP synthase-coupling factor 6, mitochondrial	0.79	0.0341873
396	P80386	Prkab1	5'-AMP-activated protein kinase subunit beta-1	0.79	0.0241881
397	Q63598	Pls3	Plastin-3	0.79	0.0176144
398	A2RUW1	Tollip	Toll-interacting protein	0.79	0.0155060
399	E9PT23	Slc38a10	Putative sodium-coupled neutral amino acid transporter 10	0.79	0.0086947
400	P21775	Acaa1a	3-ketoacyl-CoA thiolase A, peroxisomal	0.79	0.0008882
401	Q5GFD9	Impact	Protein IMPACT	0.79	0.0000745
402	P34926	Map1a	Microtubule-associated protein 1A	0.79	0.0015535
403	P47860	Pfkp	ATP-dependent 6-ph phofructokinase, platelet type	0.79	0.0000319
404	P35571	Gpd2	Glycerol-3-ph phate dehydrogenase, mitochondrial	0.79	0.0089304
405	Q63184	Eif2ak2	Interferon-induced, double-stranded RNA-activated protein kinase	0.79	0.0032215
406	Q5XI78	Ogdh	2-oxoglutarate dehydrogenase, mitochondrial	0.79	0.0003847
407	Q920L2	Sdha	Succinate dehydrogenase [ubiquinone] flavoprotein subunit, mitochondrial	0.79	0.0010525
408	Q9Z2F5	Ctbp1	C-terminal-binding protein 1	0.79	0.0221039
409	Q32KJ6	Galns	N-acetylgalact amine-6-sulfatase	0.79	0.0026002
410	Q9Z2Z8	Dhcr7	7-dehydrocholesterol reductase	0.79	0.0448463

411	Q704S8	Crat	Carnitine O-acetyltransferase	0.78	0.0168116
412	Q80Z70	Sel1l	Protein sel-1 homolog 1	0.78	0.0060134
413	Q99NA5	Idh3a	Isocitrate dehydrogenase [NAD] subunit alpha, mitochondrial	0.78	0.0012564
414	P0C5W1	Map1s	Microtubule-associated protein 1S	0.78	0.0154979
415	P61959	Sumo2	Small ubiquitin-related modifier 2	0.78	0.0000643
416	Q64057	Aldh7a1	Alpha-aminoadipic semialdehyde dehydrogenase	0.78	0.0008614
417	Q62940	Nedd4	E3 ubiquitin-protein ligase NEDD4	0.78	0.0002572
418	F1LP64	Trip12	E3 ubiquitin-protein ligase TRIP12	0.78	0.0055348
419	P97521	Slc25a20	Mitochondrial carnitine/acylcarnitine carrier protein	0.78	0.0154279
420	Q9ER34	Aco2	Aconitate hydratase, mitochondrial	0.78	0.0005769
421	P85125	Cavin1	Polymerase I and transcript release factor	0.77	0.0007397
422	Q01205	Dlst	Dihydrolipoyllysine-residue succinyltransferase component of 2-oxoglutarate dehydrogenase complex, mitochondrial	0.77	0.0217270
423	P19836	Pcyt1a	Choline-ph phate cytidylyltransferase A	0.77	0.0045096
424	P47942	Dpysl2	Dihydropyrimidinase-related protein 2	0.77	0.0000575
425	Q5XIC2	Ecsit	Evolutionarily conserved signaling intermediate in Toll pathway, mitochondrial	0.77	0.0100090
426	P32198	Cpt1a	Carnitine O-palmitoyltransferase 1, liver isoform	0.77	0.0347431
427	Q8VHF5	Cs	Citrate synthase, mitochondrial	0.77	0.0001331
428	P05708	Hk1	Hexokinase-1	0.77	0.0000347
429	P04166	Cyb5b	Cytochrome b5 type B	0.77	0.0051621
430	P15999	Atp5a1	ATP synthase subunit alpha, mitochondrial	0.77	0.0003735
431	Q62696	Dlg1	Disks large homolog 1	0.77	0.0092286
432	P05942	S100a4	Protein S100-A4	0.77	0.0003850
433	Q2TA68	Opa1	Dynamin-like 120 kDa protein, mitochondrial	0.77	0.0205501
434	P0C1X8	Aak1	AP2-associated protein kinase 1	0.77	0.0480759
435	Q64361	Lxn	Latexin	0.77	0.0261630
436	P42676	Nln	Neurolysin, mitochondrial	0.76	0.0027773
437	Q06647	Atp5o	ATP synthase subunit O, mitochondrial	0.76	0.0053029
438	P30009	Marcks	Myristoylated alanine-rich C-kinase substrate	0.76	0.0052503
439	Q9Z1E1	Flot1	Flotillin-1	0.76	0.0212713
440	Q5XIT9	Mccc2	Methylcrotonoyl-CoA carboxylase beta chain, mitochondrial	0.76	0.0000958
441	Q6AYE2	Sh3glb1	Endophilin-B1	0.76	0.0378772
442	P97700	Slc25a11	Mitochondrial 2-oxoglutarate/malate carrier protein	0.76	0.0057248
443	Q6P6R2	Dld	Dihydrolipoyl dehydrogenase, mitochondrial	0.76	0.0027338
444	P32089	Slc25a1	Tricarboxylate transport protein, mitochondrial	0.76	0.0020070
445	O70351	Hsd17b10	3-hydroxyacyl-CoA dehydrogenase type-2	0.76	0.0042540
446	P26772	Hspe1	10 kDa heat shock protein, mitochondrial	0.76	0.0369880
447	P55260	Anxa4	Annexin A4	0.76	0.0055711
448	Q2EJA0	Yap1	Transcriptional coactivator YAP1	0.75	0.0134712
449	P04041	Gpx1	Glutathione peroxidase 1	0.75	0.0115888
450	Q68FP1	Gsn	Gelsolin	0.75	0.0000217
451	Q924K2	Faf1	FAS-associated factor 1	0.75	0.0322683

452	Q4QQV3	Fam162a	Protein FAM162A	0.75	0.0476892
453	P00173	Cyb5a	Cytochrome b5	0.75	0.0015601
454	P15865	Hist1h1e	Histone H1.4	0.75	0.0143170
455	Q3B8P0	Parl	Presenilins-associated rhomboid-like protein, mitochondrial	0.75	0.0414244
456	P48037	Anxa6	Annexin A6	0.75	0.0000279
457	Q10758	Krt8	Keratin, type II cyt keletal 8	0.75	0.0000942
458	Q4V8H8	Ehd2	EH domain-containing protein 2	0.75	0.0004423
459	P97571	Capn1	Calpain-1 catalytic subunit	0.74	0.0000103
460	Q9Z1H9	Cavin3	Protein kinase C delta-binding protein	0.74	0.0044020
461	P06214	Alad	Delta-aminolevulinic acid dehydratase	0.74	0.0303985
462	Q5U2Q3	N/A	Ester hydrolase C11orf54 homolog	0.74	0.0463222
463	Q68FU3	Etfb	Electron transfer flavoprotein subunit beta	0.74	0.0003606
464	P23785	Grn	Granulins	0.74	0.0207259
465	Q62638	Glg1	Golgi apparatus protein 1	0.74	0.0050421
466	P30904	Mif	Macrophage migration inhibitory factor	0.74	0.0132020
467	P45953	Acadvl	Very long-chain specific acyl-CoA dehydrogenase, mitochondrial	0.74	0.0000231
468	P38652	Pgm1	Ph phoglucomutase-1	0.74	0.0006844
469	P21913	Sdhb	Succinate dehydrogenase [ubiquinone] iron-sulfur subunit, mitochondrial	0.74	0.0209860
470	P10688	Plcd1	1-ph phatidylin itol 4,5-bisph phate ph phodiesterase delta-1	0.74	0.0040607
471	Q8VID1	Dhrs4	Dehydrogenase/reductase SDR family member 4	0.74	0.0295825
472	P08010	Gstm2	Glutathione S-transferase Mu 2	0.74	0.0001534
473	P10719	Atp5b	ATP synthase subunit beta, mitochondrial	0.74	0.0006633
474	P52873	Pc	Pyruvate carboxylase, mitochondrial	0.73	0.0002753
475	Q4KM35	Psmb10	Proteasome subunit beta type-10	0.73	0.0404880
476	P49432	Pdhb	Pyruvate dehydrogenase E1 component subunit beta, mitochondrial	0.73	0.0000004
477	P28042	Ssbp1	Single-stranded DNA-binding protein, mitochondrial	0.73	0.0018510
478	Q63663	Gbp2	Guanylate-binding protein 1	0.73	0.0071477
479	Q4V7F2	Creld1	Cysteine-rich with EGF-like domain protein 1	0.73	0.0000831
480	B0BNF1	Sept8	Septin-8	0.73	0.0156106
481	P36201	Crip2	Cysteine-rich protein 2	0.73	0.0090930
482	Q9Z2S9	Flot2	Flotillin-2	0.73	0.0010387
483	P02454	Col1a1	Collagen alpha-1(I) chain	0.73	0.0019132
484	Q5I0C3	Mccc1	Methylcrotonoyl-CoA carboxylase subunit alpha, mitochondrial	0.73	0.0358732
485	Q99068	Lrpap1	Alpha-2-macroglobulin receptor-associated protein	0.73	0.0014664
486	Q9QZK5	Htra1	Serine protease HTRA1	0.73	0.0181115
487	Q5PQM0	Tmem168	Transmembrane protein 168	0.72	0.0196592
488	P63095	Gnas	Guanine nucleotide-binding protein G(s) subunit alpha isoforms short	0.72	0.0113979
489	P63045	Vamp2	Vesicle-associated membrane protein 2	0.72	0.0488765
490	P15651	Acads	Short-chain specific acyl-CoA dehydrogenase, mitochondrial	0.72	0.0064452
491	P07092	Serpine2	Glia-derived nexin	0.72	0.0399649
492	P56522	Fdxr	NADPH: adrenodoxin oxidoreductase, mitochondrial	0.72	0.0162405

493	Q9JHY2	Sfxn3	Sideroflexin-3	0.72	0.0018098
494	P14604	Echs1	Enoyl-CoA hydratase, mitochondrial	0.72	0.0030698
495	P35434	Atp5d	ATP synthase subunit delta, mitochondrial	0.72	0.0049924
496	P97532	Mpst	3-mercaptopyruvate sulfurtransferase	0.72	0.0004222
497	Q6P747	Hp1bp3	Heterochromatin protein 1-binding protein 3	0.72	0.0000947
498	Q8CG45	Akr7a2	Aflatoxin B1 aldehyde reductase member 2	0.71	0.0028299
499	P53534	Pygb	Glycogen ph phorylase, brain form (Fragment)	0.71	0.0000647
500	P47858	Pfkm	ATP-dependent 6-ph phofructokinase, muscle type	0.71	0.0001908
501	P10888	Cox4i1	Cytochrome c oxidase subunit 4 isoform 1, mitochondrial	0.71	0.0012368
502	Q64232	Tecr	Very-long-chain enoyl-CoA reductase	0.71	0.0129254
503	Q6Q0N3	Nt5dc2	5'-nucleotidase domain-containing protein 2	0.71	0.0022816
504	P13803	Etfa	Electron transfer flavoprotein subunit alpha, mitochondrial	0.71	0.0000466
505	Q75WE7	Vwa5a	von Willebrand factor A domain-containing protein 5A	0.71	0.0001544
506	D4ACN8	Plgrkt	Plasminogen receptor (KT)	0.71	0.0009718
507	P04182	Oat	Ornithine aminotransferase, mitochondrial	0.71	0.0047211
508	P27867	Sord	Sorbitol dehydrogenase	0.71	0.0004821
509	Q4KM98	Mff	Mitochondrial fission factor	0.71	0.0435993
510	P28077	Psmb9	Proteasome subunit beta type-9	0.70	0.0413773
511	Q4TU93	Mrc2	C-type mann e receptor 2	0.70	0.0008429
512	O54748	Stk3	Serine/threonine-protein kinase 3	0.70	0.0076585
513	P60825	Cirbp	Cold-inducible RNA-binding protein	0.70	0.0350027
514	Q63797	Psme1	Proteasome activator complex subunit 1	0.70	0.0002322
515	Q6AY84	Scrn1	Secernin-1	0.70	0.0018914
516	Q9JJ22	Erap1	Endoplasmic reticulum aminopeptidase 1	0.70	0.0009802
517	P41562	Idh1	Isocitrate dehydrogenase [NADP] cytoplasmic	0.70	0.0000098
518	P15650	Acadl	Long-chain specific acyl-CoA dehydrogenase, mitochondrial	0.70	0.0000598
519	P0C2X9	Aldh4a1	Delta-1-pyrroline-5-carboxylate dehydrogenase, mitochondrial	0.70	0.0003332
520	P11240	Cox5a	Cytochrome c oxidase subunit 5A, mitochondrial	0.70	0.0001077
521	P14882	Pcca	Propionyl-CoA carboxylase alpha chain, mitochondrial	0.70	0.0000914
522	Q60587	Hadhb	Trifunctional enzyme subunit beta, mitochondrial	0.70	0.0003499
523	Q9JIM0	Mre11	Double-strand break repair protein MRE11A	0.70	0.0083976
524	Q64428	Hadha	Trifunctional enzyme subunit alpha, mitochondrial	0.69	0.0000443
525	Q810F4	Fam3c	Protein FAM3C	0.69	0.0013938
526	Q63321	Plod1	Procollagen-lysine,2-oxoglutarate 5-dioxygenase 1	0.69	0.0000215
527	P21396	Maoa	Amine oxidase [flavin-containing] A	0.69	0.0000825
528	P25093	Fah	Fumarylacetoacetase	0.69	0.0040200
529	Q6AXU6	JPT1	Hematological and neurological expressed 1 protein	0.69	0.0014327
530	Q9Z327	Synpo	Synaptopodin	0.69	0.0039664
531	P56574	Idh2	Isocitrate dehydrogenase [NADP], mitochondrial	0.69	0.0001601
532	Q7TQ16	Uqcrq	Cytochrome b-c1 complex subunit 8	0.69	0.0474050
533	Q9JI85	Nucb2	Nucleobindin-2	0.68	0.0186665

534	P11951	Cox6c2	Cytochrome c oxidase subunit 6C-2	0.68	0.0200809
535	D3ZAF6	Atp5j2	ATP synthase subunit f, mitochondrial	0.68	0.0032847
536	Q7TPB4	Cd276	CD276 antigen	0.68	0.0001779
537	P41350	Cav1	Caveolin-1	0.68	0.0016633
538	Q10739	Mmp14	Matrix metalloproteinase-14	0.68	0.0013451
539	Q00238	Icam1	Intercellular adhesion molecule 1	0.68	0.0005359
540	Q9Z0J5	Txnrd2	Thioredoxin reductase 2, mitochondrial	0.68	0.0006278
541	P12075	Cox5b	Cytochrome c oxidase subunit 5B, mitochondrial	0.68	0.0041743
542	O88775	Emb	Embigin	0.68	0.0206963
543	B0BNA5	Cotl1	Coact in-like protein	0.68	0.0089586
544	O35854	Bcat2	Branched-chain-amino-acid aminotransferase, mitochondrial	0.68	0.0035203
545	P15978	RT1-Aw2	Class I histocompatibility antigen, Non-RT1.A alpha-1 chain	0.68	0.0041685
546	P23965	Eci1	Enoyl-CoA delta isomerase 1, mitochondrial	0.67	0.0000586
547	P18886	Cpt2	Carnitine O-palmitoyltransferase 2, mitochondrial	0.67	0.0020404
548	P04906	Gstp1	Glutathione S-transferase P	0.67	0.0132907
549	P97608	Oplah	5-oxoprolinase	0.67	0.0046135
550	Q9ER24	Atxn10	Ataxin-10	0.67	0.0153647
551	P14841	Cst3	Cystatin-C	0.67	0.0215712
552	P97546	Nptn	Neuroplastin	0.67	0.0028680
553	P97852	Hsd17b4	Peroxisomal multifunctional enzyme type 2	0.67	0.0000660
554	P06536	Nr3c1	Glucocorticoid receptor	0.67	0.0385047
555	P18437	Hmgn2	Non-histone chrom omal protein HMG-17	0.66	0.0081645
556	P50123	Enpep	Glutamyl aminopeptidase	0.66	0.0006071
557	P10860	Glud1	Glutamate dehydrogenase 1, mitochondrial	0.66	0.0002313
558	P52759	Rida	Ribonuclease UK114	0.65	0.0008711
559	P26453	Bsg	Basigin	0.65	0.0012228
560	Q5XIC0	Eci2	Enoyl-CoA delta isomerase 2, mitochondrial	0.65	0.0000079
561	Q5XIE6	Hibch	3-hydroxyisobutyryl-CoA hydrolase, mitochondrial	0.65	0.0358018
562	Q6P7C7	Gpnmb	Transmembrane glycoprotein NMB	0.65	0.0001072
563	P06760	Gusb	Beta-glucuronidase	0.65	0.0074165
564	Q6P0K8	Jup	Junction plakoglobin	0.65	0.0005066
565	P00406	Mtco2	Cytochrome c oxidase subunit 2	0.65	0.0001418
566	P15684	Anpep	Aminopeptidase N	0.64	0.0218193
567	P28037	Aldh1l1	Cyt olic 10-formyltetrahydrofolate dehydrogenase	0.64	0.0106161
568	Q920G2	Slc9a3r2	Na(+)/H(+) exchange regulatory cofactor NHE-RF2	0.64	0.0119657
569	P84817	Fis1	Mitochondrial fission 1 protein	0.64	0.0009579
570	P21708	Mapk3	Mitogen-activated protein kinase 3	0.64	0.0012310
571	P70584	Acadsb	Short/branched chain specific acyl-CoA dehydrogenase, mitochondrial	0.64	0.0002386
572	P07150	Anxa1	Annexin A1	0.63	0.0000119
573	Q4G075	Serpinb1a	Leukocyte elastase inhibitor A	0.63	0.0018797
574	P35053	Gpc1	Glypican-1	0.63	0.0001877

575	P13596	Ncam1	Neural cell adhesion molecule 1	0.63	0.0015943
576	Q9QX69	Lancl1	LanC-like protein 1	0.63	0.0007704
577	P29266	Hibadh	3-hydroxyisobutyrate dehydrogenase, mitochondrial	0.63	0.0000310
578	Q08850	Stx4	Syntaxin-4	0.63	0.0002746
579	Q1AAU6	Asap1	Arf-GAP with SH3 domain, ANK repeat and PH domain-containing protein 1	0.63	0.0057536
580	P07154	Ctsl	Cathepsin L1	0.63	0.0018394
581	Q6MG60	Ddah2	N(G),N(G)-dimethylarginine dimethylaminohydrolase 2	0.63	0.0000713
582	P70550	Rab8b	Ras-related protein Rab-8B	0.63	0.0016055
583	Q9Z252	Lin7b	Protein lin-7 homolog B	0.62	0.0109877
584	P29411	Ak3	GTP:AMP ph photransferase AK3, mitochondrial	0.62	0.0000360
585	Q9ERB4	Vcan	Versican core protein (Fragments)	0.62	0.0116038
586	Q5XI42	Aldh3b1	Aldehyde dehydrogenase family 3 member B1	0.62	0.0078887
587	P08011	Mgst1	Micr omal glutathione S-transferase 1	0.62	0.0199485
588	P18614	Itga1	Integrin alpha-1	0.61	0.0246665
589	P18297	Spr	Sepiapterin reductase	0.61	0.0009427
590	Q9QWN8	Sptbn2	Spectrin beta chain, non-erythrocytic 2	0.61	0.0019092
591	P12007	Ivd	Isovaleryl-CoA dehydrogenase, mitochondrial	0.61	0.0000446
592	Q4G017	Nisch	Nischarin	0.61	0.0407536
593	P17764	Acat1	Acetyl-CoA acetyltransferase, mitochondrial	0.61	0.0009736
594	Q5BJK8	Golim4	Golgi integral membrane protein 4	0.60	0.0000660
595	Q9WVK7	Hadh	Hydroxyacyl-coenzyme A dehydrogenase, mitochondrial	0.60	0.0000067
596	Q8K5A9	Nradd	Death domain-containing membrane protein NRADD	0.60	0.0004733
597	P04904	Gsta3	Glutathione S-transferase alpha-3	0.59	0.0012798
598	Q9EPH2	Marcksl1	MARCKS-related protein	0.59	0.0038476
599	P11915	Scp2	Non-specific lipid-transfer protein	0.59	0.0002519
600	P07633	Pccb	Propionyl-CoA carboxylase beta chain, mitochondrial	0.58	0.0000289
601	P11505	Atp2b1	Plasma membrane calcium-transporting ATPase 1	0.58	0.0000227
602	P16086	Sptan1	Spectrin alpha chain, non-erythrocytic 1	0.58	0.0000094
603	D4A1J4	Bdh2	3-hydroxybutyrate dehydrogenase type 2	0.58	0.0094715
604	P30839	Aldh3a2	Fatty aldehyde dehydrogenase	0.58	0.0004343
605	P16391	N/A	RT1 class I histocompatibility antigen, AA alpha chain	0.58	0.0048209
606	Q9JJ19	Slc9a3r1	Na(+)/H(+) exchange regulatory cofactor NHE-RF1	0.57	0.0000786
607	P12369	Prkar2b	cAMP-dependent protein kinase type II-beta regulatory subunit	0.57	0.0045010
608	Q6JE36	Ndrg1	Protein NDRG1	0.56	0.0058849
609	Q9WU82	Ctnnb1	Catenin beta-1	0.56	0.0000517
610	Q62627	Pawr	PRKC apopt is WT1 regulator protein	0.55	0.0465606
611	P13437	Acaa2	3-ketoacyl-CoA thiolase, mitochondrial	0.55	0.0000607
612	Q02253	Aldh6a1	Methylmalonate-semialdehyde dehydrogenase [acylating], mitochondrial	0.55	0.0000017
613	Q5U4F3	Fam107b	Protein FAM107B	0.55	0.0026386
614	P11884	Aldh2	Aldehyde dehydrogenase, mitochondrial	0.54	0.0000111
615	P52631	Stat3	Signal transducer and activator of transcription 3	0.54	0.0000330

616	Q5U2T3	Spats2l	SPATS2-like protein	0.52	0.0001881
617	Q5RKH6	Os9	Protein Os-9	0.51	0.0000169
618	Q62651	Ech1	Delta (3,5)-Delta (2,4)-dienoyl-CoA isomerase, mitochondrial	0.50	0.0014289
619	Q64591	Decr1	2,4-dienoyl-CoA reductase, mitochondrial	0.49	0.0002485
620	O08628	Pcolce	Procollagen C-endopeptidase enhancer 1	0.49	0.0000142
621	P04762	Cat	Catalase	0.47	0.0000000
622	Q63028	Add1	Alpha-adducin	0.44	0.0000762
623	P08430	Ugt1a6	UDP-glucuron yltransferase 1-6	0.43	0.0000274
624	O35276	Nrp2	Neuropilin-2	0.43	0.0074137
625	Q8R4C0	Capn5	Calpain-5	0.39	0.0025916
626	Q62847	Add3	Gamma-adducin	0.37	0.0052223
627	Q8VIF7	Selenbp1	Selenium-binding protein 1	0.34	0.0000377
628	P11883	Aldh3a1	Aldehyde dehydrogenase, dimeric NADP-preferring	0.22	0.0000075

Supplementary Table. 2. SRM, baicalein and IN1130 all significantly regulated proteins involved in the focal adhesion pathway. Shown here are mean fold changes of proteins expression versus TGF-β1 group, $p<0.05$, "-": not significantly regulated by drug(s).

Accession	Protein	Control	TGF-β1	TGF-β1				
				40 μg/mL SRM	80 μg/mL SRM	40 μM Baicalein	80 μM Baicalein	IN1130
P18666	Myl12b	0.55	1.00	-	0.57	0.89	-	0.52
Q9Z1P2	Actn1	0.70	1.00	-	0.83	0.72	-	0.73
P18266	Gsk3b	0.71	1.00	-	0.65	0.75	-	0.76
Q9QXQ0	Actn4	0.72	1.00	-	0.81	0.74	-	0.75
P04937	Fn1	0.75	1.00	-	1.34	0.87	-	0.83
Q01986	Map2k1	0.76	1.00	-	0.96	1.09	-	0.77
P08721	Spp1	0.81	1.00	-	1.00	1.55	-	0.81
P60711	Actb	0.91	1.00	-	0.88	0.74	-	0.92
Q9HB97	Parva	0.93	1.00	-	0.90	0.78	-	0.95
P13941	Col3a1	1.16	1.00	-	1.45	0.89	-	1.45
P02466	Col1a2	1.18	1.00	-	1.32	0.93	-	1.37
Q9JI03	Col5a1	1.22	1.00	-	1.37	0.81	-	1.36
P02454	Col1a1	1.37	1.00	-	1.43	1.16	-	1.53
P41350	Cav1	1.46	1.00	-	1.06	0.92	-	1.40
P21708	Mapk3	1.57	1.00	-	1.14	1.06	-	1.46
P18614	Itga1	1.63	1.00	-	1.07	0.96	-	1.69
Q9WU82	Ctnnb1	1.77	1.00	-	1.15	1.03	-	1.69

Supplementary Table. 3. SRM and IN1130 significantly regulated proteins involved in the amoebiasis pathway pathway. Shown here are mean fold changes of proteins expression versus TGF-β1 group, $p<0.05$.

Accession	Protein	Control	TGF-β1	TGF-β1	
				80 µg/mL SRM	IN1130
Q9Z1P2	Actn1	0.70	1.00	0.83	0.73
P42930	Hspb1	0.71	1.00	0.86	0.75
Q9QXQ0	Actn4	0.72	1.00	0.81	0.75
P04937	Fn1	0.75	1.00	1.34	0.83
P13941	Col3a1	1.16	1.00	1.45	1.45
P02466	Col1a2	1.18	1.00	1.32	1.37
Q9JI03	Col5a1	1.22	1.00	1.37	1.36
P02454	Col1a1	1.37	1.00	1.43	1.53
Q4G075	Serpinb1a	1.58	1.00	1.20	1.41

Supplementary Table. 4. Baicalein and IN1130 significantly regulated proteins involved 13 KEGG pathways. Shown here are mean fold changes of proteins expression versus TGF-β1 group, $p<0.05$, "-": not significantly regulated by drug(s).

Accession	Protein	Control	TGF-β1	TGF-β1		
				40 μM Baicalein	80 μM Baicalein	IN1130
Drug metabolism - cytochrome P450						
P06757	Adh1	1.18	1.00	1.27	0.99	1.06
P08010	Gstm2	1.36	1.00	1.04	0.92	1.38
P21396	Maoa	1.45	1.00	1.48	1.63	1.25
P04906	Gstp1	1.48	1.00	1.50	1.68	1.40
Q5XI42	Aldh3b1	1.61	1.00	1.30	1.46	1.48
P08011	Mgst1	1.62	1.00	1.15	1.03	1.62
P04904	Gsta3	1.68	1.00	1.78	1.85	1.45
P08430	Ugt1a6	2.30	1.00	1.33	1.72	2.01
P11883	Aldh3a1	4.50	1.00	1.71	1.76	4.36
Histidine metabolism						
P21396	Maoa	1.45	1.00	1.48	1.63	1.25
Q5XI42	Aldh3b1	1.61	1.00	1.30	1.46	1.48
P30839	Aldh3a2	1.73	1.00	0.85	0.87	1.62
P11884	Aldh2	1.85	1.00	1.28	1.36	1.62
P11883	Aldh3a1	4.50	1.00	1.71	1.76	4.36
Carbon metabolism						
Q5M819	Psph	0.60	1.00	0.90	0.79	0.72
P27881	Hk2	0.69	1.00	1.32	1.67	0.70
P05065	Aldoa	0.89	1.00	1.14	1.44	0.88
P85968	Pgd	0.98	1.00	1.28	1.14	1.00
P07323	Eno2	1.17	1.00	1.07	1.33	1.13
P50137	Tkt	1.25	1.00	1.40	1.56	1.18
P47860	Pfkp	1.27	1.00	1.16	1.31	1.18
Q920L2	Sdha	1.27	1.00	0.86	0.69	1.18
Q99NA5	Idh3a	1.28	1.00	1.16	1.35	1.17
Q01205	Dlst	1.29	1.00	1.16	1.29	1.14
Q6P6R2	Dld	1.32	1.00	1.12	1.30	1.18
P52873	Pc	1.36	1.00	1.29	1.33	1.21
P47858	Pfkm	1.41	1.00	1.13	1.12	1.37
P14882	Pcca	1.43	1.00	1.22	1.19	1.33
P56574	Idh2	1.46	1.00	1.18	1.22	1.30
P10860	Glud1	1.52	1.00	1.21	1.23	1.39
P17764	Acat1	1.65	1.00	1.17	1.32	1.53
P07633	Pccb	1.72	1.00	1.20	1.48	1.51
Q02253	Aldh6a1	1.83	1.00	1.22	1.32	1.60

P04762	Cat	2.11	1.00	1.84	1.69	1.77
Metabolic pathways						
Q924C3	Enpp1	0.28	1.00	0.36	0.17	0.37
P54690	Bcat1	0.52	1.00	0.80	0.91	0.61
P49088	Asns	0.54	1.00	0.89	0.83	0.57
Q5M819	Psph	0.60	1.00	0.90	0.79	0.72
Q05982	Nme1	0.61	1.00	0.94	0.57	0.73
E9PU28	Impdh2	0.62	1.00	0.98	0.93	0.69
P07314	Ggt1	0.63	1.00	1.47	1.23	0.63
D3ZUA0	Mthfd2l	0.64	1.00	1.03	1.23	0.65
P19804	Nme2	0.64	1.00	1.00	0.70	0.73
P27881	Hk2	0.69	1.00	1.32	1.67	0.70
Q5PQL5	Ptdss1	0.70	1.00	0.85	0.60	0.75
P82808	Gfpt1	0.72	1.00	0.98	0.82	0.76
P07335	Ckb	0.83	1.00	0.79	0.58	0.87
P05065	Aldoa	0.89	1.00	1.14	1.44	0.88
P18298	Mat2a	0.91	1.00	1.14	1.42	0.94
P07943	Akr1b1	0.96	1.00	1.69	1.79	0.95
P11348	Qdpr	0.97	1.00	0.98	1.27	0.92
P85968	Pgd	0.98	1.00	1.28	1.14	1.00
Q66HF1	Ndufs1	0.98	1.00	0.56	0.42	1.10
O55171	Acot2	0.99	1.00	1.31	1.46	0.72
Q5RJP0	Akr1b7	1.04	1.00	3.55	4.72	0.94
P07323	Eno2	1.17	1.00	1.07	1.33	1.13
P25286	Atp6v0a1	1.17	1.00	1.12	1.46	1.09
Q6AYQ8	Fahd1	1.18	1.00	1.33	1.24	1.12
P06757	Adh1	1.18	1.00	1.27	0.99	1.06
P69060	Cmas	1.18	1.00	1.15	1.26	1.08
P54001	P4ha1	1.19	1.00	1.21	1.54	1.14
Q80Z29	Nampt	1.21	1.00	1.29	1.36	1.13
P19234	Ndufv2	1.21	1.00	0.71	0.53	1.08
Q9WTT6	Gda	1.22	1.00	0.98	0.88	1.28
P11960	Bckdha	1.22	1.00	1.04	1.35	1.15
P45479	Ppt1	1.24	1.00	1.24	1.44	1.18
Q920D2	Dhfr	1.24	1.00	1.27	1.30	1.34
P50137	Tkt	1.25	1.00	1.40	1.56	1.18
P21571	Atp5j	1.27	1.00	1.13	1.26	1.21
P21775	Acaa1a	1.27	1.00	1.22	1.35	1.16
P47860	Pfkp	1.27	1.00	1.16	1.31	1.18
Q920L2	Sdha	1.27	1.00	0.86	0.69	1.18
Q9Z2Z8	Dhcr7	1.27	1.00	1.17	1.17	1.33
Q99NA5	Idh3a	1.28	1.00	1.16	1.35	1.17

Q01205	Dlst	1.29	1.00	1.16	1.29	1.14
P19836	Pcyt1a	1.29	1.00	1.25	1.31	1.20
Q06647	Atp5o	1.31	1.00	1.09	1.33	1.20
P48450	Lss	1.31	1.00	1.24	1.08	1.58
Q6P6R2	Dld	1.32	1.00	1.12	1.30	1.18
P06214	Alad	1.35	1.00	1.16	2.34	1.45
P38652	Pgm1	1.35	1.00	1.12	1.12	1.38
Q8VID1	Dhrs4	1.36	1.00	1.31	1.39	1.39
P10719	Atp5b	1.36	1.00	1.15	1.31	1.22
P52873	Pc	1.36	1.00	1.29	1.33	1.21
Q5I0C3	Mccc1	1.37	1.00	1.12	1.22	1.36
P19468	Gclc	1.37	1.00	1.33	1.82	1.27
P35434	Atp5d	1.39	1.00	1.17	1.27	1.33
P97532	Mpst	1.40	1.00	1.17	1.05	1.31
P53534	Pygb	1.40	1.00	1.09	1.14	1.36
P47858	Pfkm	1.41	1.00	1.13	1.12	1.37
P10888	Cox4i1	1.41	1.00	1.05	1.30	1.33
P04182	Oat	1.42	1.00	1.07	1.15	1.35
P0C2X9	Aldh4a1	1.43	1.00	1.08	1.36	1.51
P11240	Cox5a	1.43	1.00	1.09	1.36	1.35
P14882	Pcca	1.43	1.00	1.22	1.19	1.33
P21396	Maoa	1.45	1.00	1.48	1.63	1.25
P25093	Fah	1.45	1.00	1.03	1.28	1.40
P56574	Idh2	1.46	1.00	1.18	1.22	1.30
Q7TQ16	Uqcrq	1.46	1.00	0.95	1.10	1.35
D3ZAF6	Atp5j2	1.46	1.00	1.21	1.15	1.32
P12075	Cox5b	1.47	1.00	1.09	1.37	1.37
O35854	Bcat2	1.47	1.00	1.12	1.18	1.34
P97852	Hsd17b4	1.49	1.00	1.37	1.43	1.39
P10860	Glud1	1.52	1.00	1.21	1.23	1.39
P06760	Gusb	1.54	1.00	0.96	1.28	1.49
P15684	Anpep	1.55	1.00	1.05	1.29	1.26
P70584	Acadsb	1.57	1.00	1.15	1.15	1.33
P29266	Hibadh	1.59	1.00	1.22	1.32	1.44
Q5XI42	Aldh3b1	1.61	1.00	1.30	1.46	1.48
P18297	Spr	1.63	1.00	1.28	1.38	1.46
P12007	Ivd	1.64	1.00	1.12	1.19	1.40
P17764	Acat1	1.65	1.00	1.17	1.32	1.53
Q9WVK7	Hadh	1.67	1.00	1.23	1.13	1.51
P11915	Scp2	1.69	1.00	1.15	0.98	1.59
P07633	Pccb	1.72	1.00	1.20	1.48	1.51
D4A1J4	Bdh2	1.72	1.00	1.27	1.11	1.77

P30839	Aldh3a2	1.73	1.00	0.85	0.87	1.62
P13437	Acaa2	1.83	1.00	1.25	1.17	1.63
Q02253	Aldh6a1	1.83	1.00	1.22	1.32	1.60
P11884	Aldh2	1.85	1.00	1.28	1.36	1.62
P08430	Ugt1a6	2.30	1.00	1.33	1.72	2.01
P11883	Aldh3a1	4.50	1.00	1.71	1.76	4.36
Glycolysis / Gluconeogenesis						
P27881	Hk2	0.69	1.00	1.32	1.67	0.70
P06757	Adh1	1.18	1.00	1.27	0.99	1.06
Q6P6R2	Dld	1.32	1.00	1.12	1.30	1.18
P38652	Pgm1	1.35	1.00	1.12	1.12	1.38
P47858	Pfkm	1.41	1.00	1.13	1.12	1.37
Q5XI42	Aldh3b1	1.61	1.00	1.30	1.46	1.48
P17764	Acat1	1.65	1.00	1.17	1.32	1.53
P07633	Pccb	1.72	1.00	1.20	1.48	1.51
P30839	Aldh3a2	1.73	1.00	0.85	0.87	1.62
P11884	Aldh2	1.85	1.00	1.28	1.36	1.62
P04762	Cat	2.11	1.00	1.84	1.69	1.77
P11883	Aldh3a1	4.50	1.00	1.71	1.76	4.36
Tyrosine metabolism						
Q6AYQ8	Fahd1	1.18	1.00	1.33	-	1.12
P06757	Adh1	1.18	1.00	1.27	-	1.06
P21396	Maoa	1.45	1.00	1.48	-	1.25
Q5XI42	Aldh3b1	1.61	1.00	1.30	-	1.48
P17764	Acat1	1.65	1.00	1.17	-	1.53
Q9WVK7	Hadh	1.67	1.00	1.23	-	1.51
P30839	Aldh3a2	1.73	1.00	0.85	-	1.62
P11884	Aldh2	1.85	1.00	1.28	-	1.62
P04762	Cat	2.11	1.00	1.84	-	1.77
P11883	Aldh3a1	4.50	1.00	1.71	-	4.36
Glutathione metabolism						
P07314	Ggt1	0.63	1.00	1.47	-	0.63
Q91XR8	Gpx4	0.96	1.00	1.32	-	0.83
Q91XR8	Gpx4	0.96	1.00	1.32	-	0.83
P85968	Pgd	0.98	1.00	1.28	-	1.00
P85968	Pgd	0.98	1.00	1.28	-	1.00
P08010	Gstm2	1.36	1.00	1.04	-	1.38
P56574	Idh2	1.46	1.00	1.18	-	1.30
P04906	Gstp1	1.48	1.00	1.50	-	1.40
P97608	Oplah	1.48	1.00	1.02	-	1.54
P08011	Mgst1	1.62	1.00	1.15	-	1.62
P04904	Gsta3	1.68	1.00	1.78	-	1.45

Metabolism of xenobiotics by cytochrome P450						
P06757	Adh1	1.18	1.00	1.27	-	1.06
P06757	Adh1	1.18	1.00	1.27	-	1.06
P08010	Gstm2	1.36	1.00	1.04	-	1.38
Q8CG45	Akr7a2	1.40	1.00	1.09	-	1.35
P04906	Gstp1	1.48	1.00	1.50	-	1.40
Q5XI42	Aldh3b1	1.61	1.00	1.30	-	1.48
P08011	Mgst1	1.62	1.00	1.15	-	1.62
P04904	Gsta3	1.68	1.00	1.78	-	1.45
P08430	Ugt1a6	2.30	1.00	1.33	-	2.01
P11883	Aldh3a1	4.50	1.00	1.71	-	4.36
Chemical carcinogenesis						
Q9R063	Prdx5	0.75	1.00	1.16	-	0.75
P07895	Sod2	1.06	1.00	1.28	-	1.04
P06757	Adh1	1.18	1.00	1.27	-	1.06
Q704S8	Crat	1.28	1.00	1.13	-	1.32
P56574	Idh2	1.46	1.00	1.18	-	1.30
P04906	Gstp1	1.48	1.00	1.50	-	1.40
Q5XI42	Aldh3b1	1.61	1.00	1.30	-	1.48
P04904	Gsta3	1.68	1.00	1.78	-	1.45
P11915	Scp2	1.69	1.00	1.15	-	1.59
Q62651	Ech1	2.02	1.00	1.01	-	1.73
P11883	Aldh3a1	4.50	1.00	1.71	-	4.36
Peroxisome						
P07895	Sod2	1.06	1.00	1.28	-	1.04
P06757	Adh1	1.18	1.00	1.27	-	1.06
Q8VID1	Dhrs4	1.36	1.00	1.31	-	1.39
P08010	Gstm2	1.36	1.00	1.04	-	1.38
P97852	Hsd17b4	1.49	1.00	1.37	-	1.39
P08011	Mgst1	1.62	1.00	1.15	-	1.62
P04762	Cat	2.11	1.00	1.84	-	1.77
P08430	Ugt1a6	2.30	1.00	1.33	-	2.01
Biosynthesis of antibiotics						
P54690	Bcat1	0.52	1.00	-	0.91	0.61
Q5M819	Psph	0.60	1.00	-	0.79	0.72
Q05982	Nme1	0.61	1.00	-	0.57	0.73
P19804	Nme2	0.64	1.00	-	0.70	0.73
P27881	Hk2	0.69	1.00	-	1.67	0.70
P82808	Gfpt1	0.72	1.00	-	0.82	0.76
P05065	Aldoa	0.89	1.00	-	1.44	0.88
P07323	Eno2	1.17	1.00	-	1.33	1.13
P11960	Bckdha	1.22	1.00	-	1.35	1.15

P50137	Tkt	1.25	1.00	-	1.56	1.18
P21775	Acaa1a	1.27	1.00	-	1.35	1.16
P47860	Pfkp	1.27	1.00	-	1.31	1.18
Q920L2	Sdha	1.27	1.00	-	0.69	1.18
Q99NA5	Idh3a	1.28	1.00	-	1.35	1.17
Q01205	Dlst	1.29	1.00	-	1.29	1.14
P48450	Lss	1.31	1.00	-	1.08	1.58
Q6P6R2	Dld	1.32	1.00	-	1.30	1.18
P38652	Pgm1	1.35	1.00	-	1.12	1.38
P47858	Pfkm	1.41	1.00	-	1.12	1.37
P04182	Oat	1.42	1.00	-	1.15	1.35
P14882	Pcca	1.43	1.00	-	1.19	1.33
P56574	Idh2	1.46	1.00	-	1.22	1.30
O35854	Bcat2	1.47	1.00	-	1.18	1.34
P29411	Ak3	1.61	1.00	-	1.26	1.37
P17764	Acat1	1.65	1.00	-	1.32	1.53
Q9WVK7	Hadh	1.67	1.00	-	1.13	1.51
P07633	Pccb	1.72	1.00	-	1.48	1.51
P30839	Aldh3a2	1.73	1.00	-	0.87	1.62
P13437	Acaa2	1.83	1.00	-	1.17	1.63
P11884	Aldh2	1.85	1.00	-	1.36	1.62
P04762	Cat	2.11	1.00	-	1.69	1.77
Valine, leucine and isoleucine degradation						
P54690	Bcat1	0.52	1.00	-	0.91	0.61
P11960	Bckdha	1.22	1.00	-	1.35	1.15
P21775	Acaa1a	1.27	1.00	-	1.35	1.16
Q6P6R2	Dld	1.32	1.00	-	1.30	1.18
Q5I0C3	Mccc1	1.37	1.00	-	1.22	1.36
P14882	Pcca	1.43	1.00	-	1.19	1.33
O35854	Bcat2	1.47	1.00	-	1.18	1.34
P70584	Acadsb	1.57	1.00	-	1.15	1.33
P29266	Hibadh	1.59	1.00	-	1.32	1.44
P12007	Ivd	1.64	1.00	-	1.19	1.40
P17764	Acat1	1.65	1.00	-	1.32	1.53
Q9WVK7	Hadh	1.67	1.00	-	1.13	1.51
P07633	Pccb	1.72	1.00	-	1.48	1.51
P30839	Aldh3a2	1.73	1.00	-	0.87	1.62
P13437	Acaa2	1.83	1.00	-	1.17	1.63
Q02253	Aldh6a1	1.83	1.00	-	1.32	1.60
P11884	Aldh2	1.85	1.00	-	1.36	1.62
Glyoxylate and dicarboxylate metabolism						
Q6P6R2	Dld	1.32	1.00	-	1.30	1.18

P14882	Pcca	1.43	1.00	-	1.19	1.33
P17764	Acat1	1.65	1.00	-	1.32	1.53
P07633	Pccb	1.72	1.00	-	1.48	1.51
P04762	Cat	2.11	1.00	-	1.69	1.77

Supplementary Table. 5. SRM significantly regulated proteins involved 5 KEGG pathways. Shown here are mean fold changes of proteins expression versus TGF-β1 group, $p<0.05$.

Accession	Protein	Control	TGF-β1	TGF-β1 + 80 μg/mL SRM
ECM-receptor interaction				
P04937	Fn1	0.75	1.00	1.34
P13941	Col3a1	1.16	1.00	1.45
P02466	Col1a2	1.18	1.00	1.32
Q9JI03	Col5a1	1.22	1.00	1.37
P02454	Col1a1	1.37	1.00	1.43
Platelet activation				
P18666	Myl12b	0.55	1.00	0.57
P13941	Col3a1	1.16	1.00	1.45
P02466	Col1a2	1.18	1.00	1.32
Q9JI03	Col5a1	1.22	1.00	1.37
P02454	Col1a1	1.37	1.00	1.43
Protein digestion and absorption				
P13941	Col3a1	1.16	1.00	1.45
P02466	Col1a2	1.18	1.00	1.32
Q9JI03	Col5a1	1.22	1.00	1.37
P02454	Col1a1	1.37	1.00	1.43
PI3K-Akt signalling pathway				
P18266	Gsk3b	0.71	1.00	0.65
P04937	Fn1	0.75	1.00	1.34
P13941	Col3a1	1.16	1.00	1.45
P02466	Col1a2	1.18	1.00	1.32
Q9JI03	Col5a1	1.22	1.00	1.37
P02454	Col1a1	1.37	1.00	1.43
Tight junction				
P18666	Myl12b	0.55	1.00	0.57
O35889	Afdn	0.71	1.00	0.80
Q9QXQ0	Actn4	0.72	1.00	0.81
Q62915	Cask	1.16	1.00	0.80

Supplementary Table. 6. Baicalein significantly regulated proteins involved 18 KEGG pathways. Shown here are mean fold changes of proteins expression versus TGF-β1 group, $p<0.05$, "-": not significantly regulated by 40 μM or 80 μM baicalein.

Accession	Protein	Control	TGF-β1	TGF-β1	
				40 μM Baicalein	80 μM Baicalein
Galactose metabolism					
P27881	Hk2	0.69	1.00	1.32	1.67
P07943	Akr1b1	0.96	1.00	1.69	1.79
Q5RJP0	Akr1b7	1.04	1.00	3.55	4.72
P47860	Pfkp	1.27	1.00	1.16	1.31
Fructose and mannose metabolism					
P27881	Hk2	0.69	1.00	1.32	1.67
P07943	Akr1b1	0.96	1.00	1.69	1.79
Q5RJP0	Akr1b7	1.04	1.00	3.55	4.72
P47860	Pfkp	1.27	1.00	1.16	1.31
P05065	Aldoa	0.89	1.00	1.14	1.44
Cardiac muscle contraction					
P04692	Tpm1	0.76	1.00	0.52	0.30
P09495	Tpm4	0.87	1.00	0.70	0.58
P68035	Actc1	0.84	1.00	0.79	0.64
P58775	Tpm2	0.63	1.00	0.47	0.30
P17209	Myl4	0.67	1.00	0.43	1.11
P11240	Cox5a	1.43	1.00	1.09	1.36
P12075	Cox5b	1.47	1.00	1.09	1.37
P10888	Cox4i1	1.41	1.00	1.05	1.30
Dilated cardiomyopathy					
P58775	Tpm2	0.63	1.00	0.47	-
P04692	Tpm1	0.76	1.00	0.52	-
P68035	Actc1	0.84	1.00	0.79	-
P09495	Tpm4	0.87	1.00	0.70	-
P60711	Actb	0.91	1.00	0.74	-
P63095	Gnas	1.38	1.00	1.42	-
Hypertrophic cardiomyopathy (HCM)					
P58775	Tpm2	0.63	1.00	0.47	-
P04692	Tpm1	0.76	1.00	0.52	-
P68035	Actc1	0.84	1.00	0.79	-
P09495	Tpm4	0.87	1.00	0.70	-
P60711	Actb	0.91	1.00	0.74	-
Adrenergic signalling in cardiomyocytes					

P58775	Tpm2	0.63	1.00	0.47	-
P17209	Myl4	0.67	1.00	0.43	-
P04692	Tpm1	0.76	1.00	0.52	-
P68035	Actc1	0.84	1.00	0.79	-
P09495	Tpm4	0.87	1.00	0.70	-
P63095	Gnas	1.38	1.00	1.42	-
Phenylalanine metabolism					
P21396	Maoa	1.45	1.00	1.48	-
Q5XI42	Aldh3b1	1.61	1.00	1.30	-
P11883	Aldh3a1	4.50	1.00	1.71	-
Adherens junction					
Q9Z1P2	Actn1	0.70	1.00	0.72	-
O35889	Afdn	0.71	1.00	0.80	-
Q9QXQ0	Actn4	0.72	1.00	0.74	-
P60711	Actb	0.91	1.00	0.74	-
Alzheimer's disease					
P0DP29	Calm1	0.48	1.00	-	0.45
P18266	Gsk3b	0.71	1.00	-	0.75
Q9EPV5	Apaf1	0.91	1.00	-	1.36
Q66HF1	Ndufs1	0.98	1.00	-	0.42
Q63269	Itpr3	1.21	1.00	-	1.38
P19234	Ndufv2	1.21	1.00	-	0.53
P21571	Atp5j	1.27	1.00	-	1.26
Q920L2	Sdha	1.27	1.00	-	0.69
Q06647	Atp5o	1.31	1.00	-	1.33
P10719	Atp5b	1.36	1.00	-	1.31
P10888	Cox4i1	1.41	1.00	-	1.30
P11240	Cox5a	1.43	1.00	-	1.36
P12075	Cox5b	1.47	1.00	-	1.37
Parkinson's disease					
Q9JJM9	Sept5	0.84	1.00	-	0.74
Q9EPV5	Apaf1	0.91	1.00	-	1.36
Q66HF1	Ndufs1	0.98	1.00	-	0.42
P19234	Ndufv2	1.21	1.00	-	0.53
P21571	Atp5j	1.27	1.00	-	1.26
Q920L2	Sdha	1.27	1.00	-	0.69
Q06647	Atp5o	1.31	1.00	-	1.33
P10719	Atp5b	1.36	1.00	-	1.31
P10888	Cox4i1	1.41	1.00	-	1.30
P11240	Cox5a	1.43	1.00	-	1.36
P12075	Cox5b	1.47	1.00	-	1.37

Biosynthesis of amino acids					
Q5M819	Psph	0.60	1.00	-	0.79
P05065	Aldoa	0.89	1.00	-	1.44
P18298	Mat2a	0.91	1.00	-	1.42
P07323	Eno2	1.17	1.00	-	1.33
P50137	Tkt	1.25	1.00	-	1.56
P47860	Pfkp	1.27	1.00	-	1.31
Q99NA5	Idh3a	1.28	1.00	-	1.35
P52873	Pc	1.36	1.00	-	1.33
Citrate cycle (TCA cycle)					
Q920L2	Sdha	1.27	1.00	-	0.69
Q99NA5	Idh3a	1.28	1.00	-	1.35
Q01205	Dlst	1.29	1.00	-	1.29
Q6P6R2	Dld	1.32	1.00	-	1.30
P52873	Pc	1.36	1.00	-	1.33
Oxidative phosphorylation					
Q66HF1	Ndufs1	0.98	1.00	-	0.42
P25286	Atp6v0a1	1.17	1.00	-	1.46
P19234	Ndufv2	1.21	1.00	-	0.53
P21571	Atp5j	1.27	1.00	-	1.26
Q920L2	Sdha	1.27	1.00	-	0.69
Q06647	Atp5o	1.31	1.00	-	1.33
P10719	Atp5b	1.36	1.00	-	1.31
P10888	Cox4i1	1.41	1.00	-	1.30
P11240	Cox5a	1.43	1.00	-	1.36
P12075	Cox5b	1.47	1.00	-	1.37
Pentose and glucuronate interconversions					
P07943	Akr1b1	0.96	1.00	-	1.79
Q5RJP0	Akr1b7	1.04	1.00	-	4.72
P06760	Gusb	1.54	1.00	-	1.28
P11884	Aldh2	1.85	1.00	-	1.36
P08430	Ugt1a6	2.30	1.00	-	1.72
Porphyrin and chlorophyll metabolism					
P06762	Hmox1	0.70	1.00	-	2.65
P46844	Blvra	0.92	1.00	-	1.23
P06214	Alad	1.35	1.00	-	2.34
P06760	Gusb	1.54	1.00	-	1.28
P08430	Ugt1a6	2.30	1.00	-	1.72
Huntington's disease					
Q9EPV5	Apaf1	0.91	1.00	-	1.36
Q66HF1	Ndufs1	0.98	1.00	-	0.42
P62744	Ap2s1	1.08	1.00	-	0.79

P19234	Ndufv2	1.21	1.00	-	0.53
P21571	Atp5j	1.27	1.00	-	1.26
Q920L2	Sdha	1.27	1.00	-	0.69
Q06647	Atp5o	1.31	1.00	-	1.33
P10719	Atp5b	1.36	1.00	-	1.31
P10888	Cox4i1	1.41	1.00	-	1.30
P11240	Cox5a	1.43	1.00	-	1.36
P12075	Cox5b	1.47	1.00	-	1.37
Arginine and proline metabolism					
P07335	Ckb	0.83	1.00	-	0.58
P54001	P4ha1	1.19	1.00	-	1.54
P0C2X9	Aldh4a1	1.43	1.00	-	1.36
P21396	Maoa	1.45	1.00	-	1.63
P11884	Aldh2	1.85	1.00	-	1.36
Folate biosynthesis					
P11348	Qdpr	0.97	1.00	-	1.27
Q920D2	Dhfr	1.24	1.00	-	1.30
P18297	Spr	1.63	1.00	-	1.38

Supplementary Table. 7. IN1130 significantly regulated proteins involved 9 KEGG pathways. Shown here are mean fold changes of proteins expression versus TGF-β1 group, $p<0.05$.

Accession	Protein	Control	TGF-β1	TGF-β1 +1N1130
Fatty acid degradation				
P32198	Cpt1a	1.30	1.00	1.29
P18886	Cpt2	1.48	1.00	1.40
P70584	Acadsb	1.57	1.00	1.33
P17764	Acat1	1.65	1.00	1.53
Q9WVK7	Hadh	1.67	1.00	1.51
P30839	Aldh3a2	1.73	1.00	1.62
P13437	Acaa2	1.83	1.00	1.63
P11884	Aldh2	1.85	1.00	1.62
Fatty acid metabolism				
P32198	Cpt1a	1.30	1.00	1.29
Q64232	Tecr	1.41	1.00	1.37
P18886	Cpt2	1.48	1.00	1.40
P70584	Acadsb	1.57	1.00	1.33
P17764	Acat1	1.65	1.00	1.53
Q9WVK7	Hadh	1.67	1.00	1.51
P13437	Acaa2	1.83	1.00	1.63
beta-Alanine metabolism				
Q5XI42	Aldh3b1	1.61	1.00	1.48
P30839	Aldh3a2	1.73	1.00	1.62
Q02253	Aldh6a1	1.83	1.00	1.60
P11884	Aldh2	1.85	1.00	1.62
P11883	Aldh3a1	4.50	1.00	4.36
Colorectal cancer				
P14056	Araf	0.68	1.00	0.79
P18266	Gsk3b	0.71	1.00	0.76
Q63690	Bax	0.72	1.00	0.77
Q01986	Map2k1	0.76	1.00	0.77
P21708	Mapk3	1.57	1.00	1.46
Q9WU82	Ctnnb1	1.77	1.00	1.69
Propanoate metabolism				
P14882	Pcca	1.43	1.00	1.33
P17764	Acat1	1.65	1.00	1.53
P07633	Pccb	1.72	1.00	1.51
Q02253	Aldh6a1	1.83	1.00	1.60
Fatty acid elongation				

O55171	Acot2	0.99	1.00	0.72
Q64232	Tecr	1.41	1.00	1.37
Q9WVK7	Hadh	1.67	1.00	1.51
P13437	Acaa2	1.83	1.00	1.63
Endometrial cancer				
P14056	Araf	0.68	1.00	0.79
P18266	Gsk3b	0.71	1.00	0.76
Q01986	Map2k1	0.76	1.00	0.77
P21708	Mapk3	1.57	1.00	1.46
Q9WU82	Ctnnb1	1.77	1.00	1.69
Lysine degradation				
Q63321	Plod1	1.45	1.00	1.35
P17764	Acat1	1.65	1.00	1.53
Q9WVK7	Hadh	1.67	1.00	1.51
P30839	Aldh3a2	1.73	1.00	1.62
P11884	Aldh2	1.85	1.00	1.62
Prion diseases				
Q63690	Bax	0.72	1.00	0.77
Q01986	Map2k1	0.76	1.00	0.77
P21708	Mapk3	1.57	1.00	1.46
P13596	Ncam1	1.58	1.00	1.44

Supplementary Table. 8. Validation of the molecular weights of synthetic baicalein derivatives by HRMS.

Compound	Molecular formula	Measured mass (M/z)	Theoretical exact mass (m/z)	Error (ppm)	Mode
S2	$C_{17}H_{12}O_6$	No signal	313.0712$[M+H]^+$	-	ESI±/ APCI+
S3	$C_{19}H_{14}O_7$	No signal	355.0817$[M+H]^+$	-	ESI±/ APCI+
6-Acetoxy-5,7-dimethoxyflavone (S5)	$C_{19}H_{16}O_6$	341.1018 $[M+H]^+$	341.1025 $[M+H]^+$	-2.0522	ESI+
5,6,7-Trimethoxyflavone S6	$C_{18}H_{16}O_5$	313.1066 $[M+H]^+$	313.1076 $[M+H]^+$	-3.1938	ESI+
6,7-Diacetoxy-5-methoxyflavone (S7)	$C_{20}H_{16}O_7$	369.0966 $[M+H]^+$	369.0974 $[M+H]^+$	-2.1674	ESI+
5-Hydroxy-6,7-dimethoxyflavone (S8)	$C_{17}H_{14}O_5$	299.0911 $[M+H]^+$	299.0919 $[M+H]^+$	-2.6748	ESI+
6,7-Diacetoxy-5-(benzyloxy) flavone (S9)	$C_{26}H_{20}O_7$	445.1277 $[M+H]^+$	445.1287 $[M+H]^+$	-2.2465	APCI+

7-Acetoxy-6-(benzyloxy)-5-hydroxyflavone (S10)	$C_{24}H_{18}O_6$	403.1172 $[M+H]^+$	403.1181 $[M+H]^+$	-2.4807	APCI+
6,7-(Diphenylmethylenedioxy)-5-methoxyflavone (S13)	$C_{29}H_{20}O_5$	449.1379 $[M+H]^+$	449.1389 $[M+H]^+$	-2.2265	ESI+
5,6-Diacetoxy-7-(benzyloxy) flavone (S14)	$C_{26}H_{20}O_7$	445.1273 $[M+H]^+$	445.1287 $[M+H]^+$	-3.1452	APCI+
6-(Benzyloxy)-5,7-dihydroxyflavone (S15)	$C_{22}H_{16}O_5$	361.1066 $[M+H]^+$	361.1076 $[M+H]^+$	-2.7693	ESI+
5-Hydroxy-6,7-dipropyloxyflavone (S18)	$C_{21}H_{22}O_5$	355.1537 $[M+H]^+$	355.1545 $[M+H]^+$	-2.2525	ESI+
5-Methoxy-6,7-(methylenedioxy) flavone (S20)	$C_{17}H_{12}O_5$	297.0753 $[M+H]^+$	297.0763 $[M+H]^+$	-3.3661	ESI+
5,7-Dimethoxy-6-propyloxy-flavone (S22)	$C_{20}H_{20}O_5$	341.1378 $[M+H]^+$	341.1389 $[M+H]^+$	-3.2245	ESI+
5-Methoxy-6,7-dipropyloxyflavone (S23)	$C_{22}H_{24}O_5$	369.1689 $[M+H]^+$	369.1702 $[M+H]^+$	-3.5214	ESI+
6,7-Diacetoxy-8-bromo-5-hydroxyflavone (S24)	$C_{19}H_{13}BrO_7$	432.9907 $[M+H]^+$	432.9923 $[M+H]^+$	-3.6952	APCI+
8-Bromo-5,6,7-trihydroxyflavone (S25)	$C_{15}H_9BrO_5$	346.9566 $[M-H]^-$	346.9555$[M-H]^-$	3.1704	ESI-
6-Ethoxy-5,7-dihydroxyflavone (S32)	$C_{17}H_{14}O_5$	299.0907 $[M+H]^+$	299.0919 $[M+H]^+$	-4.0121	ESI+
6,7-Diethoxy-5-hydroxyflavone (S33)	$C_{19}H_{18}O_5$	327.1226 $[M+H]^+$	327.1232 $[M+H]^+$	-1.8342	ESI+
5-Hydroxy-6,7-(dioctyloxy) flavone (S34)	$C_{31}H_{42}O_5$	495.3090 $[M+H]^+$	495.3110 $[M+H]^+$	-4.0379	APCI+
6-Ethoxy-5-hydroxy-7-methoxyflavone (S38)	$C_{18}H_{16}O_5$	313.1063 $[M+H]^+$	313.1076 $[M+H]^+$	-4.1519	ESI+
5-Hydroxy-6,7-(dipentyloxy) flavone (S40)	$C_{25}H_{30}O_5$	411.2166 $[M+H]^+$	411.2171 $[M+H]^+$	-1.2159	ESI+
5-Methoxy-6,7-(dipentyloxy) flavone (S41)	$C_{26}H_{32}O_5$	425.2319 $[M+H]^+$	425.2328 $[M+H]^+$	-2.1165	ESI+
6,7-(Dihexyloxy)-5-hydroxyflavone (S42)	$C_{27}H_{34}O_5$	439.2478 $[M+H]^+$	439.2484 $[M+H]^+$	-1.3660	ESI+
6,7-(Dihexyloxy)-5-methoxyflavone (S43)	$C_{28}H_{36}O_5$	453.2631 $[M+H]^+$	453.2641 $[M+H]^+$	-2.2062	ESI+
6,7-Dibutoxy-5-hydroxyflavone (S45)	$C_{23}H_{26}O_5$	383.1847 $[M+H]^+$	383.1858 $[M+H]^+$	-2.8707	ESI+
6,7-Dibutoxy-5-methoxyflavone (S46)	$C_{24}H_{28}O_5$	397.2001 $[M+H]^+$	397.2015 $[M+H]^+$	-3.5247	ESI+